Novel radiotracers for the molecular imaging of cyclooxygenase-2 (COX-2) using positron emission tomography (PET)

by

Ole Tietz

A thesis submitted in partial fulfillment of the requirements for the degree of

Doctor of Philosophy

in

Experimental Oncology

Department of Oncology
University of Alberta

ABSTRACT

Cancer remains one of the most prevalent causes of death in the western world. Effective treatment of this disease relies on the ability to diagnose patients early and assess response to treatment accurately. This can be achieved by monitoring the expression of biomarkers relevant to the type and staging of the cancer. Inflammation has recently been recognized as a hallmark of cancer, as a result the diagnostic and therapeutic molecular targets within inflammatory pathways are of great interest in oncology.

Cyclooxygenase-2 (COX-2) is the inducible isoform of the cyclooxygenase enzyme family. COX-2 is involved in tumour development and progression, and frequent overexpression of COX-2 in a variety of human cancers has made COX-2 an important drug target for cancer treatment. Non-invasive imaging of COX-2 expression in cancer would be useful for assessing COX-2 mediated effects on chemoprevention and radiosensitization using COX-2 inhibitors as an emerging class of anti-cancer drugs, especially for colorectal cancer.

The aim of this study is the design, synthesis and characterization of novel molecular probes (radiotracers) and the preclinical assessment of those probes in cells and animals to evaluate their ability to functionally image COX-2 *in vivo* using positron emission tomography.

Herein, we describe the synthesis of various novel COX-2 inhibitors based on a pyrimidine central scaffold and the radiosynthesis of three novel ^{18}F-labeled COX-2 radiotracers. Radiosynthesis was accomplished by direct and indirect radiolabeling methods, based on a 4-[^{18}F]fluorobenzylamine ([^{18}F]FBA) building block and radiofluorination of iodyl precursors respectively. Radiotracers N-(4-[^{18}F]Fluorobenzyl)-4-[4-(methylsulfonyl)phenyl]-6-(trifluoromethyl)pyrimidin-2-amine ([^{18}F]**1a**), 4-{2-[(4-[^{18}F]Fluorobenzyl)amino]-6-(trifluoromethyl)pyrimidin-4-yl}benzenesulfonamide ([^{18}F]**2a**) and 2-[(4-[^{18}F]Fluorobenzyl)oxy]-4-[4-

(methylsulfonyl)phenyl]-6-(trifluoromethyl)pyrimidine ([^{18}F]**3a**) were evaluated in a colorectal cancer model using HCA-7 cells *in vitro* and HCA-7 xenograft tumors in NIH-III mice as *in vivo* model. Lead radiotracer [^{18}F]**1a** showed the most promising *in vitro* and *in vivo* properties and underwent the most extensive pre-clinical evaluation. *In vitro* cell uptake studies of [^{18}F]**1a** showed that the uptake of radiotracer into COX-2 positive HCA-7 cells is significantly higher than in COX-2 negative HCT-116 cells. Furthermore, the uptake of [^{18}F]**1a** in HCA-7 cells could be reduced by pre-treating cells with high doses of known COX-2 inhibitors, indicating that the uptake of [^{18}F]**1a** in HCA-7 cells is due to COX-2 specific binding. Experiments in HCA-7 tumor bearing NIH-III mice showed that the uptake of [^{18}F]**1a** in the tumor is significantly higher than the uptake in reference tissue (muscle). Furthermore, the uptake in the tumor could be reduced by pre-treatment of animals with known COX-2 inhibitors, indicating that uptake of [^{18}F]**1a** in HCA-7 xenografts is due to COX-2 specific binding. These pre-clinical studies indicate that the uptake of [^{18}F]**1a** in COX-2 positive tissues is at least partially due to specific interaction with COX-2.

Radiotracers [^{18}F]**1a**, [^{18}F]**2a** and [^{18}F]**3a** underwent further pharmacokinetic evaluation in various tissues of interest, such as blood pool, lung, tumor, muscle, brain, liver and kidney. While the pharmacokinetic properties of [^{18}F]**2a** are not favorable for the development of a radiopharmaceutical, [^{18}F]**3a** shows promising properties as a neuroimaging agent and might be investigated further as an imaging agent for neuroinflammation.

Finally, efforts were made to develop a radiotracer based on ^{125}I-labeling. An iodine containing COX-2 inhibitor was synthesized on the basis of the pyrimidine scaffold and radiolabeled using novel oxidant fluorous chloroamine-T (F-CAT), recently developed by the Valliant group at McMaster.

PREFACE

This thesis is an original work by Ole Tietz. The animal studies described in this thesis complied with the Canadian Council of Animal Care as approved by the local animal care committee (Cross Cancer Institute, University of Alberta, Protocol number: AC11182)

The literature review presented in chapter 2 is published as **Tietz, O**; Marshall, A; Wuest, M; Wang, M; Wuest, F. "Radiotracers for Molecular Imaging of Cyclooxygenase-2 (COX-2) Enzyme." *Curr. Med. Chem.*, **2013**, 20(35), 4350. I conducted the literature search and prepared the manuscript. A. Marshall, M. Wuest, M. Wang contributed to manuscript edits. F. Wuest was the supervisory author and was involved with the concept formation and manuscript composition.

Chapter 3 is published as **Tietz, O**; Sharma, S; Kaur, J; Way, J; Marshall, A; Wuest, M; Wuest, F. "Synthesis of three ^{18}F-labelled Cyclooxygenase-2 (COX-2) Inhibitors based on a Pyrimidine Scaffold." *Org. Biomol. Chem.*, **2013**, 11(46), 8052. I was involved in the conception of the study, carried out chemistry and radiochemistry experiments, and wrote the manuscript. S. Sharma performed the *in vitro* COX-1 and COX-2 enzyme inhibition experiments, J. Kaur performed the molecular docking studies, J. Way performed the automated synthesis of [^{18}F]FBA. All co-authors contributed to manuscript edits. F. Wuest was the supervisory author and was involved with the concept formation and manuscript composition.

As of July 18th 2015, Chapter 5 has been submitted for publication at the Journal of Nuclear Medicine as **Tietz, O**; Wuest, M; Marshall, A; Wang, M; Bergman, C; Way, J; Wuest, F. "PET imaging of cyclooxygenase-2 (COX-2) in a colorectal cancer model." Some of the data is submitted for publication as supplementary information. I was involved in the conception of the study, carried out radiochemistry experiments, analysed the data, and wrote the manuscript. A. Marshall and M. Wang performed the cell uptake experiments, M. Wuest performed the animal

experiments, C. Bergman and J. Way performed the automated synthesis of [^{18}F]FBA. All co-authors contributed to manuscript edits. F. Wuest was the supervisory author and was involved with the concept formation and manuscript composition.

As of July 29th 2015, Chapter 6 has been submitted for publication in Molecular Imaging and Biology as **Tietz, O**; Marshall, A; Bergman, C; Wuest, M; Wuest, F. "Molecular structure influences radiopharmacology of ^{18}F-labeled COX-2 inhibitors *in vivo*." I was involved in the conception of the study, carried out radiochemistry experiments, analysed the data, and wrote the manuscript. A. Marshall performed the cell uptake experiments, M. Wuest performed the animal experiments, C. Bergman performed the automated synthesis of [^{18}F]FBA. All co-authors contributed to manuscript edits. F. Wuest was the supervisory author and was involved with the concept formation and manuscript composition.

As of July 30th 2015, Chapter 8 has been submitted for publication in Organic & Biomolecular Chemistry as **Tietz, O**; Dzandzi, J; Bhardwaj, A; Valliant, J; Wuest, F. "Design and synthesis of ^{125}I-labelled cyclooxygenase-2 (COX-2) inhibitors using fluorous chemistry." Some of the data is submitted for publication as supplementary information. I was involved in the conception of the study, carried out chemistry and radiochemistry experiments, and wrote the manuscript. The work was a collaboration with Prof. J. Valliant's group at McMaster University, Hamilton. J. Dzandzi was instrumental in assisting with the radiochemistry described in the publication. All co-authors contributed to manuscript edits. F. Wuest was the supervisory author and was involved with the concept formation and manuscript composition.

ACKNOWLEDGEMENT

I would like to thank my supervisor Dr. Frank Wuest for all his guidance, support and encouragement. Dr. Wuest's vision and enduring optimism for this project were crucial to its success. Thank you to the members of my PhD committee, Dr. Carlos Velazquez and Dr. John Mercer for their scientific input and advice.

I would also like to thank and acknowledge former and present members of the Wuest Lab for their helpful discussion and support: Dr. Vincent Bouvet, Dr. JB Al-Hourani, Dr. James Knight, Dr. Susan Richter, Dr. Christian Foerster, Dr. Ingrit Hamann and Amanda Perreault.

Special thank and acknowledgement must go to all those who worked on the COX-2 project. Alison Marshall and Monica Wang for their work on cell uptake studies and their maintenance of cell stocks for *in vitro* studies and animal inoculation; Jenilee Way and Cody Bergman for the synthesis of 4-[^{18}F]fluorobenzylamine in the early hours of the morning; Dr. Sai Kiran Sharma, Dr. Jatinder Kaur and Dr. Atul Bhardwaj for their efforts with the enzyme inhibition assay and molecular docking studies; and most importantly Dr. Melinda Wuest for her tireless work on the *in vivo* studies and her help with data analysis.

I would like to thank Dr. John Valliant and the Valliant research group at McMaster University for welcoming me into their midst and Dr. James Dzandzi for introducing me to Iodine radiochemistry.

Acknowledgement and thanks must go to Dr. John Wilson, Dave Clendening and Blake Lazurko from the Edmonton PET Centre for radionuclide production and excellent technical support, as well as Gail Hipperson and Dan McGinn from the Vivarium of the Cross Cancer Institute for supporting the animal work.

I would further like to thank the Natural Science and Engineering Research Council (NSERC) and specifically the create Molecular Imaging Probes program for their financial and administrative assistance; the Elizabeth Tucker travel award program for enabling me to attend the ISRS 2013 in South Korea and the Herbert Meltzer Memorial Fellowship for financial assistance.

I would like to thank the Department of Oncology for their support with regards to funding and registration and special thanks to Dr. Andrew Shaw and Dr. Alan Underhill. I am grateful to Dr. David Murray and Dr. Vickie Baracos for serving on my candidacy committee.

Finally, and most importantly, I would like to thank my family and friends for their ongoing emotional support, without which none of this would have been possible.

TABLE OF CONTENTS

LIST OF TABLES

LIST OF FIGURES AND ILLUSTRATIONS

LIST OF ABBREVIATIONS AND COMPOUNDS

AA	arachidonic acid
[^{18}F]**1a**	N-(4-[^{18}F]Fluorobenzyl)-4-[4-(methylsulfonyl)phenyl]-6-(trifluoromethyl)pyrimidin-2-amine
[^{18}F]**2a**	4-{2-[(4-[^{18}F]Fluorobenzyl)amino]-6-(trifluoromethyl)pyrimidin-4-yl}benzenesulfonamide
[^{18}F]**3a**	2-[(4-[^{18}F]Fluorobenzyl)oxy]-4-[4-(methylsulfonyl)phenyl]-6-(trifluoromethyl)pyrimidine
[^{18}F]FBA	4-[^{18}F]fluorobenzylamine
[^{18}F]FBAlc	4-[^{18}F]fluorobenzyl alcohol
[^{18}F]FBN	4-[^{18}F]fluorobenzonitrile
^{99m}Tc-EC	^{99m}Tc-$_{L,L}$-ethylenedicysteine
AcOK	potassium acetate
AIDA	adaptive image deconvolution algorithm
ATPase	adenosinetriphosphatase
BBB	blood brain barrier
BCA	bicinchoninic acid
CA	carbonic anhydrases
cAMP	cyclic adenylyl monophosphate
$CDCl_3$	deuterated chloroform
CDK	cyclin-dependent kinase
CH_2Cl_2	dichloromethane

CH_3CN	acetonitrile
CH_3CO_3H	peracetic acid
COX-1	cyclooxygenase-1
COX-2	cyclooxygenase-2
coxib	cyclooxygenase-2 selective inhibitor
COXs	cyclooxygenases
cPGES	cytosolic PGE synthase
CT	computed tomography
CuI	copper iodide
DCM	dichloromethane
DMEM	Dulbecco's Modified Eagle Medium
DMF	dimethyl formamide
DMSO	dimethyl sulfoxide
DMSO-d_6	deuterated dimethyl sulfoxide
DMT	dimethoxytrityl
DMTr	4,4'-dimethoxytrityl
EFMP	6-ethoxy-3-(4-methanesulfonylphenyl)-4-(4-fluorophenyl)pyran-2-one
EGFR1	epidermal growth factor receptor 1
EOB	end of bombardment
EP receptors	prostaglandin E receptors
EP2	prostaglandin E receptor 2
EP4	prostaglandin E receptor 4

ER	estrogen receptor
Et_3N (TEA)	triethyl amine
EtOAc	ethyl acetate
EtOH	ethanol
FBS	fetal bovine serum
F-CAT	fluorous chloroamine-T
FDA	Food and drug administration
FSPE	fluorous solid phase extraction
γ–IFN	γ-interferon
GIST	gastrointestinal stromal tumors
HCl	hydrochloric acid
HEPES	2-[4-(2-hydroxyethyl)piperazin-1-yl]ethanesulfonic acid
HER2	human epidermal growth factor receptor 2
HIF1α	hypoxia induced factor 1α
HPLC	high performance liquid chromatography
HSA	human serum albumin
HSV	herpes simplex virus
i.p.	intraperitoneal
i.v.	intravenous
K_{222}	4,7,13,16,21,24-Hexaoxa-1,10-diazabicyclo[8.8.8]hexacosane
K_2CO_3	potassium carbonate
KF	potassium fluoride
LPS	lipopolysaccharides

MAP	maximum a posteriori
MeI	methyl iodide
MeOH	methanol
MeOTf	methyl triflate
MIP	maximum intensity projection
mPGES-1	microsomal PGE synthase-1
mPGES-2	microsomal PGE synthase-2
MRI	magnetic resonance imaging
mRNA	messenger ribonucleic acid
n.c.a.	no carrier added
$NaBH_4$	sodium borohydride
NaH	sodium hydride
NaI	sodium iodide
NaOAc	sodium acetate
NaOH	soduim hydroxide
NF-κB	nuclear factor κB
NMP	N-methyl-2-pyrrolidone
NNK	4-(methylnitrosamino)-1-(3-pyridyl)-1-butanone
NSAID	non-steroidal anti-inflammatory drugs
NSCLC	non-small cell lung carcinoma
$P(\text{-tolyl})_3$	tri-o-tolylphosphine
p.i.	post-injection
PBS	phosphate buffered saline

$Pd(PPh_3)_4$	tetrakis(triphenylphosphine)palladium(0)
$Pd_2(dba)_3$	tris(dibenzylideneacetone)dipalladium(0)
$PdCl_2(dppf)$	[1,1′-Bis(diphenylphosphino)ferrocene]dichloropalladium(II)
PDK-1	protein-dependent kinase 1
PET	positron emission tomography
PG	prostaglandin
PGD_2	prostaglandin D_2
PGE_2	prostaglandin E_2
$PGF_{2\alpha}$	prostaglandin $F_{2\alpha}$
PGG_2	prostaglandin G_2
PGH_2	prostaglandin H_2
PGI_2	prostaglandin I_2
PR	progesterone receptor
RCY	radiochemical yield
R_f	retention factor
RIA	radioimmuno assay
RIPA	radioimmunoprecipitation assay
ROI	region of interest
r.t.	room temperature
SEM	standard error of the mean
SIRS	systemic inflammation response syndrome
Sn_2Me_6	hexamethylditin
SPE	solid phase extraction

SPECT	single photon emission computed tomography
STAT3	signal transducer and activator of transcription 3
SUV	standardized uptake value
TAC	time-activity curve
TBAF	Tetra-n-butylammonium fluoride
TFA	trifluoro acetic acid
THF	tetrahydrofuran
$TiCl_4$	titanium tetrachloride
TLC	thin-layer chromatography
TMS	tetramethylsilane
TPA	tetradecanoylphorbol acetate
TXA_2	thromboxane A_2
UV	ultraviolet
WCT	ward colon tumor

CHAPTER 1

Introduction

Solid tumors are among the leading causes of death in Western countries, with a steadily increasing number of cancer patients every year. Approximately 1.7 million people are expected to be diagnosed with cancer over the course of the year 2014 in the United States alone. Almost 600,000 patients are expected to die from the disease [1]. Half of all new cases will be lung, colorectal, breast and prostate cancers, while lung cancer has been shown to be the most deadly in both men and women. The current lifetime risk of being diagnosed with invasive cancer is 44 % for men and 38 % for women, meaning that approximately 1 in 3 to 1 in 2 people will be diagnosed with invasive cancer over the course of their life. Diagnosis and treatment of the disease have improved significantly over the past two decades. Estimates suggest that advances in science and medicine have averted approximately 1 million cancer deaths in men and 400,000 cancer deaths in women between 1991 and 2010 (all data is for the USA only) [1]. Although the prognosis for many patients has improved over the last decade, there is still an urgent need for novel and more efficient treatment modalities.

Diagnosis and treatment of cancer is achieved by computed tomography (CT) and magnetic resonance imaging (MRI), followed by surgical, chemotherapeutic and radiotherapeutic intervention. More recently, cancer treatment has started to rely on the identification of biomarkers to personalize treatment for individual patients. Some of the most commonly used biomarkers are estrogen receptor (ER), progesterone receptor (PR) and human epidermal growth factor receptor 2 (HER2) in breast cancer, the Philadelphia chromosome (bcr-abl fusion protein) in chronic myeloid leukemia, c-KIT mutations in gastrointestinal stromal tumors (GIST) and epidermal growth factor receptor 1 (EGFR1) mutations in non-small cell lung carcinoma (NSCLC) [2]. Biomarkers can be grouped into two categories, prognostic and predictive markers. Prognostic markers provide information on the patients overall cancer outcome regardless of therapy, while

predictive markers give information on the effect of therapeutic intervention. A predictive marker can be used as a therapeutic target [2, 3]. Novel predictive biomarkers and non-invasive imaging agents selective for those biomarkers are essential for the development of personalized therapeutic approaches in oncology.

The recent inclusion of inflammation as a hallmark of cancer by Hanahan and Weinberg has led to increased interest in predictive biomarkers within the inflammatory signaling pathway [4]. Links between inflammation and cancer have existed for a long time. The first observations connecting the two conditions date back to the 19th century, when it was discovered that biopsied tumor samples contained inflammatory cells [5]. A number of recent studies have confirmed these findings on a molecular level, which has led to a resurgence of interest in the field [6-8].

1.1. Inflammation

1.1.1. Basis of inflammatory conditions

Inflammation is a host response designed to rid the body of injured tissues or combat microbial infections [9, 10]. These inflammatory functions are indispensable since the host organism would otherwise be unable to check infection or discard damaged tissues. However, inflammatory mechanisms have a tendency to cause collateral damage on healthy cells surrounding the disease center. As a result, inflammation can be harmful when inappropriately activated or poorly controlled. Much attention is paid to these harmful side effects of inflammation since they contribute to the development of many chronic diseases, such as diabetes, obesity, rheumatoid arthritis and atherosclerosis [11].

Non-steroidal anti-inflammatory drugs (NSAIDs) are some of the most commonly sold drugs in the world today. These drugs aim to combat the negative side effects of inflammation, while, ideally, retaining the positive effects.

Inflammation can be classified as being either acute or chronic. Acute inflammation serves to deliver plasma proteins and leukocytes to the site of infection or injury. This type of inflammation is induced rapidly and persists for hours or days. Increased blood flow and vascular permeability at the site of inflammation are easily detectable due to redness, warmth and swelling of the tissue [12]. Activated leukocytes, primarily neutrophils, release toxic metabolites and proteases to cause tissue damage and destroy offending agents. This process is the underlying cause of the pain usually associated with inflammation. Chronic inflammation can persist for weeks or even years. It can follow an acute inflammatory condition or manifest slowly without any of the initial hallmarks of acute inflammation [13]. It is important to note that tissue destruction and reconstruction often co-exit in some combination over the course of chronic inflammatory response [14].

If an offending agent, such as a pathogen, damaged cell or irritant, is able to escape the site of initial acute inflammatory response via the circulatory system or the lymphatic system a systematic inflammatory response follows. Systemic inflammation is not confined to a particular tissue in the body, but affects the endothelium as well as other organ systems. In extreme cases systemic inflammation can lead to the development of systemic inflammation response syndrome (SIRS), which can culminate in the failure of one or multiple organ systems. Systemic inflammation can manifest as an acute condition, as encounter in SIRS, or a chronic condition, notably studied in obesity, where inflammatory markers are up regulated chronically [15].

Acute inflammation is terminated upon the successful neutralization of the offending stimulus. Towards the end of acute inflammation the organism switches from producing pro-inflammatory to anti-inflammatory mediators. The primary function of anti-inflammatory mediators is to stop the recruitment of leukocytes and reduce vascular permeability at the site of inflammation. The principal mediators of these processes are lipoxins, resolvins and protectins [11, 16, 17]. Ideally, acute inflammation restores both structure and function of injured tissue upon resolution. In tissue types that lack regenerative potential, the site of injury is replaced by fibrous tissue in a process known as organization [17]. In the event that acute inflammation can not resolve infection or injury it transitions to chronic inflammation, which ultimately leads to tissue destruction and loss of function. Interestingly, this type of inflammation can itself cause cancer if it persists for long enough [18]. Inflammation can therefore both enable and cause cancer.

1.1.2. Inflammation and cancer

Consistent with the observation that inflammation can both enable and cause cancer, the connection between inflammation and cancer can be viewed as consisting of an extrinsic and an intrinsic pathway. The extrinsic pathway is driven by inflammatory conditions that aid the development of tumors and thereby increase the risk for developing cancer (for example: inflammatory bowl disease which can lead to the development of colorectal cancer). The intrinsic pathway has been discovered recently when researchers started to investigate why cancers develop inflammatory conditions in their microenvironments, even though there is no basis for inflammation. One of the questions that this observation raises is whether the genetic changes that lead to the development cancer are also responsible for the development of inflammatory conditions in the tumor microenvironment [5].

Inflammatory conditions are initiated through the activation of various transcription factors, most notably NF-κB, STAT3 and HIF1α [7, 19, 20]. If inflammation is initiated via the extrinsic pathway, transcription factors are activated by infection or tissue damage; if inflammation is initiated through the intrinsic pathway, transcription factors are activated by oncogenes [21]. The transcription factors facilitate the expression of various chemokines, cytokines and prostaglandins (via expression of cyclooxygenases) by tumor cells. These chemical messenger molecules work to recruit leukocytes through paracrine signaling mechanisms. The cells recruited include macrophages, eosinophils, neutrophils and mast cells, among others [22, 23]. The presence of these cells in the tumor microenvironment leads to further induction of NF-κB, STAT3 and HIF1α transcription factors in inflammatory, stromal and tumor cells. These transcription factors continue to produce chemokines, cytokines and prostaglandins in the tumor and its microenvironment. The messenger molecules are now able to act in a paracrine as well as an autocrine manner, which leads to the development of a self-sustaining pro-inflammatory environment and typical cancer related inflammation [23]. This inflammatory environment aids cell proliferation and survival, angiogenesis, tumor cell migration, invasion and metastasis, which contributes to the growth, progression and metastasis of tumors [5]. Cyclooxygenase-2 and the prostaglandin pathway are key mediators in this process.

1.2. Cyclooxygenases

1.2.1. Cyclooxygenase (COX) enzyme family and prostaglandin signaling

The Cyclooxygenase enzyme family consists of two members, the constitutively expressed Cyclooxygenase-1 (COX-1) and the inducibly expressed Cyclooxygenase-2 (COX-2). Both enzymes catalyze the conversion of arachidonic acid to prostaglandin G_2 (PGG_2) and prostaglandin

H_2 (PGH_2). PGH_2 is then further modified by to produce a variety of prostaglandin signaling molecules, such as PGE_2, PGI_2, TXA_2, PGD_2, and $PGF_{2\alpha}$. These autocrine and paracrine messenger molecules, in turn, bind to a number of G-protein coupled receptors. COX-1 is expressed in almost all resting tissue types, while COX-2 is virtually absent in healthy tissue. COX-1 functions as a housekeeping enzyme and is responsible for gastro-intestinal and renal integrity, among other things [24]. COX-2 is expressed only in response to certain pro-inflammatory stimuli, such as growth factors, cytokines, and expression is usually transient [25]. As such, COX-2 is an important mediator of inflammatory response and functions as one of the most important therapeutic targets for the treatment of inflammation and associated conditions such as pain and fever. Over the counter pain medication such as aspirin and ibuprofen are dual COX-1 / COX-2 inhibitors.

1.2.2. COX inhibitors

The first drug to be used for the treatment of pain and inflammation through the inhibition of cyclooxygenase was aspirin. The drug has been manufactured and marketed since the late 1890s, although its use as an active ingredient in willow bark goes back to antiquity. Cyclooxygenase was not identified as the molecular target of aspirin until the late 1970s and it wasn't until 1991 that COX-2 was discovered as the inducible isoform of the enzyme. The first class of compounds to be developed to inhibit cyclooxygenases were the non-steroidal anti-inflammatory drugs (NSAIDs) which inhibited both the COX-1 and COX-2 isoforms of the enzyme. The discovery of COX-2 gave rise to the scientific paradigm that COX-1 inhibition was undesirable, because it resulted in the adverse side-effects commonly encountered after long term use of NSAIDs, such as gastrointestinal bleeding and ulceration. The logical consequence of this paradigm was that only the inhibition of COX-2 is of therapeutic benefit; this lead to the development of a large number

of selective COX-2 inhibitors (coxibs) – compounds that have little or no affinity for COX-1. A few of these compounds were in broad clinical use after they obtained FDA approval in 2000. The coxib compound class includes celecoxib, valdecoxib, etoricoxib and rofecoxib. Most selective COX-2 inhibitors were withdrawn from market in 2005 following concerns over their cardiac safety profiles. The only mainstream coxib still in clinical use today is celecoxib. A study published in 2012 highlighted the underlying biochemical mechanisms of the cardioprotective effects of COX-2 [26, 27]. This has lead to a partial revision of the original paradigm, highlighting the fact that COX-2 is not only associated with negative, disease-driven expression. Due to the undiminished potential of this compound class, current efforts in pharmaceutical research are aimed at designing selective COX-2 inhibitors with minimized adverse effects [28, 29].

1.2.3. COX-2 and cancer

Elevated COX-2 expression has been demonstrated in many human cancers most notably colorectal, gastric, and breast cancer [30-34]. The COX-2 enzyme is assumed to play an important role in carcinogenesis by stimulating angiogenesis, tissue invasion, metastasis, and apoptosis inhibition. COX-2 expression is stimulated by a number of inflammatory cytokines, growth factors, oncogenes, lipopolysaccharides, and tumor promoters [34].

Numerous epidemiological studies have revealed that regular use of non-steroidal anti-inflammatory drugs (NSAIDs) is associated with a significant decreased incidence of various cancers [35-37]. The prophylactic effect of non-selective NSAIDs like aspirin, and selective COX-2 inhibitors like SC-236 and celecoxib, has been found for esophagus, stomach, breast, lung, bladder, prostate, ovary, and colon cancer [37]. The decreased risk of developing certain types of cancer through a prolonged regular intake of NSAIDs has been observed most consistently for

colon cancer, for which a reduction in tumor development of up to 50% could be achieved [38-40].

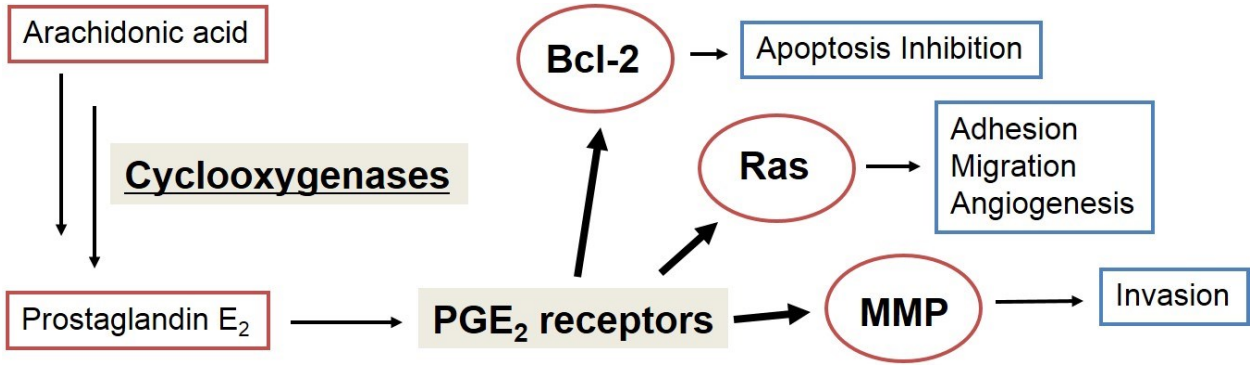

Figure 1-1: Key signaling pathways involving effects of COX-2 and specifically Prostaglaindin E_2 in inflammation and tumorigenesis. Adapted from Meric et al [34].

Several aspects of the molecular mechanisms underlying COX-2 expression in cancer and inflammatory lesions have been elucidated, and key signaling pathways involving effects of COX-2 in inflammation and tumorigenesis have been dissected [34, 41]. However, there have been notable discrepancies between the potent anticancer effects of COX-2 inhibitors in preclinical studies and their failure in a majority of clinical trials [42].

1.3. Non-invasive imaging of COX-2

Positron emission tomography (PET) is an important component of diagnostic imaging in modern medicine. Images are obtained by treating patients with targeting entities, such as drug like molecules, peptides or antibodies, radiolabeled with positron emitting short lived radioisotopes ($t_{1/2}$ > 12 h). As the radioisotope decays it emits a positron which will undergo an annihilation reaction with a nearby electron. This nuclear reaction leads to the emission of two gamma rays

that exit the annihilation site in opposite direction (180^{o} from one another). A dual coincidence PET detector registers the gamma rays and can thus determine the location of the positron-electron annihilation in three-dimensional space. Computer processing allows researchers and clinicians to reconstruct a three-dimensional image of the radioactivity distribution in the body. Appropriately targeted radiolabeled entities, so called radiotracers, can thus give functional information about biochemical process in living organisms.

Cyclooxygense-2 is an important mediator of inflammatory response. Given the importance of inflammation in the development and progression of cancer, COX-2 is a relevant diagnostic and therapeutic target in Oncology. If there were tools capable of accurately assessing COX-2 expression, the enzyme could serve as a predictive biomarker with important clinical application. To date, an exact assessment of COX-2 expression can only be achieved by laborious analyses *ex vivo*. The instability of COX-2 mRNA and protein leads to further difficulties in terms of the interval between tissue sampling and time of analysis [43].

The development of techniques for non-invasive monitoring of COX-2 functional expression would greatly facilitate our efforts to understand COX-2 pharmacology. Nuclear molecular imaging techniques like PET would provide unique opportunities to obtain data on COX-2 expression levels during disease progression and therapeutic intervention.

1.4. Aims and Objectives

This project aims to evaluate the diagnostic and therapeutic potential of COX-2 as a molecular target to further elucidate the role the enzyme plays in the development and progression of cancer. Research activities include the design, synthesis and characterization of novel molecular probes (radiotracers) and the preclinical assessment of those probes in cells and animals to evaluate their ability to visualize COX-2 *in vivo* and *in vitro*.

1.4.1. Hypothesis

^{18}F-labeled small molecule compounds containing a central pyrimidine scaffold are suitable radiotracers for molecular imaging of COX-2 expression by positron emission tomography (PET).

1.4.2. Objectives

The objective of this work is to design, synthesize and evaluate a radiolabeled COX-2 inhibitor that fulfills the following criteria:

(1) High affinity and selectivity for COX-2 in an enzyme inhibition assay

(2) Fast (< 2 half-lives), high yielding radiosynthesis that provides a product with reasonable specific activity (> 40 GBq/μmol)

(3) *In vitro* specificity for COX-2 in cell uptake experiments

(4) Favorable *in vivo* radiopharmacology, including high metabolic stability and the ability to bind specifically to COX-2 *in vivo*.

1.5. References

[1] Siegel, R.; Ma, J.; Zou, Z.; Jemal, A. Cancer statistics, 2014. *CA-Cancer J. Clin.*, **2014**, 64, 9.

[2] Oldenhuis, C.N., Oosting, S.F., Gietema, J.A., de Vries, E.G., Predictive and prognostic value of biomarkers in oncology.*Eur. J. Cancer*, **2008**, 44, 946.

[3] Braun, M.S.; Richman, S.D.; Quirke, P.; Daly, C.; Adlard, J.W.; Elliott, F.; Barrett, J.H.; et al. Predictive biomarkers of chemotherapy efficacy in colorectal cancer: results from the UK MRC FOCUS trial. *J. Clin. Onco.*, **2008**, 26, 2690.

[4] Hanahan, D., Weinberg, R., Hallmarks of cancer: The next generation. *Cell*, **2011**, 144, 646.

[5] Mantovani, A.; Allavena, P.; Sica, A.; Balkwill, F. Cancer-related inflammation. *Nature,* **2008**, 454, 436.

[6] Coussens, L.M.; Werb, Z. Inflammation and cancer. *Nature,* **2002**, 420, 860–867.

[7] Karin, M. Nuclear factor-κB in cancer development and progression. *Nature,* **2006***,* 441, 431.

[8] Koehne, C.H.; Dubois, R.N. COX-2 inhibition and colorectal cancer. *Semin. Oncol.,* **2004**, 31, 12.

[9] Benesch, M.G.K.; Ko, Y.M.; McMullen, T.P.W.; Brindely, D.N. Autotaxin in the crosshairs: Taking aim at cancer and other inflammatory conditions. *FEBS Lett.*, **2014**, 588, 2712.

[10] Weissman, G. Inflammation: Historical Perspectives in: Inflammation: Basic Principles and Clinical Correlates. *Raven Press, New York*, **1992**, 5.

[11] Krishnamoorthy, S.; Honn, K.V. Inflammation and disease progression. *Cancer Metastasis Rev.*, **2006**, 25, 481.

[12] Muller, W.A. Leukocyte-endothelia cell interactions in the inflammatory response. *Lab. Invest.*, **2002**, 82, 521.

[13] Majno, G. Chronic inflammation: links with angiogenesis and wound healing. *Am. J. Pathol.*, **1998**, 153, 1035.

[14] Lawrence, T.; Gilroy, D.W. Chronic inflammation: a failure of resolution? *Int. J. Exp. Pathol.*, **2007**, 88, 85.

[15] Kershaw, E.E.; Flier, J.S. Adipose tissue as an endocrine organ. *J. Clin. Endocrinol. Metab.*, **2004**, 89, 2548.

[16] Serhan, C.N.; Chiang, N.; Van Dyke, T.E. Resolving inflammation: dual anti-inflammatory and pro-resolution lipid mediators. *Nat. Rev. Immunol.*, **2008**, 8, 349.

[17] Serhan, C.N.; Savill, J.; Resolution of inflammation: the beginning programs the end. *Nat. Immunol.*, **2005**, 6, 1191.

[18] Balkwill, F.; Mantovani, A. Inflammation and cancer: back to Virchow? *Lancet*, **2001**, 357, 539.

[19] Yu, H.; Kortylewski, M.; Pardoll, D. Crosstalk between cancer and immune cells: role of STAT3 in the tumour microenvironment. *Nature Rev. Immunol.*, **2007**, 7, 41.

[20] Rius, J.; Guma, M.; Schachtrup, C.; Akassoglou, K.; Zinkernagel, A.S.; Nizet, V.; Johnson, R.S.; Haddad, G.G.; Karin, M. NF-κB links innate immunity to the hypoxic response through transcriptional regulation of HIF-1α. *Nature,* **2008**, 453, 807.

[21] Borrello, M.G.; Alberti, L.; Fischer, A.; Degl'Innocenti, D.; Ferrario, C.; Gariboldi, M.; Marchesi, F.; et al. Induction of a proinflammatory program in normal human thyrocytes by the *RET/PTC1* oncogene. *Proc. Natl Acad. Sci. USA,* **2005**, 102, 14825.

[22] Mantovani, A.; Bottazzi, B.; Colotta, F.; Sozzani, S.; Ruco, L. The origin and function of tumor-associated macrophages. *Immunol. Today*, **1992**, 13, 265.

[23] Ostrand-Rosenberg, S.; Sinha, P. Myeloid-derived suppressor cells: linking inflammation and cancer. *J. Immunol.,* **2009**, 182(8), 4499.

[24] Scheiman, J.M. Unmet needs in non-steroidal anti-inflammatory drug-induced upper gastrointestinal diseases. *Drugs*, **2006**, 66, 15.

[25] Seibert, K.; Zhang, Y.; Leahy, K.; Hauser, S.; Masferrer, J.; Perkins, W.; Lee, L.; Isakson, P. Pharmacological and biochemical demonstration of the role of cyclooxygenase 2 in inflammation and pain. *Proc. Natl. Acad. Sci. U S A*, **1994**, 91, 12013.

[26] Cannon, C.P.; Cannon, P.J. COX-2 Inhibitors and Cardiovascular Risk. *Science*, **2012**, 336, 1386.

[27] Yu, Y.; Ricciotti, E.; Scalia, R.; Tang, S.Y.; Grant, G.; Yu, Z.; Landesberg, G.; Crichton, I.; Wu, W.; Pure, E.; Funk, C.; FitzGerald, G. Vascular COX-2 Modulates Blood Pressure and Thrombosis in Mice. *Sci. Transl. Med.,* **2012**, 132, 54.

[28] Fiorucci, S.; Distrutti, E. COXIBs, CINODs and H2S-Releasing NSAIDs: Current Perspectives in the Development of Safer Non Steroidal Anti-Inflammatory Drugs. *Cur. Med. Chem.*, **2011**, 18, 3494.

[29] Rovati, G.E.; Sala, A.; Capra, V.; Dahlén, S.E.; Folco, G. Dual COXIB/TP antagonists: a possible new twist in NSAID pharmacology and cardiovascular risk. *Trends Pharmacol. Sci.*, **2010**, 31, 102.

[30] Edwards, J.; Mukherjee, R.; Munro, A.F.; Wells, A.C.; Almushatat, A.; Bartlett, J.M.S. HER2 and COX2 expression in human prostate cancer. *Eur. J. Cancer*, **2004**, 40, 50.

[31] Wang, D.; DuBois, R.N. The role of COX-2 in intestinal inflammation and colorectal cancer. *Oncogene*, **2010**, 29, 781.

[32] Hwang, D.; Scollard, D.; Byrne, J.; Levine, E. Expression of cyclooxygenase-1 and cyclooxygenase-2 in human breast cancer. *J. Natl. Cancer Inst.*, **1998**, 90, 455.

[33] Jiménez, P.; García, A.; Santander, S.; Piazuelo, E. Prevention of cancer in the upper gastrointestinal tract with COX-inhibition, still an option? *Curr. Pharm. Des.*, **2007**, 13, 2261.

[34] Méric, J.; Rottey, S.; Olaussen, K.; Soria, J.; Khayat, D.; Rixe, O.; et al. Cyclooxygenase-2 as a target for anticancer drug development. *Crit. Rev. Oncol.*, **2006**, 59, 51.

[35] de Groot, D.; de Vries, E.; Groen, H.; de Jong, S. Non-steroidal anti-inflammatory drugs to potentiate chemotherapy effects: from lab to clinic. *Crit. Rev. Oncol. Hematol.,* **2007**, 61, 52.

[36] Hull, M. Cyclooxygenase-2: how good is it as a target for chemoprevention? *Eur. J. Cancer.*, **2005**, 41, 1854.

[37] Liao, Z.; Mason, K.; Milas, L. Cyclooxygenase-2 and its inhibition in cancer: is there a role? *Drugs*, **2007**, 67, 821.

[38] Bansal, P.; Sonnenberg, A. Risk factors in colorectal cancer in inflammatory bowl disease. *Am. J. Gastroenterol.*, **1996**, 91, 44.

[39] Giovannucci, E.; Rimm, E.; Stampfer, M.; Colditz, G.; Ascherio, A.; Willett, W. Asperin use and the risk for colorectal cancer and adenoma in male health professionals. *Ann. Intern. Med.*, **1994**, 121, 241.

[40] Thun, M.; Namboodiri, M.; Calle E.; Flanders, W.; Heath, C. Aspirin use and risk of fatal cancer. *Cancer Res.*, **1993**, 53, 1322.

[41] Greenhough, A.; Smartt, H.; Moore, A.; Roberts, H.; Williams, A.; Paraskeva, C.; et al. The COX-2/PGE(2) pathway: Key roles in the hallmarks of cancer and adaptation to the tumour microenvironment. *Carcinogenesis*, **2009**, 30, 377.

[42] Ghosh, N.; Chaki, R.; Mandal, V.; Mandal, S. COX-2 as a target for cancer chemotherapy. *Pharmacol. Rep.*, **2010**, 62, 233.

[43] Inoue, H.; Taba, Y.; Miwa, Y.; Yokota, C.; Miyagi, M.; Sasaguri, T. Transcriptional and posttranscriptional regulation of cyclooxygenase-2 expression by fluid shear stress in vascular endothelial cells. *Arterioscler. Thromb. Vasc. Biol.*, **2002**, 22, 1415.

CHAPTER 2

Literature Review

This chapter is published as **Tietz, O**; Marshall, A; Wuest, M; Wang, M; Wuest, F. "Radiotracers for Molecular Imaging of Cyclooxygenase-2 (COX-2) Enzyme." *Curr. Med. Chem.*, **2013**, 20, 4350.

2.1. Introduction

Cyclooxygenases (COXs) control the complex conversion of arachidonic acid into prostaglandins and thromboxanes, which trigger as locally active messenger molecules many physiological and patho-physiological responses. COXs exist in two distinct isoforms, a constitutive form (COX-1) and an inducible form (COX-2). More recently, a COX-1 splice variant termed as COX-3 has also been reported [1]. COX-1 and COX-2 share arachidonic acid as their natural substrate. They both catalyze the conversion of arachidonic acid into prostaglandin PGG_2 by means of a cyclooxygenase reaction; PGG_2 is further converted to PGH_2 through a peroxidase reaction. PGH_2 is thereafter metabolized by downstream enzymes to a variety of different prostaglandins, which exert a wide range of physiological functions mediated through binding to G-protein coupled receptors.

The X-ray crystal structures of both enzymes suggest that the tertiary conformations of these proteins are very similar. The amino acids that constitute the substrate binding pocket and catalytic site are nearly identical in both enzymes [2]. A notable and significant difference is found in amino acid residues at positions 434 and 523; these are isoleucine in the case of COX-1 and valine in COX-2. Both amino acids are constituents of the binding pocket and the differences in shape they lend to the active site formed the basis for the development of selective COX-2 [3].

Since the discovery of the COX-2 enzyme in the early 1990s, numerous COX-2 selective inhibitors (coxibs) have been synthesized. Figure2-1 displays a selection of prominent selective COX-2 inhibitors [4].

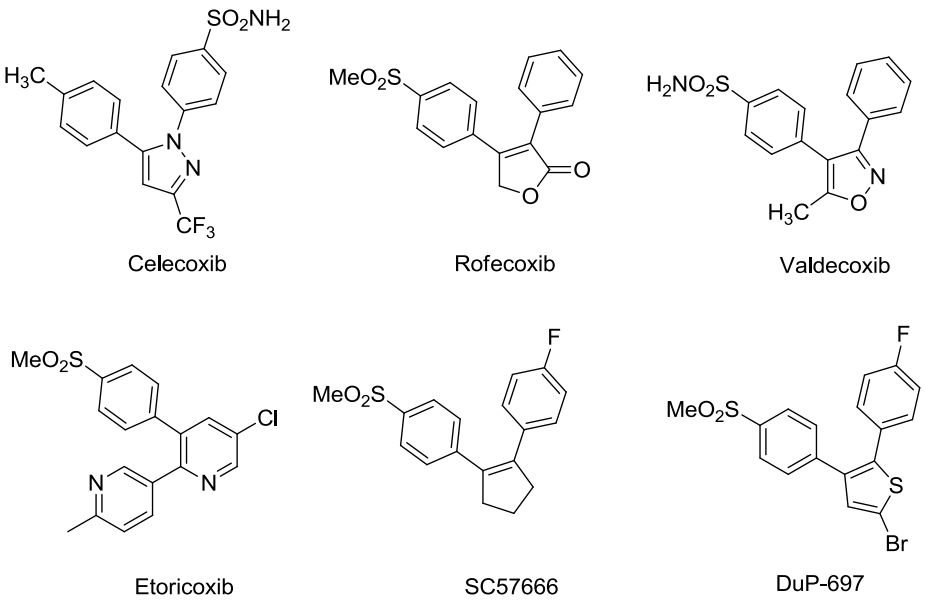

Figure 2-1: Chemical structures of selective COX-2 inhibitors.

A common structural feature of these selective COX-2 inhibitors is the presence of two vicinal aryl rings attached to a central five or six-membered heterocyclic or carbocyclic motif. Typical examples of selective COX-2 inhibitors like celecoxib, rofecoxib, valdecoxib, etoricoxib, SC57666, and DuP-697 demonstrate that a broad variety of five- or six-membered carbo- and heterocycles are acceptable for binding to the cyclooxygenase active site [5].

A number of selective COX-2 inhibitors were in broad clinical use for the treatment of pain oand inflammation after they obtained FDA approval in 2000. These compounds included celecoxib, valdecoxib, etoricoxib and rofecoxib. Rofecoxib, sold under the trade name VIOXX, was one of the world's biggest selling drugs, before it was taken off the market in 2005, along with most other selective COX-2 inhibitors, following concerns over the cardiac safety profile of coxib. The only mainstream coxib still in clinical use today is celecoxib. The reason for the increased incidence of heart attacks under coxib therapy remained unclear for a long time until a study published in 2012 highlighted the underlying biochemical mechanisms of the cardioprotective effects of COX-2 [6,

7]. Due to the undiminished potential of this compound class, current efforts in pharmaceutical research are aimed at designing selective COX-2 inhibitors with minimized adverse effects [8, 9]. The COX-1 enzyme is expressed in resting cells of most tissues. COX-1 functions as a housekeeping enzyme, and is responsible for maintaining homeostasis (gastric and renal integrity) and normal production of eicosanes [10]. COX-2 is constitutively expressed in brain and kidney while being virtually absent in most other tissues [11, 12]. However, COX-2 expression is significantly up regulated under various acute and chronic inflammatory conditions. COX-2 expression can be induced in fibroblast, epithelial, endothelial, macrophage, and smooth muscle cells in response to growth factors, cytokines, and pro-inflammatory stimuli and expression is usually transient [11].

COX-2 is furthermore involved in neurodegenerative diseases like Parkinson's and Alzheimer's disease [13], and elevated COX-2 expression was demonstrated in many human cancers such as colorectal, gastric, and breast cancer [14-17]. The COX-2 enzyme is assumed to play an important role in carcinogenesis by stimulating angiogenesis, tissue invasion, metastasis, and apoptosis inhibition. COX-2 expression is stimulated by a number of oncogenes, lipopolysaccharides, and tumor promoters [18].

Several aspects of the molecular mechanisms underlying COX-2 expression in cancer and inflammatory lesions have been elucidated, and key signalling pathways involving effects of COX-2 in inflammation and tumorigenesis have been dissected [19]. However, there are notable discrepancies between the potent anticancer effects of COX-2 inhibitors *in vitro* and their failure in a majority of clinical trials [20]. This includes COX-2 mediated effects on chemoprevention and radiosensitization using COX-2 inhibitors. The complex role of the COX-2 enzyme during the development and progression of various diseases requires more basic research on COX-2

pharmacology, including an accurate and dynamic assessment of COX-2 expression levels and/or activity in organs or tissues under various physiological conditions. However, to date an exact assessment of COX-2 expression can only be achieved by laborious *ex vivo* analyses. The instability of COX-2 mRNA and protein leads to further difficulties in terms of the interval between tissue sampling and time of analysis [21]. Frequently, detectable expression of COX-2 has ceased by the time a tissue sample has been prepared for analysis.

Therefore, the development of techniques for non-invasive monitoring of COX-2 functional expression would greatly facilitate efforts to understand COX-2 pharmacology *in vivo*. Along these lines, molecular imaging techniques like positron emission tomography (PET) and single photon emission computed tomography (SPECT) could provide unique opportunities to obtain data on COX-2 expression levels during disease development and progression and the potential role of COX-2 in various diseases. Moreover, the development and *in vivo* study of appropriately radiolabeled selective COX-2 inhibitors would provide important data on the pharmacological properties of COX-2, which might foster a better understanding of basic physiological actions and metabolic pathways of COX-2 enzyme.

The present review addresses the current status of radiotracer development for molecular imaging of COX-2 with PET and SPECT. An excellent review published by deVries in 2006 [22] provides a comprehensive overview of the advances in the field up to the date of publication. Based on the principle concepts for the design and synthesis of PET and SPECT radiotracers, the current review will discuss ^{11}C- and ^{18}F-labeled COX-2 inhibitors for PET imaging, and ^{99m}Tc-, ^{123}I- and ^{125}I-labeled COX-2 inhibitors for SPECT imaging.

2.1.1. General considerations for the design and synthesis of PET radiotracers

Positron emission tomography (PET) is a powerful non-invasive molecular imaging technique. Over the past 30 years, it has grown in sophistication, and is now able to provide detailed 3D spatial and temporal information of biochemical and pharmacokinetic processes *in vivo*. Given a suitable radiotracer, PET studies in animals and patients can provide insight into cellular function at a molecular level, providing researchers with the opportunity to investigate patho-physiological parameters in living organisms and in real time. In pharmacological research and drug development, the properties of novel substances can be assessed at sub-therapeutic dosage, to determine the suitability of a drug candidate to interact with its target.

The success of PET studies depends, to a large degree, on the availability of suitable radiotracers. Of vital importance to the design of a radiotracer are the positron-emitting isotope and the labeling position. Among the most widely used radionuclides in PET tracer development are ^{11}C ($t_{1/2}$=20.4 min) and ^{18}F ($t_{1/2}$=109.8 min) and to a lesser extent ^{13}N ($t_{1/2}$=9.9 min) and ^{15}O ($t_{1/2}$=2.0 min). The rather short half-lives of all four radionuclides generally require their in house production, using a small biomedical cyclotron. Carbon, oxygen and nitrogen are abundant constituents of most pharmaceutical molecules. The incorporation of their respective positron emitters ^{11}C, ^{13}N and ^{15}O therefore does not alter the chemical and pharmacological properties of the corresponding radiolabeled compounds. ^{15}O and ^{13}N, however, have half-lives too short for any meaningful chemistry to be accomplished before all radioactivity is decayed. Furthermore, *in vitro* and *in vivo* evaluation of radiotracers usually exceeds an hour in length, depending on the pharmacokinetics of the molecule and the biological target, making short-lived radionuclides less suitable for longer experiments.

Although a positron-emitting isotope of hydrogen is not available, this can be compensated for by the use of ^{18}F, which can act as a bioisosteric alternative to hydrogen in most molecules. ^{18}F is a highly useful radionuclide in PET studies, as its relatively long half-life allows for more complex chemistry and more sophisticated biological evaluation. As a rule of thumb, synthesis and purification, as well as formulation ready for animal or patient injection, should be accomplished within three half-lives. This allows a preparation time of up to 60 min for ^{11}C and 4-6 hours for ^{18}F labeled radiotracers. The chemistry employed to incorporate these radionuclides into target molecules must therefore be matched in complexity and reaction rate to the radionuclide used.

An important aspect in which radiosynthesis differs greatly from standard organic synthesis is in the amount of chemical substance used and the resulting extraordinary stoichiometric ratios. For any radiochemical reaction, the amount of radiolabeled compound in the reaction mixture rarely exceeds 10^{13} to 10^{15} molecules, which translates into a sub-nanomolar range. As a result, any reactant added to the mixture will always be present in large stoichiometric excess. This can have important consequences for the reactivity and feasibility of a variety of chemical reactions.

As well as presenting the investigator with chemical difficulties, the radiotracer concept might also pose biological challenges. It follows logically that a typical radiotracer injection would also contain no more than 10^{13} to 10^{15} molecules. This might be an advantage for pharmacological evaluation in drug design, where sub-therapeutic doses of novel drugs can be administered to obtain initial *in vivo* data without interfering with the biological system, well ahead of traditional clinical trials, where pharmaceutical doses have to be administered. But it does also mean that the specific activity, defined as the amount of radioactivity per unit of chemical compound, is of vital importance. The number of binding sites in a tissue of interest is usually low, and high specific

activity radiotracers are needed to produce a substantial signal. Poor specific activity would result in target saturation and leads to a reduced specific PET signal.

When reviewing radiolabeled compounds, the following should be taken into consideration: reaction efficiency (quoted as decay-corrected radiochemical yield), specific activity (quoted in GBq/μmol), and radiochemical purity (quoted as percentage of detected radioactivity corresponding to target compound).

2.2. PET Radiotracers for imaging COX-2 expression

2.2.1. ^{11}C-labeled COX-2 inhibitors

A number of selective COX-2 inhibitors have been labeled with the positron emitter ^{11}C. As a rather short-lived positron emitter ($t_{1/2}$ = 20.4 min), radiochemistry with ^{11}C is limited to simple, efficient and fast chemical reactions. Synthesis and purification are frequently carried out on remotely controlled synthesis units, to minimize synthesis time and radiation exposure.

Table 2-1 summarizes ^{11}C-labeled COX-2 inhibitors reported in the literature to date.

Table 2-1: ^{11}C-labeled COX-2 inhibitors

Compound	Radiolabeling method	Radiochemical Yield	Specific activity (GBq/µmol)	Reference
Celecoxib **1**	Stille reaction ([^{11}C]MeI)	8%	40	[23]
Celecoxib **1**	Suzuki reaction ([^{11}C]MeI) **Fig. 2-6**	63%	83	[24]
Celecoxib derivative **2**	*O*-methylation ([^{11}C]MeOTf)	47%	27-61	[25]
Celecoxib derivative **3**	*O*-methylation ([^{11}C]MeOTf)	75%	71-125	[25]
Celecoxib derivative	Methylation of CO_2H group ([^{11}C]MeOTf / [^{11}C]MeI)	50-60%	111-185	[26]
Rofecoxib **4**	methylation of masked thiol ([^{11}C]MeI)	20%	37	[27]
Etoricoxib	methylation of masked thiol ([^{11}C]MeI)			[27]
TMI **5**	methylation of masked thiol ([^{11}C]MeI)			[27]
Rofecoxib **4**	methylation of sulfinate ([^{11}C]MeI) **Fig. 2-9**	57%	14	[28]
Compound **6**	*O*-methylation ([^{11}C]MeI) **Fig. 2-11**	19%	20-25	[29]
Compound **7**	*O*-methylation ([^{11}C]MeOTf)	75%	36-264	[30]
Compound **8**	*O*-methylation ([^{11}C]MeOTf)	70%	36-264	[30]
Compound **9**	*O*-methylation ([^{11}C]MeOTf)	21%	36-264	[30]

Celecoxib and celecoxib derivatives

Celecoxib and related derivatives are promising lead structures for the design and synthesis of ^{11}C-labeled COX-2 radiotracers. Celecoxib inhibits COX-2 with a K_i value of 40 nM, while inhibiting COX-1 with a K_i value of 17000 nM, resulting in a favorable selectivity ratio of 425 [31]. Celecoxib is one of the most popular and frequently used selective COX-2 inhibitors used as an analgetic drug for the treatment of pain and inflammation. It is the only selective COX-2 inhibitor that is still in widespread clinical use. One of the main advantages to developing a celecoxib based radiotracer would be its easy transition into a clinical setting and the ease of translating information gathered through PET studies into clinically relevant data.

Prabhakaran and coworkers described the first radiosynthesis of ^{11}C-labeled celecoxib **1** in 2005 (Fig.2-2) [23]. Radiolabeling was accomplished via Stille reaction using [^{11}C]MeI as the radiolabeling agent. The final product was obtained in radiochemical yields of 8% after a total synthesis time of 40 min. Although the authors suggest that radiotracer **1** might be useful for *in vivo* assessment of COX-2 expression, no biological evaluation has been reported to date.

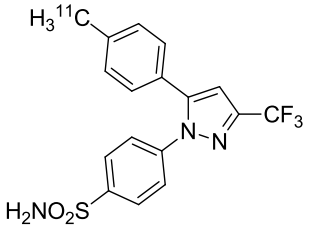

Figure 2-2: Compound **1**

In 2011, Takashima-Hirano and co-workers proposed an alternative synthesis route for ^{11}C-labeled celecoxib, based on a Suzuki cross-coupling reaction between a pinacol borate precursor and using

[^{11}C]MeI as the radiolabeling agent (Fig.2-3) [24]. Radiotracer **1** was obtained in 63% radiochemical yield. As this yield is based on [^{11}C]MeI rather than end of bombardment (EOB), it is hard to evaluate the efficacy of this method compared to the one described by Prabhakaran *et al*.

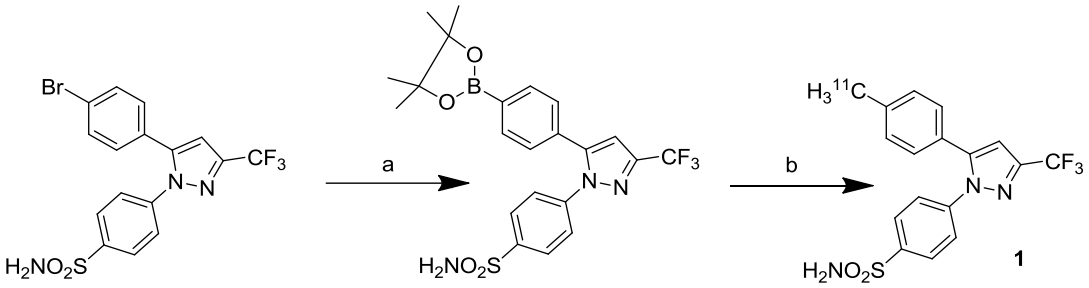

Figure 2-3: Suzuki reaction of pinacol borate precursor with [^{11}C]MeI [24]. Reagents: a) bis(pinacolato)diboron, $PdCl_2(dppf)$,·CH_2Cl_2, AcOK, DMSO, 80 °C, 16 h, 78%; b) [^{11}C]CH_3I, $Pd_2(dba)_3$, P(*o*-tolyl)$_3$, DMF, 65 °C, 4 min.

In addition to the novel chemistry presented by Takashima-Hirano *et al*, the group went on to evaluate compound **1** *in vivo*. The aim of the study, however, was the evaluation of drug transporter mechanisms in biliary excretion rather than assessment of COX-2 expression. Takashima-Hirano *et al.* found that radiotracer **1** mainly accumulates in the liver and intestines of healthy animals. Radioactivity level remained in the blood for a long time, and the radiotracer was rapidly metabolized to hydroxymethyl and carboxylic acid-containing compounds. These findings suggest that ^{11}C-labeled celecoxib **1** exhibits substantial non-specific binding and poor *in vivo* stability. Although **1** has not been evaluated in a COX-2 model, it can be concluded that [^{11}C]celecoxib, although it represents the radiolabeled equivalent of the pharmaceutical drug, is unlikely to be suitable for imaging of COX-2 expression *in vivo*.

As direct [^{11}C]methylation of aryl rings based on Stille and Suzuki cross-coupling reactions is challenging, Fujisaki and co-workers chose to radiolabel celecoxib via *O*-methylation. The result is a celecoxib derivative that includes a methoxy group in place of the methyl group on the aryl ring [25]. Methoxy containing compounds are easily radiolabeled using the corresponding phenolic precursors and [^{11}C]methyliodide or [^{11}C]methyltriflate as radiolabeling agents.

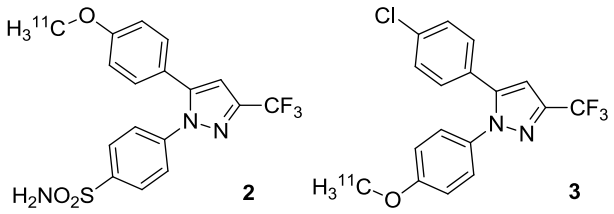

Figure 2-4: Compounds **2** and **3** [25]

Fujisaki *et al*. radiolabeled a COX-2 selective (**2**) and a COX-1 selective (**3**) derivative of celecoxib (Fig.2-4). The COX-2 selective compound **2** showed good inhibitor potential for COX-2 (K_i=8nM) over COX-1 (K_i=2.6 μM) [32], while COX-1 selective compound **3** showed good inhibitory potential for COX-1 (K_i=9 nM) over COX-2 (K_i=6.3 μM) [33]. It should be noted that the methoxy derivative of celecoxib (**2**) is in fact more potent than celecoxib itself, although these results should be considered with a note of caution. Different types of COX-2 and COX-1 inhibitory assays will give slightly different results for the same compound. It is therefore preferable to compare all results to a gold standard (such as celecoxib), measured in the same assay.

Fujisaki *et al*. obtained radiotracers **2** and **3** in radiochemical yields of 47% and 74%, using [^{11}C]methyltriflate, phenolic precursor and equimolar amounts of NaOH in acetone at room temperature. Synthesis of both tracers was accomplished within 20min. A great advantage of this synthesis is that the products do not require extensive purification, resulting in high yields and

high specific activity, as well as short synthesis times. The observed superiority of methyltriflate over methyliodide as radiolabeling agent has been confirmed by a number of other studies [34, 35].

In vivo evaluation of radiotracers **2** and **3** was carried out in AH109A tumor bearing rats. AH109A has been shown to express COX-2 using Western Blot analysis. The regional accumulation of both tracers is broadly consistent with known expression of COX-1 and COX-2 in various tissue types, such as the brain, lung, heart and kidneys [11, 12]. Blood retention of radiotracer **2** was found to be extremely high, while blood retention of **3** was comparatively low. Uptake of either tracer in COX-2 and COX-1 expressing tissues is relatively low. Compound **2** showed a slightly higher accumulation in AH109A tumor than in muscle tissue at 60min post-injection. Autoradiography studies revealed regional differences of accumulation in cross sections of tumor samples.

To further investigate whether uptake of **2** in the tumor tissue is COX-2 mediated, blocking studies were performed using indomethacin, a non-specific COX inhibitor, NS-398, a specific COX-2 inhibitor, and non-radiolabeled compounds **2** and **3**. Uptake of radiotracer **3** was significantly reduced in the small intestine and spleen. Insignificant blocking effects were observed in experiments with radiotracer **2**.

Although blocking with non-radiolabeled **2** significantly reduced uptake in blood and spleen, tumor uptake was not reduced in the presence of any of the four blocking agents. The authors suggest that injection of blocking compound at 30 min post-radiotracer injection might prevent pharmacological doses of blocking substance to reach its target and reduce uptake before the end of the experiment at 60 min post-radiotracer injection. It has been well documented that selective COX-2 inhibitors display poor pharmacokinetic properties [36, 37], a likely result is that pharmacological doses need to be administered to allow time for target saturation before

radiotracers can be administered. Despite the problems with the blocking study methodology, Fujisaki *et al*. conclude that radiotracer **2** is unlikely to be suitable for the *in vivo* evaluation of COX-2 expression due to its lack of specific binding to COX-2. Similar to celecoxib radiotracer **1**, methoxy derivative **2** displays blood retention characteristics that make unsuitable for *in vivo* application.

Another notable study on radiolabeled celecoxib derivatives was published by Gao *et al*. in 2009 [26]. Contrary to the radiotracers presented thus far, Gao *et al*. chose to methylate the sulfonamide group instead of the aryl ring. This was accomplished by linking the amide to a carboxylic acid group via an ether bridge. The carboxylic acid was subsequently radiolabeled using [^{11}C]MeOTf. The research group described the synthesis of four different radiolabeled analogues based on various carboxylic acid substituents. Radiotracers were obtained at yields of 50-60% in a synthesis time of 15-20 min based on [^{11}C]MeOTf. These compounds have not undergone biological evaluation to date, but might show promising properties [38]**,** warranting further investigation. A notable drawback of the sulfonamide labeling approach is that it is believed that an intact sulfonamide or methyl sulfone group is essential for COX-2 binding [18].

Rofecoxib

Rofecoxib is a COX-2 selective inhibitor which gained FDA approval in 1999 as an analgesic drug for the treatment of various pain related conditions, but was withdrawn from the market in 2004 following concerns over the drugs cardiac safety profile. Rofecoxib is a highly potent COX-2 inhibitor and was one of the most widely prescribed coxibs, known under its trade name VIOXX. The fact that Rofecoxib has lost approval as a pharmaceutical drug might not prohibit its use as a

potential radiotracer for diagnostic purposes. As discussed in the introduction, the tracer concept applies, which allows the use PET radiotracers at sub-therapeutic concentrations *in vivo*.

Rofecoxib is considered to be the most potent of the clinical or previously clinically used coxibs with a COX-2 inhibitory potential ranging from 18 to 44.6 nM in various assays and a K_i against COX-1 in excess of 50 μM [39].

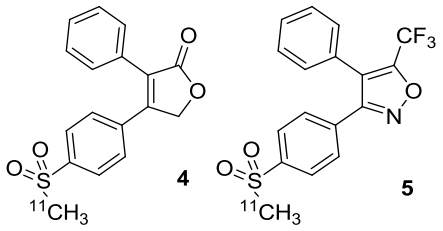

Figure 2-5: Compounds **4** and **5** [27]

Majo *et al*. first synthesized ^{11}C-labeled rofecoxib via [^{11}C]methylation of the methylsulfone groups [27]. Radiolabeling precursors contained an aryl thiol butyrate ester, which was methylated using [^{11}C]MeI in the presence of pyrrolidine and subsequently oxidized using oxone to give the radiolabeled methylsulfone. Radiosynthesis was accomplished with a radiochemical yield of 20%. Majo *et al*. further used this method to radiolabel selective COX-2 inhibitors Etoricoxib and TMI (**5**) (Fig.2-5). TMI, in particular, is considered to be a highly potent COX-2 inhibitor with a reported K_i of <1 nM and little affinity for COX-1 [40].

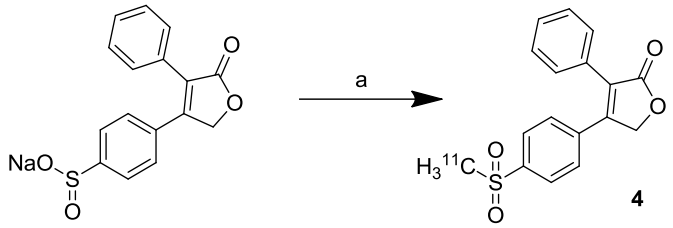

Figure 2-6: Alkylation of sulfinate precursor using [^{11}C]MeI [28]; a) [^{11}C]CH_3I, DMF, 90°C, 4 min.

In a separate study, deVries *et al.* presented an improved synthetic strategy and an extensive biological evaluation of [^{11}C]rofecoxib (**4**) (Fig. 2-5) [28]. To eliminate the second step in the radiosynthesis as described by Majo and coworkers, deVries *et al*. used a sulfinate precursor to accomplish radiolabeling using a one step methylation (Fig. 2-6). Using [^{11}C]MeI as a radiolabeling agent and subsequent HPLC purification, synthesis was accomplished within 40 min, with a yield of 57% based on [^{11}C]MeI.

deVries *et al.* used a number of biological models to evaluate [^{11}C]rofecoxib *in vivo*, with a particular emphasis on brain imaging to assess the tracer's diagnostic potential in neurodegenerative disease. It is well established that rofecoxib crosses the blood brain barrier (BBB) much better than other coxibs, resulting in cerebrospinal fluid concentrations that are fivefold higher than those of celecoxib and valdecoxib [41]. To assess tracer uptake in healthy brain tissue, healthy rats were used to perform brain distribution studies. The tracer distribution in the brain was relatively homogenous with an average Standardized Uptake Value (SUV) of 0.26 with slightly increased uptake in the frontopolar complex and hippocampus regions of the brain. To demonstrate that uptake is COX-2 mediated, rats were pretreated with 1.5 mg/kg NS398 (selective COX-2 inhibitor). Pre-treatment with pharmacological doses of NS398 significantly reduced uptake in the frontopolar complex region of the brain (-41%, p=0.01), while uptake

reduction in the hippocampus almost reached significance (-33%, p=0.06) [28]. It has been documented that both of those brain regions express significant basal levels of COX-2 [42, 43], suggesting that uptake of [^{11}C]rofecoxib is indeed mediated by the COX-2 enzyme. Interestingly, intravenous injection of NS398 5 min before tracer injection yielded the same result as injection 60min prior to tracer administration. The authors suggest that this is due to NS398 binding to COX-2 being virtually complete after 5 min. This observation is contrary with the results obtained by Fujisaki *et al.*[25], discussed previously, where the blocking doses did not reach target sites within 30 min. Given the complicated binding kinetics of COX-2 inhibitors it seems unlikely that target sites can be fully saturated 5 min post injection. An alternative explanation would be that rather than saturating the binding sites before radiotracer administration, NS398 and [^{11}C]rofecoxib compete for the available COX-2 binding sites over the 60 min time course of the experiment.

To assess whether [^{11}C]rofecoxib is capable of visualizing inflammation in brain tissue, deVries *et al*. used a herpes simplex virus (HSV) encephalitis model [44]. Six to seven days post viral infection, the virus causes severe inflammation of the brain tissue, along with increased expression of COX-2 [45]. HSV-inflamed tissue showed a moderate increase in [^{11}C]rofecoxib uptake, but increases were not statistically significant. Pretreatment of animals with 2.5 mg/kg indomethacin, 5 min prior to tracer administration via intravenous injection did not significantly lower [^{11}C]rofecoxib uptake in any brain region. It should be noted that indomethacin is not a selective COX-2 inhibitor; it also inhibits the COX-1 isoform of the enzyme.

In a follow up set of experiments performed by deVries *et al*, the research group evaluated [^{11}C]rofecoxib in a sterile inflammation model. The thigh muscles of rats were injected with turpentine, resulting in visible swelling due to inflammation and increased COX-2 expression [46,

47]. [^{11}C]rofecoxib uptake in inflamed muscle tissue was similar to uptake in control muscle. Pre-treatment with NS398 did not significantly alter [^{11}C]rofecoxib uptake, while treatment with indomethacin resulted in reduction of radiotracer uptake in both the inflamed muscle and in the control muscle as well as the blood pool. A peroxidase assay [48] on the inflamed muscle tissue found that an increase in COX-2 expression, when compared to untreated muscle tissue, was not detectable. Failure to induce COX-2 expression might be the reason for the similar uptake level of the radiotracer in the inflamed and the control muscle tissue.

While the results obtained in healthy rat brains suggested COX-2 specific binding of [^{11}C]rofecoxib (**4**), the inflammation models used in the study could not confirm those results. It seems clear that this failure was due to the lack of COX-2 expression in the sterile inflammation model. Whether that would also the case for the HSV inflammation model remains unclear.

Other COX-2 inhibitors

The relative failure of clinically used COX-2 inhibitors to provide suitable templates for ^{11}C-labeled radiotracers generated substantial interest into novel structures and scaffolds. Designing a radiotracer with a novel scaffold allows the investigator to fine-tune the structure for improved potency, pharmacokinetic properties and specificity.

In 2008, Wuest *et al*. reported the synthesis of a ^{11}C-labeled COX-2 inhibitor based on a 1,2-diarylcyclopentene central scaffold (Fig. 2-7) [29]. 1,2-diarylcyclopentenes were discovered as a class of potent and selective COX-2 inhibitors in the mid-1990's [49, 50]. A 4-methoxyphenyl derivative **6** of this compound class showed promising characteristics and a good inhibitory profile. K_i against COX-2 was determined to be 5 nM, while the K_i against COX-1 was 9.9 μM. The methoxy group on molecule **6** is easily radiolabeled using *O*-methylation (Fig. 2-8). The

radiotracer was labeled using the phenolic analogue of **6** and [^{11}C]MeI as a radiolabeling agent. Following purification using HPLC, synthesis was accomplished within 35 min, with a yield of 19%.

Radiotracer **6** was first evaluated *in vitro*. This is one of the few studies that included *in vitro* evaluation as part of pre-clinical testing. This type of evaluation, although time consuming, can yield important information with regard to suitability of different biological models. The researchers used COX-2 negative cell lines THP-1, RAW264.7 and NIH3T3, as well as COX-2 positive cell lines 3T3-L1, FaDu and HT-29. COX-2 negative cell lines exhibited baseline uptake that was not altered by pre-incubation with non-radiolabeled **6**.

COX-2 positive cell lines showed substantial uptake, which was reduced significantly upon pre-incubation with non-radiolabeled **6**. COX-2 expression was stimulated in COX-2 negative cell lines using tumor promoter TPA, resulting in increased uptake of **6** pre-incubation with non-radiolabeled **6** reduced uptake to baseline level. The *in vitro* experiments suggest specific binding of **6** to COX-2.

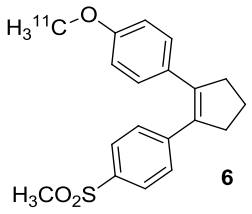

Figure 2-7: Compound **6** [29]

Biodistribution studies in healthy rats revealed atypical behaviour of **6**. Distribution patterns 5 min and 60 min post-injection suggested that radiotracer uptake decreased in all tissue types over time, with the exception of white adipose tissue. If binding was COX-2 mediated, tissue types that are

known to constitutively express COX-2, such as the kidneys, brain, lungs and heart [11, 12] would have been expected to retain **6**. Upon injection of **6** in HT-29 bearing mice, it was found that the radiotracer behaves the same in the tumor as it does in healthy tissue. Uptake peaks 10 min post-injection, followed by a slow decrease in detectable radioactivity. 60 min post-injection, **6** reaches a maximum SUV in the tumor of approximately 0.6 and a tumor-to-muscle ratio of 2.0. However, intra-peritoneal injection of 5 mg/kg non-radiolabeled **6** 10min prior to radiotracer administration did not reduce **6** uptake in the tumor. This is possibly due to the low baseline uptake of the radiotracer in the tumor, which in turn might be due to the low COX-2 expression of HT-29 xenografts *in vivo*.

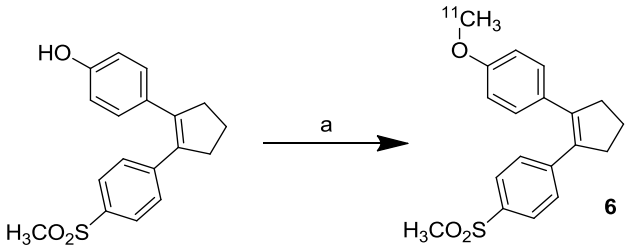

Figure 2-8: *O*-methylation using [^{11}C]MeI [29]; a) [^{11}C]CH_3I, NaOH, DMF, 60 °C, 3 min;

Metabolite analysis suggested that compound **6** was rapidly metabolized. Mouse plasma revealed only 17% of intact radiotracer 10 min post injection. This was reduced to 2% after 60 min. The instability of **6** *in vivo* is likely to be the reason why uptake in all tissues was reduced 5 min post-injection. Although the *in vitro* data on **6** was convincing, its metabolic instability makes it unsuitable for use *in vivo*. It should be noted that metabolic instability in one species does not necessarily mean that a radiotracer is unstable in other species as well [51].

A study published by Tanaka and co-workers presents a number of novel ^{11}C labeled radiotracers designed around less commonly studied heterocycles (Fig. 2-9) [30]. Tanaka *et al.* used two imidazoles and an indole species to be radiolabeled via *O*-methylation. Imidazoles **7** and **8** were

found to exhibit excellent potency and selectivity for COX-2 (**7** K_i(COX-2) = 4 nM, K_i(COX-1) >10 μM; **8** K_i(COX-2) = 5 nM, K_i(COX-1) = 3.3 μM) [52].

Indole species **9** was found to be highly potent as well, displaying similar inhibitory potency (**9** K_i (COX-2) = 6 nM, K_i(COX-1) >10 μM) [53].

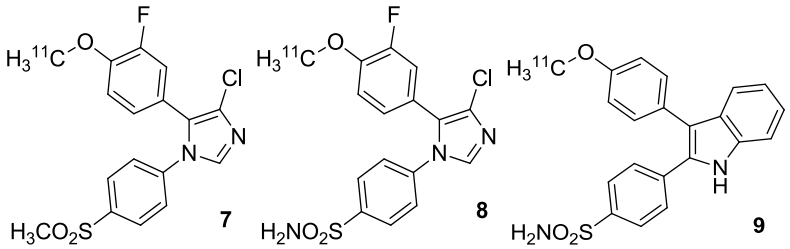

Figure 2-9: Compounds **7 - 9** [30]

Radiolabeling of all three compounds was achieved by *O*-methylation of the phenolic precursors using [^{11}C]CH_3OTf in acetone with equimolar amounts of NaOH. Radiosynthesis was accomplished with radiochemical yields of 75% (**7**), 70% (**8**) and 21% (**9**), in approximately 20 min.

The lipophilicity of compounds **7**, **8** and **9**, as determined by octanol - PBS (pH 7.4) partition, was found to be 2.2, 1.9 and 2.3, respectively. Most selective COX-2 inhibitors are quite lipophilic, with log*P* values of above 3.0, resulting in high non-specific binding as well as high intestine and liver uptake.

Biodistribution of **7** in AH109A-bearing rats showed that most of the radiotracer was taken up into the liver. Uptake in the tumor increased until 15 min post-injection and remained constant thereafter; uptake in muscle was slightly lower. Radiotracer **7** was cleared rapidly from the blood pool. In contrast, sulfonamide-bearing radiotracer **8** was retained in the blood pool, showing uptake

higher than that found in the liver. Uptake in AH109A tumors was found to be slightly higher than in muscle tissue, similar to the pattern observed with radiotracer **7**.

Radiotracer **9** showed faster clearance from the blood pool than **8**, but was retained in the blood significantly longer than tracer **7**. Uptake of **9** in AH109A tumors was slightly higher than uptake in muscle tissue. The retention of sulfonamide containing structures in the blood pool strengthens the hypothesis that sulfonamide based COX-2 inhibitors are likely to be potent carbonic anhydrase inhibitors, although blocking studies using carbonic anhydrase inhibitors were not performed to confirm the hypothesis. Expression of carbonic anhydrases in blood cells leads to the significant binding of these radiotracers to red blood cells and consequently to a long residency time of radioactivity in the blood stream [54].

To show that the uptake of tracers **7**, **8** and **9** is COX-2 specific, blocking experiments were performed with respective non-radiolabeled compounds **7**, **8** and **9**, NS-398 and celecoxib. No significant blocking effects in either the tumor or tissues known to express COX-2 [11, 12] could be observed.

None of the pre-clinical data presented on compounds **7**, **8** and **9** indicates that the uptake in various tissues or the tumor is COX-2 mediated. While high blood retention makes radiotracers **8** and **9** unsuitable as *in vivo* imaging agents, radiotracer **7** shows a pharmacokinetic profile warranting further investigation. None of the ^{11}C-labeled COX-2 radiotracers reviewed here were able to selectively visualize COX-2 *in vivo.*

2.2.2. ^{18}F-labeled COX-2 inhibitors

COX-2 inhibitors, such as celecoxib and rofecoxib were labeled with ^{11}C and also with the short-lived positron emitter fluorine-18 (^{18}F). ^{18}F is a short-lived radionuclide similar to ^{11}C but with a significantly longer half-life of 109.8 min. Working with ^{18}F is substantially less restrictive, allowing more complex reactions to be carried out. The longer half-life has another benefit, specifically for the development of COX-2 radiotracers. The clearing rates of COX-2 radiotracers out of non-COX-2 expressing tissues can be relatively slow. To achieve higher contrast, it is advantageous to be able to scan for a longer period of time post-injection. While experiments with ^{11}C are limited to 60 min time windows, ^{18}F experiments might last 4 to 6 hours.

A few selective COX-2 inhibitors include a trifluoromethyl moiety attached to the central ring as a structural element, serving as a convenient target for ^{18}F-labeling. However, most COX-2 inhibitors do not contain any fluorine. As a result, most ^{18}F-labeled COX-2 inhibitors are derivatives of their parent compounds. Because hydrogen and fluorine are bioisosteric, most ^{18}F labels are introduced in place of a hydrogen atom.

Table 2-2 summarizes ^{18}F-labeled COX-2 inhibitors reported in the literature to date.

Table 2-2: ^{18}F-labeled COX-2 inhibitors

Compound	Radiolabeling method	Yield	Specific activity (GBq/μmol)	Ref
Celecoxib **10**	Br to ^{18}F exchange reaction **Fig. 2-14**	22%	4	[31]
SC63217 **11**	microwave assisted direct radiofluorination	10-20%	37-111	[55]
SC58125 **12**	microwave assisted direct radiofluorination **Fig. 2-17**	10-20%	37-111	[55]
Celecoxib derivative **13**	microwave assisted direct radiofluorination	25%		[56]
Rofecoxib derivative **14**	Stille reaction ([^{18}F]fluoroiodobenzene) **Fig. 2-18**	93%		[57]
Compound **15**	Stille reaction ([^{18}F]fluoroiodobenzene)	68%		[57]
Valdecoxib derivative **16**	direct radiofluorination	40%	74	[58]
Desbromo DuP-697 **17**	direct radiofluorination	3%	21-47	[48]
Compound **18**	direct radriofluorination	15%	18	[59]
Compound **19**	McMuarry coupling **Fig. 2-23**	8-10%	74-91	[60]

Celecoxib and celecoxib derivatives

Celecoxib has a trifluoromethyl group attached to its central pyrazole ring and is therefore a fluorine containing compound. This eliminates the need to introduce fluorine artificially and allows celecoxib to be radiolabeled without altering its structure.

Prabhakaran *et al.* synthesized ^{18}F-labeled celecoxib **10** (Fig. 2-10), using a bromine to [^{18}F]F$^-$ exchange reaction (Fig. 2-11) [31]. The radiosynthesis uses a bromodifluoromethyl precursor with the primary amine on the sulfonamide group protected as a DMT (dimethoxytrityl) derivative. ^{18}F radiolabeling was achieved using [^{18}F]TBAF [61] in DMSO, followed by deprotection of the amine using 1:1 TFA/DCM. Radiosynthesis was accomplished with a radiochemical yield of 10%.

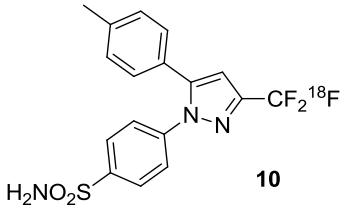

Figure 2-10: Compound **10** [31]

Evaluation of **10** in rats revealed that the radiotracer is rapidly defluorinated *in vivo*. PET scans at 0-20 min and 60-120 min revealed significant skeletal uptake, compared to uptake levels in the brain and heart, which are known to express COX-2 [62]. PET brain scans in baboons revealed that [^{18}F]celecoxib is able to cross the blood brain barrier (BBB), while time-activity-curves of various brain regions confirmed decreased uptake in the skull, compared to the brain. This suggests that the rate of radiodefluorination is much lower in baboons. However, baboon plasma analysis revealed that the fraction of intact parent compound was reduced to 17% at 60 min post-injection. The clearance rates of the radiotracer in various brain regions were consistent with the known COX-2 expression in those regions, suggesting that the uptake observed was indeed COX-2 mediated [63, 64].

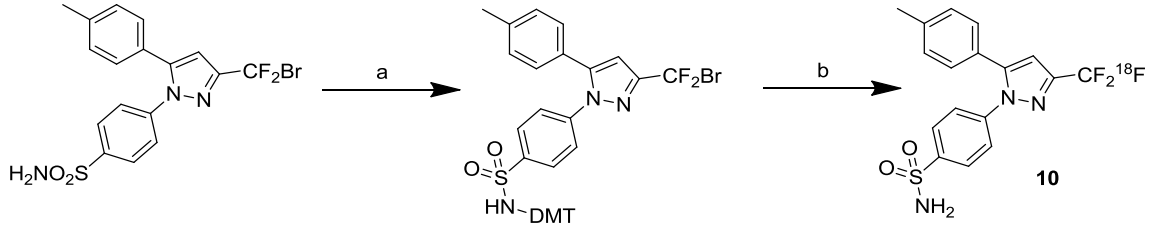

Figure 2-11: Bromine to ^{18}F exchange reaction [31]; a) DMT/Cl, TEA, CH_2Cl_2, 82%; b) i) [^{18}F]TBAF, DMSO, 135 °C, 20 min; b) ii) TFA/CH_2Cl_2 (1:1), 60 °C, 5 min;

A substantial limitation of ^{18}F-labeling of celecoxib at the trifluoromethyl position is rapid defluorination *in vivo*. It is possible that these limitations can be overcome in humans, as human metabolic rates are slower than in rats and baboons [51]. However, further evaluation of this radiotracer can only be conducted following metabolic studies *in vitro*, using human serum, *or in vivo*, using clinical protocol.

A number of researchers have attempted to introduce fluorine in alternative positions, using celecoxib as a scaffold for the development of novel COX-2 inhibitors.

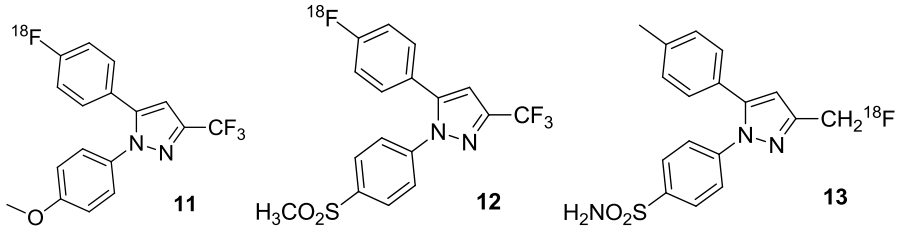

Figure 2-12: Compounds **11**, **12** [55] and **13** [56]

McCarthy *et al*. published a study comparing a COX-1 selective and a COX-2 selective radiotracer (Fig. 2-12) [55]. The compounds studied were originally developed as templates for celecoxib and share the same central scaffold. Notably, both compounds contain 4-fluoro aryl rings. SC63217 **11** is a selective COX-1 inhibitor with a K_i of <10 nM for COX-1 and >100 μM for COX-2 [65]. SC58125 **12** is a COX-2 selective inhibitor with a K_i of >100 μM for COX-1 and <86 nM for COX-2 [65].

Radiolabeling was accomplished using trimethylamino substituted trifluoroacetate salts as precursors and nucleophilic [^{18}F]KF Kryptofix in DMSO (Fig. 2-13). Fluoride incorporation was achieved using a microwave cavity, resulting in radiochemical yields of 10-20% for both tracers.

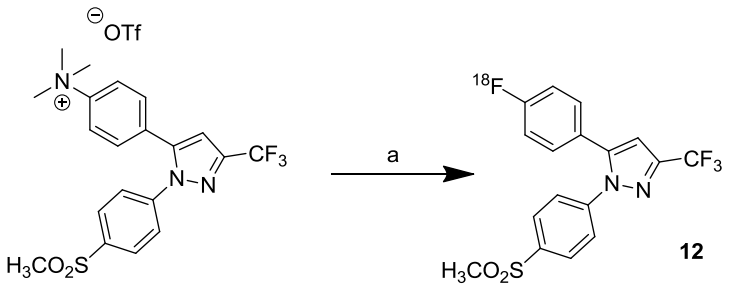

Figure 2-13: Microwave-assisted direct radiofluorination using [^{18}F]KF-Kryptofix [55]; a) [^{18}F]KF, Kryptofix, DMSO, microwave;

Radiotracers **11** and **12** were evaluated *in vitro* using murine macrophage cell line J774. COX-2 expression was stimulated by 18 h pre-incubation with a mixture of LPS and γ-interferon (γ-IFN) [66, 67]. Two hours post administration, COX-2 selective radiotracer **12** showed a 3-fold uptake increase in LPS-stimulated cells over non-stimulated cells. Uptake was reduced to baseline levels by co-incubation with 5 μM non-radiolabeled **12**.

Experiments with **12**, using the same experimental set-up, revealed that uptake was substantial in non-stimulated cells, while stimulation of cells did not significantly alter radiotracer uptake. Blocking with non-labeled **11** had a marginal effect on the uptake of **11**. This suggests that uptake of **11** is not COX-1 mediated but attributable to non-specific binding.

COX-1 specific tracer **11** accumulated in the small intestine, while COX-2 specific tracer **12** accumulated in the kidneys; both observations are consistent with known expression levels of the enzyme in the respective tissues [11, 12]. Co-injection with non-radiolabeled **11** or **12** did not decrease uptake in both tissues. COX-2 specific radiotracer **12** was found to cross the BBB and retained in the brain for up to 3 hours. Given this ability, the radiotracer was further evaluated in baboon brains. After tracer clearance from the blood (1-2 hours post-injection) no structural distribution consistent with known COX-2 expression was observed. While *in vitro* studies

suggested that COX-2 specific tracer **11** might be a suitable molecular marker for COX-2 expression *in vivo*, the experiments conducted by McCarthy *et al*. did not show that *in vivo* uptake of the radiotracer is COX-2 mediated.

One of the most promising studies to date has been presented recently by Uddin and co-workers [56]. The researchers report the synthesis of various fluorinated celecoxib and indomethacin derivatives, one of which (compound **13**, Fig. 2-12) was chosen for ^{18}F-labeling and further evaluation in different animal models.

Due to the rapid defluorination of ^{18}F-labeled celecoxib labeled at the trifluoromethyl group, Uddin *et al*. chose to replace the trifluoromethyl group with a fluoromethyl. Inhibition studies, using free COX-2 enzyme (K_i=160 nM) and a whole cell assays (K_i=80 nM), revealed that the inhibitory potential of the compound is comparable to celecoxib (K_i=40 nM in free enzyme assay [31]).^{18}F-radiofluorination was accomplished via a microwave-assisted nucleophilic [^{18}F]fluorodetosylation using a tosylate precursor. [^{18}F]KF-Kryptofix was added to the precursor in DMSO and heated at 165°C. The product was obtained in a radiochemical yield of 25%.

To evaluate the ability of compound **13** to visualize inflammation *in vivo*, Uddin *et al*. used carrageenan injections to the hind paws of rats to induce COX-2 expression. Uptake of tracer was evaluated 2 hours post injection, using a PET. It was found that carrageenan treated hind paws showed a 1.5 fold increase in uptake over non-treated hind paws. Administration of 10 mg/kg celecoxib, via intravenous injection reduced uptake in the inflamed paw to levels similar to those observed in the control paw (10% reduction). Furthermore, Uddin *et al*. used wild type and COX-2 knock-out mice in a similar experimental set up. Inflammation was induced using carrageenan injections to the hind paw. COX-2 knock-out mice showed no increased uptake in carrageenan treated versus control paws (ratio = 1.08), while wild type mice exhibited an increase in radiotracer

uptake in inflamed versus control paws (ratio = 1.48). However, uptake of **13** in the inflamed paws was relatively low, exhibiting standardized uptake values (SUV's) of only 0.2.

These experiments suggest that uptake of **13** in the carrageenan inflammation model was COX-2 mediated. These findings are at odds with a report by deVries, which found that the carrageenan inflammation model was not suitable for COX-2 radiotracer evaluation [48], as it fails to induce COX-2 expression.

Radiotracer **13** was further evaluated in a tumor model, using nude mice bearing a COX-2 positive 1483 HNSCC tumor on one flank and a COX-2 negative HCT116 tumor on the other flank. PET and biodistribution studies confirmed a threefold higher uptake of **13** in the COX-2 positive 1483 HNSCC tumor over COX-2 negative HCT116 tumor. Using nude mice carrying 1483 HNSCC xenografts only, the researches showed that tumor uptake was blocked by administration of 20 mg/kg celecoxib 2 min after tracer injection.

The tumor to muscle uptake ratio was found to be 1.01 if the mouse was pretreated with celecoxib, while administration of radiotracer lead to an uptake ratio of 2.94. These results support the evidence that the uptake of **13** in the tumor model is COX-2 mediated.

The results reported by Uddin *et al*. are promising. To date, this is the only study that has had some success in showing that radiotracer uptake might be COX-2 mediated in a COX-2 specific tumor model. To gain a better understanding of compound **13** mode of action, further evaluation of the radiotracer should be carried out. However, the present data does not allow for the relative uptake to be compared, as tracer uptake figures are not quoted as SUV's. At present there is no biodistribution or time course of uptake data available on **13**. For a more in depth discussion of the results presented by Uddin *et al*. please refer to the discussion in the summary section.

Rofecoxib analogues

As described in the paragraph on ^{11}Carbon labeled COX-2 inhibitors (pg. 30), rofecoxib is a highly potent drug and was one of the most widely prescribed coxibs. Consequently, interest in developing a suitable rofecoxib based PET radiotracer is substantial. However, the structure of rofecoxib does not contain fluorine, resulting in the need for development of fluorine containing rofecoxib analogues.

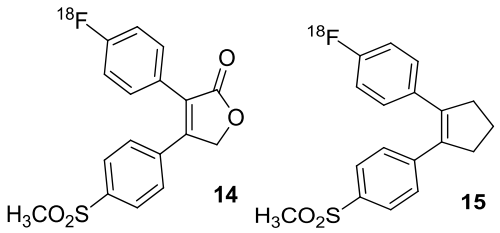

Figure 2-14: Compounds **14** and **15** [57]

Wuest *et al*. have synthesized two structural analogues of rofecoxib [57] (Fig. 2-14). Compound **14** is designed around the same furanone central scaffold as rofecoxib, while compound **15** is built around a cyclopentene central ring.

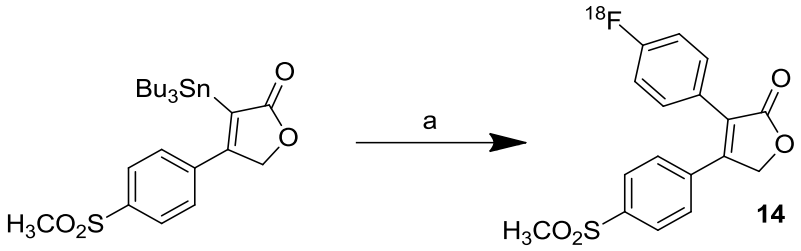

Figure 2-15: Stille reaction using [^{18}F]fluoroiodobenzene [57]; 4-[^{18}F]fluoroiodobenzene, [$Pd_2(dba)_3$/P(*o*-tol)$_3$/CuI], 1:1 DMF/toluene, 65°C, 20 min, DMF;

Radiolabeling was achieved using a Stille reaction with [^{18}F]fluoroiodobenzene acting as the radioprecursor (Fig. 2-15). The radioprecursor was prepared via a thermal decomposition of 4,4'-diiododiohenyliodonium triflate in the presence of [^{18}F]KF-Kryptofix [68].The authors optimized the Stille reaction by varying the nature of the catalyst system (palladium complex, co-ligand, additive), as well as reaction time, temperature and solvent.

Radiochemical yields of 93% and 68% for compounds **14** and **15** respectively were obtained using the catalyst complex [$Pd_2(dba)_3$/P(*o*-tol)$_3$/CuI] in 1:1 DMF/toluene, at 65°C in a reaction time of 20 min. These radiochemical yields do not include purification of the tracer, but reflect solely on the efficiency of the reaction.

The tracers described above have not been characterized *in vitro* or *in vivo*. Based on the encouraging results obtained by deVries and co-works in a different study using [^{11}C]rofecoxib [28], the ^{18}F labeled compounds reported by Wuest and co-workers are promising leads for the development of a COX-2 specific radiotracer.

Valdecoxib analogues

Valdecoxib is a COX-2 selective inhibitor, which was used in the clinic from 2000 until 2005. The drug was withdrawn from the market following concerns over adverse cardiac side effects.

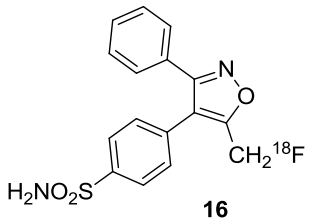

16

Figure 2-16: Compound **16** [58]

Valdecoxib, similar to rofecoxib, is not a fluorine-containing compound. Identification of a radiolabeling candidate does require the development of a fluorine-containing analogue. Toyokumi *et al*. made efforts to synthesize a number of structurally related fluorine containing analogoues of valdecoxib [58]. Compared to valdecoxib, one of the four compounds studied showed higher potency and selectivity for human recombinant COX-2 over COX-1 enzyme (Fig. 2-16). Fluorination of **16** was achieved by substituting a hydrogen atom of the methyl group on the central isoxazole ring for fluorine, using an *O*-tosylated precursor. To ensure high specificity of the radiosynthesis, the sulfonamide was protected using 4,4'-dimethoxytrityl (DMTr). Radiolabeling was achieved by nucleophilic substitution reaction using [^{18}F]KF-Kryptofix. Radiochemical yield was found to be approximately 40% after deprotection and purification.

In vivo evaluation showed rapid defluorination upon injection into mice. An evaluation of binding affinity was not possible due to rapid accumulation of ^{18}F in the skeleton. The authors suggest that this is likely due to the high metabolic activity in rodents in particular hydrogen abstraction from the methyl group via P450 catalyzed oxidation [69]. Similar to the case made for [^{18}F]celecoxib (**10**) this tracer might be used in human studies, as metabolic activity is significantly lower in humans than in rodents [51]; this coud be evaluated with by conducting an *in vitro* metabolic stability study in human serum and plasma.

DuP-697/desbromo DuP-697

DuP-697 is generally considered to be the first selective COX-2 inhibitor among the non-steroidal anti-inflammatory drugs. Its development predates conclusive proof of the existence of the COX-2 isoform. Initial screening confirmed potent anti-inflammatory activity but none of the side effects

associated with COX-1 inhibition. DuP-697 served as a template for all subsequent coxibs, such as celecoxib, rofecoxib and valdecoxib; the FDA, however, never approved DuP-697 itself.

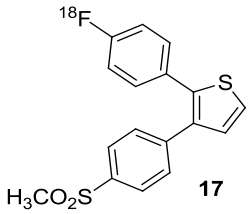

Figure 2-17: Compound **17** [48]

DuP-697 is a potent, selective and irreversible COX-2 inhibitor [70], which is not metabolized in humans [71]. DuP-697 was found to have a K_i value of 2 nM against COX-2 and 870 nM against COX-1 [72]. It is furthermore a fluorine-containing compound, which makes it a good candidate for ^{18}F-labeling. While attempting to synthesize [^{18}F]DuP-697 using a ^{18}F for ^{19}F exchange reaction, it was found that the fluorine carrier displaces the bromine on the central thiophene ring and a corresponding desbromo derivative was formed (Fig. 2-17) [48].

Experiments with desbromo-DuP-697 suggested that this compound shows good COX-2 inhibitory potential as well [73, 74]. deVries *et al*. used a nitro precursor to achieve ^{18}F labeling of desbromo-DuP-697 via nucleophilic substitution. Radiolabeling was achieved using [^{18}F]KF-Kryptofix in DMF, the radiochemical yield of the reaction was found to be 3% after a synthesis time of approximately 70 min.

For the *in vivo* evaluation of **17** a carrageenan-induced inflammation model in rats was used. Analysis of various tissue types revealed that the uptake in both inflamed and non-inflamed paws was identical. Uptake in either inflamed or control paw was not reduced by treatment with either NS-398 or indomethacin. The results of a peroxidase assay, measuring the expression of COX-2

in the analyzed tissue, revealed that, despite visible inflammation in the carrageenan treated paw, an increased COX-2 expression was not induced.

The results of biodistribution studies showed that the highest radiotracer uptake was found in the intestines and in fat tissue, this is likely to be due to the high lipophilicity of the tracer (logP = 3.7). Uptake of **17** was consistent with high COX-2 expression in the heart, brain and kidneys [11, 12], which was reduced upon treatment with indomethacin and NS398 (approximately 40% to 60% reduction in uptake). Tracer uptake in the bone was very low indicating that **17** does not suffer from significant defluorination *in vivo*.

The high lipophilicity of [^{18}F]desbromo-DuP-697 (**17**) might make it unsuitable for imaging in the abdominal region, but allows it to cross the BBB, which might enable imaging of the central nervous system. The carrageenan-induced hyperalgesia animal model was found to be unsuitable for *in vivo* COX-2 studies, although this observation is contrary with the study conducted by Uddin *et al*, which reported positive results using the same inflammation model.

Other COX-2 inhibitors

Although a number of promising radiotracers have been developed on the basis of structural templates provided by the clinical coxibs, there is a vast library of potential radiolabeling candidates among the known clinical and novel COX-2 inhibitors.

One of these structures is the COX-2 inhibitor EFMP (6-ethoxy-3-(4-methanesulfonylphenyl)-4-(4-fluorophenyl)pyran-2-one), which was chosen for development as a COX-2 specific radiotracer 18 by Tian and Lee (Fig. 2-18)[59]. The compound was discovered by Knaus et al. in 2003 and exhibits good potency (K_i = 0.10 μM) and selectivity [75]. EFMP is a fluorine-containing compound and is well suited for ^{18}F-labeling.

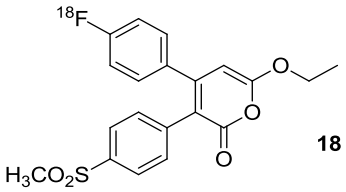

Figure 2-18: Compound **18** [59]

Radiolabeling was accomplished using a trimethylammonium precursor and [^{18}F]KF-Kryptofix in acetonitrile at 130ºC. The radiochemical yield was determined to be 15% in a reaction time of 60 to 70 min. *In vitro* or *in vivo* data on the compound has not been published to date.

Most recently, Kniess and coworkers presented a COX-2 radiotracer based on the structures designed by Tanaka *et al*. (see Carbon-11 section [30]) [60]. Kniess *et al*. used the indole-based structure **9** as a template for an ^{18}F labeled radiotracer, using the methyl sulfone derivative and replacing the methoxy substituent with fluorine **19** (Fig. 2-19). This compound has been shown to be a potent and selective COX-2 inhibitor (**19** K_i(COX-2) = 20 nM, K_i(COX-1) >10 μM) [53].

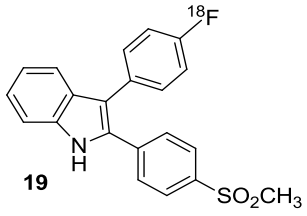

Figure 2-19: Compound **19** [60]

The radiotracer developed by Kniess *et al*. is especially notable for the innovative radiochemistry used to synthesize the title compound. The researchers used a non-cyclized trimethylamino triflate

precursor and radiolabeled it by direct fluorination using [^{18}F]KF and Kryptofix. The final compound was obtained via McMurry cyclization (Fig. 2-20).

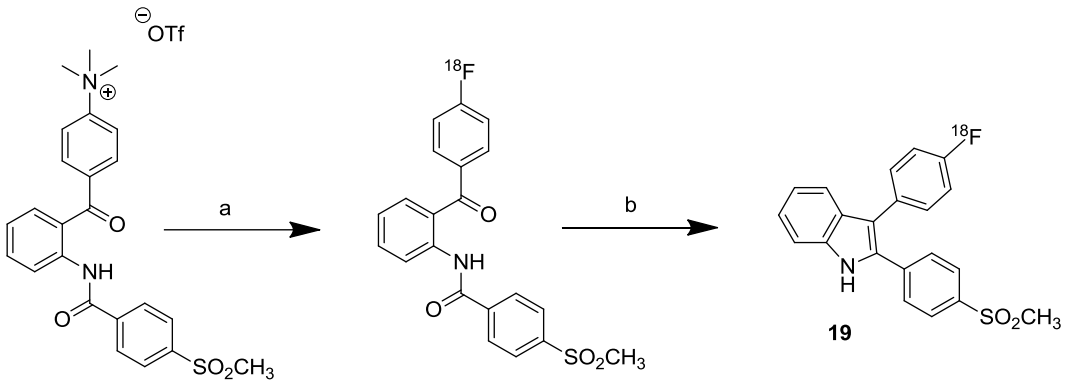

Figure 2-20: Radiosynthesis via McMurry coupling [60]; a) [^{18}F]KF, Kryptofix, CH_3CN; 100°C, 15 min b) $TiCl_4$, Zn, THF, 90°C.

Although the direct fluorination is best carried out in DMF as solvent, the researchers found that residual DMF inhibits the McMurry cyclization during the second step of the reaction. Instead the fluorination was carried out in acetonitrile followed by McMurry reaction in THF. Radiolabeling was accomplished in a yield of 8 to 10% on an automated synthesis unit and a total synthesis time of 80 min.

In vitro evaluation of radiotracer **19** in TPA stimulated THP-1 cells and various COX-2 expressing cell lines (FaDu, A375, A2058 and HT-29), confirmed that uptake in COX-2 positive cells exceeded uptake in COX-2 negative cells (non-stimulated THP-1 cells) and that the uptake was reduced by pre-treatment with 100 μM non-radiolabeled **19**. The authors furthermore showed that levels of PGE_2, a major metabolite of COX's enzymatic activity, were reduced in a concentration dependent manner in COX-2 positive cell lines after treatment with non-radiolabeled **19**. It has to be noted, however, that PGE_2 levels were reduced to below the detection limit concentrations of

10 μM, suggesting that **19** might also affect the enzymatic activity of COX-1. Kniess *et al*. went on to evaluate the selectivity ratio of **19** in a COX-1/2 K_i assay and found the ratio to be 5.5 (K_i(COX-2) = 1.2 μM, K_i(COX-1) = 6.6 μM) compared to a value of 500 reported in the literature [53]. These results indicate that compound **19** is likely to show high affinity for both COX-2 and COX-1 isoforms.

In vivo assessment of radiotracer **19** was carried out in HT-29 bearing male Wistar rats. Metabolite analysis revealed that the radiotracer suffers slow metabolism *in vivo*, with 75% of the parent compound being intact after 60 min. PET studies showed limited tumor uptake of **19**. Most of the radiotracer accumulated in the liver, small intestine and kidney. Small amounts of activity (SUV ~ 1) were detected in the brain and the blood pool. It is likely that the low affinity of **19** for COX-2 is the reason for the low tumor uptake. Affinity for COX-1 and the hydrophilic nature of the compound ($logP_{7.4}$ = 1.2) might lead to low bioavailability and general inability to cross cellular membranes.

2.2.3. COX-2 inhibitors labeled with other radionuclides

Designing SPECT imaging probes

A number of studies have used gamma-emitting radioisotopes to label COX-2 inhibitors for imaging studies utilizing SPECT (single-photon emission computed tomography). While PET imaging uses positron emitting radioisotopes, SPECT relies on gamma emitting radioisotopes. The positron, emitted in PET, collides with an electron, the collision leads to the emission of two gamma rays that exit the collision site in opposite directions. By considering "coincidence" events of gamma rays arriving at the detector, the location of the annihilation can be determined in 3D space, leading to the construction of a high-resolution 3D image. SPECT, in comparison, uses radioisotopes that emit single gamma rays directly. The origin of these photons cannot be traced in three-dimensional space, but SPECT technology is able to perform scans at multiple angles and different planes, allowing the reconstruction of a low-resolution 3D images.

Although the resolution of SPECT images is much lower compared to PET, the type of radionuclide used is much easier to handle due to their relatively longer half-lives. Radionuclides most commonly used in SPECT are ^{99m}Tc with a half-life of 6.0 hours, ^{123}I with a half-life of 13.2 hoursand ^{125}I with a half-life of 59.4 days. The long half-lives allow off-site production of radionuclides, which makes SPECT imaging significantly cheaper than PET imaging.

From a pharmacological point of view, however, PET radionuclides are more suitable for *in vivo* evaluation of drug-like molecules. As discussed previously, the short-lived positron emitters used in PET imaging are elements commonly found in drug-like molecules. Single photon emitters used in SPECT, on the other hand, are uncommon in small molecule inhibitors or larger structures, such as peptides. Iodine does exhibit properties similar to other halogens, including positron emitter ^{18}F,

but is much larger in size, which can lead to steric problems. Technetium, being a transition metal, requires a chelating agent to allow conjugation to the target molecule.

These limitations do not necessarily lead to a loss of target specificity of the SPECT tracer, but it precludes the study and subsequent pharmacokinetic evaluation of potential novel therapeutics *in vivo*.

Table 2-3 summarizes SPECT COX-2 imaging probes reported in the literature to date.

Table 2-3: SPECT labeled COX-2 inhibitors

Compound	Radiolabeling method	Radiochemical yield	Specific activity (GBq/μmol)	Ref.
Celecoxib derivative **20**	^{99m}TcO(V) N_2S_2 chelating agent			[76]
Celecoxib derivative **21**	Iododestannylation ([^{123}I]NaI) **Fig. 2-25**	90%		[77]
Celecoxib derivative **21**	Halogen exchange reaction ([^{123}I]NaI)	35%		[78]
Celecoxib derivative **22**	Halogen exchange reaction ([^{123}I]NaI)	42%		[78]
Lumiracoxib derivative **23**	Iododestannylation ([^{125}I]NaI)	36-51%	47-72	[79]

Celecoxib

Most of the work in the field of SPECT COX-2 inhibitors has been focused on celecoxib as a parent compound. Since the core structure of the celecoxib does not include iodine or technetium, all SPECT labeled tracers are celecoxib derivatives.

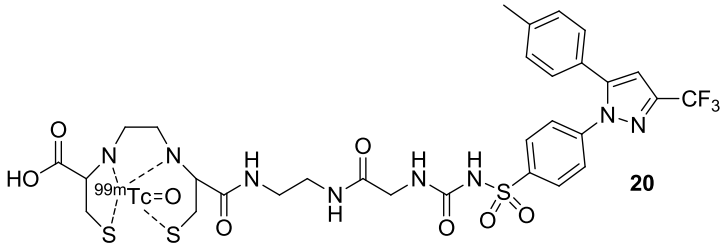

Figure 2-21: Compound **20** [76]

The first SPECT COX-2 imaging agent was developed by Yang *et al*. in 2004 (Fig. 2-21) [76]. Based on research suggesting that chelating complexes based on diaminodithiol form particularly stable technetium complexes [80], Yang *et al*. used ^{99m}Tc-$_{L,L}$-ethylenedicysteine (^{99m}Tc-EC) as the chelating group of choice [81]. ^{99m}Tc-EC conjugates have a history of wide spread use in oncologic imaging [82-84]. To achieve sufficient spatial separation between the pharmacologically active part of the molecule and the chelating agent, the sulfonamide group of celecoxib was modified using ethyl isocyanato acetate and the chain subsequently elongated using ethylene diamine. The terminal primary amine was conjugated to the EC complex to give non-radiolabeled EC-celecoxib **20**. Radiolabeling was achieved by adding [^{99m}Tc]pertechnetate and **20** into a labeling kit. Radiochemical purity was found to >95% following TLC analysis.

In vitro evaluation of **20** was carried out using three COX-2 expressing cell lines including rat-derived breast cancer cell line 13762. Counter intuitively, all three cell lines show a dose-dependent increase in uptake of **20** upon pre-incubation with celecoxib. Although it has been suggest that COX-2 expression can be induced by celecoxib treatment [85], this is unlikely to be the case here as celecoxib was administered 30 min and 2 h before tracer injection, a time frame that is likely to be too short to induce significant COX-2 expression. A more plausible explanation of the observed phenomenon was put forward by deVries [22]. It has been found that celecoxib inhibits the function of P-glycoprotein [86]. P-glycoprotein is a transmembrane pump that helps

the cell to expel a wide variety of toxins. It is plausible that an attempt to block COX-2 specific radiotracer uptake with celecoxib leads to increased tracer uptake due to celecoxib's interference with non-COX-2 related cellular mechanisms. *In vivo* studies using **20** in 13762 tumor bearing rats showed that tumor uptake was significantly higher compared to administration of [^{99m}Tc]-EC. Muscle uptake of **20** is low, resulting in favorable tumor to muscle ratios. Blood retention of **20** on the other hand is high, resulting in tumor to blood ratios of <1.

One of the drawbacks of attaching a chelating agent to the sulfonamide is that it blocks the sulfonamide functional group, which is believed to be essential to binding to COX-2 [18].

Labeling of celecoxib with ^{123}I has the advantage of not requiring the addition of a chelating agent. Kabalka *et al*. developed a ^{123}I labeled celecoxib analogue **21** (Fig. 2-23) [77]. To retain affinity and specificity, the 4-methyl group was replaced with ^{123}I, based on data suggesting that halogens in the 4-position are well tolerated [32].

The labeling precursor was synthesized from non-radiolabeled **21** via iododestannylation to give a trimethylstannyl derivative. Radiolabeling was accomplished via electrophilic iododestannylation with [^{123}I]NaI (Fig. 2-22). The product was obtained with a radiochemical yield of 90%.

The biological evaluation of radiotracer **21** was carried out by Schuller *et al*. [87]. The research group used potent carcinogen nicotine-derived nitrosamine 4-(methylnitrosamino)-1-(3-pyridyl)-1-butanone (NNK) to induce adenocarcinomas in the lungs and pancreas of hamsters. This biological model is well established in rodents [88] and immuno-histochemical analysis has shown that the resulting tumors express COX-2 [89, 90].

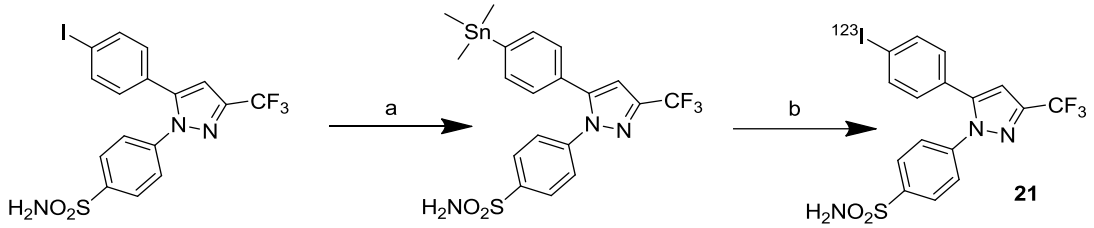

Figure 2-22: Electrophilic iododestannylation using [^{123}I]NaI [77]; a) $Sn_2(CH_3)_6$, $Pd(PPh_3)_4$, dioxane, reflux, 30min; b) CH_3CO_3H, [^{123}I]NaI, r.t., 20min;

An *in vitro* assessment of **21** radiolabeled with long-lived iodine isotope ^{125}I revealed that uptake in NNK pretreated cells was significantly higher than in non-treated control cells. The uptake of **21** was significantly reduced by pre-incubation with celecoxib, suggesting that radiotracer uptake is mediated by COX-2. Biodistribution studies performed on Syrian golden hamsters found that animals treated with NNK showed higher radiotracer uptake in the pancreas and liver and slightly higher uptake in the lung. SPECT imaging with ^{123}I labeled **21** revealed that only one of the animals treated with NNK, showed increased radiotracer uptake in the pancreas and the liver. Subsequent immuno-histochemical analysis of the tissue revealed that only the pancreas and liver of the animal in question expressed COX-2, while the organs of the other hamsters that had been treated with NNK did not show significant levels of COX-2.

The results of the immuno-histochemical analysis are in good agreement with the distribution of the radiotracer, which suggests that uptake of **21** might be COX-2 mediated.

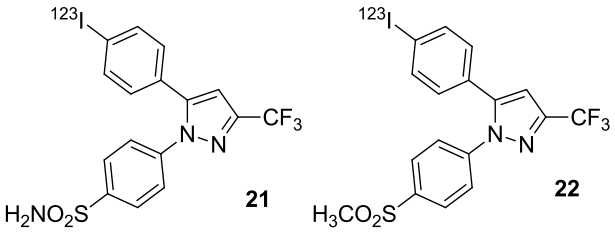

Figure 2-23: Compound **21** [77], **22** [78]

Another comprehensive study on ^{123}I labeled celecoxib derivatives was published by Kuge and coworkers [78]. In addition to the compound studied by the Kabalka group **21**, Kuge *et al*. developed a radiotracer based on the methyl sulfone derivative of celecoxib **22**. Radiolabeling was accomplished using 4-bromine precursors of **21** and **22**, [^{123}I]NaI and a copper(II) based catalyst. The radiolabeled compounds were purified by HPLC. Radiochemical yields were found to be 35% and 42% for **21** and **22** respectively. Compounds **21** and **22** showed good inhibitory potential for COX-2 while showing little to no affinity for COX-1 (K_i (COX-1 **21**) = 8.2 μM) (K_i (COX-1 **22**) = 5.2 μM).

Biodistribution of **21** and **22** in rats revealed that the sulfonamide containing **21** showed a significantly higher retention in blood, than the methyl sulfone containing **22**. This is likely to be due to affinity for carbonic anhydrase, as discussed earlier in this review [54]. Notably, Kuge *et al*. were able to show that pretreatment of blood with carbonic anhydrase inhibitors succeeded in decreasing the retention of **21**, while no change in the blood clearance of **22** could be observed, confirming the hypothesis that carbonic anhydrase is responsible for the blood retention of sulfonamide structures.

Biodistribution studies furthermore revealed little uptake of either tracer in the thyroid and the stomach, suggesting that neither compound suffers significant *in vivo* radio-deiodonation. Uptake in the kidneys and the brain was found to be high, which is consistent with known expression

levels [11, 12] of COX-2. The biodistribution pattern of **22** is comparable to that of the ^{18}F labeled sister compound **12**, suggesting that the introduction of iodine instead of fluorine does not have an adverse affect on affinity or specificity, making **22** a viable SPECT alternative to the PET tracer **12**.

Lumiracoxib

The most recent study on SPECT COX-2 radiotracer was also published by Kuge et al. [79]. The group developed a ^{125}I labeled analogue of lumiracoxib. While all COX-2 inhibitors reviewed thus far are based on a triaryl scaffold, lumiracoxib is a structural analogue to the non-selective COX inhibitor diclofenac. Much like diclofenac, lumiracoxib is based on a diaryl structure and has weakly acidic properties, due to the inclusion of a carboxylic acid group [91]. This acidic property renders the molecule less lipophilic than its triaryl colleagues and thus more suitable to act as a highly specific PET/SPECT tracer. Reduced lipophilicity leads to lower non-specific binding. Lumiracoxib's affinity and specificity for COX-2, meanwhile, is comparable to that of other coxibs [91]. The compound was retained in inflamed tissue and rapidly cleared from the plasma [92, 93]. These pharmacokinetic properties make lumiracoxib a good candidate for radiolabeling.

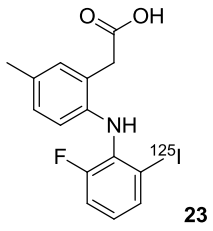

23

Figure 2-24: Compound **23** [79]

The original structure of lumiracoxib includes a chlorine substituent in position 6 of the 2-phenyl ring. Kuge *et al.* replaced the chlorine with iodine to synthesize lumiracoxib analogue **23** (Fig. 2-24). The K_i of **23** against COX-2 was found to be 2.5 μM; lumiracoxib, by comparison, was found to have a K_i of 0.8 μM in the same assay. Radiolabeling was accomplished using a trimethylstannyl precursor. The research group decided to label **23** with longer lived radioisotope [^{125}I], which was achieved via electrophilic iododestannylation of the precursor with [^{125}I]NaI. The radiotracer was purified using HPLC, with radiochemical yields of 36-51%.

In vitro experiments were carried out using LPS/IFN-γ-stimulated macrophages and untreated control cells. A Western Blot confirms the presence of COX-2 in the stimulated cell line. Uptake of **23** was significantly higher in the stimulated cell when compared to non-stimulated cells. The uptake of **23** was blocked in a concentration dependent manner using non-radiolabeled **23**.

Biodistributions in rats reveal that the compound is rapidly cleared from the blood and most other organs, with the exception of the intestine, which appears to show slow trapping of the radiotracer. Low uptake in the thyroid and stomach suggest that the radiotracer is unlikely to be subject to *in vivo* deiodination. The kidneys show high uptake of **23**; the brain, however, shows no uptake of the radiotracer, indicating that the low lipophilicity inhibits passage of the BBB.

Kuge *et al*. did not attempt to evaluate compounds **21**, **22** or **23** in COX-2 *in vivo* models. The group furthermore did not attempt to reduce the uptake patterns observed with pharmacological doses of non-radiolabeled COX-2 inhibitors. Citing the number of studies that were unsuccessful in showing *in vivo* COX-2 specificity in this way, the authors express doubt over the notion that *in vivo* blocking experiments are a viable experimental set up. Expression levels of COX-2 in animal models might be too low to successfully complete blocking models, which would make the development of a highly COX-2 expressing model necessary. Although a number of animals

model have been developed since the conclusion of these studies, the challenge to identify a standard model to test COX-2 radiotracer remains an open one.

2.3. Discussion and conclusion

Given the various chemical, radiochemical and biological properties of the different COX-2 radiotracers reviewed here, it must be concluded that a COX-2 specific radiotracer has not been identified to date. However, it appears that this is not solely due to the inadequacy of the radiotracers presented. It seems clear that the failure to show COX-2 specific binding *in vivo* is as much a chemical as it is a biological problem.

The main question that arises is how much of the relative inability of a radiotracer to specifically visualize COX-2 *in vivo* is due to shortcomings in its chemical structure and how much of it is due to limitations of the biological models. In many cases it is not possible to distinguish whether one or the other presents the main problem.

The decision made by Kuge *et al*. [78, 79] to not attempt COX-2 specific *in vivo* evaluation, in this light, is quite a valid one. Given that there are currently no well-established biological models that are know to stably express COX-2 at levels that make it suitable for *in vivo* blocking studies, any COX-2 specific *in vivo* evaluation is bound to be flawed. It is therefore not possible to conclude that failure to visualize COX-2 specifically is due to shortcomings in the design of the radiotracer. Although, it is difficult to suggest an optimal solution for this fundamental problem at this point, the data available from the various studies reviewed herein allows us to draw a number of conclusions with regard to the nature of suitable radiotracers and useful *in vivo* models.

One of the attributes that might disqualify a compound from being a suitable COX-2 radiotracer is its metabolic instability *in vivo*. A number of the compounds reviewed here have short *in vivo* half lives (**1, 6, 10, 16**). Although it is important to note that metabolic instability in rodents does not necessarily translate to their metabolic properties in primates or humans [51], it does lead to exclusion from further pre-clinical testing.

The design of COX-2 selective inhibitors generally requires the inclusion of either a methyl sulfone or a sulfonamide functional group [18]. A notable exception to this rule is lumiracoxib (**23**) [79]. A number of studies have observed high blood retention of COX-2 radiotracers that carry a sulfonamide functional group, while methyl sulfone compounds displayed much more rapid clearance from the blood pool. It is likely that the sulfonamide group causes the poor blood clearance kinetics. Tanaka *et al*. provided powerful evidence for this hypothesis, having shown the clearance of sulfonamide **8** to be retained in the blood pool, while the methyl sulfone sister compound **7** was cleared rapidly [30]. Weber *et al*. provide evidence that this is likely to be caused by sub-nanomolar affinity of sulfonamide bearing inhibitors for various carbonic anhydrase (CA) enzymes [54]. Carbonic anhydrases are expressed in various blood cells, which explains the high blood retention of these radiotracers. Although the CA binding site is similar in shape to that of the COX-2 enzyme, CA includes Zinc in its catalytic site. The high affinity of sulphonamide-based COX-2 inhibitors is largely attributed to the strong bond between the primary amine and the Zinc catalytic site. It is because of this specific interaction that methyl sulfone bearing COX-2 inhibitors show little or no affinity for CAs. Kuge *et al*. provide the most compelling evidence for CAs involvement in blood clearance behaviour [78]. Sulfonamide bearing **21** was retained in the blood pool, while methyl sulfone sister compound **22** was cleared rapidly. Pre-treatment with carbonic anhydrase inhibitors shortened the blood retention of **21** significantly, but did not alter the clearance rate of **22**.

Although the therapeutic potential of sulphonamide-based COX-2 inhibitors might be undiminished, they are not suitable for radiotracer development given the cross reactivity with carbonic anhydrase and resulting retention in the blood pool. Development of COX-2 specific radiotracers should therefore focus on methyl sulfone or none sulfone bearing COX-2 inhibitors.

It is challenging to draw similar conclusions regarding the suitability of a biological model. The array of COX-2 specific models used by various research groups for the evaluation of COX-2 radiotracers is broad. Investigators have attempted to use a number of tumor models, including mouse xenograft models HT-29 [29], 1483 HNSCC, HCT-116 [56], as well as rat models AH109A [25, 30], 13762 [76] and HT-29 [60]. Schuller *et al*. attempted to induce tumor formation by nicotine-derived nitrosamine 4-(methylnitrosamino)-1-(3-pyridyl)-1-butanone (NNK) treatment of hamsters [87]. Inflammation models have also proven popular. Researchers have induced inflammation by turpentine treatment [28], LPS or γ-interferon (IFN-γ) treatment [55], [79], carrageenan treatment [48, 56] or herpes simplex virus (HSV) treatment [28]. In addition, COX-2 positive cell lines used for *in vitro* evaluation included 3T3-L1, FaDu, HT-29 [29], A375 and A2058 [60].

Due to the large number of models used and the lack of cross over between different studies, it is difficult to make definite comments based on the suitable of biological models. Inflammation models are convenient to work with since the induction of inflammation is visible through swelling. Unfortunately, inflammation symptoms do not necessarily induce COX-2 expression [48]. Furthermore, inflammatory conditions induce a number of other physiological changes, such as increased blood flow to the area [94], which might affect the pharmacokinetics of a radiotracer. From that point of view, tumor models are more reliable, as their COX-2 expression can be assessed via protein determination before inoculation. However, as COX-2 is an inducible enzyme, an organism might easily up or down regulate COX-2 expression following inoculation. Although a cell line might express COX-2 *in vitro* there is no guarantee that it will express COX-2 at similar levels *in vivo*. The matter becomes more complicated if one considers that most tumor xenograft models induce inflammation in the tissue surrounding the inoculated tumor tissue. The problem is

very well described in recent study [95] attempting to show COX-2 mediated radiosensitization effects *in vivo*. The researches used a COX-2 positive HCA-7 xenograft mouse model and a COX-2 negative HCT-116 xenograft mouse model. Counter intuitively they found greater radiosensitization effects in the negative model than in the positive model. Closer investigation of the developed tumors post-inoculation revealed that the COX-2 expression of the HCA-7 cells had ceased *in vivo*, while HCT-116 tumors caused inflammation in the tumor microenvironment associated with significant COX-2 expression. In the end the researchers had created a negative tumor model that expressed more COX-2 than the positive tumor model.

It follows that radiotracer uptake in tumor models *in vivo* needs to be validated by *ex vivo* COX-2 assessment of the inoculated tumors. Pre-inoculation assessments might have little bearing on the COX-2 expression *in vivo*. Comparing radiotracer uptake in COX-2 positive and negative tumor models as show by Uddin *et al*. [56], can lead to misleading results, through the false positive and false negative scenario discussed above. Furthermore, comparison of uptake in two different tumor models is subject to other variables, such as efficacy of drug efflux pumps [86], which cannot be controlled for.

To show that uptake in a tumor model is COX-2 mediated despite uncertainty surrounding *in vivo* expression of positive as well as negative cell lines, a number of authors have attempted to reduce radiotracer uptake by pre-injecting animals with pharmacological doses of known COX-2 inhibitors. This is an advantageous strategy, as it is not strictly relevant whether COX-2 is expressed in the core cells of the tumor tissue or the microenvironment, as long as COX-2 expression can be confirmed post-inoculation. One of the major challenges of pre-dosing animals is the timing of the injection and the dose required to reduce uptake significantly. The

pharmacokinetic properties of most known COX-2 inhibitors are very poor [36, 37], causing slow distribution of pharmacological concentrations, as well as slow target saturation.

Definite conclusion regarding timing and dosing of pharmacological injections is very difficult at this time, because a successful direct reduction of radiotracer uptake in a COX-2 model has not been reported to date.

Uptake reduction through pre-incubation with COX-2 inhibitors *in vitro* has been successful in all studies reviewed here. Some succeed in showing alterations in regional uptake patterns *in vivo*. The work presented by Uddin *et al*. [56] has shown some success in reducing uptake of a radiolabeled celecoxib derivative **13** in a COX-2 specific inflammation model and a COX-2 specific tumor model. The researchers showed a reduction in uptake in a carrageenan-induced inflammation model. However the overall uptake level of the radiotracer at a SUV level of 0.2 might be too low to be COX-2 specific. Furthermore, compound **13** is a sulfonamide carrying substance, which means that is likely to be retained in the blood stream and to have at least one other major target (CA). The reduction in uptake shown in COX-2 positive1483 HNSCC tumorsis quoted as a change in the tumor to muscle ratio, rather than a direct measure of the total radioactivity in the tumor. It has to be noted that the uptake in the muscle tissue of animals can differ upon exposure to high concentrations of COX-2 inhibitor, which would alter the tumor to muscle ratio irrespective of the overall tumor uptake. One of the ways in which muscle uptake might be altered in response to treatment with celecoxib was reported by Awara *et al*. [86]; the researchers found that celecoxib inhibits the function of P-glycoprotein. P-glycoprotein is a transmembrane pump that helps the cell to expel a wide variety of toxins. It is plausible that an attempt to block COX-2 specific radiotracer uptake with celecoxib leads to increased tracer uptake due to celecoxib's interference with non-COX-2 related cellular mechanisms. In conclusion, the

data presented by Uddin *et al*. is promising, but does not provide a clear basis for concluding that uptake of radiotracer **13** was indeed COX-2 mediated.

The last and possibly least studied hurdle to developing a specific COX-2 radiotracer is the problem of "off-target effects". This issue has been discussed in parts of this review already, but deserves a more extensive mention. The fact that some COX-2 inhibitors show sub-nanomolar affinity for carbonic anhydrases, as well as the observation that celecoxib can alter the behavior of drug efflux pumps forces us to entertain the possibility that the "classic" COX-2 inhibitors might have a number of undiscovered molecular targets and physiological effects. Recent evidence regarding the origin of the cardiovascular toxicity of coxibs, which lead to their clinical withdrawal, underlines this observation [7]. Proving the specificity of a radiotracer for the COX-2 enzyme in a complex biological system gets more challenging with the number of undiscovered molecular targets.

Future studies and efforts to develop a COX-2 specific radiotracer would benefit from adopting a dual experimental approach. Design and optimization of the radiotracer on the one hand must be conducted in parallel to improvement and validation of the biological model. Parallel development is more likely to lead to a substantial information gain on the properties of the radiotracer and the properties of the biological model. Ideally, this would lead to the development of a "gold-standard" biological model, by which new radiotracers could be evaluated.

2.4. References

[1] Warner, T.D.; Mitchell, J.A. Cyclooxygenase-3 (COX-3): Filling in the gaps toward a COX continuum? *Proc. Natl. Acad. Sci. U S A*, **2002**, 99, 13371.

[2] Kurumbail, R.G.; Kiefer, J.R.; Marnett, L.J. Cyclooxygenase enzymes: Catalysis and inhibition. *Curr. Opin. Struct. Biol.*, **2001**, 11, 752.

[3] Luong, C.; Miller, A.; Barnett, J.; Chow, J.; Ramesha, C.; Browner, M.F. Flexibility of the NSAID binding site in the structure of human cyclooxygenase-2. *Nat. Struct. Biol.*, **1996**, 3, 927.

[4] Shi, S.; Klotz, U. Clinical use and pharmacological properties of selective COX-2 inhibitors. *Eur. J. Clin. Pharmacol.*, **2008**, 64, 233.

[5] DeWitt, D. Cox-2-selective inhibitors: The new super aspirins. *Mol. Pharmacol.*, **1999**, 55, 625.

[6] Cannon, C.P.; Cannon, P.J. COX-2 Inhibitors and Cardiovascular Risk. *Science*, **2012**, 336, 1386.

[7] Yu, Y.; Ricciotti, E.; Scalia, R.; Tang, S.Y.; Grant, G.; Yu, Z.; Landesberg, G.; Crichton, I.; Wu, W.; Pure, E.; Funk, C.; FitzGerald, G. Vascular COX-2 Modulates Blood Pressure and Thrombosis in Mice. *Sci. Transl. Med.,* **2012**, 132.

[8] Fiorucci, S.; Distrutti, E. COXIBs, CINODs and H2S-Releasing NSAIDs: Current Perspectives in the Development of Safer Non Steroidal Anti-Inflammatory Drugs. *Cur. Med. Chem.*, **2011**, 18, 3494.

[9] Rovati, G.E.; Sala, A.; Capra, V.; Dahlén, S.E.; Folco, G. Dual COXIB/TP antagonists: a possible new twist in NSAID pharmacology and cardiovascular risk. *Trends Pharmacol. Sci.*, **2010**, 31, 102.

[10] Scheiman, J.M. Unmet needs in non-steroidal anti-inflammatory drug-induced upper gastrointestinal diseases. *Drugs*, **2006**, 66, 15.

[11] Seibert, K.; Zhang, Y.; Leahy, K.; Hauser, S.; Masferrer, J.; Perkins, W.; Lee, L.; Isakson, P. Pharmacological and biochemical demonstration of the role of cyclooxygenase 2 in inflammation and pain. *Proc. Natl. Acad. Sci. U S A*, **1994**, 91, 12013.

[12] Okamoto, T.; Hino, O. Expression of cyclooxygenase-1 and -2 mRNA in rat tissues: Tissue-specific difference in the expression of the basal level of mRNA. *Int. J. Mol. Med.*, **2000**, 6, 455.

[13] Teismann, P.; Tieu, K.; Choi, D.; Wu, D.; Naini, A.; Hunot, S.; Vila, M.; Jackson-Lewis, V.; Przedborski, S. Cyclooxygenase-2 is instrumental in parkinson's disease neurodegeneration. *Proc. Natl. Acad. Sci. U S A*, **2003**, 100, 5473.

[14] Edwards, J.; Mukherjee, R.; Munro, A.F.; Wells, A.C.; Almushatat, A.; Bartlett, J.M.S. HER2 and COX2 expression in human prostate cancer. *Eur. J. Cancer*, **2004**, 40(1), 50.

[15] Wang, D.; DuBois, R.N. The role of COX-2 in intestinal inflammation and colorectal cancer. *Oncogene*, **2010**, 29, 781.

[16] Hwang, D.; Scollard, D.; Byrne, J.; Levine, E. Expression of cyclooxygenase-1 and cyclooxygenase-2 in human breast cancer. *J. Natl. Cancer Inst.*, **1998**, 90, 455.

[17] Jiménez, P.; García, A.; Santander, S.; Piazuelo, E. Prevention of cancer in the upper gastrointestinal tract with COX-inhibition, still an option? *Curr. Pharm. Des.*, **2007**, 13, 2261.

[18] Méric, J.; Rottey, S.; Olaussen, K.; Soria, J.; Khayat, D.; Rixe, O.; Spano, J.P. Cyclooxygenase-2 as a target for anticancer drug development. *Crit. Rev. Oncol.*, **2006**, 59, 51.

[19] Greenhough, A.; Smartt, H.; Moore, A.; Roberts, H.; Williams, A.; Paraskeva, C.; Kaidi, A. The COX-2/PGE(2) pathway: Key roles in the hallmarks of cancer and adaptation to the tumour microenvironment. *Carcinogenesis*, **2009**, 30, 377.

[20] Ghosh, N.; Chaki, R.; Mandal, V.; Mandal, S. COX-2 as a target for cancer chemotherapy. *Pharmacol. Rep.*, **2010**, 62, 233.

[21] Inoue, H.; Taba, Y.; Miwa, Y.; Yokota, C.; Miyagi, M.; Sasaguri, T. Transcriptional and posttranscriptional regulation of cyclooxygenase-2 expression by fluid shear stress in vascular endothelial cells. *Arterioscler. Thromb. Vasc. Biol.*, **2002**, 22, 1415.

[22] deVries, E.F.J. Imaging of cyclooxygenase-2 (COX-2) expression: Potential use in diagnosis and drug evaluation. *Curr. Pharm. Des.*, **2006**, 12, 3847.

[23] Prabhakaran, J.; Majo, V.; Simpson, N.; Van Heertum, R.; Mann, J.; Kumar, J. Synthesis of [C-11]celecoxib: A potential PET probe for imaging COX-2 expression. *J. Labelled Comp. Radiopharm.*, **2005**, 48, 887.

[24] Takashima-Hirano, M.; Takashima, T.; Katayama, Y.; Wada, Y.; Sugiyama, Y.; Watanabe, Y.; Doi, H.; Suzuki, M. Efficient sequential synthesis of PET probes of the COX-2 inhibitor [11C]celecoxib and its major metabolite [11C]SC-62807 and *in vivo* PET evaluation. *Bioorg. Med. Chem.*, **2011**, 19, 2997.

[25] Fujisaki, Y.; Kawamura, K.; Wang, W.; Ishiwata, K.; Yamamoto, F.; Kuwano, T.; Ono, M.; Maeda, M. Radiosynthesis and *in vivo* evaluation of 11C-labeled 1,5-diarylpyrazole derivatives for mapping cyclooxygenases. *Ann. Nucl. Med.*, **2005**, 19, 617.

[26] Gao, M.; Wang, M.; Miller, K.D.; Hutchins, G.D.; Zheng, Q. Synthesis of carbon-11 labeled celecoxib derivatives as new candidate PET radioligands for imaging of inflammation. *Appl. Radiat. Isot.*, **2009**, 67, 2019.

[27] Majo, V.; Prabhakaran, J.; Simpson, N.; Van Heertum, R.; Mann, J.; Kumar, J. A general method for the synthesis of aryl [C-11]methylsulfones: Potential PET probes for imaging cyclooxygenase-2 expression. *Bioorg. Med. Chem. Lett.*, **2005**, 15, 4268.

[28] de Vries, E.F.J.; Doorduin, J.; Dierckx, R.A.; van Waarde, A. Evaluation of [11C]rofecoxib as PET tracer for cyclooxygenase 2 overexpression in rat models of inflammation. *Nucl. Med. Biol.*, **2008**, 35, 35.

[29] Wuest, F.; Kniess, T.; Bergmann, R.; Pietzsch, J. Synthesis and evaluation *in vitro* and *in vivo* of a 11C-labeled cyclooxygenase-2 (COX-2) inhibitor. *Bioorg. Med. Chem.*, **2008**, 16, 7662.

[30] Tanaka, M.; Fujisaki, Y.; Kawamura, K.; Ishiwata, K.; Qinggeletu, Y.F.; Mukai, T.; Maeda, M. Radiosynthesis and evaluation of 11C-labeled diaryl-substituted imidazole and indole derivatives for mapping cyclooxygenase-2. *Biol. Pharm. Bull.*, **2006**, 29, 2087.

[31] Prabhakaran, J.; Underwood, M.; Parsey, R.; Arango, V.; Majo, V.; Simpson, N.; van Heertum, R.; Mann, J.J.; Kumar, J.S. Synthesis and *in vivo* evaluation of [F-18]-4-[5-(4-methylphenyl)-3-(trifluoromethyl)-1H-pyrazol-1-yl]benzene-sulfonamide as a PET imaging probe for COX-2 expression. *Bioorg. Med.Chem.*, **2007**, 15, 1802.

[32] Isakson, P.C.; Penning, T.D.; Talley, J.J.; Bertenshaw, S.R.; Carter, J.S.; Collins, P.W.; Docter, S.; Graneto, M.J.; Lee, L.F.; Malecha, J.W.; Miyashiro, J.M.; Rogers, R.S.; Rogier, D.J.; Yu, S.S.; AndersonG.D.; Burton E.G.; Cogburn J.N.; Gregory S.A.; Koboldt C.M.; Perkins, W.E.; Seibert, K.; Veenhuizen, A.W.; Zhang, Y.Y.; Isakson, P.C. Synthesis and

biological evaluation of the 1,5-diarylpyrazole class of cyclooxygenase-2 inhibitors: Identification of 4-[5-(4-methylphenyl)-3-(trifluoromethyl)-1H-pyrazol-1-yl]benzenesulfonamide (SC-58635, celecoxib). *J. Med. Chem.*, **1997**, 40, 1347.

[33] Smith, C.J.; Zhang, Y.; Koboldt, C.M.; Muhammad, J.; Zweifel, B.S.; Shaffer, A.; Talley, J.J.; Masferrer, J.L.; Seibert, K.; Isakson, P.C. Pharmacological analysis of cyclooxygenase-1 in inflammation. *Proc. Natl. Acad. Sci. U S A*, **1998**, 95, 13313.

[34] Kawamura, K.; Ishiwata, K. Improved synthesis of [C-11]SA4503, [C-11]MPDX and [C-11]TMSX by use of [C-11]methyl triflate. *Ann. Nucl.Med.*, **2004**, 18, 165.

[35] Nagren, K.; Halldin, C. Methylation of amide and thiol functions with [C-11]methyl triflate, as exemplified by [C-11]NMSP, [C-11]flumazenil and [C-11]methionine. *J. Labelled Comp. Radiopharm.*, **1998**, 41, 831.

[36] Gong, L.; Thorn, C.F.; Bertagnolli, M.M.; Grosser, T.; Altman, R.B.; Klein, T.E. Celecoxib pathways: pharmacokinetics and pharmacodynamics. *Pharmacogenet. Genom.,* **2012**, 22, 310.

[37] Rodriguez, G.; Luis, A.; Cea-Soriano, L.; Tacconelli, S.; Patrignani, P. Coxibs: Pharmacology, Toxicity and Efficacy in Cancer Clinical Trials. *Prospects for Chemoprevention of Colorectal Neoplasia*, **2012**, 67.

[38] Szabó, G.; Fischer, J.; Kis-Varga, A.; Gyires, K. New celecoxib derivatives as anti-inflammatory agents. *J. Med.Chem.*, **2008**, 51, 142.

[39] Ahuja, N.; Singh, A.; Singh, B. Rofecoxib: An update on physicochemical, pharmaceutical, pharmacodynamic and pharmacokinetic aspects. *J. Pharm. Pharmacol.*, **2003**, 55, 859.

[40] Habeeb, A.G.; Rao, P.N.P.; Knaus, E.E. Design and syntheses of diarylisoxazoles: Novel inhibitors of cyclooxygenase-2 (COX-2) with analgesic-antiinflammatory activity. *Drug. Dev.Res.*, **2000**, 51, 273.

[41] Dembo, G.; Park, S.B.; Kharasch, E.D. Central nervous system concentrations of cyclooxygenase-2 inhibitors in humans. *Anesthesiology*, **2005**, 102, 409.

[42] Lacroix, S.; Rivest, S. Effect of acute systemic inflammatory response and cytokines on the transcription of the genes encoding cyclooxygenase enzymes (COX-1 and COX-2) in the rat brain. *J.Neurochem.*, **1998**, 70, 452.

[43] Quan, N.; Whiteside, M.; Herkenham, M. Cyclooxygenase-2 mRNA expression in rat brain after peripheral injection of lipopolysaccharide. *Brain. Res.*, **1998**, 802, 189.

[44] Buursma, A.; de Vries, E.; Garssen, J.; Kegler, D.; van Waarde, A.; Schirm, J.; Hospers, G.; Mulder, N.; Vaalburg, W.; Klein, H. [F-18]FHPG positron emission tomography for detection of herpes simplex virus (HSV) in experimental HSV encephalitis. *J. Virol.*, **2005**, 79, 7721.

[45] Tzeng, S.; Hsiao, H.; Mak, O. Prostaglandins and cyclooxygenases in glial cells during brain inflammation. *Curr. Drug Targets Inflamm. Allergy*, **2005**, 4, 335.

[46] Yamada, S.; Kubota, K.; Kubota, R.; Ido, T.; Tamahashi, N. High accumulation of fluorine-18-fluorodeoxyglucose in turpentine-induced inflammatory tissue. *J. Nuc. Med.*, **1995**, 36, 1301.

[47] van Waarde, A.; Cobben, D.C.P.; Suurmeijer, A.J.H.; Maas, B.; Vaalburg, W.; de Vries, E,F,J.; Jager, P.L.; Hoekstra, H.J.; Elsinga, P.H. Selectivity of 18F-FLT and 18F-FDG for differentiating tumor from inflammation in a rodent model. *J. Nuc. Med.*, **2004**, 45, 695.

[48] de Vries, E.F.J.; van Waarde, A.; Buursma, A.R.; Vaalburg, W. Synthesis and *in vivo* evaluation of 18F-desbromo-DuP-697 as a PET tracer for cyclooxygenase-2 expression. *J. Nuc. Med.*, **2003**, 44, 1700.

[49] Reitz, D.B.; Li, J.J.; Norton, M.B.; Reinhard, E.J.; Collins, J.T.; Anderson, G.D.; Gregory, S.A.; Koboldt, C.M.; Perkins, W.E. Selective cyclooxygenase inhibitors: Novel 1,2-diarylcyclopentenes are potent and orally active COX-2 inhibitors. *J. Med. Chem.*, **1994**, 37, 3878.

[50] Li, J.J.; Anderson, G.D.; Burton, E.G.; Cogburn, J.N.; Collins, J.T.; Garland, D.J.; Gregory, S.A.; Huang, H.; Isakson, P.C. 1,2-diarylcyclopentenes as selective cyclooxygenase-2 inhibitors and orally active anti-inflammatory agents. *J. Med. Chem.*, **1995**, 38, 4570.

[51] Barrio, J.R.; Satyamurthy, N.; Huang, S.C.; Keen, R.E.; Nissenson, C.H.; Hoffman, J.M.; Ackermann, R.F.; Bahn, M.M.; Mazziotta, J.C.; Phelps, M.E. 3-(2'-[18F]fluoroethyl)spiperone: *In vivo* biochemical and kinetic characterization in rodents, nonhuman primates, and humans. *J. Cereb. Blood Flow Metab.*, **1989**, 9, 830.

[52] Almansa, C.; Alfón, J.; de Arriba,A.F.; Cavalcanti, F.L.; Escamilla, I.; Gómez, L.A.; Miralles, A.; Soliva, R.; Bartroli, J.; Carceller, E.; Merlos, M.; Garcia-Rafanell, J. Synthesis and structure-activity relationship of a new series of COX-2 selective inhibitors: 1,5-diarylimidazoles. *J. Med. Chem.*, **2003**, 46, 3463.

[53] Hu, W.; Guo, Z.; Chu, F.; Bai, A.; Yi, X.; Cheng, G.; Li, J. Synthesis and biological evaluation of substituted 2-sulfonyl-phenyl-3-phenyl-indoles: A new series of selective COX-2 inhibitors. *Bioorg. Med. Chem.*, **2003**, 11, 1153.

[54] Weber, A.; Casini, A.; Heine, A.; Kuhn, D.; Supuran, C.T.; Scozzafava, A.; Klebe, G. Unexpected nanomolar inhibition of carbonic anhydrase by COX-2-selective celecoxib: New pharmacological opportunities due to related binding site recognition. *J. Med. Chem.*, **2004**, 47, 550.

[55] McCarthy,T.J.; Sheriff, A.U.; Graneto, M.J.; Talley, J.J.; Welch, M.J. Radiosynthesis, *in vitro* validation, and *in vivo* evaluation of 18F-labeled COX-1 and COX-2 inhibitors. *J. Nuc. Med.*, **2002**, 43, 117.

[56] Uddin, M.; Crews, B.; Ghebreselasie, K.; Huda, I.; Kingsley, P.; Ansari, M.; Tantawy, M.N.; Reese, J.; Marnett, L.J. Fluorinated COX-2 inhibitors as agents in PET imaging of inflammation and cancer. *Can. Prev. Res.*, **2011**, 4, 1536.

[57] Wüst, F.R.; Höhne, A.; Metz, P. Synthesis of 18F-labelled cyclooxygenase-2 (COX-2) inhibitors via stille reaction with 4-[18F]fluoroiodobenzene as radiotracers for positron emission tomography (PET). *Org. Biomol. Chem.*, **2005**, 3, 503.

[58] Toyokuni, T.; Kumar, J.S.D.; Walsh, J.C.; Shapiro, A.; Talley, J.J.; Phelps, M.E.; Herschman, H.R.; Barrio, J.R; Satyamurthy, N. Synthesis of 4-(5-[18F]fluoromethyl-3-phenylisoxazol-4-yl)benzenesulfonamide, a new [18F]fluorinated analogue of valdecoxib, as a potential radiotracer for imaging cyclooxygenase-2 with positron emission tomography. *Bioorg. Med. Chem. Lett.*, **2005**, 15, 4699.

[59] Tian, H.; Lee, Z. Synthesis of 18F-labeled cyclooxygenase-2 (COX-2) inhibitor as a potential PET imaging agent. *J. Labelled Compd. Radiopharmaceut.*, **2006**, 49, 583.

[60] Kniess, T.; Laube, M.; Bergmann, F.; Sehn, F.; Graf, F.; Steinbach, J.; Wuest, F.; Pietzsch, J. Radiosynthesis of a 18F-labeled 2,3-diarylsubstituted indole via McMurry coupling for

functional characterization of cyclooxygenase-2 (COX-2) *in vitro* and *in vivo*. *Bioorg. Med. Chem.*, **2012**, 20, 3410.

[61] Alauddin, M.; Conti, P.; Mathew, T.; Fissekis, J.; Prakash, G.; Watanabe, K. Stereospecific fluorination of 1,3,5-tri-O-benzoyl-alpha-D-ribofuranose-2-sulfonate esters: Preparation of a versatile intermediate for synthesis of 2 '-[F-18]-fluoro-arabinonucleosides. *J. Fluorine Chem.*, **2000**, 106, 87.

[62] Yasojima, K.; Schwab, C.; McGeer, E.G.; McGeer, P.L. Distribution of cyclooxygenase-1 and cyclooxygenase-2 mRNAs and proteins in human brain and peripheral organs. *Brain Res.*, **1999**, 830, 226.

[63] Ho, L.; Pieroni, C.; Winger, D.; Purohit, D.P.; Aisen, P.S.; Pasinetti, G.M. Regional distribution of cyclooxygenase-2 in the hippocampal formation in alzheimer's disease. *J. Neurosci. Res.*, **1999**, 57, 295.

[64] Breder, C.D.; Dewitt, D.; Kraig, R.P. Characterization of inducible cyclooxygenase in rat brain. *J. Comp. Neurol.*, **1995**, 355, 296.

[65] Talley, J.J. Substituted pyrazolyl benzenesulfonamides. U.S. Patent No. 5,466,823. 14 Nov. **1995**.

[66] Riese, J.; Hoff, T.; Nordhoff, A.; DeWitt, D.L.; Resch, K.; Kaever, V. Transient expression of prostaglandin endoperoxide synthase-2 during mouse macrophage activation. *J. Leukoc. Biol.*, **1994**, 55, 476.

[67] Guha, M.; Mackman, N. LPS induction of gene expression in human monocytes. *Cell Signal*, **2001**, 13, 85.

[68] Wuest, F.; Kniess, T. Synthesis of 4-[F-18]fluoroiodobenzene and its application in sonogashira cross-coupling reactions. *J. Labelled Compd. Radiopharmaceut.*, **2003**, 46, 699.

[69] Zhang, J.; Yuan, J.; Wang, Y.; Bible, R.; Breau, A. Pharmacokinetics and metabolism of a COX-2 inhibitor, valdecoxib, in mice. *Drug Metab. Disposition.*, **2003**, 31, 491.

[70] Copeland, R.A.; Williams, J.M.; Giannaras, J.; Nurnberg, S.; Covington, M.; Pinto, D.; Pick, S.; Trzaskos, J.M. Mechanism of selective inhibition of the inducible isoform of prostaglandin G/H synthase. *Proc. Natl. Acad. Sci. U S A*, **1994**, 91, 11202.

[71] Joshi, A.; Raghavan, N.; Williams, R.; Takahashi, K.; Shingu, H.; King, S. Simultaneous quantification of an antiinflammatory compound (DuP-697) and a potential metabolite (X6882) in human plasma and urine by high-performance liquid chromatography. *J. Chromatogr., B: Anal. Technol. Biomed. Life Sci.,* **1994**, 660, 143.

[72] Beswick, P.J.; Blackaby, A.P.; Bountra, C.; Brown, T.; Browning, K.; Campbell, I.B.; Corfield, J.; Gleave, R.J.; Guntrip, S.B.; Hall, R.M.; Hindley, S.; Lambeth, R.F.; Lucas, F.; Mathews, N.; Naylor, A.; Player, H.; Price, H.S.; Sidebottom, P.J.; Taylor, N.L.; Webb, G.; Wiseman, J. Identification and optimisation of a novel series of pyrimidine based cyclooxygenase-2 (COX-2) inhibitors: utilisation of a biotransformation approach. *Bioorg. Med. Chem.Lett.*, **2009**, 19, 4509.

[73] Leblanc, Y.; Gauthier, J.; Ethier, D.; Guay, J.; Mancini, J.; Riendeau, D.; Tagari, P.; Vickers, P.; Wong, E.; Prasit, P. Synthesis and biological evaluation of 2,3-diarylthiophenes as selective COX-2 and COX-1 inhibitors. *Bioorg. Med. Chem. Lett.*, **1995**, 5, 2123.

[74] Pinto, D.J.P.; Copeland, R.A.; Covington, M.B.; Pitts, W.J.; Batt, D.G.; Orwat, M.J.; Lam, G.N.; Joshi, A.; Chan, Y.; Wang, S.; Trzaskos, J.M.; Magolda, R.L.; Kornhauser, D.M. Chemistry and pharmacokinetics of diarylthiophenes and terphenyls as selective COX-2 inhibitors. *Bioorg. Med. Chem. Lett.*, **1996**, 6, 2907.

[75] Praveen Rao, P.N.; Amini, M.; Li, H.; Habeeb, A.G.; Knaus, E.E. Design, synthesis, and biological evaluation of 6-substituted-3-(4-methanesulfonylphenyl)-4-phenylpyran-2-ones: A novel class of diarylheterocyclic selective cyclooxygenase-2 inhibitors. *J. Med. Chem.*, **2003**, 46, 4872.

[76] Yang, D.J.; Bryant, J.; Chang, J.Y.; Mendez, R.; Oh, C.; Yu, D.; Ito, M.; Azhdarinia, A.; Kohanim, S.; Kim, E.E.; Lin, E.; Podoloff, D.A. Assessment of cyclooxygense-2 expression with 99m-Tc-labeled celebrex. *Anticancer Drugs*, **2004**, 15, 255.

[77] Kabalka, G.; Mereddy, A.; Schuller, H. Synthesis of an iodine-123-labeled celecoxib analogue: A potential spect agent. *J. Labelled Compd. Radiopharmaceut.*, **2005**, 48, 295.

[78] Kuge, Y.; Katada, Y.; Shimonaka, S.; Temma, T.; Kimura, H.; Kiyono, Y.; Yokota, C.; Minematusa, K.; Seki, K.; Tamaki, N.; Ohkura, K.; Saji, H. Synthesis and evaluation of radioiodinated cyclooxygenase-2 inhibitors as potential SPECT tracers for cyclooxygenase-2 expression. *Nucl. Med. Biol.*, **2006**, 33, 21.

[79] Kuge, Y.; Obokata, N.; Kimura, H.; Katada, Y.; Temma, T.; Sugimoto, Y.; Aita, K.; Seki, K.; Tamaki, N.; Saji, H. Synthesis and evaluation of a radioiodinated lumiracoxib derivative for the imaging of cyclooxygenase-2 expression. *Nucl. Med. Biol.*, **2009**, 36, 869.

[80] Verbruggen, A.M.; Nosco, D.L.; Van Nerom, C.G.; Bormans, G.M.; Adriaens, P.J.; De Roo, M.J. Technetium-99m-L,L-ethylenedicysteine: A renal imaging agent, labeling and evaluation in animals. *J. Nuc. Med.*, **1992**, 33, 551.

[81] Blondeau, P.; Berse, C.; Gravel, D. Dimerization of an intermediate during the sodium in liquid ammonia reduction of l-thiazolidine-4-carboxylic acid. *Can. J. Chem.*, **1967**, 45, 49.

[82] Ilgan, S.; Yang, D.J.; Higuchi, T.; Zareneyrizi, F.; Bayhan, H.; Yu, D.; Kim, E.E.; Podoloff, D.A. 99mTc-ethylenedicysteine-folate: A new tumor imaging agent. synthesis, labeling and evaluation in animals. *Can. Biother. Radiopharm.*, **1998**, 13, 427.

[83] Zareneyrizi, F.; Yang, D.; Oh, C.; Ilgan, S.; Yu, D.; Tansey, W.; Liu, C.; Kim, E.E.; Podoloff, D.A. Synthesis of [Tc-99m]ethylenedicysteine-colchicine for evaluation of antiangiogenic effect. *Anticancer Drugs*, **1999**, 10, 685.

[84] Yang, D.J.; Azhdarinia, A.; Wu, P.; Yu, D.F.; Tansey, W.; Kalimi, S.K.; Kim, E.E.; Podoloff, D.A. *In vivo* and *in vitro* measurement of apoptosis in breast cancer cells using 99mTc-EC-annexin V. *Can. Biother Radiopharm.*, **2004**, 16, 73.

[85] Chang, H.C.; Weng, C.F. Cyclooxygenase-2 level and culture conditions influence NS398-induced apoptosis and caspase activation in lung cancer cells. *Oncol. Rep.*, **2001**, 8, 1321.

[86] Awara, W.M.; Alaa, E.E.; Magda, E.E.; Ahmed, E.G. The potential role of cyclooxygenase-2 inhibitors in the treatment of experimentally-induced mammary tumour: Does celecoxib enhance the anti-tumour activity of doxorubicin? *Pharmacol. Res.*, **2004**, 50, 487.

[87] Schuller, H.; Kabalka, G.; Smith, G.; Mereddy, A.; Akula,M.; Cekanova, M. Detection of overexpressed COX-2 in precancerous lesions of hamster pancreas and lungs by molecular imaging: Implications for early diagnosis and prevention. *Chem. Med. Chem.*, **2006**, 1, 603.

[88] Schuller, H.M.; Mechanisms of smoking-related lung and pancreatic adenocarcinoma development. *Nat. Rev. Can.*, **2002**, 2, 455.

[89] Schuller, H.; Zhang, L.; Weddle, D.; Castonguay, A.; Walker, K.; Miller, M. The cyclooxygenase inhibitor ibuprofen and the FLAP inhibitor MK886 inhibit pancreatic carcinogenesis induced in hamsters by transplacental exposure to ethanol and the tobacco carcinogen NNK. *J. Cancer Res. Clin. Oncol.*, **2002**, 128, 525.

[90] Schuller, H.; Cekanova, M. NNK-induced hamster lung adenocarcinomas over-express β2-adrenergic and EGFR signaling pathways. *Lung Cancer*, **2005**, 49, 35.

[91] Esser, R.; Berry, C.; Du, Z.; Dawson, J.; Fox, A.; Fujimoto, R.A.; Heston, W.; Kimble, E.F.; Koehler, J.; Peppard, J.; Quadros, E.; Quintavalla, J.; Toscano, K.; Urban, L.; van Duzer, J.; Zhang, X.; Zhou, S.; Marshall, P.J. Preclinical pharmacology of lumiracoxib: A novel selective inhibitor of cyclooxygenase-2. *Br. J. Pharmacol.*, **2005**, 144, 538.

[92] Buvanendran, A.; Barkin, R. Lumiracoxib. *Drugs Of Today*, **2007**, 43, 137.

[93] Bannwarth, B.; Berenbaum, F. Clinical pharmacology of lumiracoxib, a second-generation cyclooxygenase 2 selective inhibitor. *Expert Opin. Investig. Drugs.*, **2005**, 14, 521.

[94] Medzhitov, R. Origin and physiological roles of inflammation. *Nature*, **2008**, 454, 428.

[95] Debucquoy, A.; Devos, E.; Vermaelen, P.; Landuyt, W.; De Weer, S.; Van Den Heuvel, F.; Haustermans, K. 18F-FLT and 18F-FDG PET to measure response to radiotherapy combined with celecoxib in two colorectal xenograft models. *Int. J. Radiat. Biol.,* **2009**, 85, 763.

CHAPTER 3

Chemistry and Radiochemistry

This chapter is published as **Tietz, O**; Sharma, S; Kaur, J; Way, J; Marshall, A; Wuest, M; Wuest, F. "Synthesis of three ^{18}F-labelled Cyclooxygenase-2 (COX-2) Inhibitors based on a Pyrimidine Scaffold." *Org. Biomol. Chem.*, **2013**, 11(46), 8052.

3.1. Introduction

Cyclooxygenases (COXs) control the complex conversion of arachidonic acid (AA) into prostaglandins and thromboxanes, which function as locally active messenger molecules and trigger important physiological and pathophysiological processes. The COX enzyme family consists of a constitutively expressed isoform (COX-1) and an inducible isoform (COX-2). Recently, a third isoform, believed to be a COX-1 splice variant, has been reported as COX-3 [1]. Both COX-1 and COX-2 convert arachidonic acid to Prostaglandin H_2. In the first step of the reaction COXs cyclise AA to Prostaglandin G_2 which then is rapidly converted into PGH_2 by a peroxidase reaction at a second catalytic site in the same enzyme. Most COX inhibitors derive their therapeutic potential by blocking the first catalytic site of the COX enzymes. PGH_2 is converted to a variety of different prostaglandins by a number of downstream enzymes. These prostaglandins mediate various physiological processes by binding to G-protein coupled receptors [2].

The conformations of the two COX isoforms are very similar, as are the amino acids sequences that constitute the substrate-binding pocket [3]. Given these similarities, the development of COX-2 selective inhibitors has been a great challenge [4]. Since the identification of the COX-2 isoform in the early 1990's, a number of selective inhibitors have been developed. A selection of these molecules has been used extensively in clinical application. In 2005, most of these drugs were withdrawn from market following concerns over their cardiac safety profile. Among the most widely used selective COX-2 inhibitors (coxibs) were celecoxib, rofecoxib and valdecoxib [5]. More recently, the underlining biochemical mechanisms of the cardiac toxicity of the coxib compound class are starting to be unravelled [6, 7].

COX-1 functions as a housekeeping enzyme and is expressed in most resting tissues, its responsibilities include the maintenance of gastric and renal integrity [8]. COX-2 is expressed in the resting tissue of the brain and the kidney, but virtually absent in all other tissue types [9, 10]. COX-2 expression is induced in response to and maintains various acute and chronic inflammatory conditions. Expression can be triggered in fibroblast, epithelial, endothelial, macrophage, and smooth muscle cells in response to growth factors, cytokines, and pro-inflammatory stimuli [11]. Some studies have suggested that COX-2 is also involved in neurodegenerative diseases such as Parkinson's and Alzheimer's disease [12]. Elevated COX-2 expression has furthermore been found in a variety of human cancers, most prominently colorectal, gastric, and breast cancer [13-15].

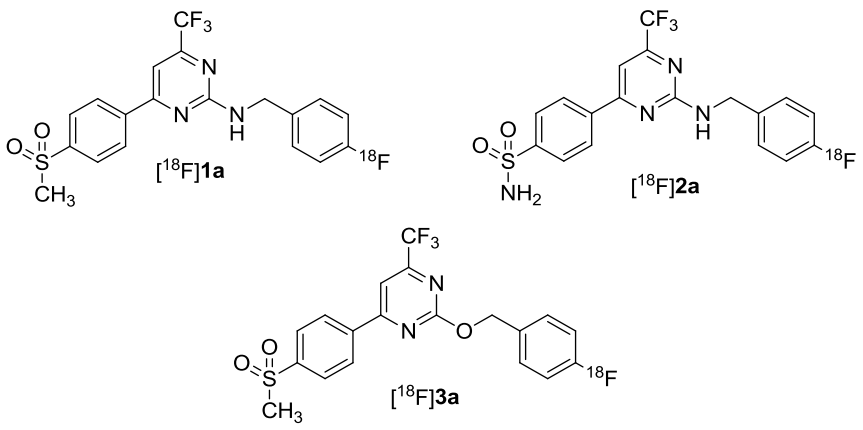

Figure 3-1: Structures of [^{18}F]**1a**, [^{18}F]**2a** and [^{18}F]**3a**

Some of the key signalling pathways involving effects of COX-2 in inflammation and tumorigenesis have been dissected [16]. There are, however, discrepancies between potent anticancer effects of COX-2 inhibitors *in vitro* and their failure in the majority of clinical trials [17].

The role that the COX-2 enzyme plays in the development and progression of various diseases appears to be very complex and requires more basic research on COX-2 pharmacology. An exact and accurate assessment of COX-2 expression levels and activity in tissues under different disease conditions is of vital importance to these efforts. To date, an exact assessment of COX-2 expression can only be achieved by *ex vivo* analysis. This type of analysis is relatively complex due to the instability of COX-2 mRNA *ex vivo* [18].

Non-invasive monitoring of COX-2 expression *in vivo* would further advance efforts into elucidating basic pharmacology of the enzyme. Over the past decade a number of COX-2 inhibitors have been radiolabeled with ^{11}C, ^{18}F, ^{99m}Tc,^{123}I and ^{125}I to assess COX-2 expression *in vivo* using positron emission tomography (PET) and single photon emission computed tomography (SPECT). Among the radiolabeled compounds were celecoxib [19-27], rofecoxib [28-30] and a number of novel structures [31-34]. Despite the large number of radiolabeled COX-2 inhibitors, COX-2 mediated uptake of a radiotracer in an *in vivo* model has not yet convincingly been demonstrated.

3.1.1. Objectives

The aim of this study is to develop a novel class of highly potent and selective radiolabeled COX-2 inhibitors as radiotracers for molecular imaging of COX-2 expression *in vivo* (Fig.3-1). The lead structure for this investigation is compound **1a**, which was originally reported by Swarbrick and co-workers [35].

3.2. Materials and Methods

3.2.1. Chemistry

All reagents and solvents were obtained from Sigma-Aldrich, unless otherwise stated and used without further purification. Nuclear magnetic resonance spectra were recorded on a 400 MHz Varian unit and a 600 MHz Burker unit. ^{1}H-NMR and ^{13}C-NMR chemical shifts are recorded in ppm relative to tetramethylsilane (TMS). ^{19}F-NMR chemical shifts are recorded in ppm relative to trichlorofluoromethane. Low resolution mass spectra were obtained using an Agilent Technologies 6220 TOF instrument. Column chromatography was conducted using Merck silica gel (mesh size 230–400 ASTM). Thin-layer chromatography (TLC) was performed using Merck silica gel F-254 aluminum plates, with visualization under UV light (254 nm). High performance liquid chromatography (HPLC) purifications and analysis were performed using a Phenomenex LUNA® C18 column (100 Å, 250 Å~10 mm, 10 μm) using a Gilson 322 Pump module fitted with a 171 Diode Array and a radio detector. Compounds **4**, **5** and **6** were prepared according to the literature procedure [35]. Compounds **1a**, **1e** and **1f** have been described by Swarbrick et al. [35].

3.2.1.1. General procedure for the synthesis of compounds 1a–1p

Compound **6** (50 mg, 0.13 mmol) was dissolved in CH_3CN (0.75–1.5 ml) and the corresponding amine (0.65 mmol, 5.0 eq.) was added. The reaction vessel was sealed and heated at 140 °C for 2–6 h. The reaction mixture was cooled to room temperature, and 8 ml of 1 N HCl was added. The reaction mixture was stirred, and the precipitating solid was filtered using filter paper. The product was thoroughly washed with cold dionized water.

3.2.1.2. N-(4-Fluorobenzyl)-4-[4-(methylsulfonyl)phenyl]-6-(trifluoromethyl)pyrimidin-2-amine (1a)

Compound **1a** (90.6 mg, 82% yield) was obtained as a pale yellow solid.

^{1}H-NMR (400MHz, $CDCl_3$): 3.10 (s, 3H, SO_2CH_3); 4.72 (s, 2H, CH_2); 5.85 (s, 1H, N-H); 7.04 (m, J=8.8Hz, 2H, Ar-H); 7.33 (s, 1H, Ar-H); 7.37 (m, J=5.27Hz, J=3.22Hz, 2H, Ar-H); 8.07 (m, J=8.8Hz, 2H, Ar-H); 8.22 (m, J=8.8Hz, 2H, Ar-H). ^{13}C-NMR (150MHz, $CDCl_3$): 44.5; 45.1; 102.6; 115.7 (d, ^{2}J(C-F) = 21Hz); 122.0 (q, ^{1}J(C-F) = 275 Hz); 128.0; 128.2; 129.2 (d, ^{3}J(C-F) = 8Hz); 134.1 (d, ^{4}J(C-F) = 3Hz); 141.4; 142.8; 162.2 (d, ^{1}J(C-F) = 245Hz); 162.7 (q, ^{2}J(C-F) = 36 Hz); 165.4; 165.5. ^{19}F-NMR (375MHz, $CDCl_3$)): -70.78 (s, 3F, CF_3); -114.83 (m, 1F, Ar-F). LR-MS: 448.1 [M+Na].

3.2.1.3. N-(4-Chlorobenzyl)-4-[4-(methylsulfonyl)phenyl]-6-(trifluoromethyl)pyrimidin-2-amine (1b)

Compound **1b** (48.4 mg, 84% yield) was obtained as a pale yellow solid.

^{1}H-NMR (400MHz, $CDCl_3$): 3.04 (s, 3H, SO_2CH_3); 4.67 (s, 2H, CH_2); 5.82 (s, 1H, N-H); 7.20 (s, 1H, Ar-H); 7.27 (m, 4H, Ar-H); 8.00 (m, J=8.8Hz, 2H, Ar-H); 8.14 (m, J=8.8Hz, 2H, Ar-H). ^{13}C-NMR (150MHz, $CDCl_3$): 44.5; 45.1; 102.7; 122.0 (q, ^{1}J(C-F) = 275 Hz); 128.0; 128.2; 128.9; 129.5; 133.4; 136.9; 141.4; 142.8; 162.2 (q, ^{2}J(C-F) = 36 Hz); 165.5; 165.6. ^{19}F-NMR (375MHz, $CDCl_3$)): -70.45 (s, 3F, CF_3). LR-MS: 464.0 [M+Na].

3.2.1.4. N-(4-Bromobenzyl)-4-[4-(methylsulfonyl)phenyl]-6-(trifluoromethyl)pyrimidin-2-amine (1c)

Compound **1c** (51.6 mg, 82% yield) was obtained as a pale yellow solid.

^{1}H-NMR (400MHz, $CDCl_3$): 3.10 (s, 3H, SO_2CH_3); 4.71 (s, 2H, CH_2); 5.87 (s, 1H, N-H); 7.28 (m, J=8.5Hz, 2H, Ar-H); 7.33 (s, 1H, Ar-H); 7.48 (m, J=8.5Hz, 2H, Ar-H); 8.07 (m, J=8.8Hz, 2H, Ar-H); 8.20 (m, J=8.8Hz, 2H, Ar-H). ^{13}C-NMR (150MHz, $CDCl_3$): 44.5; 45.1; 102.7; 121.4 (q, ^{1}J(C-F) = 275 Hz); 128.0; 128.2; 129.7; 130.9; 132.5; 137.4; 141.4; 142.8; 162.4 (q, ^{2}J(C-F) = 36 Hz); 165.5; 165.6. ^{19}F-NMR (375MHz, $CDCl_3$)): -70.7 (s, 3F, CF_3). LR-MS: 510.0 [M+Na].

3.2.1.5. N-(4-Trifluorobenzyl)-4-[4-(methylsulfonyl)phenyl]-6-(trifluoromethyl)pyrimidin-2-amine (1d)

Compound **1d** (42.3 mg, 68% yield) was obtained as a white solid.

^{1}H-NMR (400MHz, $CDCl_3$): 3.10 (s, 3H, SO_2CH_3); 4.83 (s, 2H, CH_2); 5.95 (s, 1H, N-H); 7.35 (s, 1H, Ar-H); 7.52 (m, J=8.2Hz, 2H, Ar-H); 7.61 (m, J=8.2Hz, 2H, Ar-H); 8.06 (m, J=8.5Hz, 2H, Ar-H); 8.19 (m, J=8.2Hz, 2H, Ar-H). ^{13}C-NMR (150MHz, $CDCl_3$): 44.5; 45.3; 102.9; 122.1 (q, ^{1}J(C-F) = 275 Hz); 124.0 (q, ^{1}J(C-F) = 271Hz); 125.7; 127.6; 128.0; 128.2; 129.8 (q, ^{2}J(C-F) = 32Hz); 141.3; 142.5; 162.5 (q, ^{2}J(C-F) = 36 Hz); 165.5; 165.6. ^{19}F-NMR (375MHz, $CDCl_3$)): -62.5 (s, 3F, CF_3); -70.7 (s, 3F, CF_3). LR-MS: 498.1 [M+Na].

3.2.1.6. N-(Benzyl)-4-[4-(methylsulfonyl)phenyl]-6-(trifluoromethyl)-pyrimidin-2-amine (1e)

Compound **1e** (42.9 mg, 81% yield) was obtained as a white solid.

^{1}H-NMR (400MHz, $CDCl_3$): 3.10 (s, 3H, SO_2CH_3); 4.76 (s, 2H, CH_2); 5.86 (s, 1H, N-H); 7.30 (m, 1H, Ar-H) 7.32 (s, 1H, Ar-H); 7.36 (m, 2H, Ar-H); 7.40 (m, 2H, Ar-H); 8.10 (m, J=8.8Hz, 2H, Ar-H); 8.22 (m, J=8.5Hz, 2H, Ar-H). ^{13}C-NMR (150MHz, $CDCl_3$): 44.5; 45.8; 102.4; 121.1 (q, ^{1}J(C-F) = 275 Hz); 127.5; 127.6; 128.0; 128.2; 128.7; 138.3; 141.5; 142.7; 162.4 (q, ^{2}J(C-F) = 36 Hz); 165.4; 165.5. ^{19}F-NMR (375MHz, $CDCl_3$)): -70.46 (s, 3F, CF_3). LR-MS: 430.1 [M+Na].

3.2.1.7. N-(4-Methylbenzyl)-4-[4-(methylsulfonyl)phenyl]-6-(trifluoromethyl)pyrimidin-2-amine (1f)

Compound **1f** (42.6 mg, 78% yield) was obtained as a white solid.

^{1}H-NMR (400MHz, $CDCl_3$): 2.35 (s, 3H, CH_3-Ar); 3.10 (s, 3H, SO_2CH_3); 4.71 (s, 2H, CH_2); 5.83 (s, 1H, N-H); 7.16 (m, J=7.9Hz, 2H, Ar-H); 7.29 (m, J=8.2Hz, 2H, Ar-H); 7.30 (s, 1H, Ar-H); 8.06 (m, J=8.5Hz, 2H, Ar-H); 8.22 (m, J=8.2Hz, 2H, Ar-H). ^{13}C-NMR (150MHz, $CDCl_3$): 21.1; 44.5; 45.5; 102.3; 122.2 (q, ^{1}J(C-F) = 275 Hz); 127.6; 128.0; 128.2; 129.4; 135.2; 137.3; 141.6; 142.6; 162.1 (q, ^{2}J(C-F) = 36 Hz); 165.4; 165.5. ^{19}F-NMR (375MHz, $CDCl_3$)): -70.7 (s, 3F, CF_3). LR-MS: 444.1 [M+Na].

3.2.1.8. N-(4-Phenylbenzyl)-4-[4-(methylsulfonyl)phenyl]-6-(trifluoromethyl)pyrimidin-2-amine (1g)

Compound **1g** (31.0 mg, 49% yield) was obtained as a white solid.

^{1}H-NMR (400MHz, $CDCl_3$): 3.10 (s, 3H, SO_2CH_3); 4.80 (s, 2H, CH_2); 5.91 (s, 1H, N-H); 7.33 (s, 1H, Ar-H); 7.36 (m, J=7.3Hz, 1H, Ar-H); 7.46 (m, 4H, Ar-H); 7.59 (m, 4H, Ar-H); 8.07 (m, J=8.8Hz, 2H, Ar-H); 8.24 (m, J=8.2Hz, 2H, Ar-H). ^{13}C-NMR (150MHz, $CDCl_3$): 44.5; 45.1; 103.2; 120.7 (q, ^{1}J(C-F) = 275 Hz); 123.9; 128.0; 128.2; 128.5; 129.0; 130.0; 130.5; 141.2; 142.9; 146.1; 146.2; 147.4; 162.5 (q, ^{2}J(C-F) = 36 Hz); 165.2; 165.3. ^{19}F-NMR (375MHz, $CDCl_3$)): -70.6 (s, 3F, CF_3). LR-MS: 506.1 [M+Na].

3.2.1.9. N-(4-*tert*-Butylbenzyl)-4-[4-(methylsulfonyl)phenyl]-6-(trifluoromethyl)pyrimidin-2-amine (1h)

Compound **1h** (23.9 mg, 40% yield) was obtained as a white solid.

^{1}H-NMR (400MHz, $CDCl_3$): 1.32 (s, 9H, $C(CH_3)_3$); 3.11 (s, 3H, SO_2CH_3); 4.75 (s, 2H, CH_2); 5.90 (s, 1H, N-H); 7.30 (s, 1H, Ar-H); 7.35 (m, J=7.9Hz, 2H, Ar-H); 7.38 (m, J=7.9Hz, 2H, Ar-H); 8.09 (m, J=7.9Hz, 2H, Ar-H); 8.26 (m, J=7.9Hz, 2H, Ar-H). ^{13}C-NMR (150MHz, $CDCl_3$): 31.3; 34.6; 44.5; 45.4; 102.3; 122.5 (q, ^{1}J(C-F) = 275 Hz); 125.6; 128.0; 128.2; 128.8; 135.3; 141.6; 142.6; 150.7; 162.7 (q, ^{2}J(C-F) = 36 Hz); 165.4; 165.5. ^{19}F-NMR (375MHz, $CDCl_3$)): -70.7 (s, 3F, CF_3).

3.2.1.10. N-(4-Methoxybenzyl)-4-[4-(methylsulfonyl)phenyl]-6-(tri-fluoromethyl)pyrimidin-2-amine (1i)

Compound **1i** (111.6 mg, 98% yield) was obtained as a white solid.

^{1}H-NMR (400MHz, $CDCl_3$): 3.10 (s, 3H, SO_2CH_3); 3.81 (s, 3H, CH_3-O); 4.68 (s, 2H, CH_2); 5.80 (s, 1H, N-H); 6.89 (m, J=8.5Hz, 2H, Ar-H); 7.30 (s, 1H, Ar-H); 7.33 (m, J=8.8Hz, 2H, Ar-H); 8.07 (m, J=8.5Hz, 2H, Ar-H); 8.24 (m, J=7.6Hz, 2H, Ar-H). ^{13}C-NMR (150MHz, $CDCl_3$): 44.5; 45.3; 55.3; 102.3; 121.5 (q, ^{1}J(C-F) = 275 Hz); 128.0; 128.2; 129.4; 129.8; 130.3; 141.6; 142.6; 159.1; 162.1 (q, ^{2}J(C-F) = 36 Hz); 165.4; 165.5. ^{19}F-NMR (375MHz, $CDCl_3$)): -70.7 (s, 3F, CF_3). LR-MS: 460.1 [M+Na].

3.2.1.11. N-(4-Nitrobenzyl)-4-[4-(methylsulfonyl)phenyl]-6-(trifluoro-methyl)pyrimidin-2-amine (1j)

The synthesis follows the general method described; with the exception that triethylamine (4.9 eq) was added to the reaction mixture. Compound **1j** (24.1 mg, 41% yield) was obtained as a yellow solid.

^{1}H-NMR (400MHz, $CDCl_3$): 3.10 (s, 3H, SO_2CH_3); 4.88 (s, 2H, CH_2); 6.03 (s, 1H, N-H); 7.37 (s, 1H, Ar-H); 7.57 (m, J=8.5Hz, 2H, Ar-H); 8.07 (m, J=8.5Hz, 2H, Ar-H); 8.20 (m, 4H, Ar-H). ^{13}C-NMR (150MHz, $CDCl_3$): 44.5; 45.1; 102.2; 120.1; 122.0 (q, ^{1}J(C-F) = 275 Hz); 128.0; 128.2; 129.7; 135.2; 141.6; 142.6; 158.5; 162.9 (q, ^{2}J(C-F) = 36 Hz); 165.5; 165.6. ^{19}F-NMR (375MHz, $CDCl_3$)): -70.7 (s, 3F, CF_3). LR-MS: 475.1 [M+Na].

3.2.1.12. N-(Butan-1-ol)-4-[4-(methylsulfonyl)phenyl]-6-(trifluoro-methyl)pyrimidin-2-amine (1k)

Compound **1k** (81.5 mg, 81% yield) was obtained as an off-white solid.

^{1}H-NMR (400MHz, $CDCl_3$): 1.26 (s, 1H, OH); 1.76 (m, 4H, $(CH_2)_2$); 3.12 (s, 3H, SO_2CH_3); 3.70 (m, 4H, $(CH_2)_2$); 4.83 (s, 2H, CH_2); 5.90 (s, 1H, N-H); 7.26 (s, 1H, Ar-H); 8.10 (m, J=7.9Hz, 2H, Ar-H); 8.28 (m, J=7.9Hz, 2H, Ar-H). ^{19}F-NMR (375MHz, $CDCl_3$)): -70.7 (s, 3F, CF_3). LRMS: 412.1 [M+Na].

3.2.1.13. N-(4-Pyridyl)-4-[4-(methylsulfonyl)phenyl]-6-(trifluoro-methyl)pyrimidin-2-amine (1l)

Compound **1l** (30.7 mg, 58% yield) was obtained as an off-white solid.

^{1}H-NMR (400MHz, $CDCl_3$): 3.11 (s, 3H, SO_2CH_3); 5.01 (s, 2H, CH_2); 6.74 (s, 1H, N-H); 7.43 (s, 1H, Ar-H); 7.95 (m, J=5.6Hz, 2H, Ar-H); 8.07 (m, J=8.2Hz, 2H, Ar-H); 8.28 (m, J=8.2Hz, 2H, Ar-H);8.72 (m, J=5.6Hz, 2H, Ar-H). ^{13}C-NMR (150MHz, $CDCl_3$): 44.4; 45.0; 103.9; 113.8; 121.3 (q, ^{1}J(C-F) = 275 Hz); 128.1; 128.2; 128.7; 134.3; 141.2; 143.1; 162.2 (q, ^{2}J(C-F) = 36 Hz); 165.3; 165.4. ^{19}F-NMR (375MHz, $CDCl_3$)): -70.3 (s, 3F, CF_3). LR-MS: 431.1 [M+Na].

3.2.1.14. N-(3-Pyridyl)-4-[4-(methylsulfonyl)phenyl]-6-(trifluoro-methyl)pyrimidin-2-amine (1m)

Compound **1m** (23.8 mg, 45% yield) was obtained as a pale yellow solid.

^{1}H-NMR (400MHz, $CDCl_3$): 3.10 (s, 3H, SO_2CH_3); 4.92 (s, 2H, CH_2); 6.91 (s, 1H, N-H); 7.36 (s, 1H, Ar-H); 7.69 (m, 1H, Ar-H); 8.05 (m, J=7.6Hz, 2H, Ar-H);8.16 (m, J=8.5Hz, 2H, Ar-H);8.34 (s, 1H, Ar-H); 8.62 (m, J=5.2Hz, 1H, Ar-H); 9.09 (m, 1H, Ar-H). ^{13}C-NMR (150MHz, $CDCl_3$): 42.9; 44.5; 103.3; 111.0; 121.1; 121.3 (q, ^{1}J(C-F) = 275 Hz); 125.1; 128.1; 128.2; 128.3; 133.3; 141.1; 142.9; 162.2 (q, ^{2}J(C-F) = 36 Hz); 165.4; 165.5. ^{19}F-NMR (375MHz, $CDCl_3$)): -70.4 (s, 3F, CF_3). LR-MS: 431.1 [M+Na].

3.2.1.15. N-(2-Pyridyl)-4-[4-(methylsulfonyl)phenyl]-6-(trifluoromethyl)pyrimidin-2-amine (1n)

Compound **1n** (8.5 mg, 16% yield) was obtained as a pale yellow solid.

^{1}H-NMR (400MHz, $CDCl_3$): 3.11 (s, 3H, SO_2CH_3); 3.13 (m, 2H, CH_2); 5.17 (s, 1H, N-H); 7.36 (s, 1H, Ar-H); 7.81 (m, J=6.4Hz, 1H, Ar-H); 8.00 (m, J=7.6Hz, 2H, Ar-H); 8.14 (m, J=7.6Hz, 2H, Ar-H); 8.24 (m, J=7.3Hz, 1H, Ar-H); 8.37 (m, J=7.3Hz, 1H, Ar-H); 8.67 (m, J=6.4Hz, 1H, Ar-H). ^{13}C-NMR (150MHz, $CDCl_3$): 42.6; 44.5; 103.5; 113.9; 118.9; 121.5 (q, ^{1}J(C-F) = 275 Hz); 125.3;

128.0; 128.2; 128.9; 134.5; 140.8; 143.0; 161.8 (q, ^{2}J(C-F) = 36 Hz); 165.5; 165.6. ^{19}F-NMR (375MHz, $CDCl_3$)): -70.4 (s, 3F, CF_3). LR-MS: 431.1 [M+Na].

3.2.1.16. N-(2-Fluoroethyl)-4-[4-(methylsulfonyl)phenyl]-6-(trifluoro-methyl)pyrimidin-2-amine (1o)

The synthesis follows the general method described; with the exception that triethylamine (4.9 eq) was added to the reaction mixture. Compound **1o** (26.1 mg, 52% yield) was obtained as a silvery white solid.

^{1}H-NMR (400MHz, $CDCl_3$): 3.12 (s, 3H, SO_2CH_3); 3.92 (m, J=5.5Hz, 2H, CH_2); 4.67 (m, J=5.0Hz, 2H, CH_2); 5.78 (s, 1H, N-H); 7.34 (s, 1H, Ar-H); 8.10 (m, J=7.6Hz, 2H, Ar-H); 8.25 (m, J=7.6Hz, 2H, Ar-H). ^{13}C-NMR (150MHz, $CDCl_3$): 42.1 (d, ^{2}J(C-F) = 20Hz); 44.5; 82.0 (d, ^{1}J(C-F) = 167Hz); 102.7; 121.3 (q, ^{1}J(C-F) = 275 Hz); 128.0; 128.3; 139.5; 142.8; 162.1 (q, ^{2}J(C-F) = 36 Hz); 165.4; 165.5. ^{19}F-NMR (375MHz, $CDCl_3$)): -67.9 (s, 1F, C-F); -70.8 (s, 3F, CF_3). LR-MS: 386.1 [M+Na].

3.2.1.17. N-(Butyl)-4-[4-(methylsulfonyl)phenyl]-6-(trifluoromethyl)-pyrimidin-2-amine (1p)

Compound **1p** (29.5 mg 61% yield) was obtained as a pale yellow solid.

^{1}H-NMR (400MHz, $CDCl_3$): 0.98 (m, J=7.3Hz, 3H, CH_3); 1.47 (m, J=7.0, 7.6Hz, 2H, CH_2); 1.67 (m, J=7.0, 7.6Hz, 2H, CH_2); 3.11 (s, 3H, SO_2CH_3); 3.59 (m, J=6.1, 6.4Hz, 2H, CH_2); 4.83 (s, 2H, CH_2); 5.48 (s, 1H, N-H); 7.26 (s, 1H, Ar-H); 8.10 (m, J=8.2Hz, 2H, Ar-H); 8.27 (m, J=8.2Hz, 2H, Ar-H). ^{13}C-NMR (150MHz, $CDCl_3$): 13.8; 20.0; 31.4; 41.5; 44.5; 101.7; 121.5 (q, ^{1}J(C-F) = 275

Hz); 128.2; 128.5; 140.3; 143.4; 161.2 (q, ^{2}J(C-F) = 36 Hz); 165.3; 165.4. ^{19}F-NMR (375MHz, $CDCl_3$)): -70.7 (s, 3F, CF_3). LR-MS: 396.1 [M+Na].

3.2.1.18. 2-[(4-Fluorobenzyl)oxy]-4-[4-(methylsulfonyl)phenyl]-6-(trifluoromethyl)pyrimidine (3a)

To a solution of 33 mg 4-fluorobenzyl alcohol (0.26mmol) in 3 mL of dry THF in an inert atmosphere and at 0 °C was added 11 mg of 60% NaH suspension. After 5 min, 100 mg of 2-(methylsulfonyl)-4-[4-(methylsulfonyl)phenyl]-6-(trifluoromethyl)pyrimidine **6** (0.26mmol) was added in small portions. The reaction mixture was stirred at 0 °C for 1 hour and quenched by adding an excess of 1 N HCl. Compound **3a** was extracted in ethyl acetate. The organic layer was washed with water, dried over sodium sulfate and solvent removed in vacuo. Compound **3a** was purified using a silica column eluting at 1% MeOH/CH_2Cl_2 and obtained as a white solid (78.6 mg, 71% yield).

^{1}H-NMR (600MHz, $CDCl_3$): 3.05 (s, 3H, SO_2CH_3); 5.47 (s, 2H, CH_2); 7.01 (m, J=8.2Hz, 2H, Ar-H); 7.46 (m, J=8.2Hz, 2H, Ar-H); 7.65 (s, 1H, Ar-H); 8.04 (m, J=8.4Hz, 2H, Ar-H); 8.24 (m, J=8.4Hz, 2H, Ar-H). ^{13}C-NMR (150MHz, $CDCl_3$): 44.4; 69.7; 107.1; 115.5 (d, ^{2}J(C-F) = 21Hz); 121.1 (q, ^{1}J(C-F) = 275 Hz); 128.2; 128.5; 130.7 (d, ^{3}J(C-F) = 9Hz); 131.3 (d, ^{4}J(C-F) = 3Hz); 140.3; 143.4; 159.1 (q, ^{2}J(C-F) = 36 Hz); 162.7 (d, ^{1}J(C-F) = 247Hz); 165.6; 167.4. ^{19}F-NMR (565MHz, $CDCl_3$)): -71.1 (s, 3F, CF_3); -114.1 (m, 1F, Ar-F). LR-MS: 449.1 [M+Na].

3.2.1.19. *N-tert*-Butyl-4-[2-(methylsulfanyl)-6-(trifluoromethyl)-pyrimidin-4-yl]benzenesulfonamide (7)

4-Chloro-2-(methylsulfonyl)-6-(trifluoromethyl)pyrimidine (Key Organics Ltd, Camelford, UK) (1.0 g, 4.42 mmol), *tert*-butyl 4-boronobenzenesulfonamide (Combi-Blocks Inc, San Diego, US) (1.25 g, 4.8 mmol) and tetrakis-triphenylphosphinepalladium(0) (100 mg) were dissolved in 70 ml of DME and 1.15 g of sodium carbonate in water (11 mL) added dropwise. The reaction mixture was heated under reflux for 15 hours. The solvent was reduced on a rotary evaporator and the residue partitioned between ethyl acetate and water; the organic phase was dried using sodium sulfate and concentrated in vacuo. The compound was purified using a silica column, eluting at 30% ethyl acetate/hexanes. The title compound **11** (1.27 g, 69 % yield) was obtained as a pale yellow solid. LR-MS: 444.1 [M+Na]. Low resolution mass spectrometry indicates that product is the sulfoxide. However, the product can be used directly in the next step involving oxidation with Oxone™.

3.2.1.20. *N-tert*-Butyl-4-[2-(methylsulfonyl)-6-(trifluoromethyl)-pyrimidin-4-yl]benzenesulfonamide (8)

Compound **7** (1.2 g, 2.85 mmol) was dissolved in 100 ml of dichloromethane. A solution of Oxone™ (4.37 g, 7.13 mmol) in 50 ml of water was added in small portions, and the mixture was stirred at room temperature. After 18 h, solvent was reduced on a rotary evaporator and the residue partitioned between ethyl acetate and water; the organic phase was dried over sodium sulfate and concentrated in vacuo. The title compound **8** (1.08 g, 87% yield) was obtained as a white solid. ^{1}H-NMR (600MHz, DMSO-d_6): 1.18 (s, 9H, $(CH_3)_3$); 3.64 (s, 3H, SO_2CH_3); 7.87 (s, 1H, NH); 8.13 (m, J=9.0, 2H, Ar-H); 8.69 (m, J=9.0Hz, 2H, Ar-H); 9.04 (s, 1H, Ar-H). ^{13}C-NMR (150MHz,

DMSO-d_6): 30.2; 39.6; 54.0; 117.5; 121.6 (q, ^{1}J(C-F) = 275 Hz); 127.5; 129.5; 137.0; 148.6; 158.7 (q, ^{2}J(C-F) = 36 Hz); 166.4; 167.2. ^{19}F-NMR (565MHz, DMSO-d_6): -69.02 (s, 3F, CF_3). LR-MS: 460.1 [M+Na].

3.2.1.21. 4-[2-(Methylsulfonyl)-6-(trifluoromethyl)pyrimidin-4-yl]benzenesulfonamide (9)

110 mg of compound **8** (0.252 mmol) was dissolved in 4 ml of nitromethane and 50 mg of scandium triflate was added. The mixture was heated at 80 ^{o}C overnight and subsequently concentrated in vacuo. The residue was partitioned between ethyl acetate and water; the organic phase was dried using sodium sulfate and concentrated in vacuo. Compound **9** (85 mg, 88 % yield) was obtained as a light brown solid.

^{1}H-NMR (600MHz, DMSO-d_6): 3.64 (s, 3H, SO_2CH_3); 7.68 (s, 2H, NH_2); 8.12 (m, J=8.4, 2H, Ar-H); 8.70 (m, J=8.4Hz, 2H, Ar-H); 9.05 (s, 1H, Ar-H). ^{13}C-NMR (150MHz, DMSO-d_6): 39.6; 117.5; 121.6 (q, ^{1}J(C-F) = 275 Hz); 126.8; 129.5; 137.0; 148.2; 156.7 (q, ^{2}J(C-F) = 36 Hz); 166.4; 167.3. ^{19}F-NMR (565MHz, DMSO-d_6): -69.00 (s, 3F, CF_3). LR-MS: 404.0 [M+Na].

3.2.1.22. General procedure for the synthesis of compounds 2a– 2e

Compound **9** (50 mg, 0.13 mmol) was dissolved in 1.5 ml of acetonitrile and corresponding amine (0.65 mmol, 5.0 eq) was added. The reaction vessel was sealed and heated at 140 ^{o}C for 2 to 6 hours. Solvent was removed on a rotary evaporator and the residue partitioned between ethyl acetate and 1N HCl. The organic layer was washed dried over sodium sulfate and solvent removed in vacuo. Further impurities were removed by purification on a silica column.

3.2.1.23. 4-{2-[(4-Fluorobenzyl)amino]-6-(trifluoromethyl)pyrimidin-4-yl}benzenesulfonamide (2a)

Compound **2a** (90.6 mg, 82 % yield) was obtained as a yellow solid.

^{1}H-NMR (600MHz, DMSO-d_6): 4.70 (s, 2H, CH_2); 7.21 (m, J=8.8Hz, 2H, Ar-H); 7.51 (m, J=8.8Hz, 2H, Ar-H); 7.57 (s, 2H, SO_2NH_2); 7.71 (s, 1H, Ar-H); 8.43 (m, J=8.8Hz, 2H, Ar-H); 8.62 (m, J=8.8Hz, 2H, Ar-H). ^{13}C-NMR (150MHz, DMSO-d_6): 44.1; 101.8; 115.5 (d, ^{2}J(C-F) = 23Hz); 121.5 (q, ^{1}J(C-F) = 275 Hz); 126.6; 128.4; 129.8 (d, ^{3}J(C-F) = 8Hz); 136.4 (d, ^{4}J(C-F) = 3Hz); 139.2; 146.9; 157.1 (q, ^{2}J(C-F) = 36 Hz); 161.6 (d, ^{1}J(C-F) = 243Hz); 162.5; 166.1. ^{19}F-NMR (565MHz, DMSO-d_6)): -70.03 (s, 3F, CF_3); -117.08 (m, 1F, Ar-F). LR-MS: 449.1 [M+Na].

3.2.1.24. 4-[2-(Benzylamino)-6-(trifluoromethyl)pyrimidin-4-yl]benzenesulfonamide (2b)

Compound **2b** (48.4 mg, 84 % yield) was obtained as a dark yellow solid.

^{1}H-NMR (600MHz, DMSO-d_6): 4.71 (s, 2H, CH_2); 7.28 (m, 1H, Ar-H); 7.39 (m, J=8.8Hz, 2H, Ar-H); 7.47 (m, J=8.8Hz, 2H, Ar-H); 7.57 (s, 2H, SO_2NH_2); 7.71 (s, 1H, Ar-H); 8.03 (m, J=8.8Hz, 2H, Ar-H); 8.42 (m, J=8.8Hz, 2H, Ar-H). ^{13}C-NMR (150MHz, DMSO-d_6): 44.8; 101.7; 121.2 (q, ^{1}J(C-F) = 275 Hz); 126.6; 127.3; 128.3; 128.8; 129.4; 139.3; 140.2; 146.9; 157.1 (q, ^{2}J(C-F) = 36 Hz); 162.7; 166.1. ^{19}F-NMR (565MHz, DMSO-d_6)): -70.03 (s, 3F, CF_3).LR-MS: 431.1 [M+Na].

3.2.1.25. 4-{2-[(4-Methylbenzyl)amino]-6-(trifluoromethyl)pyrimidin-4-yl}benzenesulfonamide (2c)

Compound **2c** (49.8 mg, 91 % yield) was obtained as a brown solid.

^{1}H-NMR (600MHz, DMSO-d_6): 2.31 (s, 3H, CH_3); 4.66 (s, 2H, CH_2); 7.18 (m, J=8.8Hz, 2H, Ar-H); 7.33 (m, J=8.8Hz, 2H, Ar-H); 7.57 (s, 2H, SO_2NH_2); 7.70 (s, 1H, Ar-H); 8.03 (m, J=8.8Hz,

2H, Ar-H); 8.43 (m, J=8.8Hz, 2H, Ar-H). ^{13}C-NMR (150MHz, DMSO-d_6): 38.5; 44.5; 101.6; 121.2 (q, ^{1}J(C-F) = 275 Hz); 126.6; 127.8; 128.4; 129.3; 136.7; 137.2; 139.3; 146.9; 157.1 (q, ^{2}J(C-F) = 36 Hz); 162.7; 166.1. ^{19}F-NMR (565MHz, DMSO-d_6)): -70.04 (s, 3F, CF_3). LR-MS: 445.1 [M+Na].

3.2.1.26. 4-{2-[(4-methoxybenzyl)amino]-6-(trifluoromethyl)pyrimidin-4-yl}benzenesulfonamide (2d)

Compound **2d** (32.5 mg, 57 % yield) was obtained as a dark yellow solid.

^{1}H-NMR (600MHz, DMSO-d_6): 3.72 (s, 1H, CH_3); 4.60 (s, 2H, CH_2); 6.89 (m, J=8.8Hz, 2H, Ar-H); 7.34 (m, J=8.8Hz, 2H, Ar-H); 7.52 (s, 2H, SO_2NH_2); 7.64 (s, 1H, Ar-H); 7.97 (m, J=8.8Hz, 2H, Ar-H); 8.38 (m, J=8.8Hz, 2H, Ar-H). ^{13}C-NMR (150MHz, DMSO-d_6): 44.2; 55.5; 101.6; 115.6; 121.1 (q, ^{1}J(C-F) = 275 Hz); 126.6; 128.8; 129.2; 132.1; 139.3; 146.9; 157.1 (q, ^{2}J(C-F) = 36 Hz); 158.7; 162.7; 165.6. ^{19}F-NMR (565MHz, DMSO-d_6)): -70.05 (s, 3F, CF_3).LR-MS: 461.1 [M+Na].

3.2.1.27. 4-[2-(Butylamino)-6-(trifluoromethyl)pyrimidin-4-yl]benzene-sulfonamide (2e)

Compound **2e** (31.4 mg, 65 %) was obtained as a dark yellow solid.

^{1}H-NMR (600MHz, DMSO-d_6): 0.98 (m, J=7.2Hz, 4H, $(CH_2)_2$); 1.44 (m, J=7.2Hz, 3H, CH_3); 1.64 (m, J=7.2Hz, 2H, CH_2); 7.57 (s, 2H, SO_2NH_2); 7.65 (s, 1H, Ar-H); 8.05 (m, J=8.8Hz, 2H, Ar-H); 8.43 (m, J=8.8Hz, 2H, Ar-H). ^{13}C-NMR (150MHz, DMSO-d_6): 14.2; 20.0; 31.2; 41.0; 101.6; 121.1 (q, ^{1}J(C-F) = 275 Hz); 126.6; 128.9; 139.5; 146.8; 157.1 (q, ^{2}J(C-F) = 36 Hz); 162.8; 165.7. ^{19}F-NMR (565MHz, DMSO-d_6)): -70.08 (s, 3F, CF_3).LR-MS: 397.1 [M+Na].

3.2.1.28. 2-[(4-Iodobenzyl)oxy]-4-[4-(methylsulfonyl)phenyl]-6-(trifluoromethyl)pyrimidine (10)

677 mg of 4-iodobenzyl alcohol (2.89 mmol) was dissolved in 25ml of dry THF in an inert gas atmosphere and at 0 °C, 115mg of 60% NaH (2.89 mmol) was added to the stirring mixture. After 5 min, 1.0 g of compound **6** (2.63 mmol) was added. The reaction mixture was stirred at 0 °C for 1 h and quenched by adding an excess of 1 N HCl. The title compound was extracted in ethyl acetate. The organic layer was washed with water, dried over sodium sulfate and solvent removed in vacuo. Compound **10** was purified using a silica column eluting at 1% MeOH/CH_2Cl_2 and obtained as a pale yellow solid (1.0 g, 71% yield).

^{1}H-NMR (600MHz, DMSO-d_6): 3.15 (s, 3H, SO_2CH_3); 5.55 (s, 2H, CH_2); 7.32 (m, J=8.4Hz, 2H, Ar-H); 7.75 (s, 1H, Ar-H); 7.75 (m, J=8.4Hz, 2H, Ar-H); 8.14 (m, J=8.4Hz, 2H, Ar-H); 8.33 (m, J=8.4Hz, 2H, Ar-H). ^{13}C-NMR (150MHz, DMSO-d_6): 43.7; 69.3; 95.0; 108.5; 121.7 (q, ^{1}J(C-F) = 275 Hz); 123.6; 128.1; 129.2; 131.0; 137.2; 139.8; 143.7; 157.9 (q, ^{2}J(C-F) = 36 Hz); 165.3; 167.7. ^{19}F-NMR (375MHz, DMSO-d_6)): -71.0 (s, 3F, CF_3). LR-MS: 557.0 [M+Na].

3.2.1.29. 2-[(4-Iodylbenzyl)oxy]-4-[4-(methylsulfonyl)phenyl]-6-(tri-fluoromethyl)pyrimidine (**11**)

500 mg of compound **10** (0.93 mmol) was dissolved in 100 mL of MeOH and Oxone^{TM} (2.8 g, 4.65 mmol) in 40 ml of H_2O was added drop wise. The reaction mixture was heated at 60 °C for 6 hours, cooled on ice and diluted excess water. The forming precipitate was filtered off, washed with water and dried under vacuum. The compound was purified on a silica column eluting from 10 to 50% MeOH/CH_2Cl_2. Compound **11** was obtained as a white solid (353 mg, 67 % yield).

^{1}H-NMR (600 MHz, DMSO-d_6): 3.30 (s, 3H, SO_2CH_3); 5.67 (s, 2H, CH_2); 7.76 (m, J=8.4Hz, 2H, Ar-H); 8.00 (m, J=8.4Hz, 2H, Ar-H); 8.14 (m, J=8.4Hz, 2H, Ar-H); 8.38 (s, 1H, Ar-H); 8.59 (m, J=8.4Hz, 2H, Ar-H). ^{13}C-NMR (150MHz, DMSO-d_6): 43.7; 69.3; 108.6; 121.7 (q, ^{1}J(C-F) = 275 Hz); 127.2; 128.1; 129.3; 131.0; 139.7; 139.8; 144.2; 151.2; 158.0 (q, ^{2}J(C-F) = 36 Hz); 165.3; 167.7. ^{19}F-NMR (560 MHz, DMSO-d_6)): -68.5 (s, 3F, CF_3). LR-MS: 589.0 [M+Na].

3.2.2. *In vitro* COX inhibition assay

The ability of celecoxib and compounds **1a-1p**, **2a-2e**, **3a** to inhibit ovine COX-1 and recombinant human COX-2 was determined using a COX fluorescence inhibitor assay (Cayman Chemical, Ann Arbor, USA; catalog #: 700100) according to the manufacturers protocol. Compounds were assayed in a concentration range of 10^{-9} to 10^{-3} M. PRISM5 software was used to calculate IC_{50} values.

3.2.3. Molecular docking studies

The molecular docking experiments were performed using crystal coordinates from the X-ray crystal structure of COX-1 (ovine, 1EQG, ibuprofen bound in the active site) and COX-2 (murine, 6COX, SC558 bound in the active site) were obtained from the protein data bank [48, 49]. Compounds were built using the builder toolkit of the software package ArgusLab 4.0.1 (Mark, A. ArgusLab, Version 4.0.1; Thompson Planaria Software LLC: Seattle, WA) and energy minimized using the semi-empirical quantum mechanical method PM3. The monomeric structure of the enzyme was chosen and the active site was defined around the ligand. The molecule to be docked in the active site of the enzyme was inserted in the work space carrying the structure of the enzyme. The docking program implements an efficient grid based docking algorithm, which

approximates an exhaustive search within the free volume of the binding site cavity. The conformational space was surveyed by the geometry optimization of the flexible ligand (rings are treated as rigid) in combination with the incremental construction of the ligand torsions. Thus, docking occurred between the flexible ligand parts of the compound and enzyme. The ligand orientation was determined by a shape scoring function based on Ascore and the final positions were ranked by lowest interaction energy values. The interaction is the sum of the energies involved in H-bond interactions, hydrophobic interactions and van der Waal's interactions. H-bond and hydrophobic interactions between the compound and the enzyme were explored by distance measurements.

3.2.4. Radiochemistry

No-carrier-added (n.c.a.) [^{18}F]fluoride was produced via the ^{18}O(p,n)^{18}F nuclear exchange reaction from [^{18}O]H_2O (Rotem Industries, Hyox oxygen-18 enriched water) on an ACSI TR19/9 Cyclotron (Advanced Cyclotron Systems Inc., Burnaby, Canada). [^{18}F]fluoride was trapped on a Waters SepPak® light QMA anion exchange cartridge. Radiosynthesis of 4-[^{18}F]fluorobenzylamine ([^{18}F]FBA) followed the procedure published by Way et al [42]. Please refer to the publication for a detailed description of the procedure.

3.2.4.1. Synthesis of [^{18}F]1a

To 6 mg of compound **6** was added [^{18}F]FBA in 1 ml of THF (typically 1 GBq of [^{18}F]FBA) in a sealed vessel. The reaction vessel was heated at 140^{o}C for 30 min. The mixture was diluted in 10 mL water and passed onto a SepPak® C18 cartridge, the cartridge was washed with 5 ml water and the title compound eluted using 3 ml of CH_3CN. The volume of the solvent was reduced on a

rotary evaporator to prepare a 1 ml 70/30 CH_3CN/H_2O formulation for HPLC injection. The compound was purified using HPLC (HPLC conditions: isocratic 70/30 CH_3CN/H_2O; flow rate 3 ml/min) and the product collected at retention time of 12.6 min. The solvent was evaporated using a rotary evaporator under vacuum at 30°C.

3.2.4.2. Synthesis of [^{18}F]2a

The synthesis of [^{18}F]**2a** follows the same procedure as the synthesis of [^{18}F]**1a**, excepting that [^{18}F]FBA was heated with 6 mg of compound **9** and that the desired product elutes of the HPLC after 11.1 min.

3.2.4.3. Synthesis of [^{18}F]3a

N.c.a. [^{18}F]fluoride was eluted off the QMA cartridge in Kryptofix (K_{222}) and K_2CO_3 in CH_3CN. [^{18}F]fluoride was dried under azotropic conditions, using a steady stream of nitrogen at 95 °C while adding 5 ml of CH_3CN to the mixture. To the dried [^{18}F]fluoride was added compound **11** (1 mg) dissolved in DMF (300 µl). The mixture was heated at 180°C for 20 min, 0.1 M pH 5.3 NaOAc buffer (10 ml) was added and the mixture passed through a SepPak® C18 cartridge. The cartridge was washed with water (5 ml) and [^{18}F]**3a** was eluted using acetonitrile (3 ml). The volume of the solvent was reduced on a rotary evaporator to prepare a 1 ml 70/30 CH_3CN/H_2O formulation for HPLC injection. The compound was purified using HPLC (HPLC conditions: isocratic 70/30 CH_3CN/H_2O; flowrate 3 ml/min) and the product collected at retention time of 13.4 min. The solvent was evaporated using a rotary evaporator under vacuum at 30°C.

3.2.6. Octanol-Water partition coefficient

The lipophilicity of [^{18}F]**1a**, [^{18}F]**2a** and [^{18}F]**3a** was determined by adding 10 MBq of compound the respective radiotracer in a mixture of 5ml octanol and 5 ml phosphate-buffered saline (PBS) at pH 7.4. The mixture was shaken for 30 min and the layers separated. A 10 µl sample of the organic layer and a 1 mL sample of the aqueous layer were taken and the radioactivity measured using a gamma counter.

3.3. Results and discussion

3.3.1. Chemistry

An important compound within the synthesis route of compounds **1a** and **3a** is 2-(methylsulfonyl)-4-(4-(methylsulfonyl)-phenyl)-6-(trifluoromethyl)pyrimidine (**6**) as a labeling precursor. The synthetic strategy for the preparation of compound **6** follows the route outlined by Swarbrick et al. [35] (Fig. 3-2). Claisen condensation of 1-(4-(methylthio)-phenyl)ethanone with ethyl trifluoroacetate yielded trifluoro-substituted dione (**4**) in a high yield of 92%. Pyrimidine ring formation using condensation with S-methylisothiourea afforded compound **5** in almost quantitative yield. Methylthioether groups in compound **5** were oxidized using Oxone to afford compound **6** in overall yield of 58% for the three-step reaction sequence. COX-2 inhibitors **1a–p** were prepared by heating corresponding primary amines and in the presence of compound **6** in acetonitrile in sealed vials at 140°C. Methylsulfonyl group in the 2-position of the pyrimidine ring acts as a good leaving group upon attack with primary amines. Upon completion of the reaction, excess of compound **6** and amine could easily be removed by diluting the mixture with hydrochloric acid. The desired product precipitated and was collected by filtration.

Impurities were removed using purification with column chromatography. Syntheses using benzylamine hydrochloride salts, such as 4-nitrobenzylamine, were carried out by adding triethylamine as the auxiliary base.

To synthesize compound **3a**, it was necessary to replace the secondary amine linker with an ether moiety. To this end, 4-fluorobenzyl alcohol and sodium hydride were dissolved in dry THF under a nitrogen atmosphere, and the mixture was cooled to 0°C. Addition of compound **6** allowed for the formation of fluorobenzyl ether compound **3a** (Fig. 3-2). This compound has been reported in

a patent by the Glaxo Group [36]. However, to the best of our knowledge, COX-2 potency and selectivity of this substance has not been published to date. The synthesis of methylsulfones **1a–j**, **1k–p**, and **3a** are depicted in Figure 3-2.

Many selective COX-2 inhibitors carry a methylsulfonyl group as a common COX-2 pharmacophore on one of the aryl rings. It is thought that this moiety is indispensable for high binding potency and selectively [2]. However, sulfonamide moieties are also frequently used as COX-2 pharmacophores [37, 38]. They are thought to yield compounds with comparable or even higher potency. Prominent examples of sulfonamide carrying selective COX-2 inhibitors include celecoxib and valdecoxib. Replacing a methylsulfonyl group with a sulfonamide can have significant effects on the pharmacokinetic profile of the drug.

We identified sulfonamide **2a** as a potential candidate for ^{18}F radiolabeling in addition to two methylsulfonyl group-containing compounds **1a** and **3a**. The synthesis of sulfonamide containing structures generally requires protection of the amine group to enable efficient and high yielding synthesis.

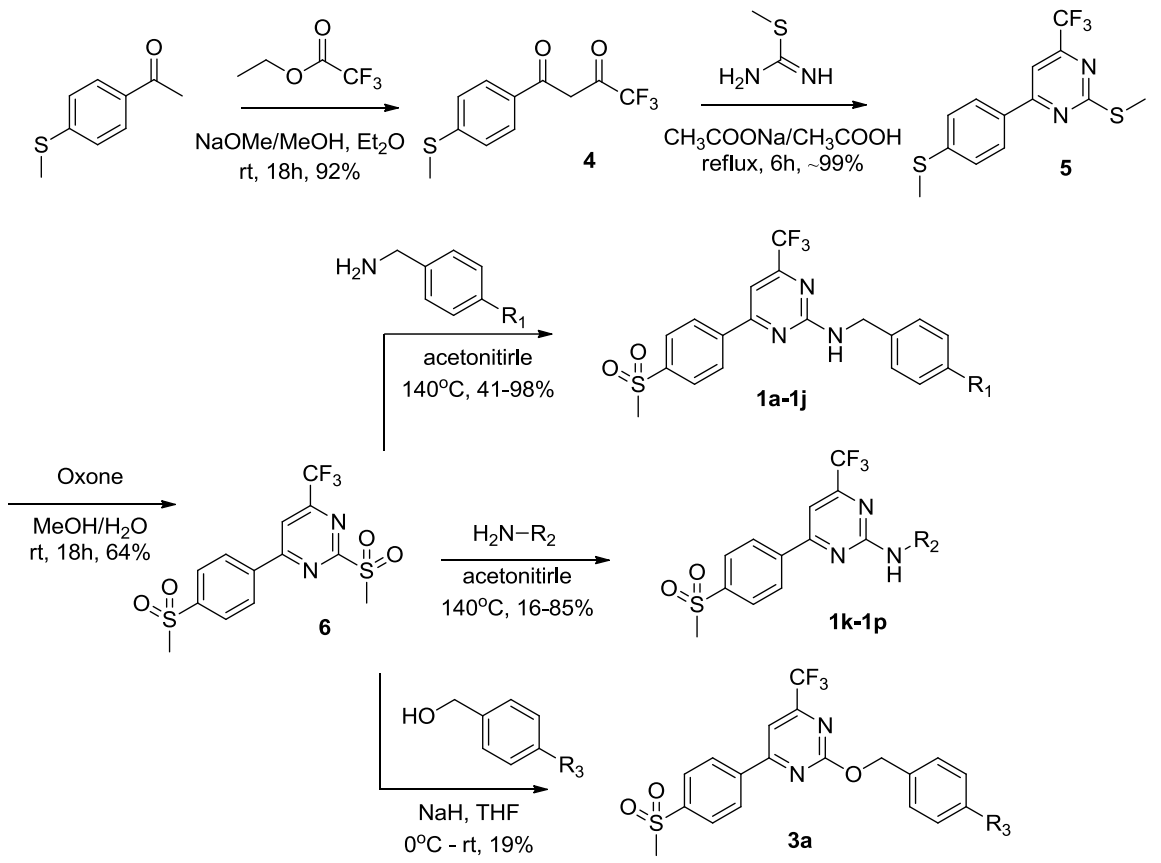

Figure 3-2: Synthesis of compounds **1a–1p**, **3a**.

A very elegant method published by Mahalingam et al. [39] described the protection of the sulfonamide groups via *tert*-butyl groups, which can easily be removed under mild conditions using catalytic amounts of Lewis acid scandium triflate. To synthesize the *tert*-butyl protected precursor **8**, we first attempted to reproduce the synthetic template that was used for the preparation of compound **6**. Reaction of 4-acetylbenzene sulfonylchloride with tert-butylamine gave *tert*-butyl-protected sulfonamide. However, subsequent Claisen condensation with ethyl trifluoroacetate failed presumably due to the basic reaction conditions. Basic reaction conditions led to the abstraction of the acidic sulfonamide proton leading to the formation of poorly soluble salt complexes.

To omit Claisen condensation, we applied the Suzuki coupling reaction between commercially available 4-chloro-2-(methylsulphonyl)-6-(trifluoromethyl)pyrimidine with *tert*-butyl 4-boronobenzenesulfonamide to form compound **7**. The methyl–sulfonyl group in compound **7** was oxidized using Oxone to afford compound **8**. Removal of the *tert*-butyl group was achieved through treatment of compound **8** with scandium triflate to give compound **9** in a total yield of 53% for the three steps. Treatment of sulfonamide **9** with various primary amines gave compounds **2a–e** in 57–91% yield. The synthesis of sulfonamides **2a–e** is summarized in Figure 3-3.

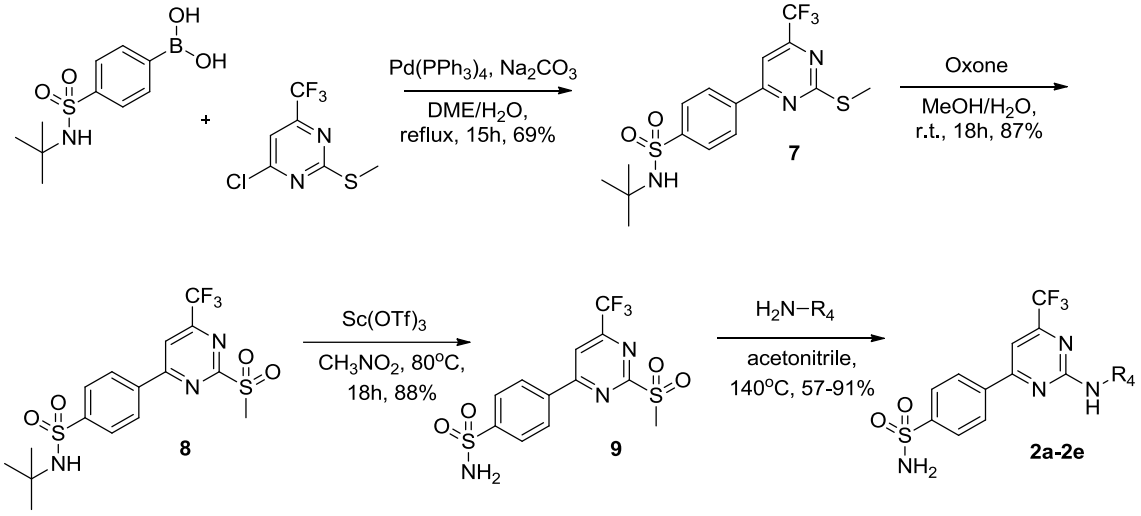

Figure 3-3: Synthesis of compounds **2a–2e**.

3.3.2. *In vitro* COX-1 and COX-2 enzyme inhibition

Compounds **1a-j**, **1l–p**, **2a–e** and **3a** were evaluated for their COX-2 inhibitory potency and selectivity profile. The determined enzyme inhibition data are summarized in Tables 3-1 to 3-4. Celecoxib was included in all assays as an internal reference compound for comparison. Celecoxib showed IC_{50} values of 40 nM against COX-2 and 15 μM against COX-1, which is in good agreement with previously reported literature values [40]. The lead structure **1a** displayed excellent

COX-2 inhibitory potency (IC_{50} (COX-2) = 7 nM) and did not show COX-1 inhibition in the concentration range tested. This makes structure **1a** more potent and many times more selective than celecoxib. In the original report, compound **1a** displayed an IC_{50} (COX-2) of 0.28 nM [35], which is an order of magnitude lower than the value we have obtained. This is likely due to differences in the inhibition assay used to determine the IC_{50} values.

Compounds **1b** to **1j** are representative of our effort to determine how structural changes to the second aryl ring effect inhibitory potency and selectivity (**Table 3-1**).

We found that changes at the 4-position of the aryl ring are usually well tolerated. Most compounds displayed better COX-2 inhibitory potency than celecoxib with IC_{50} values for COX-2 inhibition below 20 nM while possessing high selectivity over COX-1. The 4-bromine substituted compound (**1c**) is especially notable. **1c** Shows good COX-2 inhibitory potency (IC_{50} = 18 nM), despite the considerable steric bulk of bromine as a substituent. In contrast, more bulky substituents, such as *tert*-butyl and phenyl (**1h**, **1g**) show no COX-2 inhibition at the concentrations tested. It can be concluded that too much steric bulk at 4-position of the second aryl ring is detrimental to COX-2 binding potency. Despite the relatively modest steric bulk of the 4-position of the nitro-substituted compound (**1j**), we found its potency decreased by an order of magnitude in comparison to **1a**. This is likely to be due to a combination of the strongly electron withdrawing nature and modest steric bulk of the nitro group, which has a negative effect on binding potency. Compound **1i** was found to have similar COX-2 inhibitory potency and selectivity as **1a** (IC_{50} = 7 nM). Compound **1i** carries a methoxy group, which makes this compound a good candidate for ^{11}C labeling. ^{11}C labeling can be carried out via *O*-methylation of free alcohols using $^{11}CH_3I$ or [^{11}C]methyltriflate [32]. Compound **1i** would be a good radiolabeling candidate for a ^{11}C-based COX-2 radiotracer study. We found the lead compound **1a** to be relatively lipophilic (log*P* = 2.28 ± 0.05; determined

experimentally by partition in octanol–water using a ^{18}F-labeled compound). High lipophilicity of a PET radiotracer is likely to cause high non-specific binding and high intestine uptake. Compounds **1l** to **1n** as displayed in Table 3-2 are representative of our efforts to synthesize structures that are less lipophilic by substitution of the second aryl ring. The most promising candidate in this library is pyridine compound **1n**. Compound **1n** was found to have a COX-2 inhibitory potency (IC_{50} = 50 nM) comparable to that of celecoxib, but a much better COX-2 selectivity. Compound **1n** is more water-soluble than **1a** and might be developed as a ^{18}F radiotracer by including fluorine-18 at the 4-position of the pyridine ring. Various ^{18}F-labeled fluoropyridines have been reported as highly efficient radiotracers and radiopharmaceuticals [51, 52]. Efforts to synthesize alkyl substituted compounds resulted in only one high potency compound (**1p**). Compound **1p** displayed COX-2 inhibitory potency that exceeded that of celecoxibs (IC_{50} = 20 nM).

Oxygen-containing compound **3a** (IC_{50} = 20 nM) was found to be slightly less potent than the corresponding amine compound **1a** (Table 3-3). Thus, replacing nitrogen with oxygen reduces slightly binding potency, but binding potency of compound **3a** is still high when compared with an internal reference compound celecoxib.

Inhibitory potencies of sulfonamide compounds **2a** to **2e** are summarized in Table 3-4. All five compounds were slightly less potent than their corresponding methylsulfone counterparts. We can conclude that for the particular structural pyrimidine-based backbone, methylsulfone-containing compounds seem to display higher COX-2 inhibitory potency than the corresponding sulfonamides. Nonetheless, the potential candidate for ^{18}F radiolabeling **2a**, displayed inhibitory potency similar to that of celecoxib (IC_{50} = 39 nM) while showing higher COX-2 selectivity. Compound **2e**, similar to **1i**, carries a methoxy group and might therefore serve as a good ^{11}C

radiolabeling candidate. The COX-2 inhibitory potency of **2e** is comparable to that of **1i** (IC_{50} = 14 nM). Compounds **1a**, **2a** and **3a** displayed COX-2 inhibitory potency and selectivity rendering all three compounds suitable for development as ^{18}F-labeled radiotracers.

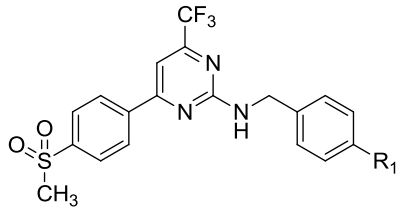

	R_1	IC_{50} (μM)[a]	
		COX-1	COX-2
celecoxib		15	0.040
1a	F	>100	0.007
1b	Cl	>100	0.006
1c	Br	>100	0.018
1d	CF_3	>100	0.017
1e	H	>100	0.016
1f	Me	>100	0.005
1g	Ph	>100	>10
1h	t-Bu	>100	>10
1i	OMe	>100	0.007
1j	NO_2	>100	0.086

Table 3-1: IC_{50} (COX-1) and IC_{50} (COX-2) values for compounds **1a–1j** ([a] Values are means of two determinations)

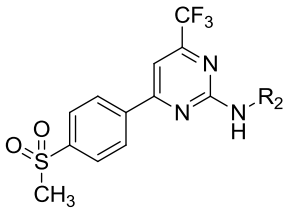

	R_2	IC_{50} (μM)[a]	
		COX-1	COX-2
celecoxib		15	0.040
1k	N-(Butan-1-ol)	n.d.*	n.d.*
1l	N-(4-pyridyl)-CH2-	>100	0.30
1m	N-(3-pyridyl)-CH2-	>100	0.080
1n	N-(2-pyridyl)-CH2-	>100	0.050
1o	N-(2-fluoroethyl)	>100	2.0
1p	N-Butyl	>100	0.020

Table 3-2: IC_{50} (COX-1) and IC_{50} (COX-2) values for compounds **1k–1o** ([a] Values are means of two determinations) (* not determined)

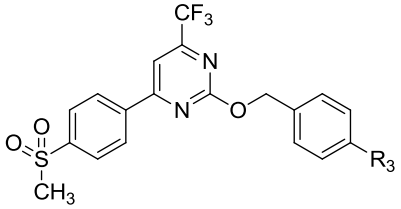

	R_3	IC_{50} (μM)[a]	
		COX-1	COX-2
celecoxib		15	0.040
3a	F	>100	0.020

Table 3-3: IC_{50} (COX-1) and IC_{50} (COX-2) values for compound **3a** ([a] Values are means of two determinations)

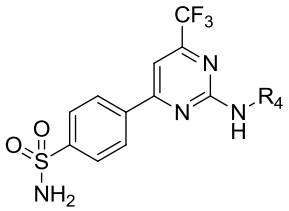

	R_4	IC_{50} (μM)[a]	
		COX-1	COX-2
celecoxib		15	0.040
2a	N-(4-fluorobenzyl)	>100	0.039
2b	N-Benzyl	>100	0.034
2c	N-(4-methylbenzyl)	>100	0.028
2d	N-(4-methoxybenzyl)	>100	0.014
2e	N-Butyl	>100	0.031

Table 3-4: IC_{50} (COX-1) and IC_{50} (COX-2) values for compound **2a–2e** ([a] Values are means of two determinations)

3.3.3. Molecular docking studies

Molecular docking experiments were performed using X-ray crystal structure data for COX-1 and COX-2 obtained from the protein data bank to explore possible interaction of compounds **1a**, **2a** and **3a** with the active site of COX-1 and COX-2 enzymes. High inhibitory potency of compound **1a** (COX-2, IC_{50} = 7 nM) suggests a favorable orientation within the COX-2 binding site. The SO_2CH_3 group in compound **1a** completely enters into the secondary pocket region of the COX-2 active site, where it is oriented towards Q192, R513, H90, and A516 residues (Fig. 3-4, left). One of the oxygen atoms of the SO_2CH_3 group undergoes hydrogen-bonding interactions with the nitrogen atom of H90 (S=O···N = 2.64 Å). The other oxygen atom indicates hydrogen-bonding interactions with the nitrogen atom of Q192 amino acid residue (S=O···N = 2.23 Å).

Moreover, the phenyl ring bearing a fluorine atom is placed in the vicinity of R120, A527 and

V349 amino acid residues. On the other side, docking studies of compound **1a** into COX-1 enzyme indicated that compound **1a** was not able to enter into the COX-1 active site completely (Fig. 3-4, right). The fluorine containing phenyl ring is situated near A527, S530 and L531 residues while the SO_2CH_3 group is positioned outside the active site of COX-1 enzyme. This finding is in good agreement with the determined high inhibitory potency and selectivity of compound **1a** towards COX-2.

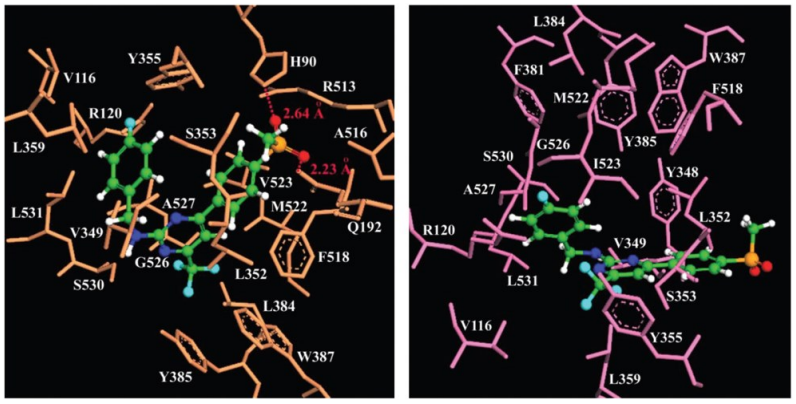

Figure 3-4: (Left) Molecular docking of compound **1a** (carbon atoms in green) positioned in the binding site of COX-2 (PDB ID: 6COX; $E_{intermolecular} = -10.70$ kcal mol^{-1}) and (right) COX-1 (PDB ID: 1EQG; $E_{intermolecular} = -8.03$ kcal mol^{-1}). Hydrogen atoms of amino acid residues have been removed for clarity.

Docking studies with compound **2a** (COX-2, IC_{50} = 39 nM) indicated that the phenyl ring bearing the SO_2NH_2 group is inserted into the secondary pocket region of the COX-2 active site where it is surrounded by H90, Q192, A516 and R513 residues (Fig. 3-5, left). The nitrogen atom of the SO_2NH_2 group displays hydrogen bonding to carbonyl oxygen of Q192 (N···O=C = 2.85 Å), and to carbonyl oxygen of L352 (N···O=C = 2.78 Å). One oxygen atom of the SO_2NH_2 group is hydrogen bonded to the nitrogen atom of H90 residue (S=O···N = 2.57 Å). The 4-fluoro phenyl

ring of compound **2a** is positioned in the vicinity of R120, V349, V116, L531 and A527 amino acid residues. The CF_3 group of compound **2a** is positioned at the entrance of COX-2 hydrophobic pocket constituted by W387, Y385 and F518 residues. Compound **2a** shows only partial entry into the COX-1 enzyme active site and did therefore not exhibit significant interactions with the COX-1 active site residues (Fig. 3-5, right). This is also in agreement with the determined COX-2 inhibitory potency and selectivity of compound **2a**.

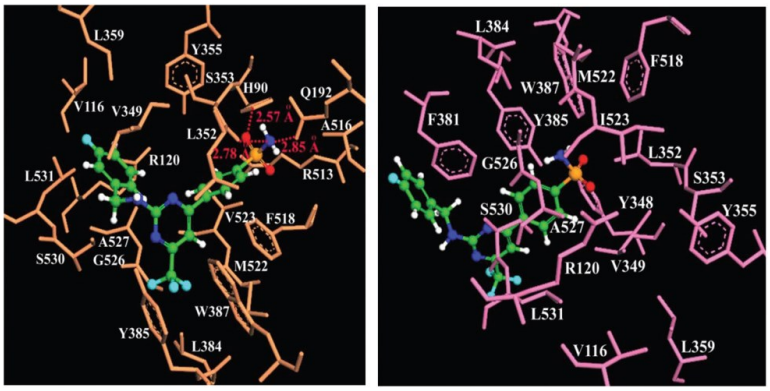

Figure 3-5: (Left) Molecular docking of compound **2a** (carbon atoms in green) positioned in the binding site of COX-2 (PDB ID: 6COX; $E_{intermolecular} = -10.55$ kcal mol^{-1}) and (right) COX-1 (PDB ID: 1EQG; $E_{intermolecular} = -8.39$ kcal mol^{-1}). Hydrogen atoms of amino acid residues have been removed for clarity.

The top scored docking pose of compound **3a** (COX-2 IC_{50} = 20 nM) displays a favorable orientation into the COX-2 active site wherein the SO_2CH_3 group is sloping towards the secondary pocket region of COX-2 active site lined by H90, R513, S353 and L352 residues (Fig. 3-6, left). One of the oxygen atoms of the SO_2CH_3 group is hydrogen bonded to the nitrogen atom of H90 residue (S=O···N = 2.64 Å), and the other oxygen atom shows hydrogen-bonding interactions with nitrogen atom of R513 amino acid residue (S=O···N = 2.79 Å). The CF_3 group of compound **3a** is

located in close proximity of the S530 residue where the measured distance between one of the F atom of the CF_3 group and the –OH group of S530 is 1.36 Å. The 4-fluoro phenyl ring of compound **3a** is positioned in the vicinity of L359, V116 and R120 amino acid residues. However, docking of compound **3a** within the COX-1 active site clearly indicates that the SO_2CH_3 pharmacophore, which probably contributes to potent COX-2 inhibition, is not able to enter into the COX-1 active site, whereas the F-phenyl ring is sandwiched between the Y385 and W387 amino acid residues of the hydrophobic region.

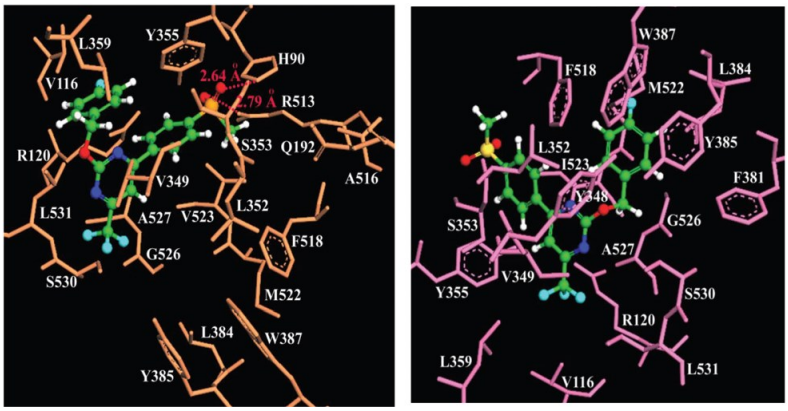

Figure 3-6: (Left) Molecular docking of compound **3a** (carbon atoms in green) positioned in the binding site of COX-2 (PDB ID: 6COX; $E_{intermolecular} = -10.12$ kcal mol^{-1}) and (right) COX-1 (PDB ID: 1EQG; $E_{intermolecular} = -9.03$ kcal mol^{-1}). Hydrogen atoms of amino acid residues have been removed for clarity.

3.3.4. Radiochemistry

Radiotracers [^{18}F]**1a** and [^{18}F]**2a** were synthesized using a 4-[^{18}F]fluorobenzylamine ([^{18}F]FBA) as a building block. [^{18}F]FBA was synthesized using a method recently described by our group [41, 42] (Fig. 3-7). 4-Cyano-N,N,N-trimethylanilinium trifluoromethansulfonate as a labeling precursor was radio-fluorinated using nucleophilic no-carrier-added (n.c.a.) [^{18}F]KF in the

presence of Kryptofix K_{222} in dry DMSO at elevated temperature. The resulting 4-[^{18}F]fluorobenzonitrile ([^{18}F]FBN) was reduced to [^{18}F]FBA using transition metal-assisted $NaBH_4$ reduction. A fully automated [^{18}F]FBA synthesis was recently developed by Way et al. [42]. This work also describes the usefulness of [^{18}F]FBA as a building block for the synthesis of a variety of ^{18}F-labeled compounds like prosthetic groups for peptide labeling or built-up synthesis of complex molecules as ^{18}F-labeled Hsp90 inhibitor geldanamycin.

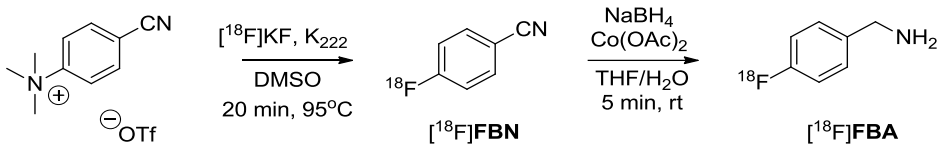

Figure 3-7: Radiosynthesis of 4-[^{18}F]fluorobenzylamine [^{18}F]FBA.

Radiotracer [^{18}F]**1a** was prepared through the reaction of compound **6** with [^{18}F]FBA. The reaction was carried out in THF at 140°C for 20 min (Fig. 3-8). Total synthesis time for the preparation of [^{18}F]**1a**, including HPLC purification, was 95 min. Decay-corrected radiochemical yield based on [^{18}F]FBA was 27 ± 11%. In a typical experiment, starting from 1 GBq of [^{18}F]FBA prepared on an automated synthesis unit provided 160 MBq of radiotracer [^{18}F]**1a**. Specific activity of [^{18}F]**1a** at the end of synthesis was determined to be greater than 40 GBq μmol^{-1}.

Synthesis of radiotracer [^{18}F]**2a** was accomplished by the same methodology described for [^{18}F]**1a** but using labeling precursor **9** as the starting material. Radiosynthesis was carried out within 110 min with a decay-corrected radiochemical yield of 23 ± 1 %. Specific activity of [^{18}F]**2a** was greater than 40 GBq μmol^{-1} at the end of synthesis. Radiosyntheses of compounds of [^{18}F]**1a** and of [^{18}F]**2a** are depicted in Figure 3-8.

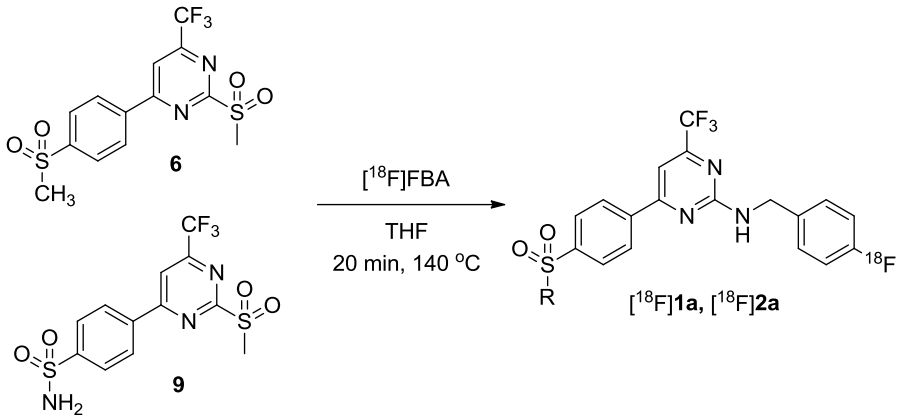

Figure 3-8: Radiosynthesis of [^{18}F]**1a** (R = CH_3) and [^{18}F]**2a** (R = NH_2).

We also attempted to synthesize radiotracer [^{18}F]**3a** by expanding the concept of nucleophilic substitution reactions with compound **6** as the labeling precursor. To replace the nitrogen present in compound [^{18}F]**1a** with an oxygen, we performed radiosyntheses with 4-[^{18}F]fluorobenzyl alcohol ([^{18}F]-FBAlc) as a building block. This strategy would allow the extension of feasible radiochemistry as exemplified for compounds [^{18}F]**1a** and [^{18}F]**2a** to the readily available ^{18}F building block [^{18}F]FBAlc.

As described in the chemistry section, we successfully synthesized reference compound **3a** by the reaction of 4-fluorobenzyl alcohol with compound **6** in the presence of sodium hydride. Radiosynthesis of [^{18}F]FBAlc as a ^{18}F building block was accomplished following a protocol developed by Donohue et al. [43]. (4-Trimethylamino)benzaldehyde trifluoromethanesulfonate was treated with a powerful radiofluorination agent [^{18}F]KF in the presence of Kryptofix K_{222} in dry acetonitrile at elevated temperature to yield 4-[^{18}F]fluorobenzaldehyde. 4-[^{18}F]Fluorobenzaldehyde was reduced to [^{18}F]FBAlc using $NaBH_4$. $NaBH_4$ was dissolved in water and passed through a solid phase extraction cartridge containing 4-[^{18}F]- fluorobenzaldehyde.

[^{18}F]FBAlc was purified using HPLC, and the solvent was evaporated under reduced pressure. Dried [^{18}F]FBAlc was redissolved in dry solvent to be used in subsequent reaction steps. Despite extensive efforts to promote the substitution reaction between [^{18}F]FBAlc and labeling precursor **6**, it was not possible to obtain reasonable amounts of the desired product [^{18}F]**3a**. Radiochemical yields were below 1 % as indicated by radio-TLC analysis of the reaction mixture.

Radiosynthesis of [^{18}F]**3a** based on the reaction between [^{18}F]FBAlc and compound **6** was performed using different reaction conditions. This included variation of reaction temperature (0 °C to 180 °C) use of different bases (no base, triethylamine, potassium *tert*-butoxide, sodium hydride), and the use of different solvents (THF, CH_3CN, DMF). To our disappointment, no product formation of **3a** was achieved as confirmed by radio-TLC and radio-HPLC analyses. We hypothesize that the ratio of [^{18}F]FBAlc to a base and a precursor is crucial for the success of the reaction. The reaction does not proceed in the absence of a base. During the radiosynthesis only trace amounts of [^{18}F]FBAlc are present in the reaction mixture, therefore any added base will be in large stoichiometric excess. We believe that the excess of base interferes with the reaction.

Moreover, the reaction tended to be very water sensitive. Although most residual water can be removed during the radiosynthesis, even trace amounts of water seem to have a detrimental effect on the reaction using tracer concentrations of 4-fluorobenzyl alcohol.

As a result, it seems to be very challenging to fine-tune the amount of base required for successful radiosynthesis of compound [^{18}F]**3a** based on the reaction of labeling precursor **6** with [^{18}F]FBAlc. The difficulties to prepare compound [^{18}F]**3a** according to the synthesis method of cold reference compound **3a** (Fig. 3-2) prompted us to envisage an alternative synthesis route. Direct nucleophilic aromatic radiofluorination has been reported using iodylbenzene derivatives as labeling precursors. Iodylbenzene derivatives substituted with electron donating as well as electron

withdrawing groups on the aromatic ring were shown to readily undergo radiofluorination reaction with n.c.a. [^{18}F]fluoride as exemplified for various compounds described in a recent patent publication [44]. Synthesis of the iodyl group-containing compound **11** as a labeling precursor for the preparation of radiotracer [^{18}F]**3a** is given in Fig. 3-9. Synthesis of iodylaryl compound **11** was achieved by the reaction of compound **6** with 4-iodobenzyl alcohol and sodium hydride, applying similar reaction conditions described for the synthesis of **3a** to form compound **10** in 71 % yield. 4-Iodobenzyl compound **10** was oxidized to iodyl compound **11** using Oxone in a mixture of water and methanol, while being gently heated. Dilution of the reaction mixture with water and collection of the formed precipitate by filtration yielded iodyl compound **11**. The product also contained small amounts of starting material **10** and the mono-oxidized iodine intermediate. Both small impurities could be removed by column chromatography to give pure iodyl compound **11** in 38 % yield.

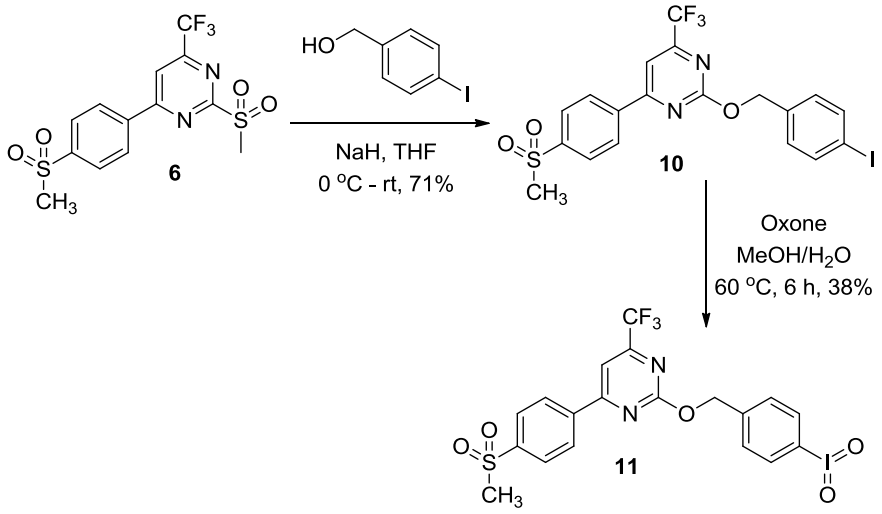

Figure 3-9: Synthesis of iodylaryl compound **11**.

Radiolabeling with n.c.a. [^{18}F]fluoride was achieved by heating 1 mg of iodylaryl compound **11** in 300 µl of dry DMF in the presence of Kryptofix K_{222} at 180°C for 20 min (Fig. 3-10). A range of different solvents (DMF, DMSO, NMP), temperatures (80°C to 180°C) and different precursor concentrations were tested. It was found that optimal radiochemical yields of 5 to 10 % (as determined by radio-TLC) could be achieved by using 1 mg of iodyl compound **11** in DMF at 180°C. To prepare [^{18}F]**3a** in radiopharmaceutical quality for *in vitro* and *in vivo* work, the reaction mixture was diluted in 0.1 M NaOAc buffer (pH 5.3) and passed through a solid phase extraction cartridge. The cartridge was washed with water and product [^{18}F]**3a** was eluted with CH_3CN. The radiotracer was further purified using HPLC. After evaporation of the solvent, the radiotracer was redissolved in 10% EtOH–saline for further radiopharmacological evaluation. Total synthesis was accomplished in 120 min. A starting activity of 300 MBq [^{18}F]fluoride typically yielded 3–5 MBq of purified product [^{18}F]**3a**. The identity of the radiotracer was confirmed by HPLC co-injection with the non-radiolabeled reference compound.

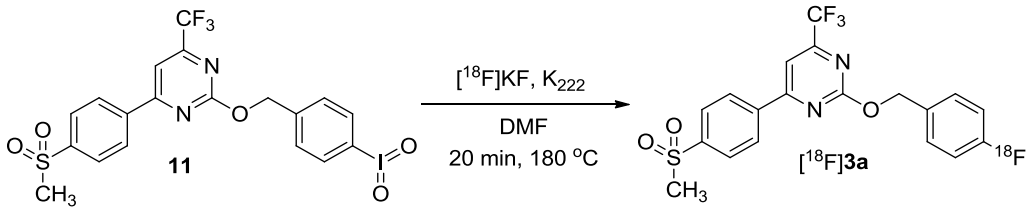

Figure 3-10: Radiosynthesis of [^{18}F]**3a** from precursor **11**.

Upon further reaction optimization of the reaction conditions, the iodylaryl-based direct radiofluorination approach could prove to be a versatile strategy for the site specific radiolabeling of more complex drug-like molecules in sufficient radiochemical yields.

Other direct radiolabeling strategies using nucleophilic aromatic substitution reactions with

[^{18}F]KF on non-activated aromatic systems involve iodonium and sulfonium salts. However, syntheses of iodonium and sulfonium salts of structurally more complex compounds tend to be challenging, making them generally less versatile with respect to their incorporation of n.c.a. fluorine-18 at specific sites in a given molecule [45–47].

3.4. Summary and conclusion

We have prepared a series of novel COX-2 inhibitors based on a pyrimidine scaffold in continuation to the original work reported by Swarbrick and co-workers [35]. *In vitro* COX-1 and COX-2 enzyme inhibition studies revealed the great potential of pyrimidine-based compounds as highly potent and selective COX-2 inhibitors. Except for bulky substituents such as phenyl and *tert*-butyl groups attached to the para position of the benzyl ring (compounds **1g** and **1h**), COX-2 enzyme seems to accept a broad variety of electron-donating (Me, OMe,) and electron-withdrawing (F, Cl, Br, CF_3, NO_2) groups. Molecular docking studies confirmed the determined high COX-2 inhibitory potency and selectivity of fluorine-containing compounds **1a**, **2a** and **3a**. The high COX-2 inhibitory potency and selectivity of fluorine-containing compounds **1a**, **2a** and **3a** make them interesting compounds for the development of corresponding ^{18}F-labeled radiotracers. Radiolabeling was achieved through two different routes, using the indirect labeling method with 4-[^{18}F]fluoro-benzylamine as the building block, and the direct radiolabeling method with iodylaryl derivative **11** as the labeling precursor. All radiotracers could be prepared in radiochemical yields and radiopharmaceutical quality suitable for subsequent radiopharmacological evaluation. First results on radiopharmacological evaluation of radiotracers [^{18}F]**1a**, [^{18}F]**2a**, and [^{18}F]**3a** have been reported during the 20th International Symposium on Radiopharmaceutical Sciences 2013 in Jeju, Korea [50].

3.5. References

[1] Warner, T.D.; Mitchell, J.A. Cyclooxygenase-3 (COX-3): filling in the gaps toward a COX continuum? *Proc. Natl. Acad. Sci. U. S. A.*, **2000**, 99, 13371.

[2] Méric, J.; Rottey, S.; Olaussen, K.; Soria, J.; Khayat, D.; Rixe, O.; et al. Cyclooxygenase-2 as a target for anticancer drug development. *Crit. Rev. Oncol.*, **2006**, 59, 51.

[3] Kurumbail, R.G.; Kiefer J.R.; Marnett, L.J. Cyclooxygenase enzymes: catalysis and inhibition. *Curr. Opin. Struct. Biol.*, **2001**, 11, 752.

[4] Luong, C.; Miller, A.; Barnett, J.; Chow, J.; Ramesha C.; Browner, M.F. Flexibility of the NSAID binding site in the structure of human cyclooxygenase-2. *Nat. Struct. Biol.*, **1996**, 3, 927.

[5] Shi, S.; Klotz, U. Proton pump inhibitors: an update of their clinical use and pharmacokinetics. *Eur. J. Clin. Pharmacol.*, **2008**, 64, 233.

[6] Cannon C. and P. Cannon, COX-2 inhibitors and cardiovascular risk. Science, 2012, 336, 1386.

[7] Yu, Y.; Ricciotti, E.; Scalia, R.; Tang, S.; Grant, G.; Yu, Z.; Landesberg, G.; et al. Vascular COX-2 modulates blood pressure and thrombosis in mice. *Sci. Transl. Med.*, **2012**, 132.

[8] Scheiman, J.M. Unmet needs in non-steroidal anti-inflammatory drug-induced upper gastrointestinal diseases. *Drugs*, **2006**, 66, 15.

[9] Seibert, K.; Zhang, Y.; Leahy, K.; Hauser, S.; Masferrer, J.; Perkins, W.; et al. Pharmacological and biochemical demonstration of the role of cyclooxygenase 2 in inflammation and pain. *Proc. Natl. Acad. Sci. U. S. A.*, **1994**, 91, 12013.

[10] Okamoto, T.; Hino, O. Expression of cyclooxygenase-1 and-2 mRNA in rat tissues: tissue-specific difference in the expression of the basal level of mRNA. *Int. J. Mol. Med.*, **2000**, 6, 455.

[11] Seibert, K.; Zhang, Y.; Leahy, K.; Hauser, S.; Masferrer, J.; Perkins, W.; et al. Pharmacological and biochemical demonstration of the role of cyclooxygenase 2 in inflammation and pain. *Proc. Natl. Acad. Sci. U. S. A.*, **1994**, 91, 12013.

[12] Teismann, P.; Tieu, K.; Choi, D.; Wu, D.; Naini, A.; Hunot, S.; et al. Cyclooxygenase-2 is instrumental in Parkinson's disease neurodegeneration. *Proc. Natl. Acad. Sci. U. S. A.*, **2003**, 100, 5473.

[13] Edwards, J.; Mukherjee, R.; Munro, A.F.; Wells, A.C.; Almushatat, A.; Bartlett, J.M.S. HER2 and COX2 expression in human prostate cancer. *Eur. J. Cancer*, **2004**, 40, 50.

[14] Wang, D.; DuBois, R.N. The role of COX-2 in intestinal inflammation and colorectal cancer. *Oncogene*, **2010**, 29, 781.

[15] Hwang, D.; Scollard, D.; Byrne J.; Levine, E. Expression of cyclooxygenase-1 and cyclooxygenase-2 in human breast cancer. *J. Natl. Cancer Inst.*, **1998**, 90, 455.

[16] Greenhough, A.; Smartt, H.; Moore, A.; Roberts, H.; Williams, A.; Paraskeva, C.; et al. The COX-2/PGE2 pathway: key roles in the hallmarks of cancer and adaptation to the tumour microenvironment. *Carcinogenesis*, **2009**, 30, 377.

[17] Ghosh, N.; Chaki, R.; Mandal, V.; Mandal, S. COX-2 as a target for cancer chemotherapy.*Pharmacol. Rep.*, **2010**, 62, 233.

[18] Inoue, H.; Taba, Y.; Miwa, Y.; Yokota, C.; Miyagi, M.; Sasaguri, T. Transcriptional and posttranscriptional regulation of cyclooxygenase-2 expression by fluid shear stress in vascular endothelial cells. *Arterioscler. Thromb. Vasc. Biol.*, **2002**, 22, 1415.

[19] Prabhakaran, J.; Underwood, M.; Parsey, R.; Arango, V.; Majo, V.; Simpson, N.; et al. Nuclear imaging of neuroinflammation: a comprehensive review of [11C] PK11195 challengers. *Bioorg. Med. Chem.*, **2007**, 15, 1802.

[20] Uddin, M.; Crews, B.; Ghebreselasie, K.; Huda, I.; Kingsley, P.; Ansari, M.; et al. Fluorinated COX-2 inhibitors as agents in PET imaging of inflammation and cancer. *Cancer Prev. Res.*, **2011**, 4, 1536.

[21] Prabhakaran, J.; Majo, V.; Simpson, N.; Van Heertum, R.; Mann, J.; Kumar, J. Synthesis of [11C] celecoxib: a potential PET probe for imaging COX-2 expression. *J. Labelled Compd. Radiopharm.*, **2005**, 48, 887.

[22] Takashima-Hirano, M.; Takashima, T.; Katayama, Y.; Wada, Y.; Sugiyama, Y.; Watanabe, Y.; et al. Efficient sequential synthesis of PET Probes of the COX-2 inhibitor [11C] celecoxib and its major metabolite [11C] SC-62807 and *in vivo* PET evaluation. *Bioorg. Med. Chem.*, **2011**, 19, 2997.

[23] Fujisaki, Y.; Kawamura, K.; Wang, W.; Ishiwata, K.; Yamamoto, F.; Kuwano, T.; et al. Radiosynthesis and *in vivo* evaluation of 11C-Iabeled 1,5-diarylpyrazole derivatives for mapping cyclooxygenases. *Ann. Nucl. Med.*, **2005**, 19, 617.

[24] Gao, M.; Wang, M.; Miller, K.D.; Hutchins, G.D.; Zheng, Q. Synthesis and preliminary *in vitro* biological evaluation of new carbon-11-labeled celecoxib derivatives as candidate PET tracers for imaging of COX-2 expression in cancer. *Appl. Radiat. Isot.*, **2009**, 67, 2019.

[25] Yang, D.; Bryant, J.; Chang, J.; Mendez, R.; Oh, C.; Yu, D.; et al. Assessment of cyclooxygense-2 expression with 99mTc-labeled celebrex. *Anticancer Drugs*, **2004**, 15, 255.

[26] Kabalka, G.; Mereddy, A.; Schuller,H. Synthesis of an iodine-123-labeled celecoxib analogue: a potential spect agent. *J. Labelled Compd. Radiopharm.*, **2005**, 48, 295.

[27] Kuge, Y.; Katada, Y.; Shimonaka, S.; Temma, T.; Kimura, H.; Kiyono, Y.; et al. Synthesis and evaluation of radioiodinated cyclooxygenase-2 inhibitors as potential SPECT tracers for cyclooxygenase-2 expression. *Nucl. Med. Biol.*, **2006**, 33, 21.

[28] Majo, V.; Prabhakaran, J.; Simpson, N.; Van Heertum, R.; Mann, J.; Kumar, J. Synthesis and *in vivo* evaluation of [18F]-4-[5-(4-methylphenyl)-3-(trifluoromethyl)-1H-pyrazol-1-yl] benzenesulfonamide as a PET imaging probe for COX-2 expression. *Bioorg. Med. Chem. Lett.*, **2005**, 15, 4268.

[29] de Vries, E.; Doorduin, J.; Dierckx, R.; van Waarde, A. Evaluation of [11C] rofecoxib as PET tracer for cyclooxygenase 2 overexpression in rat models of inflammation. *Nucl. Med. Biol.*, **2008**, 35, 35.

[30] Wuest, F.; Hoehne, A.; Metz, P. Synthesis of 18F-labelled cyclooxygenase-2 (COX-2) inhibitors via Stille reaction with 4-[18F]fluoroiodobenzene as radiotracers for positron emission tomography (PET). *Org. Biomol. Chem.*, **2005**, 3, 503.

[31] Tanaka, M.; Fujisaki, Y.; Kawamura, K.; Ishiwata, K.; Yamamoto, F.; Mukai, T.; Maeda, M. Radiosynthesis and evaluation of 11C-labeled diaryl-substituted imidazole and indole derivatives for mapping cyclooxygenase-2. *Biol. Pharm. Bull.*, **2006**, 29, 2087.

[32] Wuest, F.; Kniess, T.; Bergmann, R.; Pietzsch, J. Synthesis and evaluation *in vitro* and *in vivo* of a 11C-labeled cyclooxygenase-2 (COX-2) inhibitor. *Bioorg. Med. Chem.*, **2008**, 16, 7662.

[33] Tian, H.; Lee, Z. Synthesis of 18F-labeled cyclooxygenase-2 (COX-2) inhibitor as a potential PET imaging agent. *J. Labelled Compd. Radiopharm.*, **2006**, 49, 583.

[34] Kniess, T.; Laube, M.; Bergmann, R.; Sehn, F.; Graf, F.; Steinbach, J.; et al. Radiosynthesis of a 18F-labeled 2, 3-diarylsubstituted indole via McMurry coupling for functional characterization of cyclooxygenase-2 (COX-2) *in vitro* and *in vivo*. *Bioorg. Med. Chem.*, **2012**, 20, 3410.

[35] Swarbrick, M.; Beswick, P.; Gleave, R.; Green, R.; Bingham, S.; Bountra, C.; et al. Identification of [4-[4-(methylsulfonyl) phenyl]-6-(trifluoromethyl)-2-pyrimidinyl] amines and ethers as potent and selective cyclooxygenase-2 inhibitors. *Bioorg. Med. Chem. Lett.*, **2009**, 19, 4504.

[36] Hagan, J.; Ratti, E.; Routledge, C.; et al. Use of cyclooxygenase- 2 inhibitors for the treatment of depressive disorders, WO, 2005048999 A3, **2005**.

[37] Gaulier, S.M.; Reuben, M.; Swain, N.A. A novel three-step synthesis of Celecoxib via palladium-catalyzed direct arylation. *Tetrahedron Lett.*, **2011**, 52, 6000.

[38] Puig, C.; Crespo, M.; Godessart, N.; Feixas, J.; Ibarzo, J.; Jiménez, J.; et al. Synthesis and biological evaluation of 3, 4-diaryloxazolones: a new class of orally active cyclooxygenase-2 inhibitors. *J. Med. Chem.*, **2000**, 43, 214.

[39] Mahalingam, A.; Xiongyu, W.; Yiqian, W.; Alterman, M. Scandium Triflate as an Efficient and Recyclable Catalyst for the Deprotection of Tert-Butyl Aryl Sulfonamides.*Synth. Commun.*, **2005**, 35, 95.

[40] Penning, T.; Talley, J.; Bretenshaw, S.; Carter, J.; Collins, P.; Docter, S.; Graneto, M.; et al. Synthesis and biological evaluation of the 1, 5-diarylpyrazole class of cyclooxygenase-2 inhibitors: identification of 4-[5-(4-methylphenyl)-3-(trifluoromethyl)-1 H-pyrazol-1-yl] benzenesulfonamide (SC-58635, celecoxib). *J. Med. Chem.*, **1997**, 40, 1347.

[41] Koslowsky, I.; Mercer J.; Wuest, F.; Synthesis and application of 4-[18F] fluorobenzylamine: A versatile building block for the preparation of PET radiotracers. *Org. Biomol. Chem.*, **2010**, 8, 4730.

[42] Way, J.; Wuest, F. Fully automated synthesis of 4-[18F] fluorobenzylamine based on borohydride/NiCl2 reduction. *Nucl. Med. Biol.*, **2013**, 2013, 40, 430.

[43] Donohue, S.; Halldin, C.; Schou, M.; Hong, J.; Phebus, L.; Chernet, E.; Hitchcock, S.; et al. Radiolabeling of a high potency cannabinoid subtype-1 receptor ligand, N-(4-fluoro-benzyl)-4-(3-(piperidin-1-yl)-indole-1-sulfonyl) benzamide (PipISB), with carbon-11 or fluorine-18. *J. Labelled Compd. Radiopharm.*, **2008**, 51, 146.

[44] Satyamurthy, N.; Barrio, J. No-carrier-added nucleophilic [F-18] fluorination of aromatic compounds, WIPO Patent, WO/2010/117435, **2010**.

[45] Littich, P.; Scott, P. Novel Strategies for Fluorine-18 Radiochemistry. *Angew. Chem., Int. Ed.*, **2012**, 51, 1106.

[46] Kim, D.; Jeong, H.-J.; Lim, S.; Sohn, M.-H. Recent Trends in the Nucleophilic [18F]-radiolabeling Method with No-carrier-added [18F] fluoride. *Nucl. Med. Mol. Imaging*, **2010**, 44, 25.

[47] Lehmann, L.; Stellfeld, T.; Graham, K.; Becaud, J.; Mu, L. Triaryl-sulphonium compounds, kit and methods for labeling positron emitting isotopes, US Patent, US/2012/0020881, **2012**.

[48] Selinsky, B.S.; Gupta, K.; Sharkey C.T.; Loll, P.J. Structural analysis of NSAID binding by prostaglandin H2 synthase: time-dependent and time-independent inhibitors elicit identical enzyme conformations. *Biochemistry*, **2001**, 40, 5172.

[49] Kurumbail, R.G.; Stevens, A.M.; Gierse, J.K.; McDonald, J.J.; Stegeman, R.A.; Pak, J.Y.; Gildehaus, D.; Miyashiro, J.M.; Penning, T.D.; Seibert, K.; Isakson, P.; Stallings, W.C. Structural Basis for Selective-Inhibition of Cyclooxygenase-2 by Antiinflammatory Agents. *Nature*, **1996**, 384, 644.

[50] Tietz, O.; Wang, M.; Marshall, A.; Sharma, S.; Way, J.; Wuest, M.; Wuest, F. 18F-Labelled radiotracers for molecular imaging of cyclooxygenase-2 (COX-2) expression in cancer. *J. Labelled Compd. Radiopharm.*, **2013**, 56, S3.

[51] Dollé, F. [18F]fluoropyridines: From conventional radiotracers to the labeling of macromolecules such as proteins and oligonucleotides, *Ernst Schering Res. Found Workshop*, **2007**, 62, 113.

[52] Dollé, F. Fluorine-18-labelled fluoropyridines: advances in radiopharmaceutical design, *Curr. Pharm. Des.*, **2005**, 11, 3221.

CHAPTER 4

Evaluation of [^{18}F]1a in a rat model of colorectal cancer

4.1. Introduction

Lead radiotracer [^{18}F]**1a** was initially evaluated in the Ward Colon Tumor (WCT) rat model. The WCT rat model has been used primarily to study cachexia and the efficacy of drug treatments in colorectal cancer [1 – 4]. WCT tumors are grown via subcutaneous injection of WCT cells into female Fisher 344 rats. The advantages of this rat model are the size of rats, which allows higher resolution PET images to be obtained, and the immunocompetency of WCT-bearing Fisher 344 rats. Injection of human cell lines into animals requires the use of partially immunocompromised strains of mice to ensure that the tumor cells are not rejected by the immune system and a solid tumor is allowed to graft. The Ward Colon Tumor cells are a rat cell lines and can be by used immunocompetent animals, providing a model that is more closely related to clinical scenarios. The WCT / Fisher 344 rat model has been used by faculty member Prof. Vickie Baracos to study cachexia [3, 4]and her expertise were instrumental in establishing the model for imaging studies.

4.1.1. Objectives

The objective of this set of experiments was to gather preliminary data on the behavior of [^{18}F]**1a** in WCT cells *in vitro*, as well as, initial metabolic stability, biodistribution and tumor uptake studies *in vivo*. Furthermore, these experiments seek to establish a reliable procedure for pre-treating rats with pharmacological doses of COX-2 inhibitor for the purpose of blocking studies *in vivo.*

4.2. Materials and Methods

All regents and solvents were obtained from Sigma-Aldrich, unless otherwise stated and used without further purification. Nuclear magnetic resonance spectra were recorded on a 400MHz Varian (Palo Alto, CA, USA) unit and a 600 MHz Bruker (Billerica, MA, USA) unit. ^{1}H-NMR chemical shifts are recorded in ppm relative to tetramethylsilane (TMS). ^{19}F-NMR chemical shifts are recorded in ppm relative to trichlorofluoromethane. Low resolution mass spectra were obtained using am Agilent Technologies (Santa Clara, CA, USA) 6220 oaTOF instrument. Column chromatography was conducted using Merck silica gel (mesh size 230–400 ASTM). Thin-layer chromatography (TLC) was performed on Merck silica gel F-254 aluminum plates, with visualization under UV light (254 nm). High performance liquid chromatography (HPLC) purifications and analysis were performed using a Phenomenex LUNA® C18 column (100Å, 250x10mm, 10mm) on a Gilson 322 Pump module fitted with a 171 Diode Array and a radio detector.

4.2.1. Formulation of radiotracer for *in vitro* and *in vivo* studies

[^{18}F]**1a** was dissolved in ethanol (EtOH) and diluted in Krebs buffer for *in vitro* studies (final percentage of EtOH < 1 % of final volume). For *in vivo* studies, 25 µL of radiotracer in EtOH was added to 475 µL sterile saline solution. For *in vivo* studies using human serum albumin (HSA) as a carrier protein, 25 µL of radiotracer in EtOH was added to 475 µL of 3.5 % HSA in saline solution. The mixture was sonicated in a water bath for 15 min.

4.2.2. Cell uptake studies

Experiments for the *in vitro* evaluation of [^{18}F]**1a** in the ward colon tumor model were performed with cell lines WCT (rat-derived colon carcinoma; provided by Dr. Vickie Baracos, Department of Oncology, University of Alberta) and EMT-6 (murine mammary carcinoma; ATCC CRL-2755). Cells were routinely cultivated in Dulbecco's Modified Eagle Medium: Nutrient Mixture F-12 (DMEM/F-12, in house) medium, supplemented with 10 % (v/v) heat-inactivated fetal bovine serum (FBS, Gibco 12483), penicillin-streptomycin (1 %; Gibco 15140), 2-[4-(2-hydroxyethyl)piperazin-1-yl]ethanesulfonic acid (HEPES, 10 mM; Gibco 15630), and L-glutamine (2 mM; Gibco 25030) at 37 ºC and 5 % CO_2 in a humidified incubator. For the uptake studies, cells were seeded in 12-well plates at a density of 400,000 cells/mL and grown to 90-95 % confluence. The radiotracer uptake experiments using [^{18}F]**1a** (300 KBq/mL; specific activity: >40 GBq/μmol) were performed in triplicates in KREBS buffer at 37 ºC for 5, 10, 15, 30 and 60 min incubation time. For blocking studies, the cells were pre-incubated with 10 μM of non-radiolabeled **1a** and celecoxib for 30 min before the radiotracer was added. Radiotracer uptake was stopped with 1 mL ice-cold PBS, the cells were washed subsequently two times with PBS and lysed in 0.4 mL radioimmunoprecipitation assay buffer (RIPA buffer). The radioactivity in the cell lysates was determined with a WIZARD2 Automatic gamma counter (Perkin Elmer; Waltham, MA, U.S.A.). Total protein concentration in the samples was determined by the bicinchoninic acid method (BCA; Pierce, Thermo Scientific 23227) using bovine serum albumin (800, 600, 400, 300, 200, 100, 50 μg/mL, blank) as protein standard. Cell uptake data for all experiments are expressed as percent of measured radioactivity per l mg protein (% radioactivity / mg protein).

4.2.3. *In vivo* tumor model

Positron emission tomography (PET) experiments in the ward colon tumor model were performed using WCT tumor-bearing Fisher-344 rats (Charles River Laboratories, Quebec, Canada). All animal experiments were carried out in accordance with the guidelines of the Canadian Council on Animal Care (CCAC) and approved by the local animal care committee (Cross Cancer Institute, University of Alberta). Female Fisher-344 rats were housed under standard conditions with free access to standard food and tap water. WCT cells ($1x10^7$ cells in 400 µl PBS) were injected into the upper left flank of female Fisher-344 rats (170-200 g). After 14 to 21 days post-inoculation, WCT tumors reached sizes of approximately 1 cm^3 which were suitable for all *in vivo* experiments.

4.2.4. Metabolite analysis

The radiotracer [^{18}F]**1a** was injected intravenously into female Fisher-344 rats (50 MBq) under isoflurane anesthesia. Blood samples from the tail vein were collected at 5, 15, 30, 60, 90, and 120 min post-injection. Plasma was separated by centrifugation (5 min, 13000 g) followed by precipitation of the plasma proteins using ice-cold methanol (2 parts per 1 part plasma) and centrifugation (5 min, 13000 g), and the supernatants were analyzed by radio-thin layer chromatography (radio-TLC). TLCs were developed in 1% MeOH/CH_2Cl_2 and analyzed using a BAS-5000 reader (Fuji Photo Film Co., LTD) and Adaptive Image Deconvolution Algorithm (AIDA) Image Analyzer v.450 software.

4.2.5. Small animal PET imaging

General anesthesia of WCT tumor-bearing Fisher-344 rats was induced with inhalation of isoflurane in 40 % oxygen / 60 % nitrogen (gas flow = 2.5 ml/min), and rats were subsequently fixed in prone position. The body temperature was kept constant at 37 °C for the entire experiment. For PET experiments, 30–40 MBq of [^{18}F]**1a** in 400-500 µL of solution (formulation see above) was administered intravenously as a bolus via the tail vein. PET data were collected dynamically over 2 h to 4 h on a microPET® R4 or an Inveon® PET/CT scanner (Siemens Preclinical Solutions, Knoxville, TN U.S.A.). A transmission scan for attenuation correction was not acquired. The radioactivity of the injection solution in a 0.5 ml syringe was determined with a dose calibrator (Atomlab™ 300, Biodex Medical Systems, New York, U.S.A.). After the PET emission scan was started the radioactivity was injected with a delay of approximately 15 s. Data acquisition continued for 120 to 240 min in 3D list mode. The dynamic list mode data were sorted into sinograms with up to 72 time frames (10x2, 8x5, 6x10, 6x20, 8x60, 10x120, 5x300, 19x600 s). The frames were reconstructed using maximum a posteriori (MAP) reconstruction modes. The pixel size was 0.085x0.085x0.12 cm, and the resolution in the center field of view was 1.8 mm. Correction for partial volume effects was not performed. The image files were further processed using the ROVER v2.0.51 software (ABX GmbH, Radeberg, Germany). Masks defining 3D regions of interest (ROI) were set and the ROIs were defined by thresholding. ROIs covered all visible tumor mass of the subcutaneous tumors, and the thresholds were defined by 50 % of the maximum radioactivity uptake level for WCT tumor in each animal. Mean standardized uptake values [SUV_{mean} = (activity/mL tissue)/(injected activity/body weight), mL/g] were calculated for each ROI. Time-activity curves (TAC) were generated from the dynamic scans. All semi-quantified PET data are presented as means ± SEM.

In the blocking experiments, the COX-2 inhibitor celecoxib (50 mg/kg body weight) in 100 μL DMSO was injected intraperitoneally 30 min prior to and radiotracer administration and PET acquisition. Pilot blocking experiments were performed as described in the results section.

4.2.6. Protein analysis

For the Western Blot analysis of COX-2 expression, 50 μg of protein for each sample was loaded and run for 120V for 1 hour on IDGel (IR121s). Transfer from the SDS-PAGE to membrane was done at 4ºC overnight at 35 V. The membrane was then washed in PBS once for 5 minutes before blocking in 5 % skim milk + 0.1 % Tween-20 + PBS for 1 hour at room temperature (rt). The membrane was then washed once with PBST (PBS + 0.1 %Tween-20) for 5 minutes, followed by incubation with the COX-2 primary antibody (1:500; Santa Cruz sc-70879 mouse monoclonal) and β-actin primary antibody (1:1000; Sigma A5060 rabbit monoclonal) for 1 hour at room temperature. Two more washes with PBST for 5 minutes each were done, followed by incubation of the membrane with the COX-2 secondary antibody (1:1500; Santa Cruz sc-2005 goat anti mouse) and β-actin secondary antibody (1:10000; Sigma A0545 goat anti rabbit) for 1 hour at rt. The membrane was washed with PBST 4 times for 5 minutes each, followed by one wash with PBS for 5 minutes. The membrane was then incubated with a 1:1 mixture of substrates from Pierce ECL Western Blotting Substrate (Thermo Scientific 32209) for 1 minute before gently rinsing with water.

4.2.7. Statistical analysis

All data are expressed as means ± SEM. Graphs were constructed using GraphPad Prism 5.0 (GraphPad Software). Where applicable, statistical differences were tested by unpaired Student's t-test and were considered significant for $p<0.05$.

4.3. Results and discussion

4.3.1. Cell uptake studies

Initial evaluation of [^{18}F]**1a** was carried out in ward colon tumor (WCT) cells; mouse derived tumor cell line EMT-6 was used as negative control cell line. Protein analysis showed that EMT-6 cells do not express COX-2. COX-2 expression in WCT cells was confirmed by Western Blot analysis (Fig. 4-1).

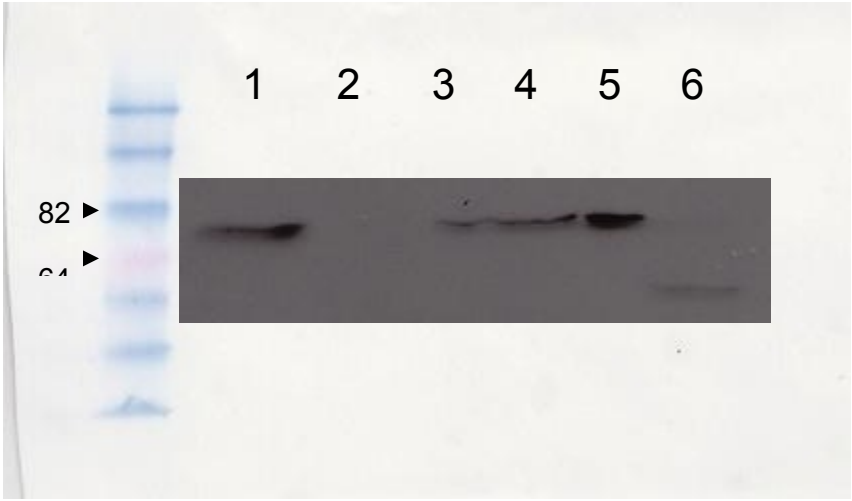

Figure 4-1: Western blot analysis of COX-2 expression in cell lysates of WCT (4, 5) and EMT-6 (6). (1) Cell lysate of 293 cells (COX-2 positive); (2) Cell lysate of A549 cells (COX-2 negative); (3) Cell lysate of A172 cells (COX-positive); (4) Lysate of WCT cells isolated from tumor I; (5) Lysate of WCT cells isolated from tumor II; (6) Cell lysate of EMT6 cells)

Accumulation of [^{18}F]**1a** in COX-2 positive WCT and COX-2 negative EMT-6 cells was almost identical. After 60 min incubation time radioactivity reached a level of 42 ± 4 % radioactivity/mg

of protein (n=3) in WCT cells, while uptake in EMT-6 cells reached 41 ± 6 % radioactivity/mg of protein (n=3; Fig. 4-2a).

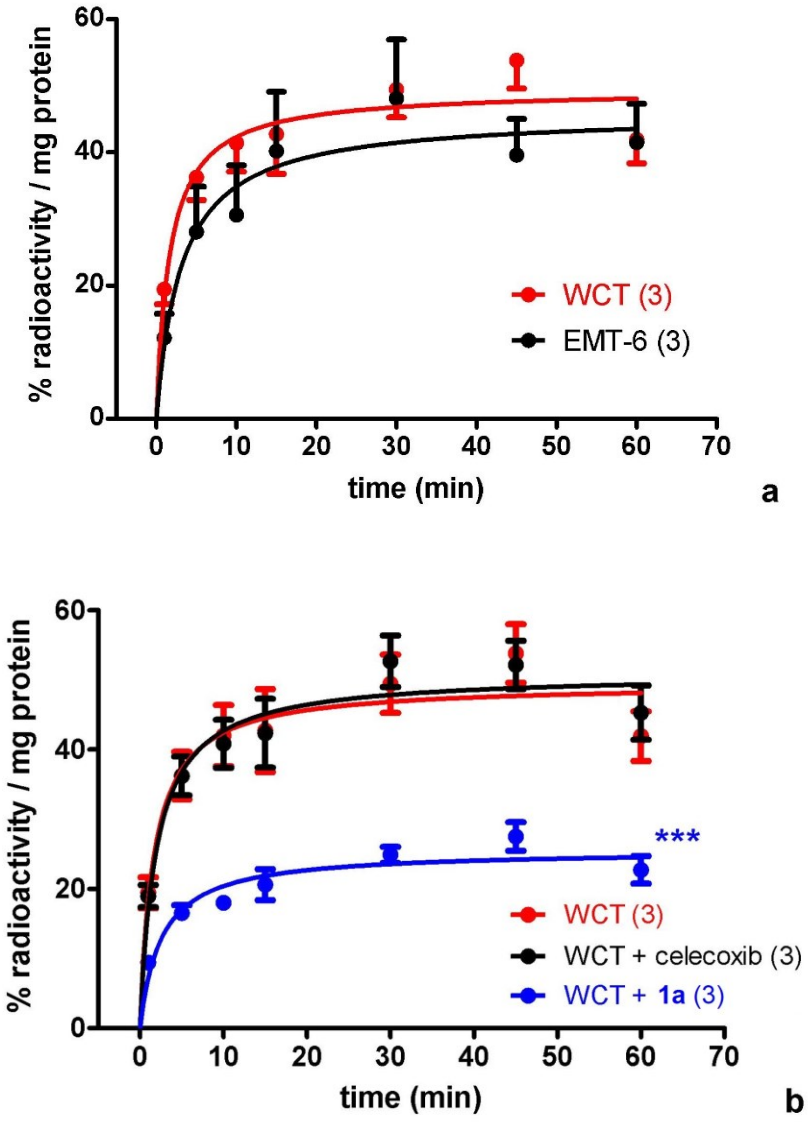

Figure 4-2a, 4-2b: (a) *In vitro* cell uptake of [^{18}F]**1a** into WCT and EMT-6 cells; (b) *In vitro* cell uptake of [^{18}F]**1a** into WCT cells and WCT cells pretreated with 10 μM celecoxib and 10 μM **1a**. All data as mean ± SEM.

The specificity of radiotracer uptake was tested by performing blocking experiments in WCT cells. Cells were pre-incubated with 10 μM of known COX-2 inhibitor celecoxib, as well as non-radiolabeled **1a** for 30 min prior to the addition of the radiotracer.Uptake of [^{18}F]**1a**in WCT cells was reduced significantly by pre-treating the cells with 10 μM **1a** (Fig. 4-2b). However, pre-incubation with celecoxib did not alter the amount of radioactivity detected in WCT cells.

These results suggest that uptake of the radiotracer into WCT cells might be due to binding to non-COX targets. The observation that uptake can be reduced with non-radiolabeled sister compound, but not with known COX-2 inhibitors (celecoxib) suggests that **1a** binds to an unknown non-COX target that is expressed in WCT cells; further, the results suggest that celecoxib does not bind to this target. The uptake of [^{18}F]**1a** is generally low in both WCT and EMT-6 cells at approximately 40 % radioactivity per mg of protein.

4.3.2. Metabolite analysis

Metabolite analysis of venous blood samples by radio-TLC revealed that [^{18}F]**1a** is not metabolized in Fisher-344 rats. The radiotracer was found to be fully intact 2 hours post-injection. Images of radio-TLC plates developed in 50 % ethyl acetate / hexanes are shown in Figure 4-3. **1a** has an R_f of approximately 0.5 in the solvent system used.

The content of detectable radioactivity in rat plasma increased from approximately 40 % after 5 min to around 60 % after 2 h post injection while it decreased in the blood cell fraction. Levels of radioactivity bound to plasma proteins increased slightly over the 2 hour time course of the experiment (Fig. 4-4).

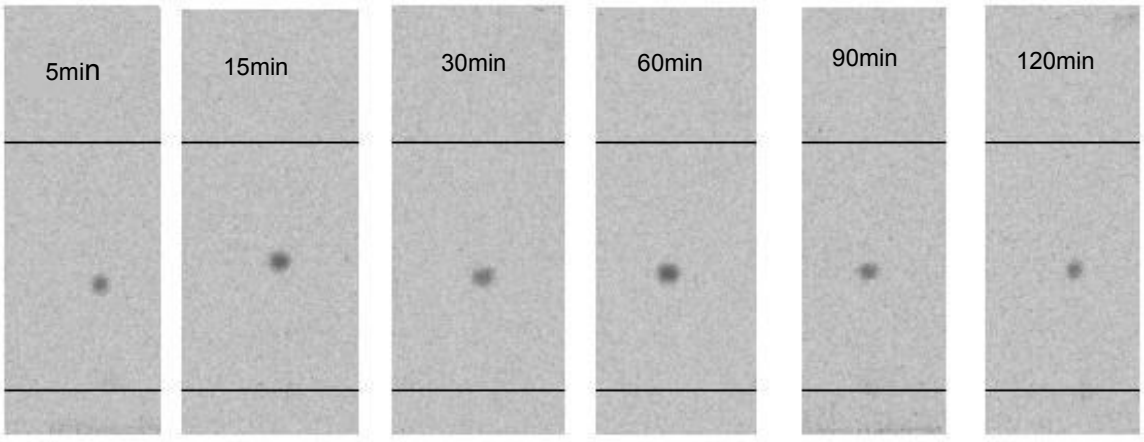

Figure 4-3: TLC plates spotted with plasma samples obtained from the venous blood of Fisher-344 rats at 5 min, 15 min, 30 min, 60 min, 90 min and 120 min post-injection of [^{18}F]**1a** analyzed using a BAS-5000 reader.

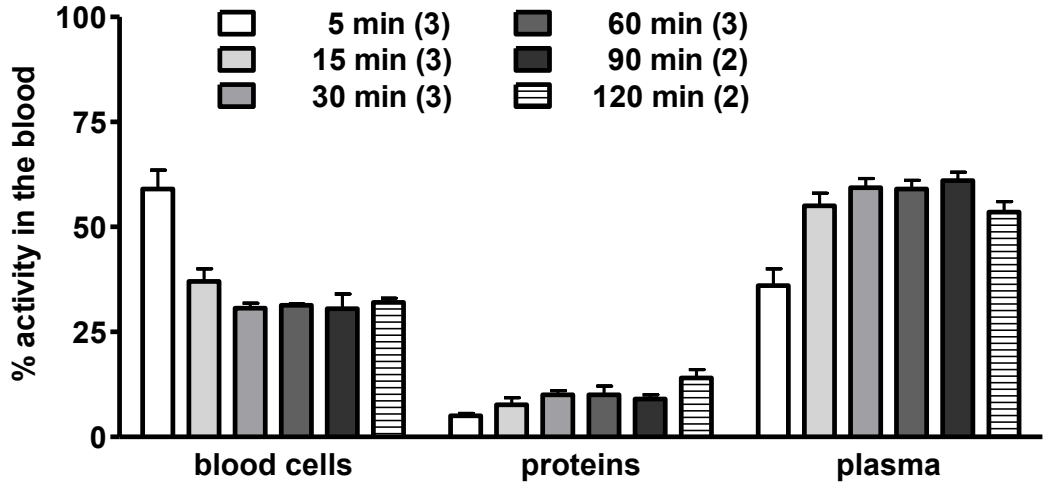

Figure 4-4: Distribution of radioactivity in the blood of Fisher-344 rats 5 min, 15 min, 30 min, 60 min, 90 min and 120 min post-injection of [^{18}F]**1a**.

4.3.3. *In vivo* small animal PET imaging

The initial *in vivo* studies of [^{18}F]**1a** were carried out in WCT bearing Fisher-344 rats using small animal PET imaging. These experiments were carried out to investigate whether [^{18}F]**1a** could serve as a COX-2 specific radiotracer *in vivo*.

Upon injection of [^{18}F]**1a** into the tail vein of a Fisher-344 rat, the tracer was transported with the venous blood to the heart and thereupon passed into the pulmonary arterial blood to reach the lung. Upon reaching the lung the radiotracer was extracted from the blood stream and retained in the lung. After approximately 30 min the radiotracer slowly starts to diffuse out of the pulmonary tissue. Figure 4-5 shows the lung of a Fisher-344 rat 1, 30, 60 and 120 min post-injection of [^{18}F]**1a** in 5 % EtOH / saline solution. This phenomenon is known as first pass pulmonary retention effect and has been studied in the context of local anesthetics [5, 6]. A thorough discussion of the first pass pulmonary retention effect can be found in Chapter 7.

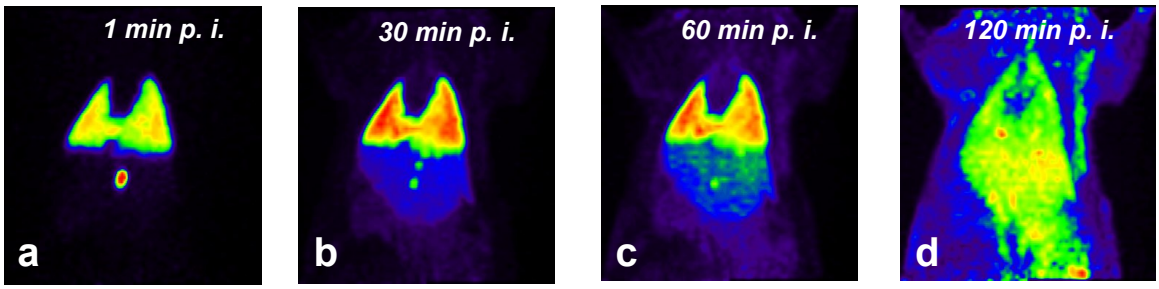

Figure 4-5a to 4-5d: PET images at 1 min to 120 min post-injection of [^{18}F]**1a** (in 5 % ethanol / saline) into the tail vein of a Fisher-344 rat under isoflurane anesthesia.

To by-pass the first pass pulmonary retention effect, radiotracer was bound to carrier protein human serum albumin (HSA) before being injected into the tail vein of Fisher-344 rats. The use of HSA as a carrier protein for radiotracers has been described previously been described in the

literature [7, 8]. HSA-bound radiotracer was diffuse out of the lung much more rapidly and distribute throughout the body at an improved rate. Based on that observation all subsequent WCT model *in vivo* experiments were conducted using HSA-bound [^{18}F]**1a** only.

Experiments with [^{18}F]**1a** (5 % EtOH / saline / 3.5 % HSA) in WCT tumor-bearing Fisher-344 rats resulted in a mean standardized uptake value ($SUV_{tumor, 2h}$) of 1.52 ± 0.16 (n=7) after 120 min. The observed muscle uptake $SUV_{muscle, 2h}$ was 0.72 ± 0.04 (n=7) at the same time, resulting in a tumor-to-muscle ratio of 2.16 ± 0.27 (n=7). The radioactivity measured in WCT tumors reaches it's maximum after approximately 90 min and remains relatively unchanged thereafter, suggesting that the radioactivity measured is target bound in the tumor. Uptake into muscle tissue also does decrease over the time course of the experiment indicating some unspecific binding of the radioactivity in non-target tissue (Fig. 4-6a). This property of [^{18}F]**1a** leads to an almost steady-state tumor-to-muscle-ratio from 90 min post-injection onward. Maximum intensity projection (MIP) PET images of radioactivity distribution 90 min post injection (Fig. 4-6b) show significant accumulation of radioactivity in the WCT tumor.

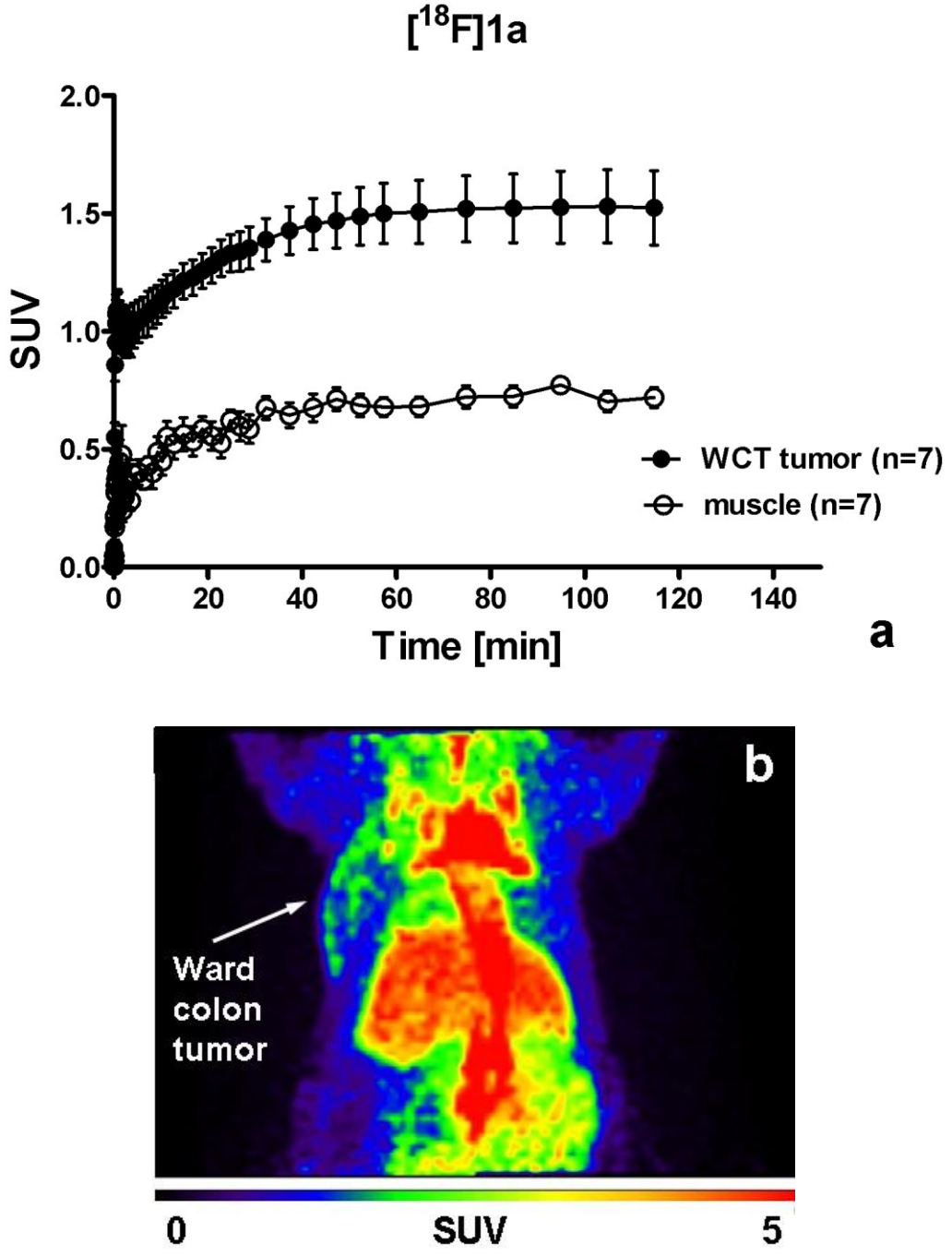

Figure 4-6a, 4-6b: (a) Time activity curves of the uptake of [^{18}F]**1a** in WCT tumor (black dot) and muscle (white dot) of Fisher-344 rats. Data as mean ± SEM. (b) Maximum intensity projection PET image at 90 min post-injection of [^{18}F]**1a** into WCT bearing (left flank) Fisher-344 under isoflurane anesthesia.

To investigate whether the uptake of [^{18}F]**1a** into WCT tumors is due to specific binding to the COX-2 enzyme a number of *in vivo* blocking studies were carried out. The aim of these studies was to achieve saturation of the target by pre-treating animals with pharmacological doses of COX-2 inhibitors. Attempts to administer large doses of COX-2 inhibitors **1a** and celecoxib by intravenous (i.v.) injection failed due to poor solubility of drug molecules and resulting crystallization in the catheter and the tail vein of the test animals. Intraperitoneal (i.p.) injections of COX-2 inhibitors, on the other hand, were successful when drug molecules were dissolved in 100 % DMSO. Distribution of COX-2 inhibitors throughout the body and saturation of COX-2 binding sites following intreperitoneal injections is expected to be significantly slower than following intravenous injection. We investigated the possibility of administering pharmacological dose 5 min, 30 min and 1 h prior to tail vein injection of the radiotracer. We found that i.p. injection of COX-2 inhibitor 30 min prior to administration of the radiotracer yielded the most consistent results. To account for differences in tumor size and COX-2 expression in the tumor between different test animals, every WCT-bearing Fisher-344 rat underwent a control scan on day one, where the animal was treated with radiotracer only, followed by a blocking scan on day two, where the animal was treated with both pharmacological dose of COX-2 inhibitor and radiotracer.

Figures 4-7a to 4-7c summarize the results of the blocking studies that were carried out in WCT bearing Fisher 344 rats. Figure 4-7a shows the time activity curves of [^{18}F]**1a** uptake in WCT tumors of untreated animals (control scans). The accumulation of radiotracer in the WCT tumors of the four animals is relatively inconsistent. Tumor uptake of the radiotracer in animal (1) reaches $aSUV_{tumor,\ 2h}$ of 2.15, while tumor uptake in animals (2), (3) and (4) reaches $aSUV_{tumor,\ 2h}$ of approximately 1.27 only. Furthermore, the flat line time activity curves observed in animals (2),

(3) and (4) suggest that the uptake of [^{18}F]**1a** in the WCT tumors of these animals is not due to specific interaction with a biological target. The time activity curve in animal (1) on the other hand shows a continuous increase in radioactivity accumulation, suggesting that the radiotracer binds to a specific target in the tumor.

Figure 4-7b shows the time activity curves of [^{18}F]**1a** uptake in WCT tumors of the same Fisher-344 animals treated with celecoxib (blocking scans). For these experiments WCT tumor bearing Fisher-344 rats were treated with 50 mg/kg celecoxib i.p. injection 30 min prior to radiotracer administration. Blocking scans were carried out one day after control scans for each animal. A blocking effect could be shown for animal (1) only. Radiotracer uptake in the WCT tumor of animal (1) treated with celecoxib showed an $SUV_{tumor,\ 2h}$ of 1.85 (compared to 2.15 in the control scan), while the $SUV_{tumor,\ 2h}$ in animals (2), (3) and (4) was approximately 1.35 (compared to 1.27 in control scans). The shape of the time activity curves in the animals treated with celecoxib is similar to those encountered in the control scans. While a continuous accumulation of radiotracer is observed in the WCT tumor of animal (1), the time activity curves for animals (2), (3) and (4) are flat and indicative of non-specific accumulation.

In Figure 4-7c the mean tumor SUV's of the control scans (black dot) are compared to the mean tumor SUVs for the blocking scans (white dot). A significant reduction in radiotracer uptake in the presence of celecoxib could not be observed for this group of test animals.

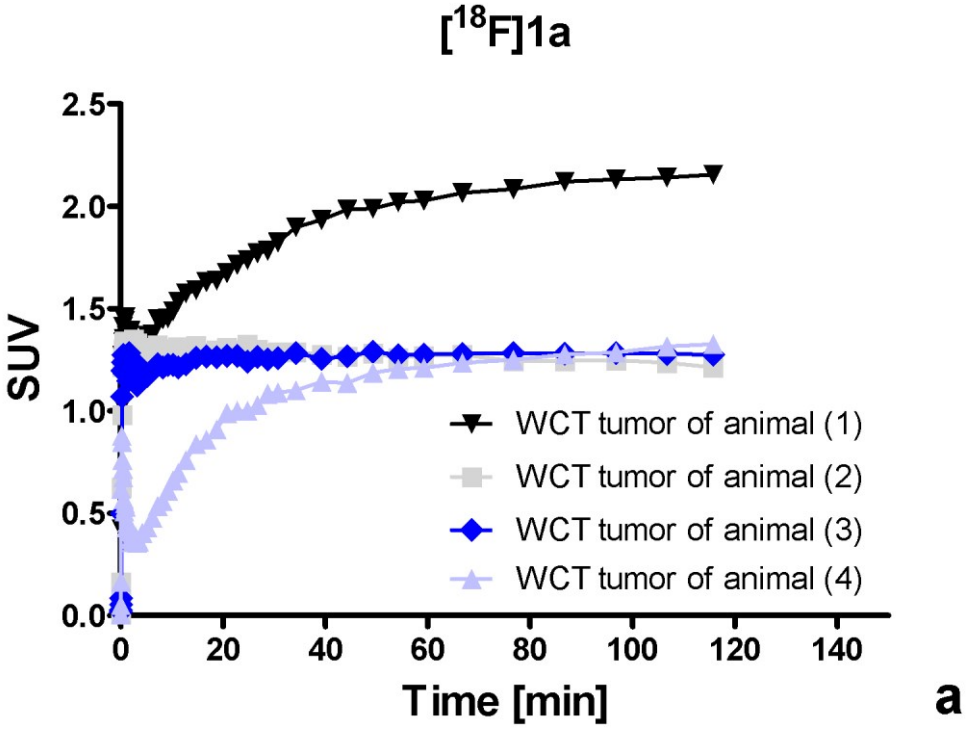
[18F]1a
SUV
2.5
2.0
1.5
1.0
0.5
0.0
0
20
40
60
80
100
120
140
Time [min]
WCT tumor of animal (1)
WCT tumor of animal (2)
WCT tumor of animal (3)
WCT tumor of animal (4)
a

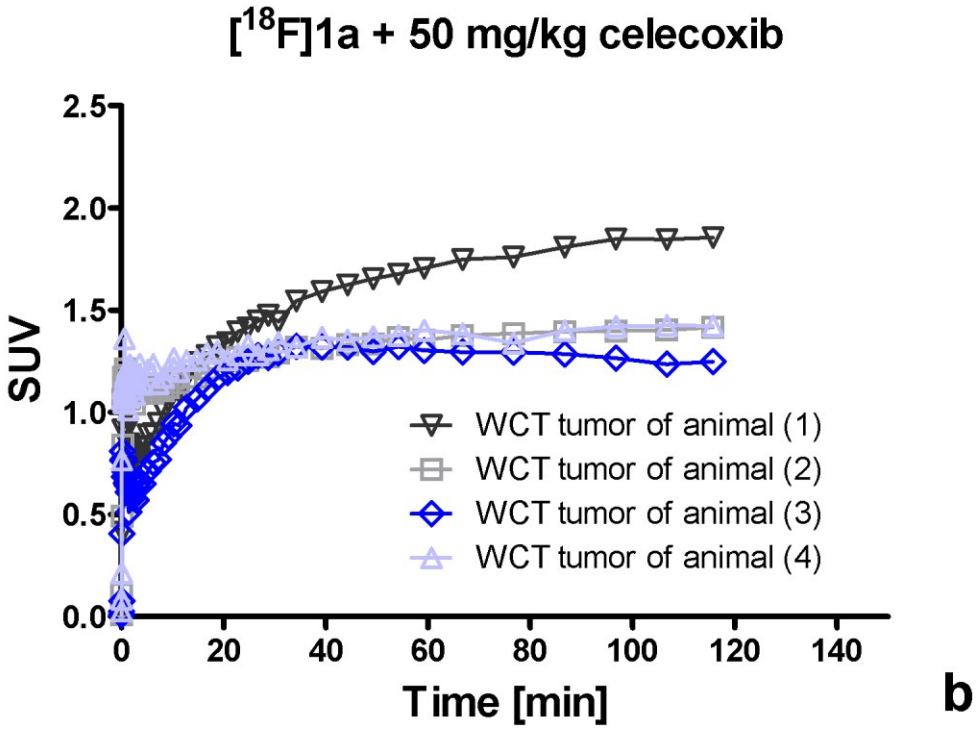
[18F]1a + 50 mg/kg celecoxib
SUV
2.5
2.0
1.5
1.0
0.5
0.0
0
20
40
60
80
100
120
140
Time [min]
WCT tumor of animal (1)
WCT tumor of animal (2)
WCT tumor of animal (3)
WCT tumor of animal (4)
b

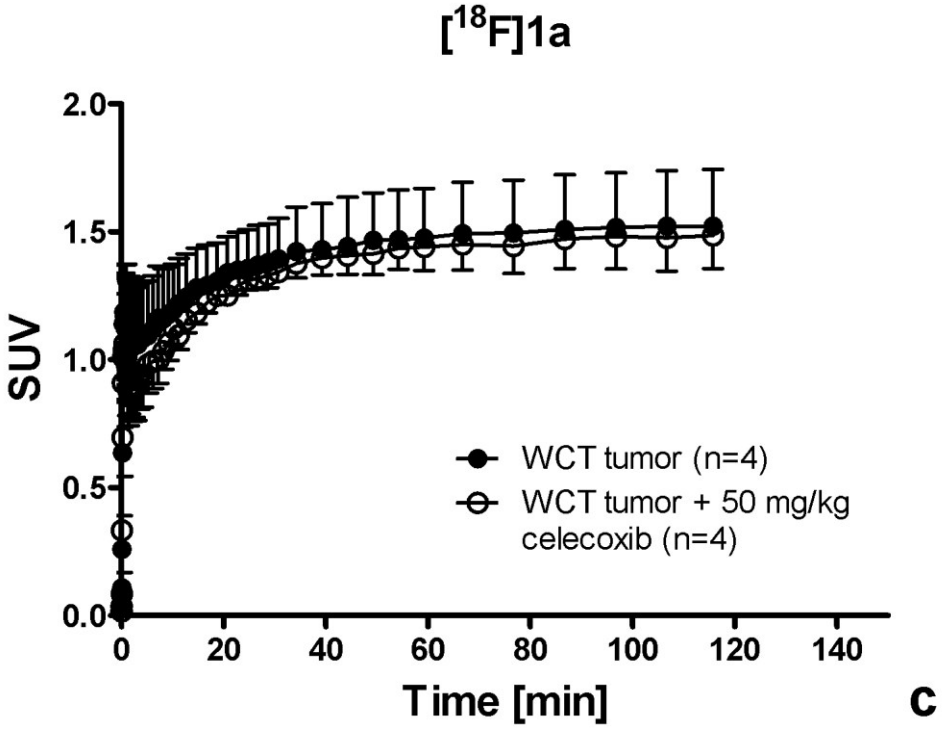

Figure 4-7a, 4-7b, 4-7c: (a) Time activity curves of the uptake of [^{18}F]**1a** in WCT tumors of Fisher-344 rats. Data as single measurements in four animals. (b) Time activity curves of the uptake of [^{18}F]**1a** in WCT tumors of Fisher-344 rats treated with 50 mg/kg celecoxib (i.p. injection) 30 min prior to radiotracer administration. Data as single measurements in four animals. (c) Time-activity curve for the uptake of [^{18}F]**1a** into WCT tumors of Fisher-344 rats (black dot); effect of 50 mg/kg celecoxib per rat, 30 min before radiotracer injection (white dot). Data expressed as mean standardized uptake value (SUV) ± SEM.

The results shown in Figure 4-7c suggest that [^{18}F]**1a** does not bind to COX-2 in WCT tumors of Fisher-344 rats. The uptake of radiotracer into the tumor grafts is likely due to binding to unknown secondary targets or due to non-specific mechanisms. If COX-2 specific binding was (at least partially) responsible for accumulation of the radiotracer in tumor grafts, a reduction of uptake in

the presence of selective COX-2 inhibitor celecoxib would be expected. The analysis of the individual control and blocking scans (Figures 4-7a and 4-7b) suggest that the failure to show COX-2 specific binding might be due to limitations in the biological model. We hypothesized that [^{18}F]**1a** did not fail to bind to COX-2 generally, but that the WCT tumor cells failed to express COX-2 in some of the animals studied. Animal (1) (Figures 4-7a and 4-7b) appears to carry a tumor that does express COX-2, hence the observation that the control uptake time activity curve (Figure 4-7a - black triangle) shows typical binding kinetics and radiotracer accumulation on the tumor can be reduced upon treatment with celecoxib ($SUV_{tumor,\ 2h}$ 2.15 vs. 1.85). Animals (2), (3) and (4), on the hand, appear to lack COX-2 expression. Western Blot analysis of WCT cell cultures used to inoculate Fisher-344 rats confirmed that COX-2 expression could not be detected (data not shown). WCT cells undergo rapid changes in morphology and protein expression patterns. Since COX-2 is inducible protein, its expression is especially susceptible to cellular changes.

4.4. Summary and conclusion

[^{18}F]**1a** underwent preliminary evaluation in WCT cells *in vitro* and in WCT-bearing Fisher 344 rats *in vivo*. The uptake of [^{18}F]**1a** in WCT cells *in vitro* was modest and did not appear to be due COX-2 specific binding. The radiotracer was found to be stable *in vivo*, and appeared to be taken up into WCT tumors *in vivo*. Definite conclusion on the suitability of [^{18}F]**1a** as an *in vivo* marker of COX-2 could not be drawn, due to inconsistencies in the biological model. A suitable protocol for *in vivo* blocking studies was developed over the course of these experiments.

Reliable *in vitro* and *in vivo* models are need to study the suitability of [^{18}F]**1a** to function as a COX-2 specific radiotracer. The initial evaluation of [^{18}F]**1a** lead to encouraging results and warrants further investigation of the radiotracer in improved biological models.

4.5. References

[1] Cao, S.; Rustum, Y.M. Synergistic antitumor activity of irinotecan in combination with 5-fluorouracil in rats bearing advanced colorectal cancer: role of drug sequence and dose. *Cancer Res.*, **2000**, 60, 3717.

[2] Grossie Jr, V.B.; Mailman, D. Influence of the Ward colon tumor on the host response to endotoxin. *J. Cancer Res. Clin.Oncol.*, **1997**, 123, 189.

[3] Xue, H.; Sawyer, M.B.; Field, C.J.; Dieleman, L.A.; Baracos, V.E. Nutritional modulation of antitumor efficacy and diarrhea toxicity related to irinotecan chemotherapy in rats bearing the ward colon tumor. *Clin. Cancer Res.*, **2007**, 13, 7146.

[4] Lin, X.B.; Farhangfar, A.; Valcheva, R.; Sawyer, M.B.; Dieleman, L.; Schieber, A.; Gänzle, M.G.; Baracos, V. The role of intestinal microbiota in development of irinotecan toxicity and in toxicity reduction through dietary fibres in rats. **2014**, e83644.

[5] Bakhle, Y.S. Pharmacokinetic and metabolic properties of lung. *Brit. J. Anaest.*, **1990**, 65, 79.

[6] Boer, F. Drug handling by the lungs. *Brit. J. Anaest.*, **2003**, 91, 50.

[7] Welch, M.J.; Dence, C.S.; Marshall, D.R.; Kilbourn, M.R. Remote system for production of Carbon-11 labelled palmitic acid. *J. labelled Compd. Radiopharm.*, **1983**, 10, 1087.

[8] Seedher, N.; Bhatia, S. Reversible binding of celecoxib and vadecoxib with human serum albumin using fluorescence spectroscopic technique. *Pharmacol. Res.*, **2006**, 54, 77.

CHAPTER 5

Evaluation of [^{18}F]1a in a mouse model of colorectal cancer

As of July 18th 2015, Chapter 5 has been submitted for publication at the Journal of Nuclear Medicine as **Tietz, O**; Wuest, M; Marshall, A; Wang, M; Bergman, C; Way, J; Wuest, F. "PET imaging of cyclooxygenase-2 (COX-2) in a colorectal cancer model."; some of the data is submitted for publication as supplementary information.

Note: The publication manuscript refers to [^{18}F]**1a** as [^{18}F]Pyricoxib. For consistency, the name [^{18}F]**1a** is retained for this thesis.

5.1. Introduction

Cyclooxgenases (COXs) are responsible for the complex conversion of arachidonic acid into prostaglandins, which exert a wide range of physiological functions mediated through binding to G-protein coupled receptors [1]. The COX enzyme family consists of two distinct isoforms; COX-1, which is a constitutively expressed enzyme and COX-2, which is the inducible form of the enzyme. COX-1 functions as a housekeeping enzyme and is expressed in most tissues types. The enzyme is responsible for maintaining homeostasis (gastric and renal integrity) and normal production of eicosanes [1]. COX-2 is only expressed in response to inflammatory stimuli and virtually absent in most resting tissues [2]. COX-2 expression is usually significantly upregulated under acute and chronic inflammatory conditions [3], as well as in neurodegenerative diseases like Parkinson and Alzheimer [4] and a variety of cancers [5].

COX-2 has become an extensively studied drug target, and numerous selective COX-2 inhibitors (coxibs) have been developed [6]. Various selective COX-2 inhibitors were in widespread clinical use from when they first gained FDA approval in 2000. However, most coxibs were withdrawn from the market in 2005 following concerns over their cardiac safety profiles [7]. Despite its evident involvement in a variety of diseases, the multiple pathogenic and non-pathogenic roles of COX-2 in human physiology have not been fully explored yet. A recent shift in COX paradigm suggests that balance between COX-1 and COX-2 expression is of crucial importance. Recent studies on biochemical mechanisms that underline the cardiac toxicity of coxibs support this theory [8, 9].

Elevated COX-2 expression was also demonstrated in many human cancers such as colorectal, gastric, and breast cancer [10-13]. Although several aspects of the molecular mechanisms underlying COX-2 expression in cancer and inflammatory lesions have been elucidated [14], there

are discrepancies between the potent anticancer effects of several COX-2 inhibitors in preclinical studies and their failure in the majority of clinical trials [15].

The development of techniques for non-invasive monitoring of COX-2 functional expression would greatly facilitate efforts to understand the COX-2 pharmacology in a living organism. To date, an exact assessment of COX-2 expression can only be achieved by laborious analyses *ex vivo*. *Ex vivo* analysis of COX-2 is not particularly accurate since COX-2 mRNA and protein are not stable outside the body and degrade rapidly [16]. Nuclear molecular imaging techniques such as positron emission tomography (PET) and single photon emission computed tomography (SPECT) would provide unique opportunities to collect data on COX-2 expression levels *in vivo* during disease development, its progression and the involvement of COX-2 in various diseases. Over the past decade more than two dozens of PET and SPECT radiotracers for COX-2 imaging have been developed. A comprehensive overview of the advances in the field and the challenges surrounding the identification of a suitable radiotracer for COX-2 imaging has been the subject of several recent reviews [17-19]. However, despite the large number of structurally diverse radiolabeled COX-2 inhibitors, none was suitable for molecular imaging of COX-2 in pre-clinical models of cancer. The purpose of the present study was to evaluate novel COX-2 radiotracer [^{18}F]**1a** as an imaging biomarker for assessment of functional expression of COX-2 in a preclinical human colorectal cancer model *in vitro* and *in vivo*.

5.2. Materials and Methods

All regents and solvents were obtained from Sigma-Aldrich, unless otherwise stated and used without further purification. Thin-layer chromatography (TLC) was performed on Merck silica gel F-254 aluminum plates, with visualization under UV light (254 nm). TLCs were developed in 1% MeOH/CH_2Cl_2 and analyzed using a BAS-5000 reader (Fuji Photo Film Co., LTD) and Adaptive Image Deconvolution Algorithm (AIDA) Image Analyzer v.450 software. High performance liquid chromatography (HPLC) purifications and analysis were performed using a Phenomenex LUNA® C18 column (100Å, 250x10mm, 10mm) on a Gilson 322 Pump module fitted with a 171 Diode Array and a radioactivity detector.

5.2.1. Radiochemistry

Radiosynthesis of [^{18}F]**1a** was performed as recently described [20]. Radiosynthesis of *N*-(4-[^{18}F]fluorobenzyl)-4-[4-(methylsulfonyl)phenyl]-6-(trifluoro-methyl)pyrimidin-2-amine ([^{18}F]**1a**): To 6 mg of radiolabeling precursor **1** was added 4-[^{18}F]fluorobenzylamine ([^{18}F]FBA) in 1 ml of THF (typically 1 GBq of [^{18}F]FBA) in a sealed vessel[1]. The reaction vessel was heated at 140 °C for 30 min. The mixture was diluted in 10 mL water and passed onto a SepPak® C18 cartridge, the cartridge was washed with 5 ml water and radiotracer [^{18}F]**1a** was eluted with 3 ml of CH_3CN. The volume of the solvent was reduced on a rotary evaporator to prepare a 1 ml 70/30 CH_3CN/H_2O formulation for HPLC purification. [^{18}F]**1a** was purified using HPLC (HPLC conditions: isocratic 70/30 CH_3CN/H_2O; flow rate 3ml/min) and the product collected at retention time of 12.6 min. The solvent was evaporated using a rotary evaporator under vacuum at 30 °C.

Decay-corrected radiochemical yield was 27±11%, and specific activity exceeded 40 GBq/μmol.[^{18}F]**1a** was then dissolved in EtOH and diluted in Krebs buffer for *in vitro* studies (% of EtOH in final volume: <1 %). For *in vivo* studies, 20 μL of [^{18}F]**1a** in EtOH was added to 180 μL of saline solution (10 % EtOH / saline solution).

5.2.2. Cell uptake studies

In vitro evaluation of [^{18}F]**1a** was performed with cell lines HCA-7 (human colon adenocarcinoma; colony 29, ECACC 2091238) and HCT-116 (human colorectal carcinoma; ATCC CCL-247). Cells were routinely cultivated in Dulbecco's Modified Eagle Medium: Nutrient Mixture F-12 (DMEM/F-12, in house) medium, supplemented with 10% (v/v) heat-inactivated fetal bovine serum (FBS, Gibco 12483), penicillin-streptomycin (1%; Gibco 15140), 2-[4-(2-hydroxyethyl)piperazin-1-yl]ethanesulfonic acid (HEPES, 10mM; Gibco 15630), and L-glutamine (2 mM; Gibco 25030) at 37 ºC and 5% CO_2 in a humidified incubator. For the uptake studies, cells were seeded in 12-well plates at a density of 400,000 cells/mL and grown to 90-95% confluence.Cellular uptake experiments using [^{18}F]**1a** (300 KBq/mL; specific activity: >40 GBq/μmol) were performed in triplicates in KREBS buffer at 37 °C with 5, 10, 15, 30, 60, 90 and 120 min incubation time. For blocking studies, cells were pre-incubated for 30 min with 10 μM and 100 μM of **1a**, celecoxib, rofecoxib, or SC58125 prior to the addition of [^{18}F]**1a**.
Blocking experiments were performed at 60 min. Radiotracer uptake was stopped by the addition of 1 mL of ice-cold PBS. Then, cells were washed two times with PBS and lysed in 0.4 mL of radio-immunoprecipitation assay buffer (RIPA buffer). Radioactivity of cell lysates was determined with a WIZARD2 Automatic gamma counter (Perkin Elmer; Waltham, MA, U.S.A.). Total protein concentration in the samples was determined by the bicinchoninic acid method

(BCA; Pierce, Thermo Scientific 23227) using bovine serum albumin (800, 600, 400, 300, 200, 100, 50 μg/mL, blank) as protein standard. Cell uptake data are expressed as percent of measured radioactivity per 1 mg protein (%radioactivity/mg protein).

5.2.3. *In vivo* tumor model

All animal experiments were carried out in accordance with the guidelines of the Canadian Council on Animal Care (CCAC) and approved by the local animal care committee (Cross Cancer Institute, University of Alberta).

Positron emission tomography (PET) and biodistribution experiments were carried out in HCA-7 tumor-bearing NIH-III nude mice (Charles River Laboratories, Quebec, Canada). Female NIH-III nude mice were housed under standard conditions with free access to standard food and tap water. HCA-7 cells ($5x10^6$ cells in 100 μl of PBS) were injected into the upper left flank of female NIH-III nude mice (20-24 g). After 14 to 21 days post-inoculation, HCA-7 tumors reached sizes of approximately 1 cm^3 which were suitable for all *in vivo* experiments.

5.2.4. Biodistribution studies in mice

NIH-III mice (body weight 21±2g) bearing subcutaneous HCA-7 tumors were intravenously injected with 3-7 MBq of [^{18}F]**1a** in 200 μL of solvent (10% EtOH/H_2O). A second group of NIH-III mice (body weight 21± 2 g) bearing HCA-7 tumors were treated with 2 mg of celecoxib administered via intraperitoneal injection in 100% DMSO 60 min prior to intravenous injection of [^{18}F]**1a** (3-7 MBq) in 200 μL of solvent (10% EtOH / H_2O). Animals were sacrificed at 60 min p.i.. Organs and tissues of interest were rapidly excised, weighed, and the radioactivity was determined using the automatic gamma counter (see above). Radioactivity in selected tissues and

organs was calculated as percent injected dose per gram tissue (%ID/g). Data were analyzed as means ± standard error of mean (mean ± SEM) for n = 4 animals.

5.2.5. Radiometabolite analysis

The radiotracer [^{18}F]**1a** (10 MBq) was injected intravenously into female NIH-III nude mice under isoflurane anesthesia. Blood samples from the tail vein were collected at 5, 30, 60, and 120 min p.i.. Plasma was separated by centrifugation (5 min, 13,000 x g) followed by plasma protein precipitation using ice-cold methanol (2 parts per 1 part plasma) and centrifugation (5 min, 13,000 x g). Supernatants were analyzed by radio-thin layer chromatography (radio-TLC). TLCs were developed in 1% MeOH/CH_2Cl_2 and analyzed using a BAS-5000 reader.

5.2.6. Pre-clinical PET imaging

General anesthesia of HCA-7 tumor-bearing mice was induced with inhalation of isoflurane in 40 % oxygen / 60 % nitrogen (gas flow = 1 ml/min), and mice were subsequently fixed in prone position. The body temperature was kept constant at 37 °C for the entire experiment. For PET experiments, 3-8 MBq of [^{18}F]**1a** in 150 µL of solution (formulation see supplementary information) was administered intravenously as a bolus injection into the tail vein. PET data was collected dynamically over 60 min using an Inveon® PET/CT scanner (Siemens Preclinical Solutions, Knoxville, TN U.S.A.).

A transmission scan for attenuation correction was not acquired. The radioactivity of the injection solution in a 0.5 ml syringe was determined with a dose calibrator (Atomlab™ 300, Biodex Medical Systems, New York, U.S.A.). After the PET emission scan was started the radioactivity was injected with a delay of approximately 15 s. Data acquisition continued for 60 min in 3D list

mode. The dynamic list mode data were sorted into sinograms with up to 54 time frames (10x2, 8x5, 6x10, 6x20, 8x60, 10x120, 6x300 s). The frames were reconstructed using maximum a posteriori (MAP) reconstruction modes. The pixel size was 0.085x0.085x0.12 cm, and the resolution in the center field of view was 1.8 mm. Correction for partial volume effects was not performed. The image files were further processed using the ROVER v2.0.51 software (ABX GmbH, Radeberg, Germany). Masks defining 3D regions of interest (ROI) were set and the ROIs were defined by thresholding. ROIs covered all visible tumor mass of the subcutaneous tumors, and the thresholds were defined by 50% of the maximum radioactivity uptake level for HCA-7 tumor in each animal.

Mean standardized uptake values [SUV_{mean} = (activity/mL tissue)/(injected activity/body weight), mL/g] were calculated for each region of interest (ROI) with a threshold defined at 50% of radioactivity uptake. Time-activity curves (TAC) were generated from dynamic PET scans. All semi-quantified PET data are presented as means ± SEM. In the blocking experiments, COX-2 inhibitor celecoxib (2 mg per animal) in 100 μL DMSO was injected intraperitoneally 60 min prior to radiotracer administration.

5.2.7. Protein analysis

50 μg of protein was loaded and run for 120V for 1 hour on IDGel (IR121s). Transfer from the SDS-PAGE to membrane was carried out at 4 ºC overnight at 35V. The membrane was then washed in PBS once for 5 minutes before blocking in 5% skim milk + 0.1% Tween-20 + PBS for 1 hour at room temperature (rt). The membrane was washed once with PBST (PBS+0.1%Tween-20) for 5 minutes, followed by incubation with the COX-2 primary antibody (1:500; Santa Cruz sc-70879 mouse monoclonal) or COX-1 primary antibody and β-actin primary antibody (1:1000;

Sigma A5060 rabbit monoclonal) for 1 hour at rt. After two more washes with PBST for 5 minutes the membrane was incubated with the COX-2 secondary antibody (1:1500; Santa Cruz sc-2005 goat anti mouse) or COX-1 secondary antibody and β-actin secondary antibody (1:10000; Sigma A0545 goat anti rabbit) for 1 hour at room temperature. The membrane was washed with PBST 4 times for 5 minutes each, followed by one wash with PBS for 5 minutes. The membrane was incubated with a 1:1 mixture of substrates from Pierce ECL Western Blotting Substrate (Thermo Scientific 32209) for 1 min before gently rinsing with water.

An immuno-reactive band for COX-2 was detected at 72 kDa in HCA-7 cell lysate, which is consistent with the reported molecular weight of COX-2. Neither cell line showed expression of COX-1.

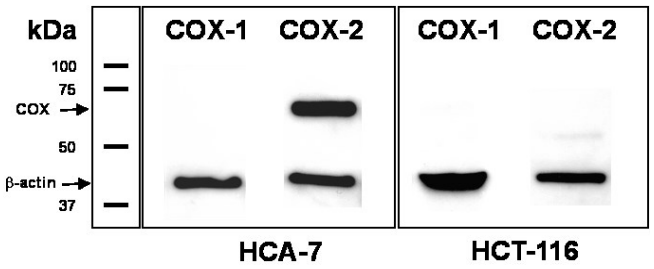

Figure 5-S1: Western blot analysis of COX-2 and COX-1 in cell lysates of HCA-7 and HCT-116 cell lines.

5.2.8. Statistical analysis

All data are expressed as means ± SEM. Graphs were constructed using GraphPad Prism 5.0 (GraphPad Software). Where applicable, statistical differences were tested by unpaired Student's t-test and were considered significant for $p<0.05$.

5.3. Results

5.3.1. Chemistry and radiochemistry

Synthesis of **1a** (*N*-(4-fluorobenzyl)-4-[4-(methylsulfonyl)phenyl]-6-(trifluoro-methyl)pyrimidin-2-amine) 1 and [^{18}F]**1a** have previously been described by Tietz *et al.* [20, 21]. **1a** was evaluated for its COX-2 inhibitory potency and selectivity profile in an *in vitro* inhibition assay. **1a** displayed excellent COX-2 inhibitory potency (IC_{50} = 7 nM) which was higher than that of celecoxib (IC_{50} = 40 nM). **1a** did not show COX-1 inhibition in the concentration range tested [20]. Radiosynthesis of [^{18}F]**1a** based on the reaction of bis-methylsulfone precursor **1** with 4-[^{18}F]fluoro-benzylamine ([^{18}F]FBA) was accomplished within 95 min including HPLC purification in decay-corrected radiochemical yields of 27±11% (Fig.5-1).

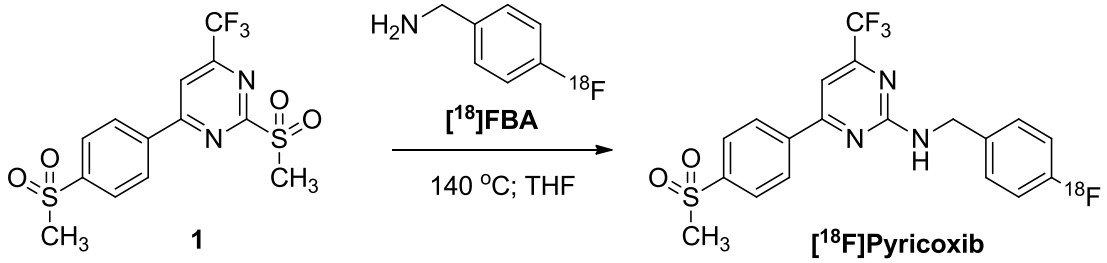

Figure 5-1: Radiosynthesis of [^{18}F]**1a** ([^{18}F]Pyricoxib).

5.3.2. Cell uptake studies

Human colorectal cancer cell lines HCA-7 (COX-2 positive) and HCT-116 (COX-2 negative) were used to study the uptake of [^{18}F]**1a** *in vitro*. High baseline expression of COX-2 in HCA-7 cells is well documented, as well as the lack of COX-2 expression in HCT-116 cells [22]. These

observations were confirmed by Western blot analysis (Fig.5-S1, Materials and methods). Cellular uptake of [^{18}F]**1a** was significantly higher in HCA-7 cells compared to HCT-116 cells (Fig.5-2).

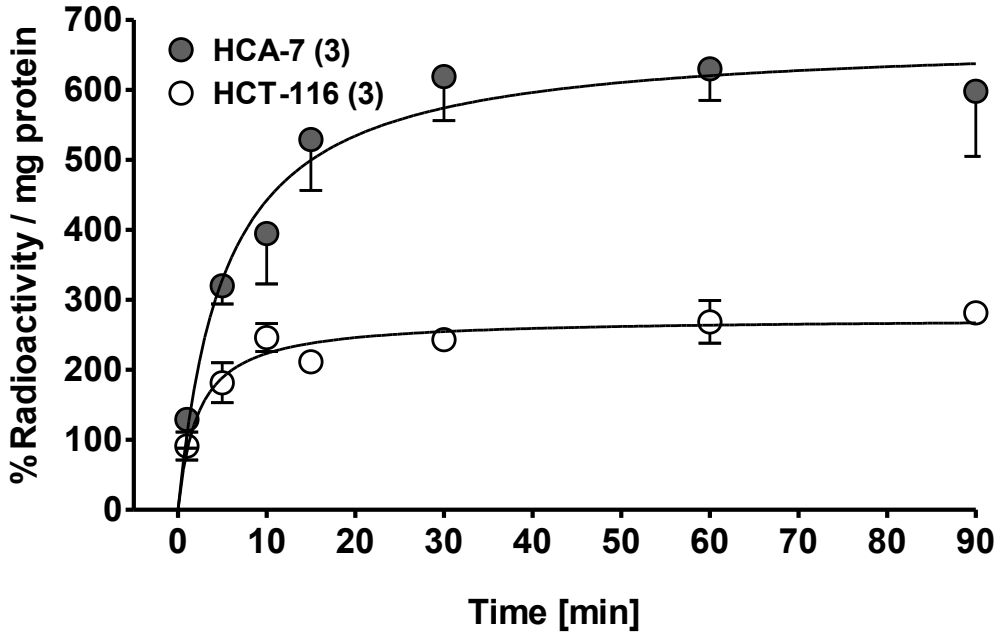

Figure 5-2: Cellular uptake of [^{18}F]**1a** in HCA-7 and HCT-116 cells. Data represented as mean ± SEM.

After 60 min, uptake in HCA-7 cells reached 630 ± 45 % radioactivity/mg of protein (n=3), while uptake in HCT-116 cells only reached 268 ± 30 % radioactivity/mg of protein (n=3) at the same time point. Specificity of radiotracer uptake in HCA-7 cells was tested by using blocking experiments (Fig.5-3).

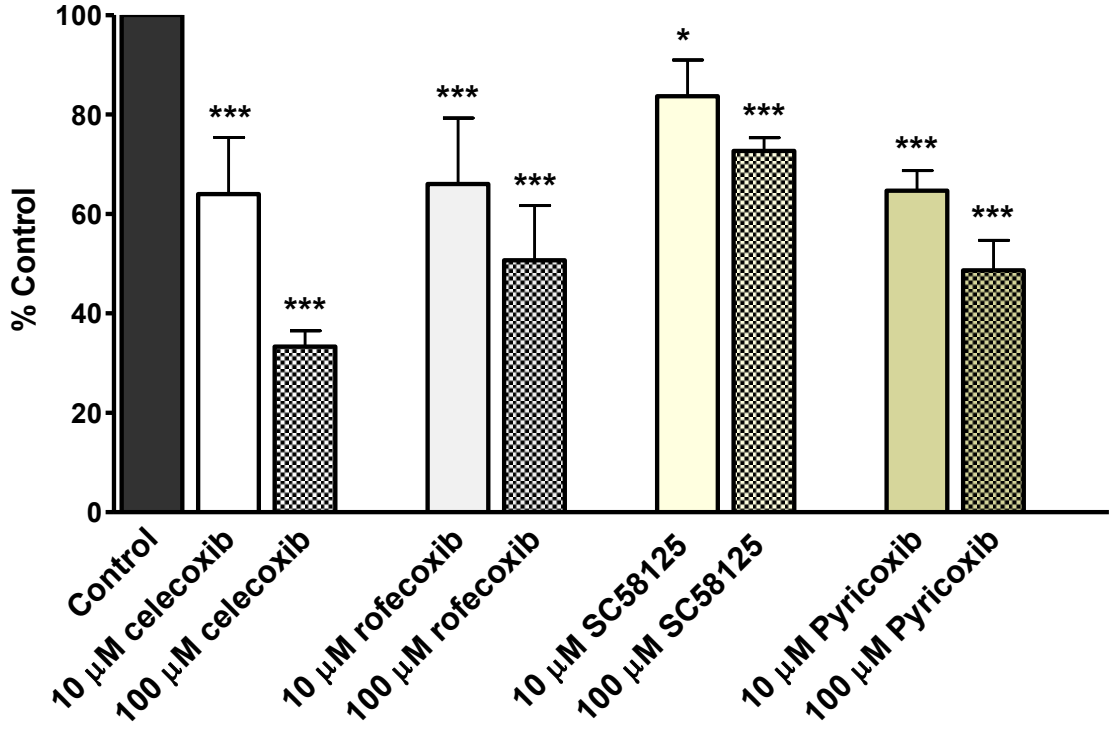

Figure 5-3: Cellular uptake inhibition studies of [^{18}F]**1a** with COX-2 inhibitors celecoxib, rofecoxib, SC58125 and **1a**. Each bar represents the mean ± SEM (n=3). * P< .05; *** P< .001.

Cells were pre-incubated with 10 and 100 μM of various COX-2 inhibitors (celecoxib, rofecoxib, SC58125 and **1a**) for 30 min prior to the addition of radiotracer [^{18}F]**1a**. Radiotracer uptake in HCA-7 cells could be reduced in a concentration-dependent manner, although to a different extent. Inhibition of radiotracer uptake was strongest with celecoxib which resulted in an inhibition of 35% at 10 μM and 65% at 100 μM. **1a** inhibited radiotracer uptake by 35% and 50% at inhibitor concentrations of 10 μM and 100 μM, respectively.

5.3.3. Biodistribution studies in mice

Biodistribution profile of [^{18}F]**1a** in the presence and absence of 2 mg celecoxib (~100mg/kg) was studied in HCA-7 tumor bearing NIH-III mice at 60 min p.i. Pre-treatment of HCA-7 tumor-bearing NIH-III mice with 2 mg of celecoxib led to a significant reduction of radiotracer uptake into HCA-7 tumors. Control animals showed a tumor uptake of 2.20 ± 0.26 %ID/g after 60 min, while treated animal displayed significantly reduced tumor uptake of 1.04 ± 0.15 %ID/g (**$p<0.01$). Presence of celecoxib also led to an increase in blood retention (**$p<0.01$) as well as an increase in uptake in a number of other tissues and organs (heart, lung, liver, kidney, stomach, pancreas, brain). Biodistribution data are summarized in Table 5-1.

Table 5-1: Biodistribution of [^{18}F]**1a** in control (left) and treated (right) HCA-7 tumor-bearing NIH-III mice (n=4). Data are dispayed as means ± SEM %ID/g after 60 min p.i.. ** $p<0.05$.

Organ	**[^{18}F]1a**	**[^{18}F]1a** *+ 2 mg celecoxib*
Blood	0.65 ± 0.06	0.98 ± 0.04
Heart	2.52 ± 0.27	5.70 ± 0.79
Lung	3.75 ± 0.33	52.26 ± 21.54
Liver	17.13 ± 0.61	25.47 ± 1.22
Kidneys	4.38 ± 0.36	8.40 ± 0.27
Spleen	1.24 ± 0.16	2.72 ± 0.32
Stomach	1.08 ± 0.14	3.96 ± 1.37
Duodenum	4.59 ± 0.37	5.18 ± 0.65
Intestine (small)	8.08 ± 1.16	6.66 ± 0.97
Intestine (large)	4.21 ± 0.87	3.48 ± 0.40
Pancreas	3.92 ± 0.69	7.22 ± 1.43
Bone	0.67 ± 0.09	1.05 ± 0.08
Ovaries	8.22 ± 0.74	4.97 ± 2.01
Brain	1.74 ± 0.26	3.79 ± 0.28
Fat	12.67 ± 2.72	5.80 ± 1.92
Muscle	1.42 ± 0.27	1.59 ± 0.32
HCA-7 Tumor	2.12 ± 0.26	1.04 ± 0.15 **
Tumor / Muscle	1.81 ± 0.52	0.70 ± 0.10
Tumor / Blood	3.39 ± 0.27	1.09 ± 0.20

5.3.4. Radio-metabolite analysis

Radio-metabolite analysis of blood samples revealed that radiotracer [^{18}F]**1a** was slowly metabolized in NIH-III mice. The amount of intact [^{18}F]**1a** decreased from 98% at 5 min p.i. to 60% at 2 h p.i.. The content of detectable radioactivity in plasma fraction increased from 20 % after 5 min to 55% after 2 h p.i., while radioactivity amount in the blood cell fraction decreased

over time. Levels of radioactivity bound to plasma proteins did not change over 2 h and remained low in the range of 2 to 7 %.

5.3.5. Pre-clinical PET imaging

PET imaging was performed in HCA-7 tumor-bearing NIH-III mice (Fig.5-4).

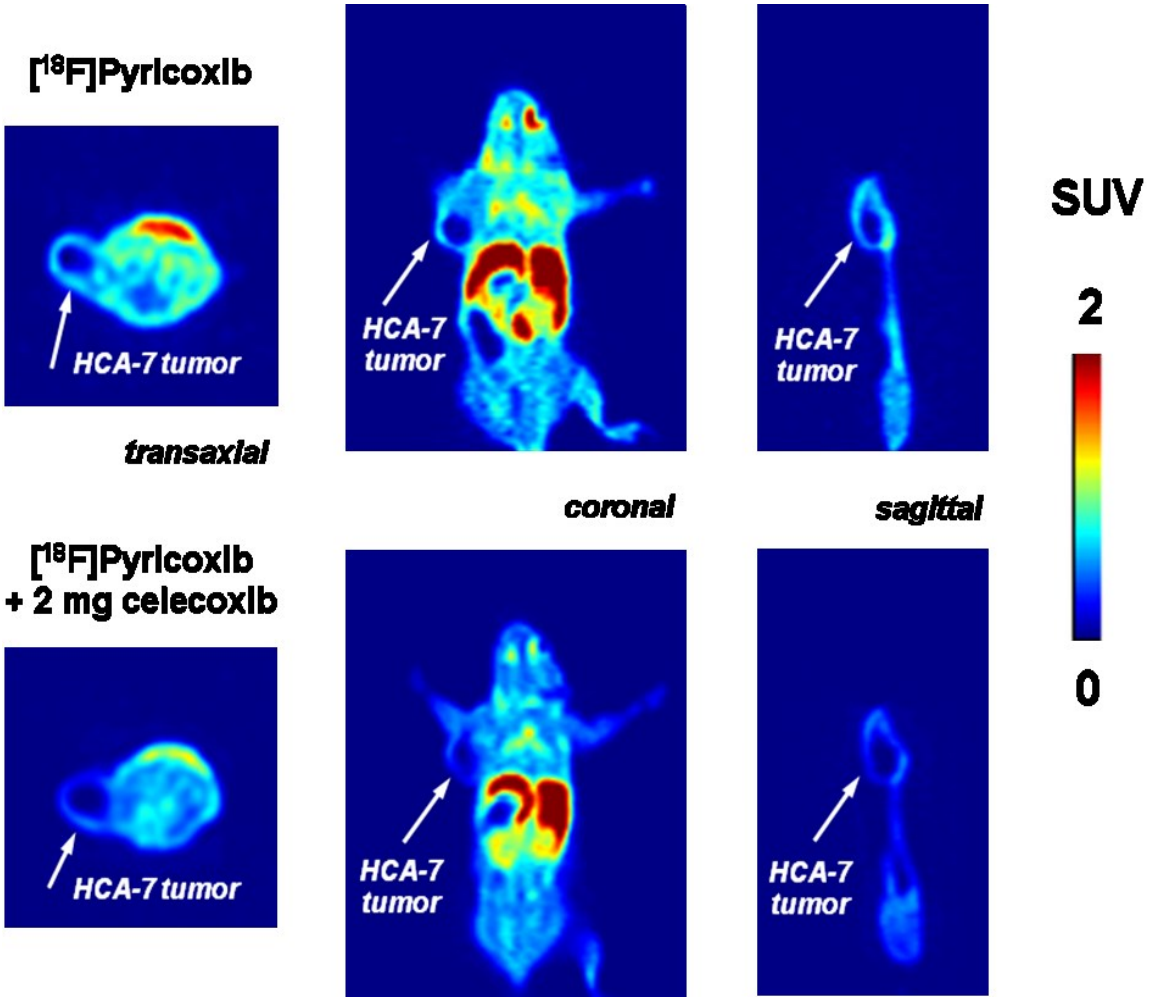

Figure 5-4: (Top) Transaxial, coronal and sagittal PET images at 60 min p.i. injection of [^{18}F]**1a** into HCA-7 tumor-bearing NIH-III mouse (control) (injected activity = 5.84 MBq); (Bottom) Transaxial, coronal and sagittal PET images at 60 min p.i. of [^{18}F]**1a** into HCA-7 tumor-bearing

NIH-III mouse (pre-treated with 2 mg of celecoxib 60 min prior to radiotracer administration, injected activity = 4.62 MBq).

Radiotracer [^{18}F]**1a** uptake in HCA-7 tumors after 60 min p.i. resulted in a mean standardized uptake value ($SUV_{tumor,1h}$) of 0.75 ± 0.05 (n=6), which was significantly higher than radioactivity uptake found in muscle tissue ($SUV_{muscle,1h}$ of 0.50 ± 0.04 (n=6)) at the same time point (***$p<0.001$). The resulting tumor-to-muscle ratio was 1.5 ± 0.2 (n=6), which was consistent with the data from the biodistribution study. Radiotacer uptake in muscle also remained high, and no clearance of radioactivity from muscle tissue was observed. Transaxial, coronal, and sagittal PET images of radioactivity distribution after 60 min p.i. clearly showed uptake in HCA-7 tumors in control animals. The same animals were pre-treated with 2 mg of celecoxib prior to radiotracer administration which led to a significant decrease of tumor uptake. Analysis of time-activity curves of radioactivity uptake in HCA-7 tumors and muscle in the absence (control) and presence of celecoxib further confirmed the blocking effect (Fig. 5-5).

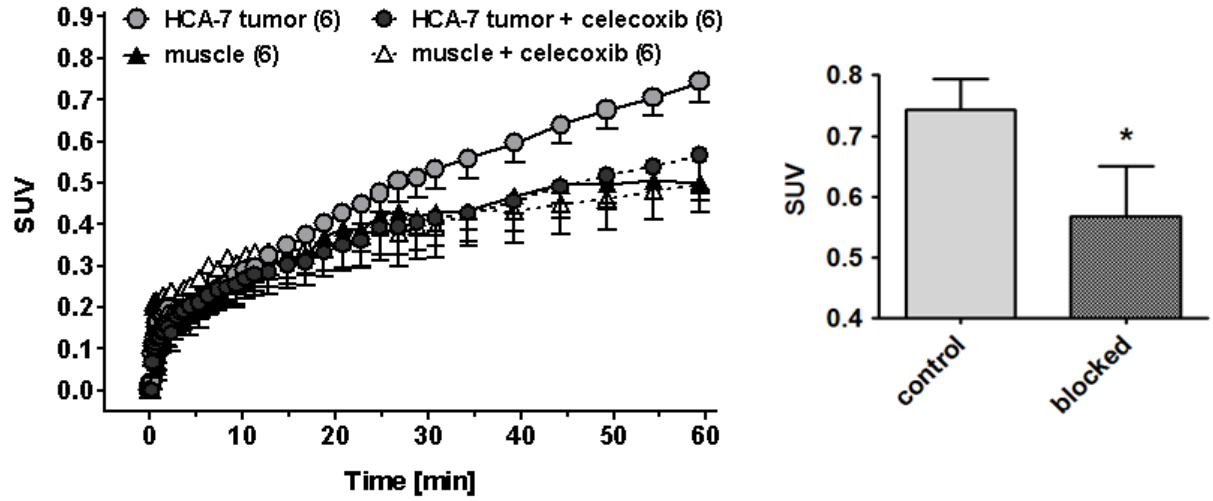

Figure 5-5: Analyzed standardized uptake values at 60 min p.i. for the uptake of [^{18}F]**1a** into HCA-7 tumors and muscle in control and treated animals.

Each blocking experiment was performed on consecutive days in the same animal with a baseline scan (control) followed by a PET scan after treatment of the animal with celecoxib treated scan. The uptake of [^{18}F]**1a** in HCA-7 tumors ($SUV_{tumor,1h}$ of 0.75 ± 0.058; n=6) was significantly reduced upon treatment to$SUV_{tumor,1h}$ of 0.57 ± 0.08 (n=6) (*p=0.05), which was in the same range as the SUV measured in muscle.

5.4. Discussion

Over the last two decades, numerous PET and SPECT radiotracers have been developed for COX-2 imaging. Several radiotracers have been subject of preclinical evaluation for molecular imaging of COX-2 expression in inflammation and cancer [17-19]. However, most of the reported radiotracers failed to visualize COX-2 *in vivo* due to multiple challenges including low metabolic stability, insufficient inhibitory potency and specificity for COX-2, and high non-specific binding to other targets. These challenges are especially pronounced for experiments aimed at molecular imaging of COX-2 in various preclinical cancer models. As a result, none of the reported radiotracers could demonstrate specific interaction with COX-2 *in vivo*. Therefore, to date no successful imaging strategy for COX-2 in cancer has been described.Reasons for the failure of successful molecular imaging of COX-2 *in vivo* can be attributed to a major extent tounfavourable radiopharmacological profile of the radiotracers tested, but the selection and utilization of suitable pre-clinical models to study COX-2 radiotracers seems to be equally challenging.

In this study we have evaluated novel COX-2 radiotracer [^{18}F]**1a** in HCA-7 mouse xenografts as a preclinical model of colorectal cancer. Radiotracer [^{18}F]**1a** contains a 6-membered trifluoromethyl pyrimidine core structure and a methylsulfone COX-2 pharmacophore, which is different to most of the recently tested COX-2 inhibitors like celecoxib and valdecoxib containing 5-membered heterocyclic core structure and a sulphonamide COX-2 pharmacophore.

Radiotracer [^{18}F]**1a** was prepared in good radiochemical yields of 27±11% using 4-[^{18}F]fluorobenzylamine as readily available ^{18}F building block[21] within a substitution reaction using 2-(methyl-sulfonyl)-4-(4-(methyl-sulfonyl)phenyl)-6-(trifluoromethyl)-pyrimidine 1 as the radiolabeling precursor. The radiotracer was shown to possess reasonable metabolic stability*in vivo*, reaching 60% of intact [^{18}F]**1a** after 2 h p.i. in mice. Moreover, radiotracer [^{18}F]**1a** exhibited

high inhibitory potency and selectivity for COX-2 (IC_{50} = 7 nM) versus COX-1(IC_{50}>100 μM). Therefore, [^{18}F]**1a** meets two basic requirements for a successful PET imaging agents – high metabolic stability and high inhibitory potency and selectivity for the target in the nanomolar range. However, COX-2 is located inside the membrane of the endoplasmic reticulum. Consequently, radiotracers need to cross various biological membranes to reach the COX-2 binding site.

For this purpose, a favourable lipophilicity profile is required, and the lipophilicity of [^{18}F]**1a** was determined to be log*P* = 2.28 ± 0.05. This value is in the range to allow for passive diffusion, and it is also in the same range as reported lipophilicity values of other radiolabeled COX-2 inhibitors [17-19]. Cellular uptake studies of [^{18}F]**1a** in human colorectal cell lines HCA-7 and HCT-116 demonstrated significantly higher radiotracer uptake and retention in COX-2 positive HCA-7 cells, reaching 630±45% of radioactivity/mg protein after 60 min. However, overall uptake of the radiotracer was also high in COX-2 negative HCT-116 cells, reaching 268±30% of radioactivity/mg protein. This finding is indicative of a favourable passive diffusion profile of the radiotracer in combination with COX-2 mediated uptake and retention mechanisms in the case of COX-2 expressing HCA-7 cells. In COX-2 negative HCT-116 cells, several COX-2 independent uptake and retention mechanisms are likely to be responsible for the observed radiotracer uptake. ATP-independent passive diffusion of radiotracer [^{18}F]**1a** through cell membranes was confirmed by cellular uptake studies at 37 °C and 4 °C, which led to comparable cellular uptake levels in both cell lines (data not shown). Reduction of radiotracer uptake in HCA-7 cells in response to pre-treatment with various COX-2 inhibitors in a concentration-dependent manner indicated that cellular uptake and retention of [^{18}F]**1a** is largely related to specific binding to COX-2. However, blocking efficacy varied among the used COX-2 inhibitors and was most evident with celecoxib.

No complete blockage of radiotracer uptake could be achieved and remaining radioactivity levels of >35% even at high inhibitor concentrations of 100 μM is indicative of some non-specific intracellular binding of the radiotracer. Interactions of radiotracer [^{18}F]**1a** with COX-2 and non-COX targets would explain the observed broad variety in blocking efficacy using different COX-2 inhibitors, assuming that every used compound possesses a distinct affinity and selectivity profile for both COX and non-COX targets.

However, given the data determined during the present study, it is not possible to speculate about the nature of potential non-COX targets, although some secondary targets have been identified in the literature. Most of the research in this area focused on celecoxib [23-25]. COX-2 inhibitors like celecoxib do not interact with COX-2 exclusively; they can also interact with a variety of other molecular targets. Celecoxib was shown to directly target Ca^{2+} ATPase, protein-dependent kinase 1 (PDK-1), cycline-dependent kinases (CDKs) in concert with various cyclins, and carbonic anhydrases (CA) [23]. Direct inhibition of these proteins by celecoxib allows the drug to exert anti-carcinogenic properties in a COX-2 independent manner. Although coxibs are selective for COX-2 over COX-1, the assumption that these molecules are truly "selective drugs" is faulty. The therapeutic efficacy of drugs like celecoxib and rofecoxib can not only be attributed to inhibition of arachidonic acid metabolism through inhibition of COX-2 enzyme exclusively. Data on the non-COX affinity profile for **1a** is not available, but since celecoxib, rofecoxib and **1a** share a number of key COX-2 pharmacophores, the possibility that they share a number of non-COX molecular targets must be considered. However, at this point, potential non-COX interactions of radiotracer [^{18}F]**1a** were not further analyzed during this study.

Pre-clinical PET imaging experiments provided further evidence of COX-2 mediated uptake of [^{18}F]**1a** in COX-2 expressing HCA-7 tumors. Consistent with cellular uptake results in COX-2

expressing HCA-7 cells, radiotracer showed steady uptake in HCA-7 tumors with no wash-out of radioactivity over the time course of the PET study. COX-2 mediated retention of [^{18}F]**1a** in HCA-7 tumors was confirmed by blocking studies. Pre-dosing of HCA-7 tumor bearing mice with 2 mg of celecoxib resulted in a 25% decrease of radioactivity uptake in the tumor at 60 min p.i. compared to radioactivity uptake in tumors of control animals. Pre-treatment with celecoxib reduced SUV of HCA-7 tumors to the SUV level of that of muscle as reference tissue.

However, overall uptake in muscle was also high, and no clearance of radioactivity from muscle tissue was observed. Under normal physiological conditions, muscle tissue does not express COX-2 [2]. Therefore, the observed high uptake and retention of radioactivity in muscle tissue can also be related to non-COX-2 mediated interactions of [^{18}F]**1a**. Comparison of radiotracer uptake in control animals and animals pre-treated with celecoxib showed that tumor uptake was reduced to levels similar to those found in muscle as reference tissue. This 25% reduction of radiotracer uptake in the tumor upon blocking with celecoxib represents the COX-2 mediated fraction of radiotracer uptake, while the remaining 75% is related to non-specific and non-COX-2 mediated interactions. The biodistribution data in control and treated animals revealed a 50% blocking effect which confirmed COX-2 mediated uptake of [^{18}F]**1a** in HCA-7 tumors. Interestingly, biodistribution data also showed an increase in radiotracer uptake in response to celecoxib treatment in the lung, heart, liver, kidney, stomach, pancreas and brain. This observation further suggests that celecoxib has the ability to interact with other molecular targets responsible for the active accumulation and retention of small molecules like radiotracer [^{18}F]**1a**. The literature provides some examples of possible mechanisms. A recent study showed that celecoxib is able to inhibit G-protein coupled drug efflux pumps and thereby enhance the intracellular retention of drugs [23]. Drug-efflux pumps serve as one possible example of targets for non-COX-2 specific

interactions of molecules designed on the typical coxib structural scaffold. A number of these non-COX targets have been identified for celecoxib as typical example of the coxib drug family [23-25].

A COX-2 radiotracer recently developed by Uddin *et al*. serves as a good comparison to [^{18}F]**1a** in terms of non-COX-2 specific interaction [26]. The researchers developed an ^{18}F-labeled celecoxib derivative and evaluated the radiotracer in a COX-2 inflammation model and a COX-2 tumor model. They showed a reduction of radiotracer uptake in a carrageenan-induced inflammation model in response to pre-treatment with celecoxib. However, the observed overall uptake level of the radiotracer (SUV = 0.2) might be too low to be COX-2 specific, especially considering the high non-specific uptake of celecoxib in a variety of organs and tissues. Celecoxib contains the typical sulfonamide COX-2 pharmacophore. Various sulfonamides including celecoxib are also known to have low nanomolar affinity for members of the carbonic anhydrase (CA) enzyme family [24]. A reduction in uptake of a radiolabeled celecoxib derivative in response to treatment with celecoxib might therefore be representative of an interaction with CA rather than with COX-2. In contrast, [^{18}F]**1a** contains a methylsulfone COX-2 pharmacophore which does not interact with CAs, and[^{18}F]**1a** displayed COX-2 specific interactions *in vitro* and *in vivo*.However, the observed multiple non-COX-2 mediated interactions of radiotracer [^{18}F]**1a** still represent a major challenge.The non-specific interactions of COX-2 inhibitors like [^{18}F]**1a** are inevitable due to theirrather high lipophilic nature, which is necessary to cross biological membranes to reach the binding site of COX-2 located inside of the endoplasmic reticulum.

5.5. Conclusion

We have developed a novel PET imaging strategy for non-invasive detection of functional expression of COX-2 in cancer using radiolabeled COX-2 inhibitor [^{18}F]**1a**. The novel imaging strategy has the potential to assess COX-2 *in vivo* which fills a critical clinical need to monitor COX-2 expression non-invasively over time. Non-invasive imaging of COX-2 expression with [^{18}F]**1a** in cancer would be useful for assessing COX-2 mediated effects on chemoprevention and radiosensitization using COX-2 inhibitors as an emerging class of anti-cancer drugs, especially for colorectal cancer.

5.6. References

[1] Kurumbail, R.G.; Kiefer, J.R.; Marnett, L.J. Cyclooxygenase enzymes: Catalysis and inhibition. *Curr. Opin. Struct. Biol*., **2001**, 11, 752.

[2] Okamoto, T.; Hino, O. Expression of cyclooxygenase-1 and -2 mRNA in rat tissues: Tissue-specific difference in the expression of the basal level of mRNA. *Int. J. Mol. Med.,* **2000**, 6, 455.

[3] Seibert, K.; Zhang, Y.; Leahy, K.; Hauser, S.; Masferrer, J.; Perkins, W.; et al. Pharmacological and biochemical demonstration of the role of cyclooxygenase 2 in inflammation and pain. *Proc. Natl. Acad. Sci. U S A.,***1994**, 91, 12013.

[4] Teismann, P.; Tieu, K.; Choi, D.; Wu, D.; Naini, A.; Hunot, S.; et al. Cyclooxygenase-2 is instrumental in parkinson's disease neurodegeneration. *Proc. Natl. Acad. Sci. U S A.,* **2003**, 100, 5473.

[5] Méric, J.; Rottey, S.; Olaussen, K.; Soria, J.; Khayat, D.; Rixe, O.; et al. Cyclooxygenase-2 as a target for anticancer drug development. *Crit. Rev. Oncol.,* **2006**, 59, 51.

[6] Shi, S.; Klotz, U. Clinical use and pharmacological properties of selective COX-2 inhibitors. *Eur. J. Clin. Pharmacol.,* **2008**, 64, 233.

[7] FitzGerald, G.A. Coxibs and cardiovascular disease. *N. Engl. J. Med.,* **2004**, 351, 1709.

[8] Cannon, C.P.; Cannon, P.J. COX-2 Inhibitors and Cardiovascular Risk. *Science.,* **2012**, 336, 1386.

[9] Yu, Y.; Ricciotti, E.; Scalia, R.; Tang, S.Y.; Grant, G.; Yu, Z.; Landesberg, G.; et al. Vascular COX-2 Modulates Blood Pressure and Thrombosis in Mice. *Sci. Transl. Med.,* **2012**, 132.

[10] Edwards, J.; Mukherjee, R.; Munro, A.F.; Wells, A.C.; Almushatat, A.; Bartlett, J.M.S. HER2 and COX2 expression in human prostate cancer. *Eur. J. Cancer.,* **2004**, 40, 50.

[11] Wang, D.; DuBois, R.N. The role of COX-2 in intestinal inflammation and colorectal cancer. *Oncogene.,* **2010**, 29, 781.

[12] Hwang, D.; Scollard, D.; Byrne, J.; Levine, E. Expression of cyclooxygenase-1 and cyclooxygenase-2 in human breast cancer. *J. Natl. Cancer. Inst.,* **1998**, 90, 455.

[13] Jiménez, P.; García, A.; Santander, S.; Piazuelo, E. Prevention of cancer in the upper gastrointestinal tract with COX-inhibition, still an option? *Curr. Pharm. Des.,* **2007**, 13, 2261.

[14] Greenhough, A.; Smartt, H.; Moore, A.; Roberts, H.; Williams,A.; Paraskeva, C.; et al. The COX-2/PGE(2) pathway: Key roles in the hallmarks of cancer and adaptation to the tumour microenvironment. *Carcinogenesis,* .**2009**, 30, 377.

[15] Ghosh, N.; Chaki, R.; Mandal, V.; Mandal, S. COX-2 as a target for cancer chemotherapy. *Pharmacol. Rep.,* **2010**, 62, 233.

[16] Inoue, H.; Taba, Y.; Miwa, Y.; Yokota, C.; Miyagi, M.; Sasaguri, T. Transcriptional and posttranscriptional regulation of cyclooxygenase-2 expression by fluid shear stress in vascular endothelial cells. *Arterioscler. Thromb. Vasc. Biol.,* **2002**, 22, 1415.

[17] Tietz, O.; Marshall, A.; Wuest, M.; Wang,M.; Wuest, F. Radiotracers for Molecular Imaging of Cyclooxygenase-2 (COX-2) Enzyme. *Curr. Med. Chem.,* **2013**, 20, 4350.

[18] Pacelli, A.; Greenman, J.; Cawthorne, C.; Smith, G. Imaging COX- 2 expression in cancer using PET/SPECT radioligands: current status and future directions. *J.Labelled Compd. Radiopharm.*, **2014**, 57, 317.

[19] Laube, M.; Kniess, T.; Pietzsch, J. Radiolabelled COX-2 inhibitors for non-invasive visualization of COX-2 expression and activity-A critical update. *Molecules.,* **2013**, 18, 6311.

[20] Tietz, O.; Sharma, S.K.; Kaur, J.; Way, J.; Marshall, A.; Wuest, M.; Wuest, F. Synthesis of three ^{18}F-labelled cyclooxygenase-2 (COX-2) inhibitors based on a pyrimidine scaffold. *Org. Biomol. Chem.,* **2013**, 11, 8052.

[21] Way, J.; Wuest, F. Fully automated synthesis of 4-[^{18}F]fluorobenzylamine based on borohydride/$NiCl_2$ reduction.*Nucl. Med. Biol.,* **2013**, 40, 430.

[22] Debucquoy, A.; Devos, E.; Vermaelen, P.; Landuyt, W.; De Weer, S.; Van Den Heuvel, F.; Haustermans, K. 18F-FLT and 18F-FDG PET to measure response to radiotherapy combined with celecoxib in two colorectal xenograft models. *Int. J. Radiat. Biol.,* **2009**, 85, 763-771.

[23] Awara, W.M.; El-Sisi, E.A.; El-Sayad, M.E.; Goda, A.E. The potential role of cyclooxygenase-2 inhibitors in the treatment of experimentally-induced mammary tumour: does celecoxib enhance the anti-tumour activity of doxorubicin? *Pharmacol. Res.,* **2004**, 50, 487-498.

[24] Weber, A.; Casini, A.; Heine, A.; Kuhn, D.; Supuran, C.T.; Scozzafava, A.; Klebe, G. Unexpected nanomolar inhibition of carbonic anhydrase by COX-2-selective celecoxib: New pharmacological opportunities due to related binding site recognition. *J. Med. Chem.,* **2004**, 47, 550.

[25] Grosch, S.; Maier, T.J.; Schiffmann, S.; Geisslinger, G. Cyclooxygenase-2 (COX-2) independent anticarcinogenic effects of selective COX-2 inhibitors. *J. Nat. Cancer Inst.,* **2006**, 98, 736.

[26] Uddin, M.; Crews, B.; Ghebreselasie, K.; Huda, I.; Kingsley, P.; Ansari, M.; et al. Fluorinated COX-2 inhibitors as agents in PET imaging of inflammation and cancer. *Can. Prev. Res.,* **2011**, 4, 1536.

CHAPTER 6

Structure-activity relationship of three ^{18}F-labeled COX-2 inhibitors

As of July 29th 2015, Chapter 6 has been submitted for publication in Molecular Imaging and Biology as **Tietz, O**; Marshall, A; Bergman, C; Wuest, M; Wuest, F. "Molecular structure influences radiopharmacology of ^{18}F-labeled COX-2 inhibitors *in vivo*."

6.1. Introduction

The cyclooxygenase (COX) enzyme family consists of COX-1 and COX-2. Non-steroidal anti-inflammatory drugs (NSAIDs) such as aspirin, ibuprofen, paracetamol, diclofenac and others were developed first before the COX enzyme family was discovered and identified in the 1970s [1,2]. Most NSAIDs are not selective in inhibiting COX-1 and COX-2 enzyme. Selective COX-2 inhibitors were developed only after the discovery after two distinct isoforms, the constitutively expressed COX-1 and the inducible expressed COX-2 in 1991 [3]. The discovery resulted in a scientific paradigm which postulated that maintenance of normal physiological processes was mediated by COX-1, while pathophysiological conditions were mediated by COX-2 [4]. Inhibition of the housekeeping enzyme COX-1 is one of the main reason for several severe gastrointestinal side-effects associated with long term NSAID use [5].

The discovery of the COX-2 isoform led to the development of numerous COX-2 selective inhibitors, so called coxibs, such as celecoxib, rofecoxib, valdecoxib and others. These drugs promised to deliver the same relief from pain and inflammation as NSAIDs, but without gastrointestinal side-effects. Development of highly selective compounds through molecular screening has made COX-2 also an attractive target for molecular imaging [6]. Moreover, COX-2 was found to be involved in the development and progression of a variety of cancers and neurodegenerative diseases [7, 8]. As a result, a large number of COX-2 selective radiotracers have been developed to visualize functional expression of COX-2 in cancer, inflammation and other diseases [9-11].

Despite initial promise, the therapeutic and diagnostic value of coxibs as drugs and radiolabeled coxibs as molecular probes remained challenging. The majority of coxibs in clinical use during the early 2000's had to be withdrawn from market following concerns over their cardiac toxicity

profile. Although a large number more than two dozen of PET and SPECT radiotracers have been developed over the past decade, none of them has progressed past initial preclinical testing stages [6].

The failure of coxibs and their radiolabeled analogues in preclinical and clinical settings is due to multiple challenges associated with the molecular target and the coxib compound class itself. Both COX enzymes are membrane bound on the inside of the endoplasmic reticulum, and the active site of both enzymes is located at the end of a long hydrophobic channel with the entrance located inside the membrane [12]. These characteristics make COX-2 a very challenging molecular target, which has formidable consequences for the design of radiopharmaceuticals with good membrane crossing properties through active or passive diffusion. Potential radiotracer candidates must therefore be lipophilic enough to readily diffuse through membranes. However, in that case the non-specific background uptake of these radiotracers in adipose and muscle tissue is expected to lead to unfavorable target-to-background ratios.

In addition to the complexity of the nature of the molecular target, other challenges encountered in specific targeting of COX-2 derived from the molecular structure and pharmacokinetic properties of the coxib compound class. Most COX-2 selective inhibitors are designed around a central aryl or heteroaryl core structure plus two aryl rings on either side of the central motif. A large number of coxibs further include a methyl sulfone or sulfonamide motif on the COX-2 pharmacophore attached to one of the two aryl rings as well as a hydrophobic moiety bound to the central core structure [13]. It was demonstrated that typical coxib compounds exhibit various interactions with non-COX targets. This phenomenon is best studied for celecoxib, which has been shown to possess affinity for NF-kB, cyclins A and E, carbonic anhydrases, and others [14]. Observed anti-cancer effects of celecoxib in various pre-clinical and clinical studies were

demonstrated to involve multiple non-COX pathways [14]. Some of the non-COX mediated effects have been shown to be particularly caused by specific interactions with members of the carbonic anhydrase family [15].

There are also notable discrepancies between the performance of COX-2 radiotracers in various *in vitro* screening assays and their pharmacological properties in complex *in vivo* systems. We have previously designed and synthesized novel ^{18}F-labeled COX-2 selective radiotracers based on a pyrimidine scaffold (Fig. 6-1) [16]. All compounds displayed high COX-2 inhibitory potencies in the lower nanomolar range. Furthermore we have evaluated COX-2 mediated radiopharmacology of radiotracer [^{18}F]**1a** ([^{18}F]Pyricoxib) in a human colorectal xenograft cancer model [17]. The goal of the present study was to compare the radiopharmacological profile of [^{18}F]**1a** to its sister compounds [^{18}F]**2a** and [^{18}F]**3a**. We wanted to elucidate how small structural alterations influence pharmacokinetic parameters such as distribution, accumulation, retention and elimination.

6.2. Materials and methods

All regents and solvents were obtained from Sigma-Aldrich, unless otherwise stated and used without further purification. Nuclear magnetic resonance spectra were recorded on a 400MHz Varian (Palo Alto, CA, USA) unit and a 600 MHz Bruker (Billerica, MA, USA) unit. ^{1}H-NMR chemical shifts are recorded in ppm relative to tetramethylsilane (TMS). ^{19}F-NMR chemical shifts are recorded in ppm relative to trichlorofluoromethane. Low resolution mass spectra were obtained using am Agilent Technologies (Santa Clara, CA, USA) 6220 oaTOF instrument. Column chromatography was conducted using Merck silica gel (mesh size 230–400 ASTM). Thin-layer chromatography (TLC) was performed on Merck silica gel F-254 aluminum plates, with visualization under UV light (254 nm). High performance liquid chromatography (HPLC) purifications and analysis were performed using a Phenomenex LUNA® C18 column (100Å, 250x10mm, 10mm) on a Gilson 322 Pump module fitted with a 171 Diode Array and a radio detector.

6.2.1. Chemistry and Radiochemistry

Non-radiolabeled compounds **1a** (N-(4-fluorobenzyl)-4-[4-(methylsulphonyl)phenyl]-6-(trifluoromethyl)pyrimidin-2-amine), **2a** (4-{2-[(4-fluorobenzyl)amino]-6-(trifluoromethyl)pyrimidin-4-yl}benzenesulphonamide) and **3a** (2-[(4-fluorobenzyl)oxy]-4-[4-(methylsulphonyl)phenyl]-6-(trifluoromethyl)pyrimidine), labeling precursors, as well as radiotracers [^{18}F]**1a**, [^{18}F]**2a** and [^{18}F]**3a** were prepared as previously reported [16 -19].

6.2.2. Octanol-water partition coefficient

The lipophilicity of [^{18}F]**1a**, [^{18}F]**2a** and [^{18}F]**3a** was determined by adding 10 MBq of compound the respective radiotracer in a mixture of 5 ml octanol and 5 ml phosphate-buffered saline (PBS) at pH 7.4. The mixture was shaken for 30 min and the layers separated. A 10µl sample of the organic layer and a 1 mL sample of the aqueous layer were taken and the radioactivity measured using a gamma counter.

6.2.3. Formulation of radiotracers for *in vitro* and *in vivo* studies

Radiotracers [^{18}F]**1a**, [^{18}F]**2a** and [^{18}F]**3a** were dissolved in ethanol (EtOH) and diluted in Krebs buffer for *in vitro* studies (final percentage of EtOH < 1 % of final volume). For *in vivo* studies, 20 µL of radiotracer in EtOH was added to 180 µL of saline solution.

6.2.4. Cell uptake studies

Experiments for the *in vitro* evaluation of radiotracers [^{18}F]**1a**, [^{18}F]**2a** and [^{18}F]**3a** were performed with HCA-7 cells (human colon adenocarcinoma; colony 29, ECACC 2091238). Cells were routinely cultivated in Dulbecco's Modified Eagle Medium: Nutrient Mixture F-12 (DMEM/F-12, in house) medium, supplemented with 10% (v/v) heat-inactivated fetal bovine serum (FBS, Gibco 12483), penicillin-streptomycin (1%; Gibco 15140), 2-[4-(2-hydroxyethyl)piperazin-1-yl]ethanesulfonic acid (HEPES, 10mM; Gibco 15630), and L-glutamine (2 mM; Gibco 25030) at 37 ºC and 5% CO_2 in a humidified incubator. For the uptake studies, cells were seeded in 12-well plates at a density of 400,000 cells/mL and grown to 90-95% confluence. Radiotracer uptake experiments were performed in triplicates in KREBS buffer at 37 ºC for 5, 10, 15, 30, 60 and 90 min incubation time. Radiotracer uptake was stopped with 1 mL ice-cold PBS, the cells were

washed subsequently two times with PBS and lysed in 0.4 mL radioimmunoprecipitation assay buffer (RIPA buffer). The radioactivity in the cell lysates was determined with a WIZARD2 Automatic gamma counter (Perkin Elmer; Waltham, MA, U.S.A.). Total protein concentration in the samples was determined by the bicinchoninic acid method (BCA; Pierce, Thermo Scientific 23227) using bovine serum albumin (800, 600, 400, 300, 200, 100, 50 μg/mL, blank) as protein standard. Cell uptake data for all experiments are expressed as percent of measured radioactivity per l mg protein (%radioactivity / mg protein).

6.2.5. Animal model

Positron emission tomography (PET) experiments were performed using HCA-7 tumor-bearing NIH-III nude mice (Charles River Laboratories, Quebec, Canada). All animal experiments were carried out in accordance with the guidelines of the Canadian Council on Animal Care (CCAC) and approved by the local animal care committee (Cross Cancer Institute, University of Alberta). Female NIH-III nude mice were housed under standard conditions with free access to standard food and tap water. HCA-7 cells ($5x10^6$ cells in 100 μl PBS) were injected into the upper left flank of female NIH-III nude mice (20-24 g). After 14 to 21 days post-inoculation, HCA-7 tumors reached sizes of approximately 1 cm^3 which were suitable for all *in vivo* experiments.

6.2.6. Dynamic PET imaging

General anesthesia of HCA-7 tumor-bearing mice was induced with inhalation of isoflurane in 40 % oxygen / 60 % nitrogen (gas flow = 1 ml/min), and mice were subsequently fixed in prone position. The body temperature was kept constant at 37°C for the entire experiment. For PET experiments, 3–8 MBq of radiotracer in 150-200 μL of solution (formulation see above) was

administered intravenously as a bolus via the tail vein. PET data were collected dynamically over 60 min to 120 min on an Inveon® PET/CT scanner (Siemens Preclinical Solutions, Knoxville, TN U.S.A.). A transmission scan for attenuation correction was not acquired. The radioactivity of the injection solution in a 0.5 ml syringe was determined with a dose calibrator (Atomlab™ 300, Biodex Medical Systems, New York, U.S.A.). After the PET emission scan was started the radioactivity was injected with a delay of approximately 15 s. Data acquisition continued for 120 to 240 min in 3D list mode. The dynamic list mode data were sorted into sinograms with up to 72 time frames (10x2, 8x5, 6x10, 6x20, 8x60, 10x120, 5x300, 19x600 s). The frames were reconstructed using maximum a posteriori (MAP) reconstruction modes. The pixel size was 0.085x0.085x0.12 cm, and the resolution in the center field of view was 1.8 mm. Correction for partial volume effects was not performed. The image files were further processed using the ROVER v2.0.51 software (ABX GmbH, Radeberg, Germany). Masks defining 3D regions of interest (ROI) were set and the ROIs were defined by thresholding. ROIs covered all visible tumor mass of the subcutaneous tumors, and the thresholds were defined by 50% of the maximum radioactivity uptake level for each HCA-7 tumor in each animal. Mean standardized uptake values [SUV_{mean} = (activity/mL tissue)/(injected activity/body weight), mL/g] were calculated for each ROI. Time-activity curves (TAC) were generated from the dynamic scans. All semi-quantified PET data are presented as means ± SEM.

6.2.7. Statistical Analysis

All data are expressed as means ± SEM. Graphs were constructed using GraphPad Prism 4.0 (GraphPad Software). Where applicable, statistical differences were tested by unpaired Student's t-test and were considered significant for $p<0.05$.

6.3. Results

6.3.1. Chemistry and Radiochemistry

Three small molecule COX-2 inhibitors based on a trifluoromethyl-pyrimidine scaffold ([^{18}F]**1a**, [^{18}F]**2a**, [^{18}F]**3a** – Fig. 6-1) were designed and synthesized as previously reported [16]. The compounds were labeled with ^{18}F via direct and indirect labeling methods and purified by HPLC to yield injectable radiotracers with a specific activity of >40 GBq/μM and a radiochemical purity of >99% [16]. Radiotracer [^{18}F]**1a** carries a methylsulfone COX-2 pharmacophore, while radiotracer [^{18}F]**2a** carries a sulfonamide pharmacophore (Fig. 6-1 – highlighted in blue). The main structural difference between the radiotracers [^{18}F]**1a** and [^{18}F]**3a** is that [^{18}F]**1a** contains an amine linker, while [^{18}F]**3a** contains an oxygen bridge (Fig. 6-1 – highlighted in red). IC_{50} values against COX-2 for **1a**, **2a** and **3a** were determined as 7, 39 and 20 nM, respectively. All inhibitors tested displayed no affinity for COX-1 in the concentration range tested [16]. Lipophilicity was also comparable for all three radiotracer. The log*P* values for **1a**, **2a** and **3a** were determined as 2.28 (±0.05), 2.30 (±0.03) and 2.19 (±0.09), respectively.

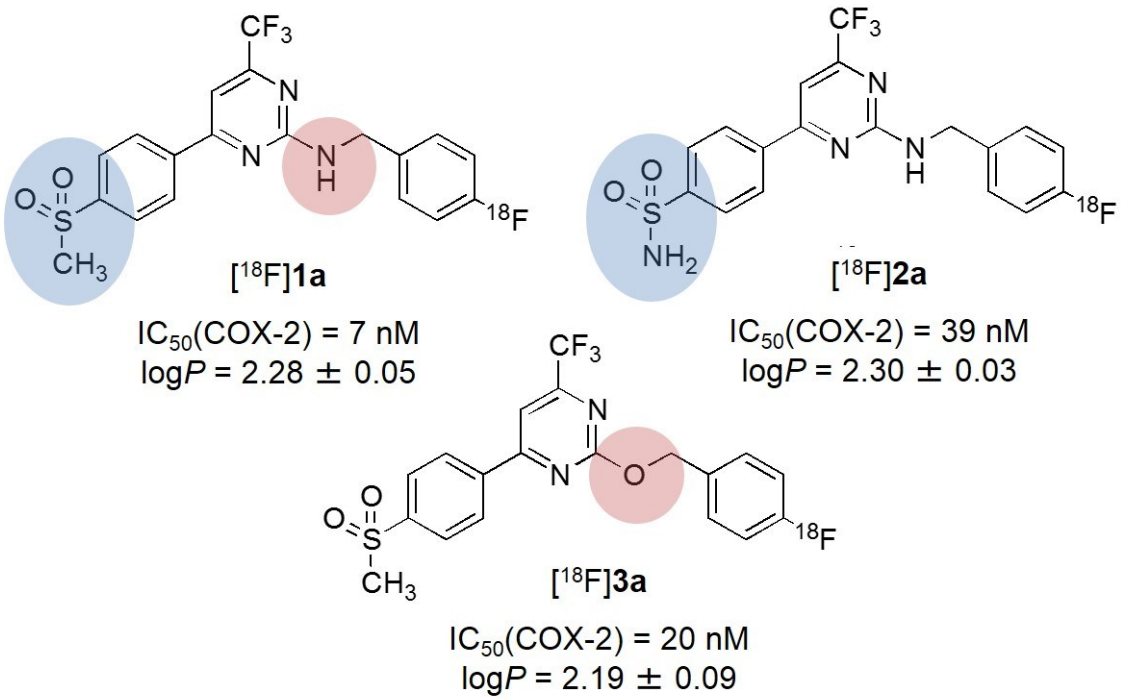

Figure 6-1: Structures of radiotracers [^{18}F]**1a**, [^{18}F]**2a**, [^{18}F]**3a**; IC_{50} values for COX-2 [16] and experimentally determined log*P* values.

6.3.2. Cell uptake studies

HCA-7 human colorectal cancer cells were used to study the uptake of radiotracers *in vitro*. The COX-2 expression of HCA-7 cells is well document [20, 21], and has been confirmed in the cells used for the present experiments [17]. The HCA-7 cells showed no expression of COX-1. The uptake kinetics and pattern of radiotracers [^{18}F]**1a**, [^{18}F]**2a**, [^{18}F]**3a** into HCA-7 cells was markedly different (Fig. 6-2). After 90 min incubation with [^{18}F]**1a** showed the highest uptake of 598±55% radioactivity/mg protein (n=9), compared to 443±17% and 296±25% radioactivity/mg protein (both n=6) for [^{18}F]**2a** and [^{18}F]**3a**. Interestingly, the minor differences in IC_{50} values seemed not to be responsible for the observed larger differences in [^{18}F]**2a** and [^{18}F]**3a** radiotracer uptake.

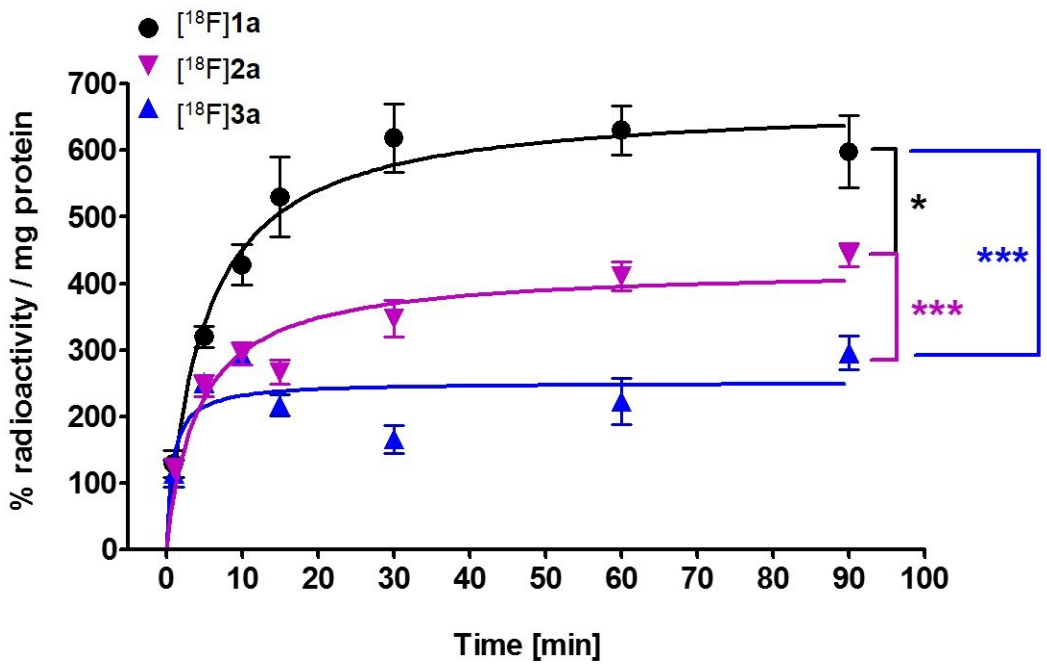

Figure 6-2: *In vitro* cell uptake of [^{18}F]**1a**, [^{18}F]**2a**, [^{18}F]**3a** into HCA-7 cells at 37ºC. Data expressed as mean % radioactivity / mg protein ± SEM.

6.3.3. *In vivo* small animal PET imaging

[^{18}F]**1a**, [^{18}F]**2a**, [^{18}F]**3a** were further assessed by dynamic PET imaging. Figure 6-3 shows uptake and distribution of the three different radiotracers after 60 min p.i.

PET images indicated that *in vivo* profile of the three tracers was different. Highest uptake into HCA-7 tumors was observed with [^{18}F]**1a** compared [^{18}F]**2a** and [^{18}F]**3a** (Fig. 6-3). High retention of radioactivity in the heart and blood pool as well as high liver uptake was detected after 60 min p.i. of [^{18}F]**2a**. Injection of [^{18}F]**3a** resulted in higher accumulation in intestines, kidneys and bladder.

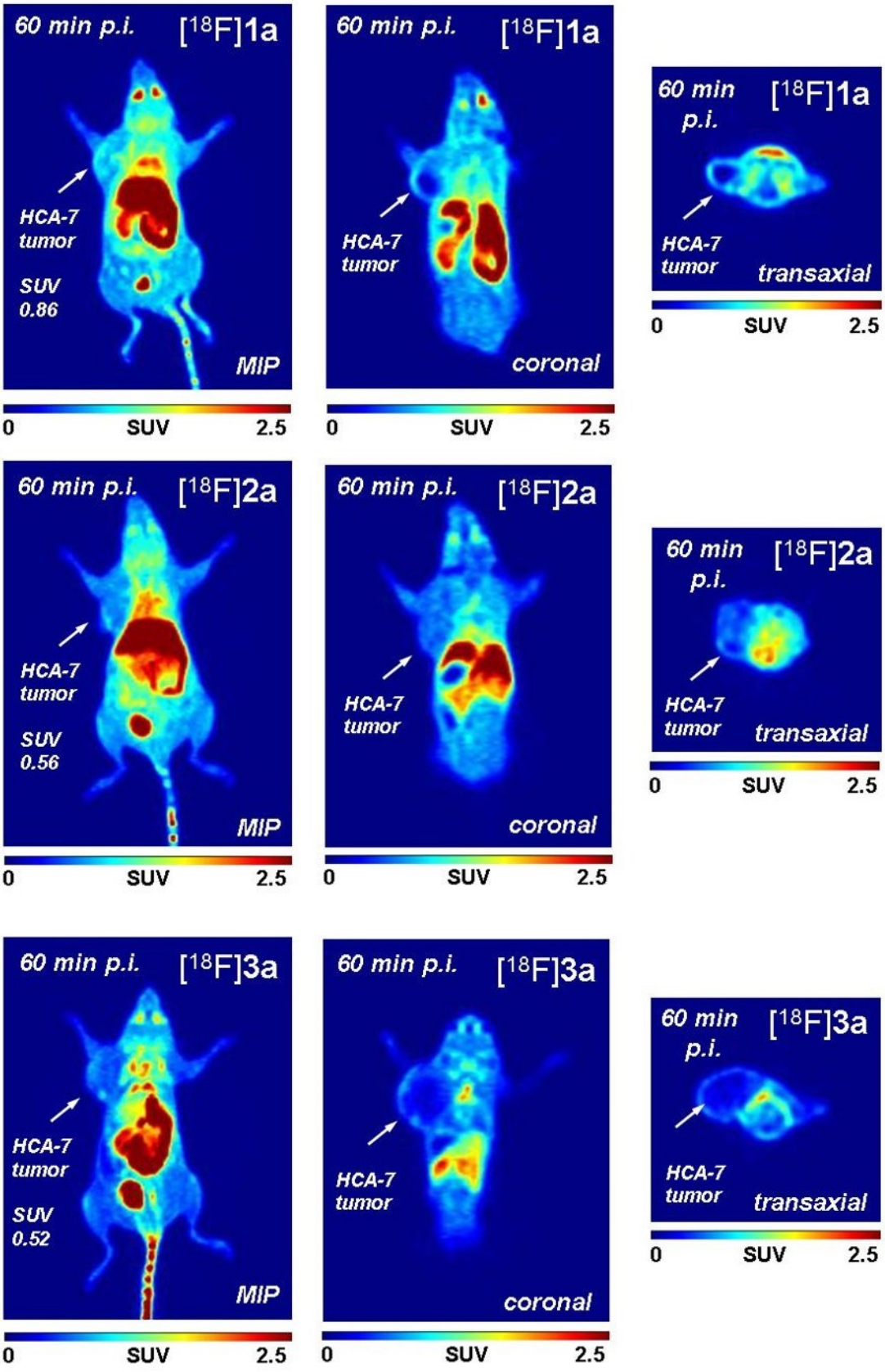
60 min p.i.
[18F]1a
HCA-7 tumor
SUV 0.86
MIP
0
SUV
2.5
60 min p.i.
[18F]1a
HCA-7 tumor
coronal
0
SUV
2.5
60 min p.i.
[18F]1a
HCA-7 tumor
transaxial
0
SUV
2.5
60 min p.i.
[18F]2a
HCA-7 tumor
SUV 0.56
MIP
0
SUV
2.5
60 min p.i.
[18F]2a
HCA-7 tumor
coronal
0
SUV
2.5
60 min p.i.
[18F]2a
HCA-7 tumor
transaxial
0
SUV
2.5
60 min p.i.
[18F]3a
HCA-7 tumor
SUV 0.52
MIP
0
SUV
2.5
60 min p.i.
[18F]3a
HCA-7 tumor
coronal
0
SUV
2.5
60 min p.i.
[18F]3a
HCA-7 tumor
transaxial
0
SUV
2.5

Figure 6-3: PET images at 60 min post injection of [^{18}F]**1a** (top), [^{18}F]**2a** (middle) and [^{18}F]**3a** (bottom) in HCA-7 bearing (left shoulder) NIH-III mice. Images are shown as maximum intensity projections (MIP, left), coronal (middle) and transaxial (right) slices.

Detailed perfusion, distribution, accumulation, retention and clearance pattern were further analyzed with of time-activity curves (TACs) over respective ROIs. Figure 6-4 summarizes the TACs for lung, heart (blood pool), HCA-7 tumors and muscle tissue, Figure 6-5 the TACs for brain, liver, kidneys and bladder.

In contrast to radiotracers [^{18}F]**2a** and [^{18}F]**3a** blood clearance of [^{18}F]**1a** was not analyzed due to insufficient lung clearance after i.v. injection. Instead, an enhanced retention upon first passage of the lung was observed with [^{18}F]**1a**. After 10min p.i. mean SUV of [^{18}F]**1a** in the lung was 4.9±1.5 (**$p<0.05$) compared to 1.8±0.26 and 1.1±0.08 (all n=4) for [^{18}F]**2a** and [^{18}F]**3a**, respectively. High retention of radioactivity in the blood pool was detected in the case of sulfonamide containing compound [^{18}F]**2a** (Fig. 6-4**,** top right). The SUV_{60min} was 1.55±0.09 (n=4) compared to 0.32±0.10 (n=3, (***$p<0.001$) after injection of [^{18}F]**3a**. Previous biodistribution experiments for [^{18}F]**1a** indicated that radioactivity rapidly cleared from the blood pool [17]. However, direct comparison of blood clearance profile to sister compounds [^{18}F]**2a** and [^{18}F]**3a** cannot be done because of the delayed lung clearance of [^{18}F]**1a**.

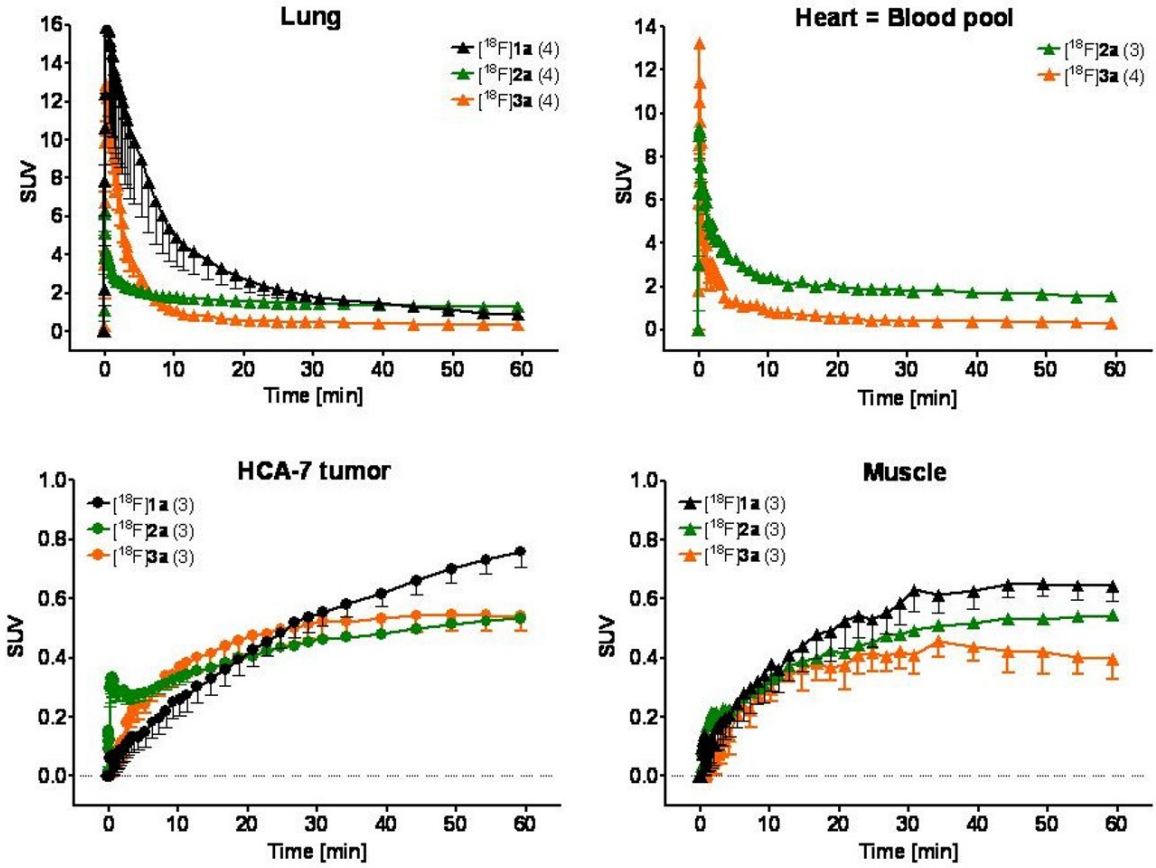

Figure 6-4: Time-activity curves for [^{18}F]**1a**, [^{18}F]**2a** and [^{18}F]**3a** in lung (top left), heart (top right), HCA-7 tumors (bottom left) and muscle tissue (bottom right) of HCA-7 tumor bearing NIH-III mice. Data are shown as SUV and mean ± SEM from n experiments.

Tumor uptake of [^{18}F]**1a** was significantly higher than that of [^{18}F]**2a** and [^{18}F]**3a**: SUV_{60min} 0.76±0.06 versus 0.53±0.01 (*$p<0.05$) and 0.54±0.05 (*$p<0.05$; all n=3) (Fig. 6-4**,** bottom left). However, uptake of [^{18}F]**1a** into non-targeting muscle tissue was also high (Fig. 6-4**,** bottom right). While TACs analysis indicated a delayed muscle clearance for [^{18}F]**2a** over time whereas compounds [^{18}F]**1a** and [^{18}F]**3a** did not show noticeable muscle clearance over the same time period of the PET study. Consequently, tumor-to-muscle (T/M) ratios at 60 min p.i. were

determined as 1.19±0.13 for [^{18}F]**1a**, 0.98±0.03 for [^{18}F]**2a** and 1.43±0.19 for [^{18}F]**3a** (all n=3), respectively.

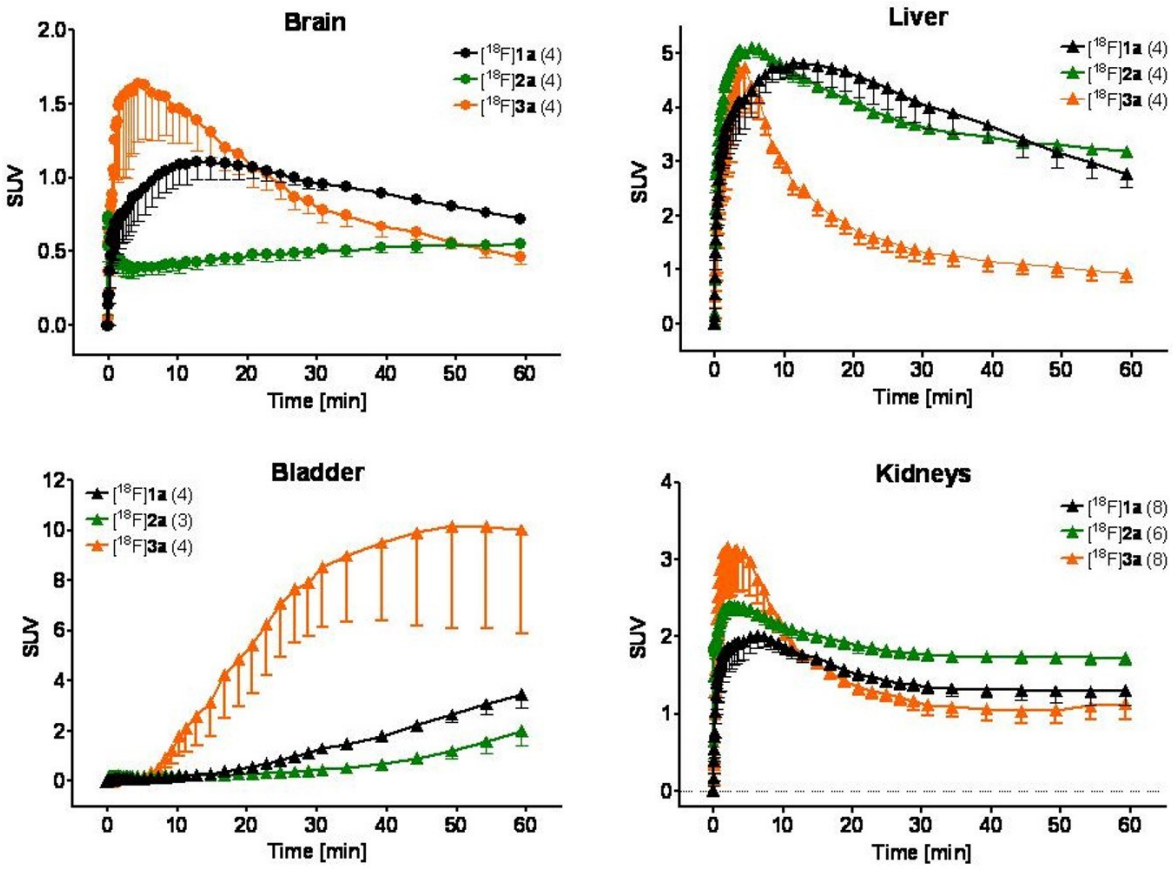

Figure 6-5: Time-activity curves for [^{18}F]**1a**, [^{18}F]**2a** and [^{18}F]**3a** in brain (top left), liver (top right), bladder (bottom left) and kidneys (bottom right) of HCA-7 tumor bearing NIH-III mice. Data are shown as SUV and mean ± SEM from n experiments.

ROI analysis over the whole brain suggested that all three radiotracers are capable of crossing the blood-brain barrier (Fig. 6-5**,** top left). SUV_{20min} were determined as 1.07±0.08 (n=4), 0.48±0.04 (n=4) and 1.07±0.13 (n=3) for [^{18}F]**1a**, [^{18}F]**2a** and [^{18}F]**3a**. Liver and kidney clearance did differ

for all three radiotracers despite lipophilicity was in the same range for all three compounds (see Fig. 6-1). Liver retention of [^{18}F]**1a** and [^{18}F]**2a** was more profound after 60 min p.i., whereas [^{18}F]**3a** showed a more rapid clearance from liver tissue over time (Fig. 6-5, top right). Also, after injection of [^{18}F]**3a** higher activity amounts were detected in the bladder compared to the other two radiotracers (Fig. 6-5, bottom left) indicating that [^{18}F]**3a** favors a more renal clearance, while the other two radiotracers show a higher hepatobilary clearance pattern. Overall clearance of radioactivity via kidneys is slowed with remarkable amounts of activity left after 60 min p.i., however, [^{18}F]**3a** also showed faster and more dominant clearance through the kidneys supporting a favored renal elimination pattern.

6.4. Discussion

During this study three structurally related COX-2 radiotracers were evaluated in a human colorectal cancer xenograft model. The following main results were obtained: i) lipophilicity was comparable for [^{18}F]**1a**, [^{18}F]**2a** and [^{18}F]**3a**; ii) cell uptake into COX-2 expressing HCA-7 cells was highest for [^{18}F]**1a** following [^{18}F]**2a** and [^{18}F]**3a**; iii) uptake into HCA-7 tumors *in vivo* was also highest for [^{18}F]**1a** following [^{18}F]**2a** and [^{18}F]**3a** with similar uptake levels; iv) only [^{18}F]**1a** showed first pass retention in the lungs while blood clearance was slowest for [^{18}F]**2a** and v) [^{18}F]**1a** and [^{18}F]**2a** favor a hepatobilary clearance while [^{18}F]**3a** is cleared more via the renal elimination pathway.

The radiotracers used in this study were designed based on the same trifluoromethyl pyrimidine central scaffold. They displayed similar inhibitory potency and specificity profiles in an *in vitro* COX-2 enzyme inhibition assay. They also possess a near identical lipophilicity. The structural differences between the three radiotracers are the substitution of a methylsulfone for a sulfonamide COX-2 pharmacophore ([^{18}F]**1a** vs. [^{18}F]**2a**) and the substitution of a secondary amine linker for an oxygen bridge ([^{18}F]**1a** vs. [^{18}F]**3a**). Compound **1a** was determined to be the most potent structure in the enzyme inhibition assay: **1a**>**3a**>**2a** (IC_{50} (COX-2) 7nM>20nM>39nM). Cellular uptake into HCA-7 cells revealed slightly different results with more uptake of [^{18}F]**2a** than [^{18}F]**3a** (Δ 33%). The results for [^{18}F]**1a**, on the other hand, were consistent: highest IC_{50} and highest uptake into HCA-7 cells. Very few COX-2 radiotracers have been evaluated in *in vitro* cell-based assays to date [6]. Furthermore, those that have undergone *in vitro* assessment were often analyzed in different biological models, making direct comparison challenging.

A notable characteristic of radiotracer [^{18}F]**1a** was its high retention in the lung upon first passage. This phenomenon has been described as first pass pulmonary retention effect, particularly with

reference to local anesthetic drugs such as lidocaine and prilocain as well as systemic anesthetics like thiopental and ketamine [22, 23]. A first pass pulmonary retention effect is evident when a drug is injected i.v., transported to the heart and onwards to the lung and retained there. Literature on this phenomenon identifies a number of different properties that affect the extent of pulmonary retention most importantly molecular weight, lipophilicity and pK_a of the drug molecule, as well as blood pH, ventilation, perfusion and oxygenation of the blood and lungs of the test animal [23]. Pulmonary space is slightly more acidic than vascular space (pH 6.5 vs pH 7.4), while various acidic compartments can be significantly more acidic. If the drug is ionized anywhere in pulmonary space it is unable to diffuse back into vascular space and is thus retained in the lung. A common structural motif involved in this trapping mechanisms are secondary amines that are easily ionized [22]. Interestingly, both [^{18}F]**1a** and [^{18}F]**2a** contain secondary amine motifs, but the extent of pulmonary retention is lower for [^{18}F]**2a**. [^{18}F]**3a** contains an ether linker in place of the secondary amine and shows significantly improved lung clearance in comparison to [^{18}F]**1a**.

The ability of radiotracer [^{18}F]**2a** to pass the lung faster than [^{18}F]**1a** might be linked to its increased retention in the blood pool. It is well documented that celecoxib-related structures containing a sulfonamide moiety are prone to bind to carbonic anhydrases (CA) [15]. Specifically CA I and CA II are expressed on red blood cells, and both are a possible binding site for a sulfonamide containing molecule [24]. The cross-affinity of sulfonamide containing COX-2 compounds for carbonic anhydrases and their resulting retention in the blood pool have been demonstrated before. Pretreatment with a known anhydrase inhibitor improves blood clearance of sulfonamide-containing radiotracers towards the clearance pattern of methyl sulfone-containing structures [25]. Rapid binding of [^{18}F]**2a** to CAs expressed on red blood cells might be the reason for improved

lung clearance. Protein or cell bound radiotracers are unable to diffuse out of the vascular space and therefore exhibit normal lung passage [26].

All three COX-2 radiotracers have shown a substantial brain uptake demonstrating sufficient capacity to cross the blood-brain barrier. Strong differences were observed regarding the kinetic profiles of brain accumulation. While the ether compound [^{18}F]**3a** possessed the highest initial brain uptake following washout, [^{18}F]**1a** has a slower kinetic for brain penetration may due to its first pulmonary retention and therefore longer distribution and slower blood clearance pattern. [^{18}F]**2a** on the other hand initially perfused the brain but tended to accumulate slowly over the observed 60 min reaching a brain-to-blood ratio of 0.35 only, suggesting that most of the radiotracer is blood bound and diffusion out of vascular space may slow. In contrast, with [^{18}F]**3a** a brain-to-blood ratio of 1.44 at 60 min p.i. was measured which would be indicative of a high brain tissue uptake. Only few COX-2 radiotracers have undergone extensive evaluation as a neuroimaging agent. As one candidate ^{11}C-labelled rofecoxib was studied by de Vries *et al* [27]. It was shown to cross the blood-brain-barrier and be heterogeneously distributed in different brain regions broadly consistent with known expression patterns of basal level COX-2. A mean SUV_{60min} of 0.26 in rat brain was determined which is slightly lower than the SUV_{60min} of 0.46 for [^{18}F]**3a** with the latter one determined in mice during the current study. Given an appropriate neuroinflammation model further studies could be carried out to determine the potentials for [^{18}F]**3a** as a neuroimaging agent.

HCA-7 tumor uptake of [^{18}F]**2a** and [^{18}F]**3a** is significantly lower than of [^{18}F]**1a**. [^{18}F]**1a** has been extensively studied as a specific COX-2 targeting radiotracer in the HCA-7 tumor model [17]. Tumor uptake of [^{18}F]**1a** was insignificantly higher than the uptake in non-targeting muscle tissue amounting to a T/M ratio of 1.19 after 60 min. However, longer PET studies showed that the

accumulation of [^{18}F]**1a** in HCA-7 tumor tissue is significantly higher than in muscle tissue reaching a T/M ratio of about 2 after 120 min p.i. (data shown in Chapter V). [^{18}F]**3a** also shows a sufficient T/M ratio of 1.43 after 60 min indicative for specific tumor tissue uptake while [^{18}F]**2a** displays homogeneous uptake in both tumor and muscle tissue reaching a T/M ratio of 0.98 only which points toward a non-specific uptake in both COX-2 targeting HCA-7 tumor tissue and non-targeting muscle reference tissue. The latter might be based on [^{18}F]**2a** higher binding possibility to CAs.

The favorable hepatobilary clearance pattern for [^{18}F]**1a** and [^{18}F]**2a** was shifted towards a more renal clearance pattern when the ether-functions was introduced in [^{18}F]**3a**. While this cannot be resulting from a change in lipophylicity since all three compounds possess a similar log*P* value, it may due to much faster blood clearance and lower overall residential time of [^{18}F]**3a**. However, even if a faster blood clearance is favorable for development of a good PET radiotracer, here for this compound class of COX-2 inhibitors and the goal to reach an intracellular target site a slower blood clearance may be of advantage. Therefore, [^{18}F]**1a** ideally combines a delayed clearance from blood pool due to its first pass pulmonary retention together with a delayed and therefore prolonged delivery to the intracellular target site. In addition, a sulfonamide functionality as in [^{18}F]**2a** may prohibits specificity for COX-2 based on a higher interaction with carboanhydrases as seen in the higher levels of non-specific uptake and missing clearance form non-COX-2 muscle tissue as well as longer and higher blood pool retention.

It still remains a formidable challenge to design an optimal PET radiotracer for selective imaging of COX-2 *in vivo* [6, 10, 11]. Despite good *in vitro* affinities for isolated COX-2 in enzyme assays, different indole and imidazole derivatives did not display suitable properties for specific interaction with COX-2 *in vivo* [28, 29]. Past attempts to use a celecoxib derivative may lack

specificity between COX-2 and non-selective target sites since they still contain a sulfonamide pharmacophore showing substantial binding to carboanhydrase [30]. We have recently shown that pyrimidine scaffold-based [^{18}F]**1a** ([^{18}F]Pyricoxib) does possess specific COX-2 mediated interaction *in vivo* [16-18]. During the present study we have shown that small modifications such as changing the methylsulfone COX-2 pharmacophore to a sulfonamide group and the change from the amine to the ether linker results in a substantial loss of affinity towards the COX-2 enzyme, general lower into COX-2 expressing cells as well loss of radiotracer accumulation in COX-2 expressing tumors *in vivo*. Beside that perfusion, distribution and clearance parameters were also impaired. Taken together, those small structure modifications of COX-2 targeting radiotracers can be well studied with dynamic PET imaging in order to evaluate structure-relation-ships in a living organism.

6.5. Conclusion

Three highly potent and selective ^{18}F-labeled COX-2 inhibitors have been designed and synthesized. Despite structural similarity and comparable inhibitory potency against COX-2, the *in vivo* and *in vitro* metabolic profiles of these radiotracers varies significantly.The reasons for the discrepancy between inhibitory potency and suitability as a radiotracer have been partially elucidated using dynamic PET imaging.

Depending on the complexity of the biological target, studies might benefit from starting with a library of structurally related radiotracer to allow the fine tuning of a lead compound radiopharmaceutical.

6.6. References

[1] Moncada, S.; Gryglewski, R.J.; Bunting, S.; Vane, J.R. An enzyme isolated from arteries transforms prostaglandin endoperoxides to an unstable substance that inhibits platelet aggregation. *Nature*, **1976**, 263, 663.

[2] Zheng, W.; Thorne, N.; McKew, J.C. Phenotypic screens as a renewed approach for drug discovery. *Drug Discov. Today*, **2013**, 18, 1067.

[3] Vane, J.R.; Bakhle, Y.S.; Botting, R.M. Cyclooxygenase-1 and 2. *Annu. Rev. Pharmacol.,***1998**, 38, 97.

[4] Dubois, R.N.; Abramson, S.B.; Crofford, L.; Gupta, R.A.; Simon, L.S.; Van De Putte, L.B.A.; Lipsky, P.E. Cyclooxygenase in biology and disease. *FASEB J.*, **1998**, 12, 1063.

[5] Scheiman, J.M. Unmet needs in non-steroidal anti-inflammatory drug-induced upper gastrointestinal diseases. *Drugs*, **2006**, 66, 15.

[6] Tietz, O.; Marshall, A.; Wuest, M.; Wang, M.; Wuest, F. Radiotracers for Molecular Imaging of Cyclooxygenase-2 (COX-2) Enzyme. *Curr. Med. Chem.*, **2013**, 20, 4350.

[7] Méric, J.; Rottey, S.; Olaussen, K.; Soria, J.; Khayat, D.; Rixe, O.; et al. Cyclooxygenase-2 as a target for anticancer drug development. *Crit. Rev. Oncol.*, **2006**, 59, 51.

[8] Minghetti, L. Cyclooxygenase-2 (COX-2) in inflammatory and degenerative brain diseases. *J. Neuropath. Exp. Neuro.*, **2004**, 63, 901.

[9] deVries, E.F.J. Imaging of cyclooxygenase-2 (COX-2) expression: Potential use in diagnosis and drug evaluation. *Curr. Pharm. Des.*, **2006**, 12, 3847.

[10] Pacelli, A.; Greenman, J.; Cawthorne, C.; Smith, G. Imaging COX-2 expression in cancer using PET/SPECT radioligands: current status and future directions. *J. labelled Compd. Radiopharmaceut.*, **2014**, 57, 317.

[11] Laube, M.; Kniess, T.; Pietzsch, J. Radiolabelled COX-2 inhibitors for non-invasive visualization of COX-2 expression and activity—A critical update. *Molecules*, **2013**, 18, 6311.

[12] Godsell, D.S. The molecular perspective: cyclooxygenase-2. *Oncologist*, **2000**, 5, 169.

[13] Shi, S.; Klotz, U. Clinical use and pharmacological properties of selective COX-2 inhibitors. *Eur. J. Clin. Pharmacol.*, **2008**, 64, 233.

[14] Grosch, S.; Maier, T.J.; Schiffmann, S.; Geisslinger, G. Cyclooxygenase-2 (COX-2) independent anticarcinogenic effects of selective COX-2 inhibitors. *J. Nat. Cancer Inst.*, **2006**, 98, 736.

[15] Weber, A.; Casini, A.; Heine, A.; Kuhn, D.; Supuran, C.T.; Scozzafava, A.; Klebe, G. Unexpected nanomolar inhibition of carbonic anhydrase by COX-2-selective celecoxib: New pharmacological opportunities due to related binding site recognition. *J. Med. Chem.*, **2004**, 47, 550.

[16] Tietz, O.; Sharma, S.K.; Kaur, J.; Way, J.; Marshall, A.; Wuest, M.; Wuest, F. Synthesis of three ^{18}F-labelled cyclooxygenase-2 (COX-2) inhibitors based on a pyrimidine scaffold. *Org. Biomol. Chem.*, **2013**, 11, 8052.

[17] Tietz, O.; Wang,M.; Marshall, A.; Sharma, S.K.; Way, J.; Wuest, M.; Wuest, F. F-18-Labelled radiotracers for molecular imaging of cyclooxygenase-2 (COX-2) expression in cancer. *J. labelled Compd. Radiopharm.*,**2013**, 56, S3.

[18] Tietz, O.; Wang,M.; Marshall, A.; Sharma, S.K.; Way, J.; Wuest, M.; Wuest, F. Functional imaging of COX-2 in cancer: A challenge for desgining a PET tracer and choosing the right *in vivo* model. *Mol. Imaging Biol.*, **2013**, 15, S929.

[19] Swarbrick, M.; Beswick, P.; Gleave, R.; Green, R.; Bingham,S.; Bountra, C.; et al. Identification of [4-[4-(methylsulfonyl)phenyl]-6-(trifluoromethyl)-2-pyrimidinyl] amines and ethers as potent and selective cyclooxygenase-2 inhibitors. *Bioorg. Med. Chem. Lett.*, **2009**, 19, 4504.

[20] Debucquoy, A.; Devos, E.; Vermaelen, P.; Landuyt, W.; De Weer, S.; Van Den Heuvel, F.; Haustermans, K. 18F-FLT and 18F-FDG PET to measure response to radiotherapy combined with celecoxib in two colorectal xenograft models. *Int. J. Radiat. Biol.*, **2009**, 85, 763.

[21] Yoshida, K.; Fujino, H.; Otake, S.; Seira, N.; Regan, J.; Murayama, T. Induction of cyclooxygenase-2 expression by prostaglandin E2 stimulation of the prostanoid EP4 receptor via coupling to Gαi and transactivation of the epidermal growth factor receptor in HCA-7 human colon cancer cells. *Eur. J. Pharmacol.*, **2013**, 8, 408.

[22] Bakhle, Y.S. Pharmacokinetic and metabolic properties of lung. *Brit. J. Anaest.*, **1990**, 65, 79.

[23] Boer, F. Drug handling by the lungs. *Brit. J. Anaest.*, **2003**, 91, 50.

[24] Supuran, C.T. Carbonic anhydrases: novel therapeutic applications for inhibitors and activators. *Nat. Rev. Drug Discov.*, **2008**, 7, 168.

[25] Kuge, Y.; Katada, Y.; Shimonaka, S.; Temma, T.; Kimura, H.; Kiyono, Y.; et al. Synthesis and evaluation of radioiodinated cyclooxygenase-2 inhibitors as potential SPECT tracers for cyclooxygenase-2 expression. *Nucl. Med. Biol.*, **2006**, 33, 21.

[26] Welch, M.J.; Dence, C.S.; Marshall, D.R.; Kilbourn, M.R. Remote system for production of Carbon-11 labelled palmitic acid. *J. labelled Compd. Radiopharm.*, **1983**, 10, 1087.

[27] de Vries, E.F.J.; Doorduin, J.; Dierckx, R.A.; van Waarde, A. Evaluation of [11C]rofecoxib as PET tracer for cyclooxygenase 2 overexpression in rat models of inflammation. *Nucl. Med. Biol.*, **2008**, 35, 35.

[28] Tanaka, M.; Fujisaki, Y.; Kawamura, K.; Ishiwata, K.; Qinggeletu, Y.F.; Mukai, T.; Maeda, M. Radiosynthesis and evaluation of 11C-labelled diaryl-substituted imidazole and indole derivatives for mapping cyclooxygenase-2. *Biol. Pharm. Bull.*, **2006**, 29, 2087.

[29] Kniess, T.; Laube, M.; Bergmann, F.; Sehn, F.; Graf, F.; Steinbach, J.; Wuest, F.; Pietzsch, J. Radiosynthesis of a 18F-labeled 2,3-diarylsubstituted indole via McMurry coupling for functional characterization of cyclooxygenase-2 (COX-2) *in vitro* and *in vivo*. *Bioorg. Med. Chem.*, **2012**, 20, 3410.

[30] Uddin, M.; Crews, B.; Ghebreselasie, K.; Huda, I.; Kingsley, P.; Ansari, M.; Tantawy, M.N.; Reese, J.; Marnett, L.J. Fluorinated COX-2 inhibitors as agents in PET imaging of inflammation and cancer. *Can. Prev. Res.*, **2011**, 4, 1536.

CHAPTER 7

Drug delivery of [^{18}F]1a using HSA as a carrier protein

7.1. Introduction

[^{18}F]**1a** has undergone extensive evaluation in a rat model and a colorectal cancer model and has been shown to interact with COX-2 specifically *in vivo* (Chapter 4 and 5). A comparison of [^{18}F]**1a** and its sister compounds [^{18}F]**2a** and [^{18}F]**3a** revealed that [^{18}F]**1a** is the most suitable for the non-invasive assessment of COX-2 expression in cancer. However, [^{18}F]**1a** exhibited poor lung clearance parameters in comparison to its sister compounds (Chapter 6). Poor lung clearance upon first passage of a small drug-like molecule is known as first-pass pulmonary retention and has been studied particularly in the field of anesthesiology [1-4]. Local anesthetics containing a secondary amine moiety in particular a susceptible to poor lung clearance on first pass. Most of our knowledge concerning first-pass pulmonary retention comes from work in the field of anesthesiology, where significant retention in the lung can have an impact on patient dosing. However, the phenomenon is starting to be recognized as a major obstacle to the intravenous delivery of larger therapeutic agents, such as stem cells, as well [5].

First-pass pulmonary retention is most easily studied using dynamic PET-imaging. The accumulation and retention of radioactivity in the lung is easy to follow using dynamic imaging. By contrast, if a radiotracer is analyzed by 60 min post-injection biodistribution only, first-pass pulmonary retention might go unnoticed. Even perfusion phase biodistribution (5 min p.i.) might not yield pharmacokinetic data that unambiguously suggests that a radiotracer suffers from first-pass pulmonary retention.

The first-pass pulmonary retention properties of [^{18}F]**1a** might have implications for the use of the tracer as a radiopharmaceutical in humans in the future. Significant retention of radioactivity in the lung leads to a higher radioactive dose delivered to the organ during the perfusion phase. Drug delivery of [^{18}F]**1a** to avoid first-pass pulmonary retention would be desirable.

7.1.1. Objectives

The purpose of this study is to further investigate the possible origin of this lung retention phenomenon and to assess whether the delivery of the radiopharmaceutical to organs of interest can be improved by using human serum albumin as a carrier protein.

7.2. Materials and methods

All regents and solvents were obtained from Sigma-Aldrich, unless otherwise stated and used without further purification. Nuclear magnetic resonance spectra were recorded on a 400MHz Varian (Palo Alto, CA, USA) unit and a 600 MHz Bruker (Billerica, MA, USA) unit. ^{1}H-NMR chemical shifts are recorded in ppm relative to tetramethylsilane (TMS). ^{19}F-NMR chemical shifts are recorded in ppm relative to trichlorofluoromethane. Low resolution mass spectra were obtained using am Agilent Technologies (Santa Clara, CA, USA) 6220 oaTOF instrument. Column chromatography was conducted using Merck silica gel (mesh size 230–400 ASTM). Thin-layer chromatography (TLC) was performed on Merck silica gel F-254 aluminum plates, with visualization under UV light (254 nm). High performance liquid chromatography (HPLC) purifications and analysis were performed using a Phenomenex LUNA® C18 column (100Å, 250x10mm, 10mm) on a Gilson 322 Pump module fitted with a 171 Diode Array and a radio detector.

7.2.1. Formulation of [^{18}F]1a for *in vivo* studies

[^{18}F]**1a** was dissolved in 20 µL ethanol and added to 180 µL of 3.5 % human serum albumin (HSA) in saline solution. The mixture was sonicated in a water bath for 15 min. Binding of [^{18}F]**1a** to HSA was monitored by radio-TLC prior to injection of the formulation into the tail vein of the animal. To study the first pass pulmonary retention, the radiotracer was dissolved in 10 % EtOH in saline solution only.

7.2.2. *In vivo* tumor model

Positron emission tomography (PET) experiments were performed using HCA-7 tumor-bearing NIH-III and non-tumor-bearing Balb/c mice (Charles River Laboratories, Quebec, Canada). All animal experiments were carried out in accordance with the guidelines of the Canadian Council on Animal Care (CCAC) and approved by the local animal care committee (Cross Cancer Institute, University of Alberta). Female NIH-III and female Balb/c mice were housed under standard conditions with free access to standard food and tap water. HCA-7 cells ($5x10^6$ cells in 100 µl PBS) were injected into the upper left flank of female NIH-III nude mice (20-24 g). After 14 to 21 days post-inoculation, HCA-7 tumors reached sizes of approximately 1 cm^3 which were suitable for all *in vivo* experiments.

7.2.3. Small animal PET imaging

General anesthesia of HCA-7 tumor-bearing NIH-III and non-tumor-bearing Balb/c mice was induced with inhalation of isoflurane in 40 % oxygen / 60 % nitrogen (gas flow = 1 ml/min), and mice were subsequently fixed in prone position. The body temperature was kept constant at 37°C for the entire experiment. For PET experiments, 3–8 MBq of [^{18}F]**1a** in 150-200 µL of solution (formulation see above) was administered intravenously as a bolus via the tail vein. PET data were collected dynamically over 2h to 4h on a microPET® R4 or an Inveon® PET/CT scanner (Siemens Preclinical Solutions, Knoxville, TNU.S.A.). A transmission scan for attenuation correction was not acquired. The radioactivity of the injection solution in a 0.5 ml syringe was determined with a dose calibrator (Atomlab™ 300, Biodex Medical Systems, New York, U.S.A.). After the PET emission scan was started the radioactivity was injected with a delay of approximately 15 s. Data acquisition continued for 120 to 240 min in 3D list mode. The dynamic list mode data were sorted

into sinograms with up to 72 time frames (10x2, 8x5, 6x10, 6x20, 8x60, 10x120, 5x300, 19x600 s). The frames were reconstructed using maximum a posteriori (MAP) reconstruction modes. The pixel size was 0.085x0.085x0.12 cm, and the resolution in the center field of view was 1.8 mm. Correction for partial volume effects was not performed. The image files were further processed using the ROVER v2.0.51 software (ABX GmbH, Radeberg, Germany). Masks defining 3D regions of interest (ROI) were set and the ROIs were defined by thresholding. ROIs covered all visible mass of organs of interest, and the thresholds were defined by 50% of the maximum radioactivity uptake level. Mean standardized uptake values [SUV_{mean} = (activity/ml tissue)/(injected activity/body weight), ml/g] were calculated for each ROI. Time-activity curves (TAC) were generated from the dynamic scans. All semi-quantified PET data are presented as means ± SEM.

7.2.4. Statistical Analysis

All data are expressed as means ± SEM. Graphs were constructed using GraphPad Prism 5.0 (GraphPad Software). Where applicable, statistical differences were tested by unpaired Student's t-test and were considered significant for $p<0.05$.

7.3. Results and discussion

7.3.1. PET-imaging of first-pass pulmonary retention

The first pass pulmonary retention of [^{18}F]**1a**was studied using dynamic PET-imaging. PET was performed in HCA-7 tumor-bearing NIH-III mice and the radiotracer administered via tail vein injection in 10 % ethanol / saline solution.

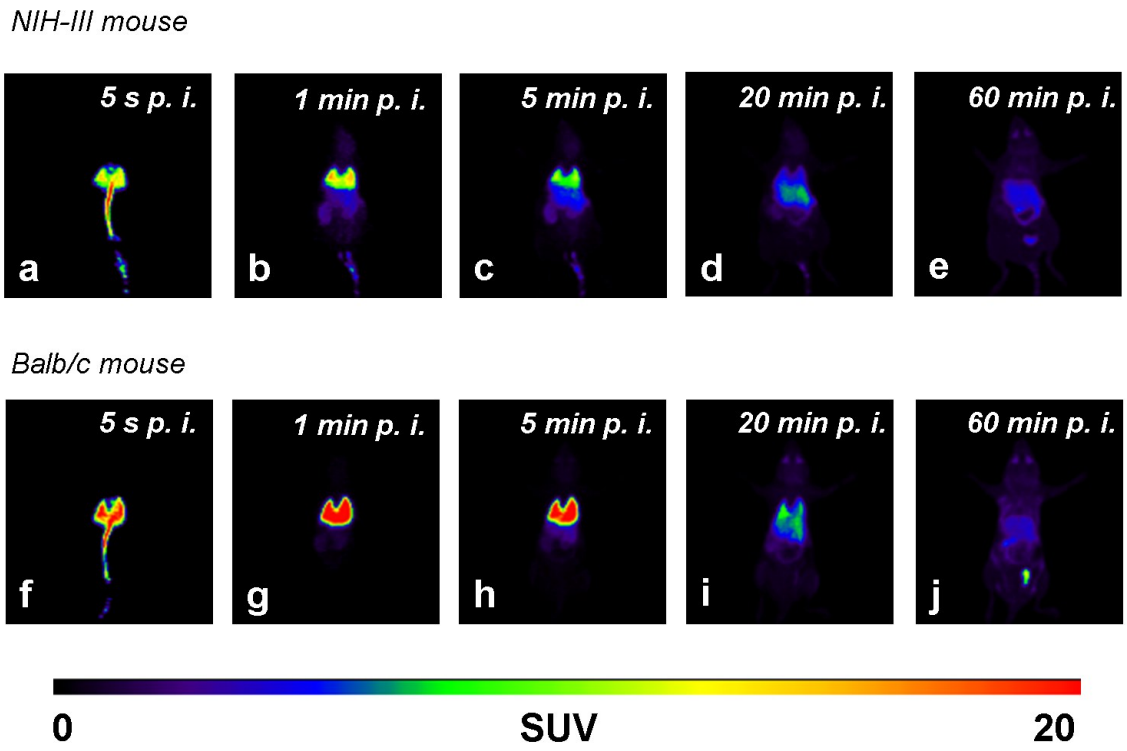

Figure 7-1a to7-1j: PET images at 5 s to 60 min post-injection of [^{18}F]**1a** (in 10 % ethanol / saline) into the tail vein of an NIH-III (7-1a to7-1e) (injected activity = 2.51 MBq) and BALB/c mouse (7-1f to7-1j) (injected activity = 2.81 MBq) under isoflurane anesthesia.

Upon injection of [^{18}F]**1a** into the tail vein of an HCA-7 tumor bearing NIH-III mouse, the tracer was transported with the venous blood to the heart and onwards to the lung with the pulmonary

arterial blood. Interestingly, upon reaching the lung the radiotracer did not enter the pulmonary venous blood stream and distribute throughout the body via the arterial blood vessels as expected. Instead [^{18}F]**1a**was retained in the lung over the first 5 min of a distribution phase and only slowly started to diffuse out after that time. The PET images shown in Figure 7-1a to7-1e are maximum intensity projections of an HCA-7 tumor bearing NIH-III mouse at time points 5 sec, 1 min, 5 min, 20 min and 60 min post-injection. The 5 sec post-injection image clearly shows the bolus of the radiotracer injection traveling up the tail vein and radioactivity starting to distribute throughout the lung. Images 7-1b and 7-1c (1 min and 5min post-injection) clearly show the right and the left lung as major sites of radioactivity accumulation with almost no radioactivity found elsewhere in the mouse. 60 min post-injection (Image 7-1e) the radioactivity found in the lung is reduced to levels similar to the rest of the organism.

To ensure that the effect observed here is not due to a defect in the mouse strain or the tumor model, the radiotracer was injected into non-tumor-bearing Balb/c mice. Tail vein administration of [^{18}F]**1a** in a Balb/c mouse led to an apparent increase in first-pass pulmonary retention. The PET images shown in Figure 7-1f to 7-1j are maximum intensity projections of a Balb/c mouse. The images show a higher maximum retention of radioactivity in the lung and a lower diffusion speed out of the lung in comparison to the images take of the NIH-III mouse.

These observations were quantified using lung clearance curves analyzed from ROIs over the lung (Fig.7-2a). 60 min p.i. the amount of radioactivity found in the lung of NIH-III and Balb/c mice reaches similar levels. The data presented here shows only one Balb/c mouse and NIH-III mouse, so such the increase in pulmonary retention in Balb/c is only an observation that cannot be verified statistically without conducting further experiments. Importantly, however, we observed first-pass pulmonary retention of [^{18}F]**1a** in two strains of mouse, one tumor bearing and one non-tumor

bearing. This suggests that the pulmonary retention of [^{18}F]**1a** is not a result of defects with the animal model.

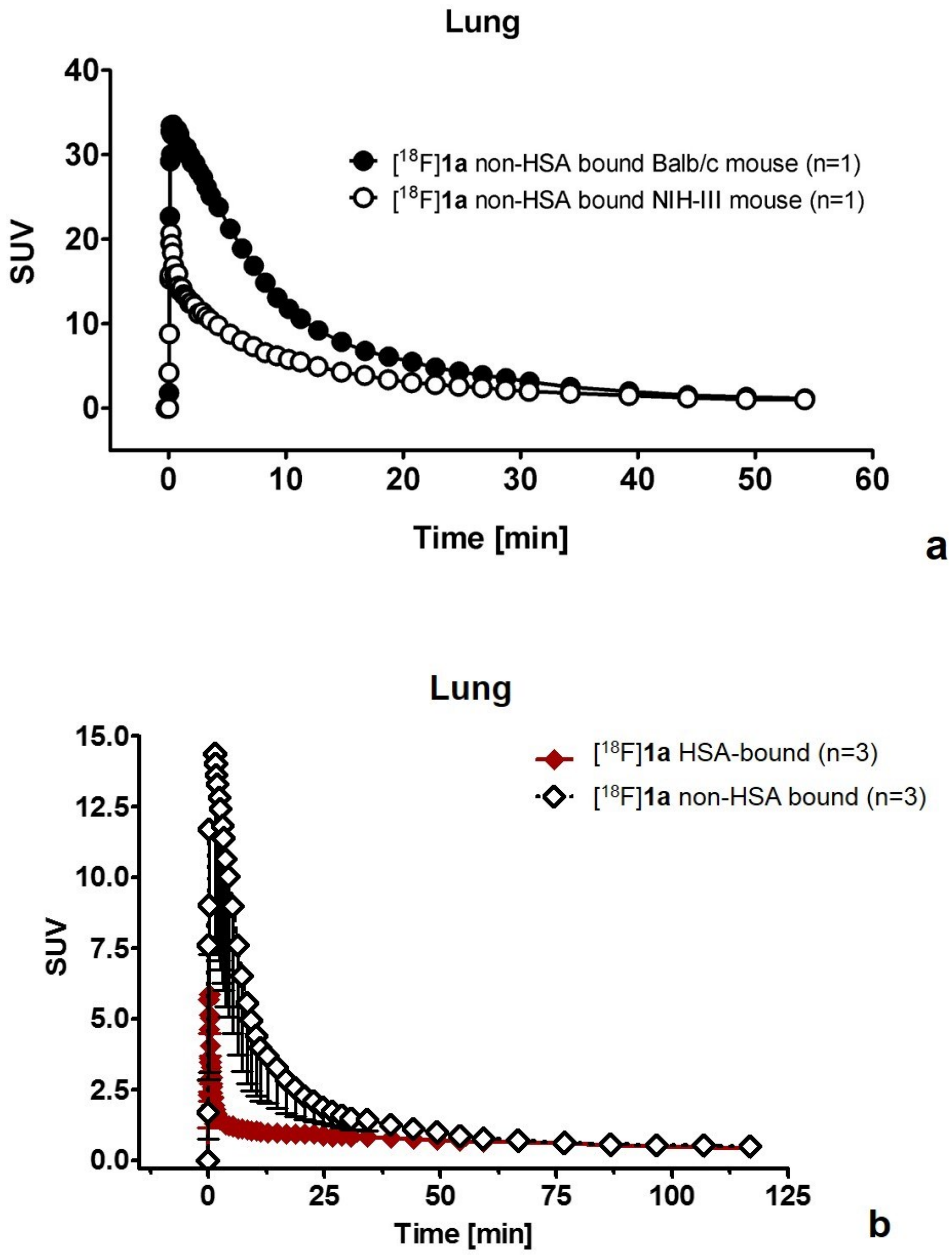

Figure 7-2a, 7-2b: Time-activity curves for the uptake of [^{18}F]**1a** in the lung of NIH-III and Balb/c mice. (a) Injection of [^{18}F]**1a** in 10% ethanol / saline into the tail vein of NIH-III mice (white circle) and Balb/c mice (black circle). (b) Injection of [^{18}F]**1a** in 10% ethanol / saline (white square)

and [^{18}F]**1a** in 3.5 % human serum albumin, 10 % ethanol and saline (red square) into the tail vein of NIH-III mice. Data as mean ± SEM.

Factors known to influence the pulmonary retention of a drug are its molecular weight, lipophilicty and pK_a, as well as blood pH, ventilation, perfusion and oxygenation of the blood and lungs of the test animal [2]. Further, factors such as plasma protein binding, lung disease, ageing and co-administration with other drugs have been identified as having a significant effect on pulmonary retention as well. The full mechanism of pulmonary retention has been described for a few agents only. Most drugs appear to diffuse from vascular into non-vascular space and are thereafter retain in specific compartments of the lung. The general model proposed by Boer [2] recognizes three different states of the drug while it is in vascular space – ionized drug, non-ionized drug and blood bound drug. Ionized compounds and blood bound compounds will pass the lung without be retained; non-ionized drug will diffuse from vascular into pulmonary space provided the drug is lipophilic enough to do so. Once the drug has entered pulmonary space it can be bound in lipophilic or non-lipophilic compartments, further the drug can be ionized in pulmonary space or in acidic compartments (such as the lysosome). Pulmonary space is slightly more acidic than vascular space (pH 6.5 vs pH 7.4), while various acidic compartments can be significantly more acidic. If the drug is ionized anywhere in pulmonary space it is unable to diffuse back into vascular space and is thus retained in the lung. The extent of first pass retention and the rate of release of a molecule in the pulmonary tissue depends on the properties of the drug itself and the mechanism by which it is retained, as well as the distinct properties of the pulmonary tissue in the test animal.

By these mechanisms and bearing in mind that local anesthetics with secondary amine moieties are susceptible to first-pass pulmonary retention, it is likely that the secondary amine on **1a** is the

site of protonation in acidic pulmonary tissue. **1a** is a lipophilic molecule and therefore expected readily penetrate the membrane between vascular and pulmonary space. The pyrimidine ring and the characteristic guanidine moiety at the core of the molecule might help to stabilize the protonated drug through resonance structures. Unfortunately, efforts to monitor the formation of the protonated drug were unsuccessful. We attempted to measure the log*D* of [^{18}F]**1a**by partition between octanol and buffers ranging in pH from 1 to 13, but were unable to detect a significant change in that range (data not shown). Attempts to analyze the radiotracer in formulations of ethanol and buffers (ranging in pH from 1 to 13) by radio-TLC analysis also did not yield any significant results (data not shown). It is unlikely that [^{18}F]**1a** does not undergo protonation, deprotonation or degradation at the extreme ends of the pH range tested. It is possible that the experimental set up is not sufficiently adapted for the purpose.

To facilitate first pass distribution of the radiotracer with a strongly reduced retention in the lung, the radiotracer was bound to human serum albumin (HSA) before injection into the test animal as previously described in the literature [6, 7]. HSA-bound radiotracer was able to pass the lung much faster and distribute throughout the body at an improved rate (Fig. 7-2b).

Non-HSA bound radiotracer showed a maximum SUV in the lung of 17.9 ± 7.2, 45 seconds post-injection, compared to 3.5 ± 0.75 for HSA-bound radiotracer. The difference of SUVs in the lung at 45 sec p.i., 2 min p.i. and 5 min p.i., between non-HSA bound and HSA-bound [^{18}F]**1a** approaches significance ($p=0.12$, $p=0.11$ and $p=0.16$ for the three time points respectively). 10 min post-injection the SUV of non-HSA bound radiotracer in the lung is 4.4 ± 2.1, compared to 1.1 ± 0.28 for HSA bound radiotracer. The SUV in the lung of unbound and bound radiotracer is almost identical after 60 min (0.8 ± 0.20 and 0.7 ± 0.15 respectively).

After successful altering the first-pass pulmonary passage of [^{18}F]**1a** we wanted to investigate whether HSA effects the accumulation and clearance of radiotracer in other organs as well.

7.3.2. Effect of HSA on the pharmacokinetic profile of [^{18}F]1a

Interestingly, comparisons of [^{18}F]**1a** HSA bound and [^{18}F]**1a** non-HSA bound uptake in the HCA-7 tumors of NIH-III mice showed that although non-HSA bound tracer shows a lower accumulation in the tumor during the perfusion phase, the radioactivity detected in the tumor is almost identical 10 min post-injection. 10 min p.i. the SUV of non-HSA bound tracer is 0.26 ± 0.06, while the SUV of HSA-bound tracer is 0.29 ± 0.09 (Fig. 7-3a). Another interesting observation is that, at the end point of the experiment (120 min post-injection), the accumulation of non-HSA bound tracer in the tumor is higher than the accumulation HSA-bound tracer(Fig. 7-3b). 120 min p.i. the SUV of non-HSA bound [^{18}F]**1a** is 0.91 ± 0.09, compared to 0.76 ± 0.05 for the HSA-bound tracer. The difference is insignificant ($p=0.22$), but notable because it suggests that the lung might act as a "reservoir" for the radiotracer. The slow release of [^{18}F]**1a** trapped in the lung keeps the radiotracer bioavailable for longer and leads to higher accumulation in tissues that express COX-2.

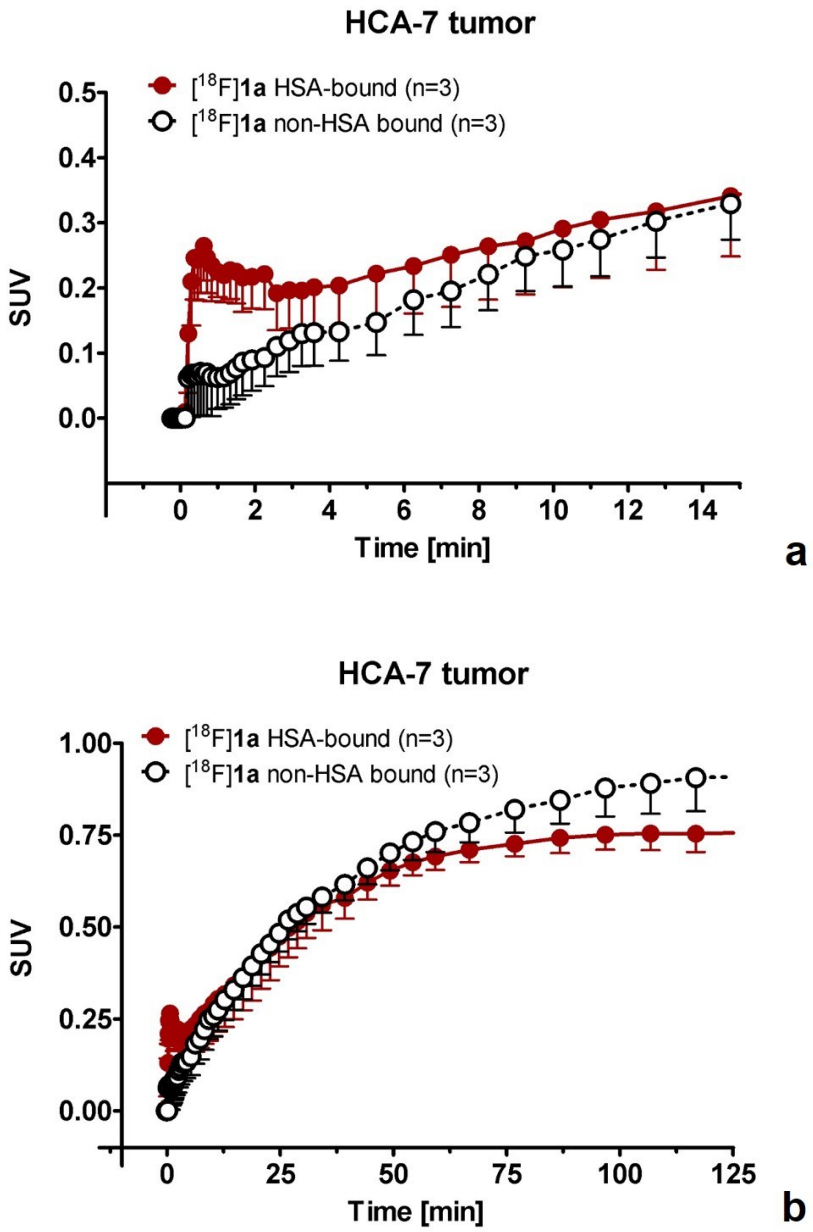

Figure 7-3a, 7-3b: Standardized uptake values of HSA bound [^{18}F]**1a** (red circle) and non-HSA bound [^{18}F]**1a** (white circle) in the HCA-7 tumor of NIH-III mice at (a) 0 min p.i. to 15 min p.i. and (b) 0 min p.i. to 120 min p.i. All data as mean ± SEM.

To investigate whether this enhanced accumulation due to slow release of the drug from the lung is general or specific to COX-2 expressing tissues, we evaluated the radiotracer uptake in the

muscle, as COX-2 negative reference tissue. Similar to the observations made in HCA-7 tumors, the initial uptake in the muscle is lower for non-HSA bound radiotracer, but almost identical 10 min post-injection (Fig. 7-4a). 10 min p.i. the SUV of non-HSA bound [^{18}F]**1a** is 0.38 ± 0.09, compared to 0.34 ± 0.07 for HSA-bound radiotracer. SUV of non-HSA bound [^{18}F]**1a**in the muscle is higher than HSA-bound radiotracer 30 min post-injection (0.63 ± 0.07 vs. 0.47 ± 0.03; p=0.11), however, in contrast to the uptake observed in the tumor, the uptake of non-HSA bound and HSA-bound [^{18}F]**1a** is almost identical 120 min post-injection. 120 min p.i. the SUV of non-HSA bound radiotracer is 0.53 ± 0.03, compared to 0.51 ± 0.07 for HSA-bound radiotracer (Fig. 7-4b). Interestingly, this suggests that non-HSA bound [^{18}F]**1a** "washes out" of reference tissue from approximately 60 min p.i. onward. As a result of this "wash out effect" in the muscle and the higher accumulation of non-HSA bound [^{18}F]**1a** in the tumor, the tumor to muscle ratio (120 min p.i.) is higher for non-HSA bound tracer (1.72) than for HSA-bound tracer (1.49). Furthermore, the difference between uptake in the tumor and uptake in the muscle is more significant for non-HSA bound [^{18}F]**1a** (p=0.017) when compared to HSA bound [^{18}F]**1a** (p=0.038). Counterintuitively, that means that non-HSA bound [^{18}F]**1a** is better for imaging studies due to the improved target to background ratio, despite its extended residency time in pulmonary tissue. HSA does improve the first-pass pulmonary passage of radiotracer [^{18}F]**1a** but reduces its ability to bind two COX-2 selectively.

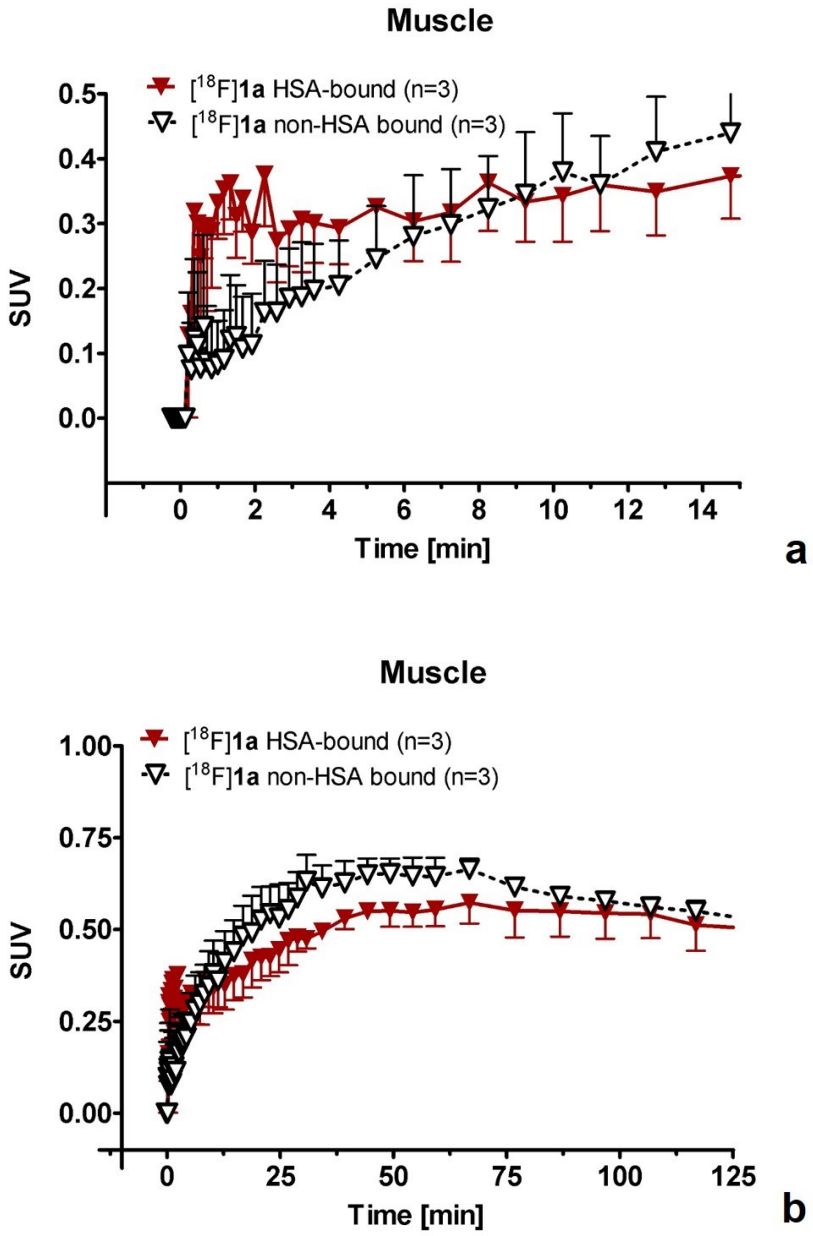

Figure 7-4a, 7-4b: Standardized uptake values of HSA bound [^{18}F]**1a** (red triangle) and non-HSA bound [^{18}F]**1a** (white triangle) in the muscle tissue of NIH-III mice at (a) 0 min p.i. to 15 min p.i. and (b) 0 min p.i. to 120 min p.i. All data as mean ± SEM.

Another organ of interest in COX-2 radiotracer studies is the brain. COX-2 is involved in a number of neurodegenerative diseases and COX-2 imaging in the central nervous system would be

advantageous. Our lab does not have a COX-2 positive neuro model, but pharmacokinetics in brain tissue can nonetheless be assessed. Similar to the observations made in muscle and tumor, the accumulation of non-HSA bound [^{18}F]**1a** in the brain is low during the perfusion phase, but reaches similar levels as HSA bound [^{18}F]**1a** 10 min post-injection(Fig. 7-5a). 10 min p.i. the SUV of non-HSA bound tracer in the brain is 1.17 ± 0.16, compared to 1.18 ± 0.18 for HSA-bound tracer. In contrast to both muscle and tumor, the clearance rates of non-HSA bound and HSA bound [^{18}F]**1a**are similar thereafter (Fig. 7-5b). 120 min p.i. the SUV of non-HSA bound [^{18}F]**1a** is 0.52 ± 0.06, compared to 0.49 ± 0.04 for HSA bound radiotracer. At this point, it is not possible to speculate whether the accumulation of non-HSA bound [^{18}F]**1a** might be higher in a COX-2 positive neuroinflammation model, similar to the uptake pattern observed in tumor tissue.

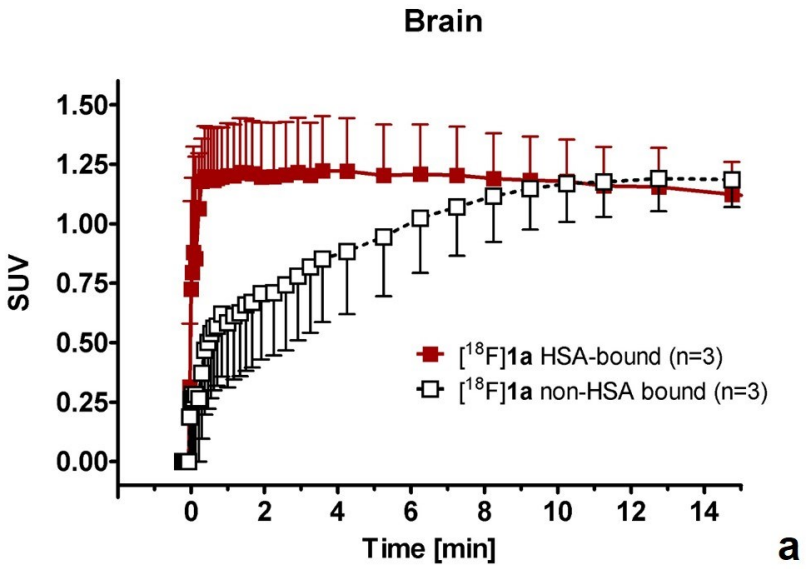

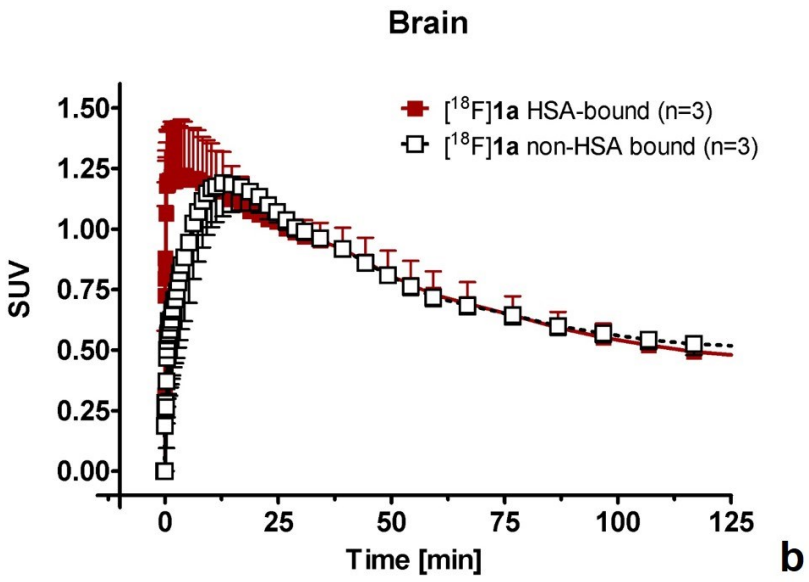

Figure 7-5a, 7-5b: Standardized uptake values of HSA bound [^{18}F]**1a** (red square) and non-HSA bound [^{18}F]**1a** (white square) in the brain of NIH-III mice at (a) 0 min p.i. to 15 min p.i. and (b) 0 min p.i. to 120 min p.i. All data as mean ± SEM.

7.4. Conclusion

Radiotracer [^{18}F]**1a** is effected by first-pass pulmonary retention through mechanisms that are not known at this time. We hypothesize that the secondary amine on **1a** is protonated in an acidic lung compartment and that the ionized radiotracer is unable to cross membranes to diffuse back into vascular space.

Normal lung passage could be achieved by binding [^{18}F]**1a** to carrier protein HSA prior to injection. The carrier protein had a minimal effect on the pharmacokinetics of the radiotracer and improved distribution during the perfusion phase. 10 min post-injection the radioactivity found in HCA-7 tumors, muscle and brain was similar for both HSA bound and non-HSA bound radiotracer. Non-HSA bound radiotracer appeared to show improved accumulation in the tumor 120 min post-injection, leading to a higher tumor to muscle ratio, however, this finding was not statistically significant.

HSA binding of the radiotracer might be used to reduce the radiation exposure of the pulmonary tissue in potential clinical trials. However, the use of a carrier protein also leads to exposure of the patient to a biological agent (i.e. protein) and might diminish the target to background ratio of resulting PET scans.

7.5. References

[1] Bakhle, Y.S. Pharmacokinetic and metabolic properties of lung. *Brit. J. Anaest.*, **1990**, 65, 79.

[2] Boer, F. Drug handling by the lungs. *Brit. J. Anaest.*, **2003**, 91, 50.

[3] Boer, F.; Bovill J.G.; Burm, A.G.L.; Hak, A. Effect of ventilation on first-pass pulmonary retention of alfentanil and sufentanil in patients undergoing coronary artery surgery. *Brit. J. Anaest.*, **1994**, 73, 458.

[4] Roerig, D.L.; Kotrly, K.J.; Dawson, C.A.; Ahlf, S.B.; Gualtieri, J.F.; Kampine, J.P. First-pass uptake of verapamil, diazepam, and thiopental in the human lung. *Anesth. Analg.*, **1989**, 69, 461.

[5] Fischer, U.M.; Harting, M.T.; Jimenez, F.; Monzon-Posadas, W.O.; Xue, H.; Savitz, S.I.; Laine, G.A.; Cox, C.S. Pulmonary passage is a major obstacle for intravenous stem cell delivery: the pulmonary first-pass effect. *Stem cells Dev.*, **2009**, 18, 683.

[6] Welch, M.J.; Dence, C.S.; Marshall, D.R.; Kilbourn, M.R. Remote system for production of Carbon-11 labelled palmitic acid. *J. labelled Compd. Radiopharm.*, **1983**, 10, 1087.

[7] Seedher, N.; Bhatia, S. Reversible binding of celecoxib and vadecoxib with human serum albumin using fluorescence spectroscopic technique. *Pharmacol. Res.*, **2006**, 54, 77.

CHAPTER 8

Synthesis of a ^{125}I-labeled COX-2 inhibitor using fluorous chemistry

As of July 30th 2015, Chapter 8 has been submitted for publication in Organic & Biomolecular Chemistry as **Tietz, O**; Dzandzi, J; Bhardwaj, A; Valliant, J; Wuest, F. "Design and synthesis of ^{125}I-labelled cyclooxygenase-2 (COX-2) inhibitors using fluorous chemistry." Some of the data is submitted for publication as supplementary information.

8.1. Introduction

The ongoing interest in COX-2 as an emerging drug target has also led to the development of various radiolabeled COX-2 inhibitors for non-invasive assessment of functional COX-2 expression to assess COX-2 using PET and SPECT imaging techniques [1-3]. In this regard, the use of prominent PET radioisotope fluorine-18 (^{18}F) was particularly popular and successful for the design and synthesis of radiolabeled COX-2 inhibitors. COX-2 is a membrane-bound enzyme that is located on the inside of the endoplasmic reticulum, and access to the active site of the enzyme is located inside the membrane bound portion of the protein [4]. Effective drug delivery to the active site of the COX-2 enzyme requires compounds with a favourable lipophilicity profile. However, highly lipophilic compounds also inherent high non-specific binding potential, which especially in the case of radiotracers results in the need of long waiting times for sufficient clearance of radioactivity from non-target tissue to achieve a reasonably high imaging contrast. Long waiting times >4 h as required for sufficient clearance are not compatible with the fairly short half life of 109.8 min for ^{18}F. Therefore, use of longer-lived radioisotopes would allow extended imaging experiments to achieve more favourable imaging contrast as reflected by better target-to-background ratios.

Iodine-125 (^{125}I) is a gamma-emitting radioisotope with a physical half-life of 59.4 days. It has found multiple applications in clinical *in vitro* diagnostics, especially for radioimmuno assay (RIA) analyses. As a low energy gamma- and efficient Auger electron-emitter ^{125}I is also a radionuclide suitable for the development of radio-pharmaceuticals for imaging and therapy. ^{125}I can be replaced by other isotopes of Iodine suitable for single photon emission computed tomography (SPECT), such as ^{123}I and ^{131}I, and positron emission tomography (PET), such as ^{124}I. The ease of oxidizing radioiodide into an electrophilic radioiodine species and subsequent mild and efficient

incorporation into aromatic compounds via electrophilic aromatic substitution reactions make electrophilic labeling strategies among the most frequently and most popular employed radioiodination methods. In recent decades, radioiodination methods have been reviewed extensively in the literature with special emphasis on labeling methods, mechanistic aspects, and applications of radioiodinated compounds in medical research [5-7].

We have recently described the synthesis and evaluation of a series of novel COX-2 inhibitors based on a diaryl-trifluoromethyl-pyrimidine scaffold [8]. Compounds contained different substitution pattern at the para-position of one of the aryl rings, and several compounds displayed favourable nanomolar inhibitory potency and a high selectivity profile towards COX-2. Selected candidates were further developed as PET radiotracers through labeling with short-lived positron emitter ^{18}F. However, the recent series of novel diaryl trifluoromethyl-pyrimidines as COX-2 inhibitors did not include iodine-containing compounds. The objective of this work was the design and synthesis of ^{125}I-labeled radiotracers based on a diaryl-trifluoromethyl-pyrimidine scaffold for molecular targeting of COX-2.

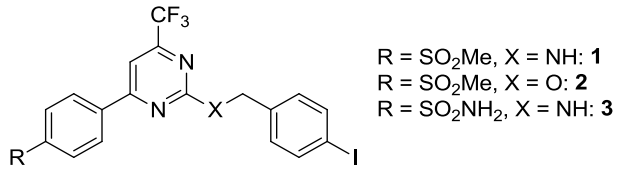

Figure 8-1: Structures of compounds **1**, **2**, and **3**

8.2. Materials and methods

All regents and solvents were obtained from Sigma-Aldrich, unless otherwise stated and used without further purification. Nuclear magnetic resonance spectra were recorded on a 600 MHz Bruker (Billerica, MA, USA) unit. ^{1}H-NMR chemical shifts are recorded in ppm relative to tetramethylsilane (TMS).

^{19}F-NMR chemical shifts are recorded in ppm relative to trichlorofluoromethane. Low resolution mass spectra were obtained using am Agilent Technologies (Santa Clara, CA, USA) 6220 oaTOF instrument. Column chromatography was conducted using Merck silica gel (mesh size 230–400 ASTM). Thin-layer chromatography (TLC) was performed on Merck silica gel F-254 aluminum plates, with visualization under UV light (254 nm). High performance liquid chromatography (HPLC) purifications and analysis were performed using a Phenomenex LUNA® C18 column (100Å, 250x10mm, 10mm) on a Gilson 322 Pump module fitted with a 171 Diode Array and a radio detector. Compounds **4** and **5** were prepared according to literature procedure [8, 11].

8.2.1. Chemistry

***N*-(4-Iodobenzyl)-4-[4-(methylsulfonyl)phenyl]-6-(trifluoromethyl)pyrimidin-2-amine (1).** Compound **4** (200 mg, 0.52 mmol) and 140 mg of 4-iodobenzylamine (0.52 mmol, 1.0 eq) were added to the reaction vessel and 2.0 ml CH_3CN with 69 μL triethyl amine (0.49 mmol, 0.9 eq) added. The reaction vessel was sealed and heated at 140^{o}C for 4 h. The reaction mixture was cooled to room temperature, and 10 ml of 1N HCl was added. The reaction mixture was stirred, and the precipitating solid was filtered off. The product was thoroughly washed with water. Compound **1** (171.2 mg, 62% yield) was obtained as a pale yellow solid.^{1}H-NMR (600MHz, $CDCl_3$): 3.10 (s, 3H, SO_2CH_3); 4.70 (s, 2H, CH_2); 5.85 (s, 1H, N-H); 7.14 (m, J=8.4Hz, 2H, Ar-H); 7.33 (s, 1H, Ar-

H); 7.68 (m, J=8.4Hz, 2H, Ar-H); 8.07 (m, J=8.4Hz, 2H, Ar-H); 8.21 (m, J=8.4Hz, 2H, Ar-H). ^{19}F-NMR (375MHz, $CDCl_3$)): -70.60 (s, 3F, CF_3). LR-MS: 556.2 [M+Na].

2-[(4-Iodobenzyl)oxy]-4-[4-(methylsulfonyl)phenyl]-6-(trifluoromethyl)pyrimidine (2). To a solution of 67 mg 4-iodobenzyl alcohol (0.29 mmol) in 3 mL of dry THF in an inert atmosphere and at 0 °C was added 11 mg of 60% NaH suspension. After 5 min, 100 mg of 2-(methylsulfonyl)-4-[4-(methylsulfonyl)phenyl]-6-(trifluoromethyl)pyrimidine **4** (0.26 mmol) was added in small portions. The reaction mixture was stirred at 0°C for 1 hour and quenched by adding an excess of 1 N HCl. Compound **2** was extracted in ethyl acetate. The organic layer was washed with water, dried over sodium sulfate and solvent removed in vacuo. Compound **2** was purified using a silica column eluting at 1% CH_3OH/CH_2Cl_2 and obtained as a pale yellow solid (98.1 mg, 71% yield). 1H-NMR (600 MHz, DMSO-d_6): 3.15 (s, 3H, SO_2CH_3); 5.55 (s, 2H, CH_2); 7.32 (m, J=8.4 Hz, 2H, Ar-H); 7.55 (s, 1H, Ar-H); 7.75 (m, J=8.4 Hz, 2H, Ar-H); 8.14 (m, J=8.4 Hz, 2H, Ar-H); 8.33 (m, J=8.4 Hz, 2H, Ar-H). 19F-NMR (565 MHz, DMSO-d_6)): -71.0 (s, 3F, CF_3). LR-MS: 557.0 [M+Na].

4-{2-[(4-Iodobenzyl)amino]-6-(trifluoromethyl)pyrimidin-4-yl}benzenesulfonamide (3). Compound **5** (100 mg, 0.26 mmol) and 140 mg of 4-iodobenzylamine (0.52 mmol, 2.0 eq) were added to the reaction vessel and dissolved in 1.0 ml CH_3CN with 69 µL triethyl amine (0.49 mmol, 1.9 eq). The vessel was heated at 140ºC for 4 hours, the reaction mixture was cooled to room temperature thereafter, and 10 ml of 1 N HCl was added. The reaction mixture was stirred and the extracted using ethyl acetate. The organic phase was washed with water and dried over sodium sulfate. The title compound was purified using a silica column eluting at 5% CH_3OH/CH_2Cl_2. Compound **3** (80.1 mg, 58 % yield) was obtained as a pale yellow solid. 1H-NMR (600 MHz, d_6-

DMSO): 4.70 (s, 2H, CH_2); 7.29 (m, J=7.8Hz, 2H, Ar-H); 7.57 (s, 2H, SO_2NH_2); 7.73 (m, J=9.6Hz, 2H, Ar-H); 7.75 (s, 1H, Ar-H); 8.01 (m, J=7.8Hz, J=9.6Hz, 2H, Ar-H); 8.40 (m, J=7.8Hz, 2H, Ar-H). 19F-NMR (375 MHz, d_6-DMSO)): -69.21 (s, 3F, CF_3). LR-MS: 554.1 [M+Na].

***N*-(4-trimethylstannyl-benzyl)-4-[4-(methylsulfonyl)phenyl]-6-(trifluoromethyl)pyrimidin-2-amine (7).** 37 mg of hexamethylditin (0.11 mmol, 1.5eq) and compound **1** were sequentially added to 10 mg tetrakistriphenylphosphine palladium(0) (0.008 mmol, 0.1 eq) in 1 mL dioxane in an inert atmosphere. The reaction vessel was sealed and heated at 120ºC for 2 hours. The mixture was allowed to cool, filtered and volume reduced on a rotary evaporator. The product was purified using a silica column stepwise eluting from 10 % EtOAc/Hexanes to 100 % EtOAc. Compound **7** (14.0 mg, 33 % yield) was obtained as a pale yellow solid. ^{1}H-NMR (600MHz, $CDCl_3$): 0.24 (m, J=27.0Hz, J=1.2Hz, 9H, $Sn(CH_3)_3$); 3.10 (s, 3H, SO_2CH_3); 4.70 (s, 2H, CH_2); 5.85 (s, 1H, N-H); 7.31 (s, 1H, Ar-H); 7.38 (m, J=7.8Hz, 2H, Ar-H); 7.49 (m, J=7.8Hz, 2H, Ar-H); 8.06 (m, J=4.8Hz, J=1,8Hz, 2H, Ar-H); 8.22 (m, J=7.8Hz, 2H, Ar-H). ^{19}F-NMR (375MHz, $CDCl_3$)): -70.61 (s, 3F, CF_3).LR-MS: 594.1 [M+Na].

8.2.2. *In vitro* COX binding assay

The ability of celecoxib and compounds **1, 2, 3** and **6** to inhibit ovine COX-1 and recombinant human COX-2 was determined using a COX fluorescence inhibitor assay (Cayman Chemical, Ann Arbor, USA; catalog #: 700100) according to the manufacturers protocol. Compounds were assayed in a concentration range of 10^{-9} to 10^{-3} M. PRISM5 software was used to calculate IC_{50} values.

8.2.3. Preparation of oxidant coated Eppendorf tubes

The walls of an eppendorf tube were treated with either 40 μL of a solution of F-CAT in $CHCl_3$ (125 μg, 3.1 mg/mL) or 20μL of a solution of iodogen in $CHCl_3$ (20 μg, 1 mg/mL) and solvent evaporated under a steady stream of Nitrogen N_2 to form a film of the oxidant at the bottom of the tube.

8.2.4. Radiochemistry

Sodium [^{125}I]iodide with a specific activity of ~17 Ci/mg was purchased from the McMaster Nuclear Reactor (Hamilton, ON, Canada). A CAPINTEC CRC-15W dose calibrator was used for measuring the amount of radioactivity employed during the radiosynthesis protocols. Analytical HPLC was performed using a Waters 2489 HPLC equipped with a Waters 2489 UV/Vis, a Bioscan glow count gamma detector (model 106), and a Phenomenex® Gemini-C18 column (4.6×250 mm, 110 Å, 5 mm). Dual wavelength for UV detection was set at 215 and 254 nm, and the dwell time in the gamma detector was 5 sec using a 10 mL loop. The mobile phase was composed of solvent A = H_2O (0.1 % TFA), and solvent B = CH_3CN (0.1 % TFA). Elution method: 0-10 min, 60-80 % B; 10-15 min, 80-100 % B; 15-24 min, 100 % B; 24-25 min, 100-60% B. The novel oxidant fluorouse Chloroamine-T (F-CAT) was synthesized at McMaster University according to literature procedure [9, 10].

Synthesis of [^{125}I]1. 50 μL of a 2 mg/mL solution of compound **7** (in 5 % CH_3COOH/CH_3OH) was added to an oxidant coated Eppendorf tube (for experiments with F-CAT or iodogen coated Eppendorf tubes), followed by addition of 20 μL of Na^{125}I (30 – 45 MBq) solution in a mildly basic solution (pH 8-11) of concentration of 1.85 GBq/mL. The radioactivity of the reaction

mixture was measured and the reaction quenched after 5 min with a solution of sodium metabisulfite (50 μL, 0.2 M). A portion of the reaction mixture was diluted in water (20 μL with 180 μL of water) and the radioactivity measured prior to HPLC purification. The activity of the purified sample was also measured to calculate the radiochemical yield (RCY).For experiments with non-coated Eppendorf tubes, precursor (**7**) was added to Eppendorf tubes containing a solution of F-CAT in CH_3OH (50 μL, 2 mg/mL), or a single iodobead®.

8.3. Results and discussion

8.3.1. Chemistry

Introduction of radioiodine was accomplished through iodo-destannylation reaction employing fluorous chemistry with fluorous chloroamine T (F-CAT) as novel and innovative oxidizing agent for radioiodide [9, 10]. Structures of novel iodine-containing compounds **1**, **2**, and **3** as novel COX-2 inhibitors are given in Figure 8-1.

Synthesis of compounds **1**, **2** and **3** followed the general synthesis route recently described using trifluoromethyl-pyrimidines **4** and **5** as starting materials carrying either a methylsulfone ($MeSO_2$) or a sulfonamide (NH_2SO_2) COX-2 pharmacophore [8, 11] (Fig. 8-2).

Reaction of 2-(methylsulfonyl)-4-(4-(methylsulfonyl)phenyl)-6-(trifluoro-methyl)pyrimidine **4** and 4-[2-(methylsulfonyl)-6-(trifluoromethyl)pyrimidin-4-yl]benzenesulfonamide **5** with 4-iodobenzylamine to give compounds **1** and **3** proceeded at elevated temperatures in CH_3CN in the presence of Et_3N in a sealed tube in good chemical yields of 62% and 58%, respectively. Incorporation of 4-iodobenzylalcohol into bis-methylsulfone 4 required NaH as the base in THF to give compound **2** in 71% yield.

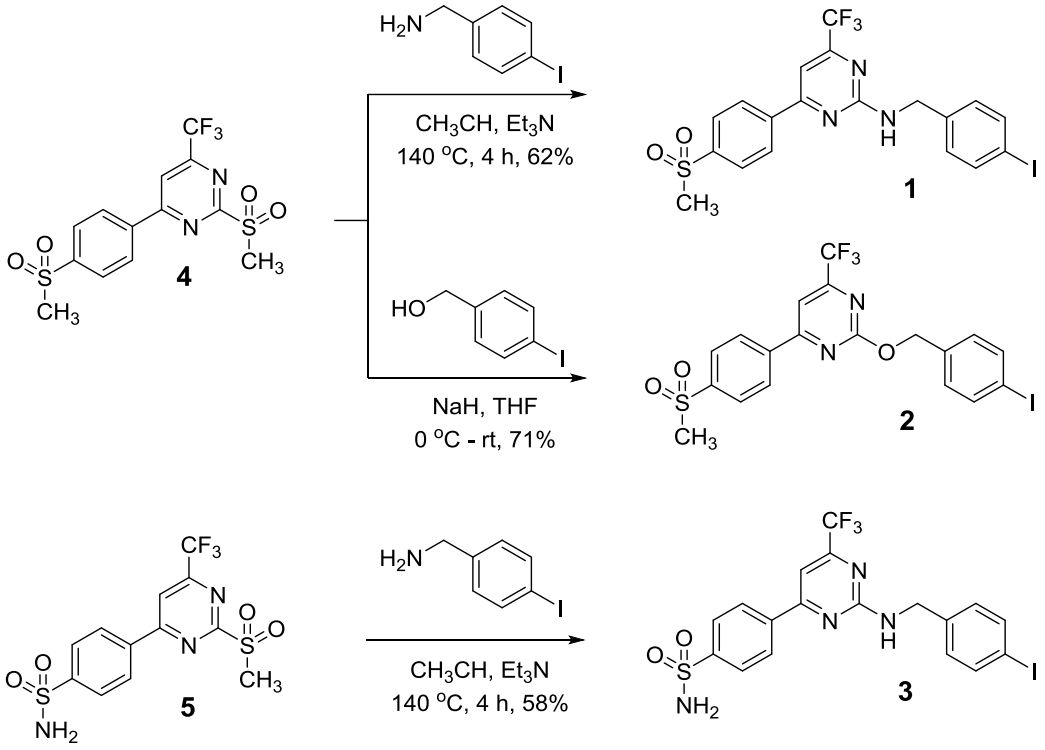

Figure 8-2: Synthesis of compounds **1**, **2**, and **3**

8.3.2. *In vitro* COX inhibition assay

4-Iodoaryl compounds **1**, **2** and **3** were further evaluated for their COX-2 inhibitory potency and selectivity profile in an *in vitro* COX enzyme inhibition assay. The enzyme inhibition data is summarized in Table 8-1.

Highly potent and selective COX-2 inhibitors celecoxib and previously reported fluorine-containing trifluoromethyl-pyrimidine compound **6** were also included into the assay as internal references for comparison [8].

All three novel iodine-containing COX-2 inhibitors compounds displayed submicromolar inhibitory potency towards COX-2 with no inhibition of COX-1 in the concentration range tested. This resulted in favourable COX-2/COX-1 selectivity profiles. However, inhibitory potency of compounds **1**, **2** and **3** was significantly lower compared to other recently studied halogen

substituted trifluoromethyl-pyrimidines and celecoxib.Corresponding iodine substituted inhibitors **1**, **2** and **3** showed two to three orders of magnitude lower inhibitory potencies when especially compared with corresponding fluorine-containing compounds. This finding suggest that increased steric bulk from iodine substitution is not well tolerated in the COX-2 binding pocket.

Despite its lowest inhibitory potency among all tested iodine-containing trifluoromethyl-pyrimidines, compound **1** was selected for radiolabeling with ^{125}I employing fluorous CAT as novel oxidizing agent for electrophilic radioiodinations. Compound **1** contains an oxidation-sensitive secondary amine which makes the compound ideal for testing radioiodination reactions under oxidative conditions.

Table 8-1: IC_{50} (COX-1) and IC_{50} (COX-2) values

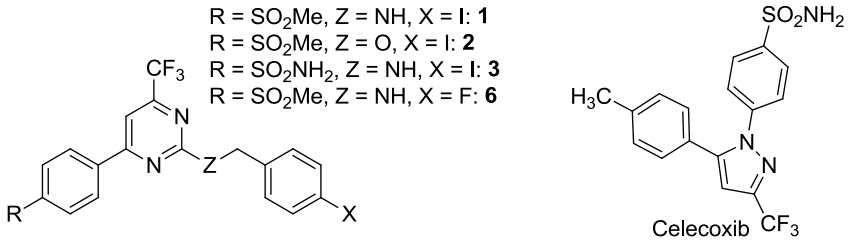

	IC_{50} (μM)[a]	
	COX-1	**COX-2**
Celecoxib	15	0.040
1	>100	0.85
2	>100	0.14
3	>100	0.28
6	>100	0.002

[a] Values are means of two determinations

.

8.3.3. Radiochemistry

Several radioiodination reactions involving organometallic intermediates have been shown to be very effective, rapid and site-specific methods for the incorporation of iodine isotopes into small molecules [5-7]. Especially the use of aromatic and vinylic organostannanes as labeling precursors gave very good results for radioiodinations via iodo-destannylation reactions. Thus, we prepared organostannane **7** as labeling precursor for radiolabeling with ^{125}I. Organostannanes **7** was prepared via Pd-catalyzed cross-coupling reaction between iodine compound **1** and hexamethylditin (Sn_2Me_6).

The reaction was carried out in dry dioxane in a sealed reaction vessel using $Pd(PPh_3)_4$ as the palladium complex under an inert atmosphere. Trimethylstannane **7** was isolated from staring material **1** after silica-gel column chromatography in 33% yield. Quality control by HPLC showed that the labeling precursor **7** did not contain any iodine-containing starting material **1**. Synthesis of trimethylstannane **7** is given in Figure 8-3.

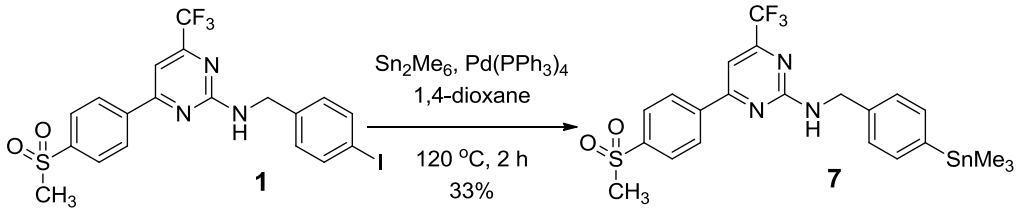

Figure 8-3: Synthesis of compound **7**

Radiotracer [^{125}I]**1** was synthesized via electrophilic iodo-destannylation from labeling precursor **7**. The reaction was optimized using a number of different oxidizing agents: Iodobeads®, iodogen coated on an Eppendorf vial and novel oxidant, which is a fluorous analogue of chloroamine-T (F-CAT), coated on an Eppendorf vial and in solution. F-CAT is a novel compound [9, 10], that is

structurally related to chloroamine-T, but modified so it and any reaction byproducts can be removed using simple fluorous solid phase extraction (FSPE). To coat oxidizing agent on the inside of an Eppendorf vial the oxidant was dissolved in chloroform, added to the vial and solvent reduced under nitrogen until the oxidant was evenly coated on the walls of the vial. The structure of various oxidizing agents (chloroamine-T, F-CAT and iodogen) and their use in the radiosynthesis of [^{125}I]**1** is given in Figure 8-4.

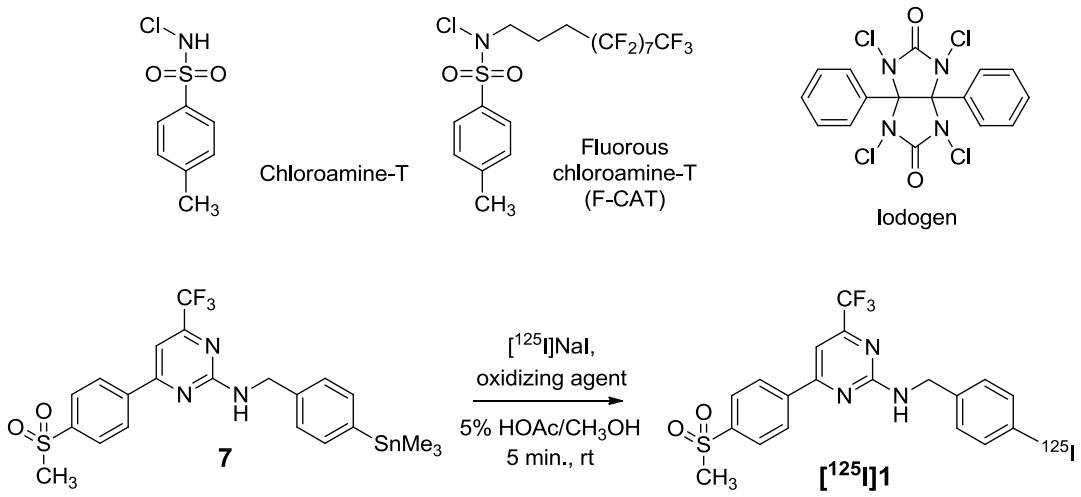

Figure 8-4: (Top) Structures of tested oxidizing agents. (Bottom) Radiosynthesis of [^{125}I]**1**.

Radiosynthesis of [^{125}I]**1** was accomplished within 30 min, including HPLC purification. Radiochemical yields (starting from [^{125}I]NaI compared to product recovered from HPLC) for reactions carried out in F-CAT coated vials were 91±4 % (n=3) compared to 81±3 % (n=3) using iodogen-coated vials. The radiochemical yields in reactions using F-CAT in solution (49 %) or Iodobeads® (32 %) were significantly lower. Radiochemical purity of [^{125}I]**1** was found to be >99 %. These results demonstrate that novel oxidizing agent F-CAT is highly effective in iodo-destannylation reactions.

Because it is simple to remove F-CAT from labelling reactions, larger quantities can be used to promote higher radiochemical yields. An additional note was that the labelling conditions did not cause decomposition of the product where the secondary amine attached to the pyrimidine ring in **7** is known to be unstable under oxidative conditions. The mild oxidization potential in connection with purification advantages make fluorous chloroamine-T an ideal oxidizing agent for electrophilic radioiodination reactions. F-CAT is able to minimize damage to oxidation sensitive structures, while being reactive enough to promote oxidation of iodide ion to an electrophilic radioiodine species required for the radioiodination reaction.

8.4. Conclusion

Radiotracer **[^{125}I]1** was prepared using fluorous chemistry with F-CAT as the oxidizing agent. The novel ^{125}I-labelled COX-2 inhibitor reported here represents an interesting lead compound for longer-lived radiotracers for molecular imaging of COX-2 and it is a new reagent to study COX-2 *in vitro*.

8.5. References

[1] Tietz, O.; Marshall, A.; Wuest, M.; Wang, M.; Wuest, F. Radiotracers for Molecular Imaging of Cyclooxygenase-2 (COX-2) Enzyme. *Curr. Med. Chem.*, **2013**, 20, 4350.

[2] Pacelli, A.; Greenman, J.; Cawthorne, C.; Smith, G. Imaging COX-2 expression in cancer using PET/SPECT radioligands: current status and future directions. *J. labelled Compd. Radiopharmaceut.*, **2014**, 57, 317.

[3] Laube, M.; Kniess, T.; Pietzsch, J. Radiolabelled COX-2 inhibitors for non-invasive visualization of COX-2 expression and activity—A critical update. *Molecules*, **2013**, 18, 6311.

[4] Godsell, D.S. The molecular perspective: cyclooxygenase-2. *Oncologist*, **2000**, 5, 169.

[5] Adam, M.J.; Wilbur, D.S. Radiohalogens for imaging and therapy. *Chem. Soc. Rev.*, **2005**, 34, 153.

[6] Seevers, R.H.; Counsell, R.E. Radioiodination techniques for small organic molecules. *Chem. Rev.*, **1982**, 82, 575.

[7] Koehler, L.; Gagnon, K.; McQuarrie, S.; Wuest, F. Iodine-124: a promising positron emitter for organic PET chemistry. *Molecules*, **2010**, 15, 2686.

[8] Tietz, O.; Sharma, S.K.; Kaur, J.; Way, J.; Marshall, A.; Wuest, M.; Wuest, F. Synthesis of three ^{18}F-labelled cyclooxygenase-2 (COX-2) inhibitors based on a pyrimidine scaffold. *Org. Biomol. Chem.*, **2013**, 11, 8052.

[9] Dzandzi, J.P.K.; Beckford Vera, D.R.; Genady, A.R.; Albu, S.A.; Eltringham-Smith, L.J.; Capretta, A.; Sheffield, W.P.; Valliant, J.F. Fluorous Analogue of Chloramine-T: Preparation, X-ray Structure Determination, and Use as an Oxidant for Radioiodination and s-Tetrazine Synthesis. *J. Org. Chem.*, **2015**, 80, 7117.

[10] Dzandzi, J.P.K.; Beckford Vera, D.R.; Valliant, J.F. A hybrid solid-fluorous phase radioiodination and purification platform. *J. labelled Compd Radiopharm.*, **2014**, 57, 551.

[11] Swarbrick, M.; Beswick, P.; Gleave, R.; Green, R.; Bingham, S.; Bountra, C.; et al. Identification of [4-[4-(methylsulfonyl) phenyl]-6-(trifluoromethyl)-2-pyrimidinyl] amines and ethers as potent and selective cyclooxygenase-2 inhibitors. *Bioorg. Med. Chem. Lett.*, **2009**, 19, 4504.

CHAPTER 9

Summary, Conclusion and Future direction

9.1. Summary of results

1 – Introduction

The effective treatment of cancer relies on accurate diagnosis and precise evaluation of response to treatment. Cancer is hard to describe and define as single entity in terms of molecular biology, due to the large diversity and complexity of the disease. Diagnosis must therefore be personalized for individual patients to assess the best treatment options. For this personalized medicine approach to function in a clinical setting, prognostic and predictive biomarkers are need, which can give feedback on disease stage and treatment option. Inflammation has recently been included as a hallmark of cancer [1] and various molecular targets are being investigate as biomarkers of inflammation in cancer.

Cyclooxygense-2 is an important mediator of inflammatory response and instrumental in the development and progression of cancer. As such, the enzyme has immense value as a diagnostic and therapeutic target. The efficacy of COX-2 as therapeutic target has already been exploited in the field of oncology and the treatment of pain related conditions. Exploitation of the diagnostic potential of COX-2 has been hampered by the difficulties associated with assessing COX-2 expression *ex vivo*. The instability of COX-2 mRNA and protein *ex vivo* leads to problems in terms of the interval between tissue sampling and time of analysis [2]. The development of techniques for non-invasive monitoring of COX-2 functional expression is therefore essential for the translation of COX-2's diagnostic potential to clinical reality.

2 – Literature Review

The literature review conducted here shows that there is a clear need for the development of COX-2 radiotracers. Approximately 25 PET and SPECT radiotracers have been developed to date, but none could be shown to interact with COX-2 specifically *in vivo*. In the context of successful COX-2 targeting *in vivo*, the work presented by Uddin *et al*. [3] was discussed extensively in Chapters 2 and 5. The researchers presented their ^{18}F-labeled celecoxib analogue as capable of specifically interact with COX-2 *in vivo*. In our opinion, the data presented by Uddin *et al.* does not support this conclusion. There are some inconsistencies in reporting the uptake of the radiotracer, such as quoting tumor to muscle ratios only, but one of the major faults of the study is the cross-affinity of the radiotracer for carbonic anhydrases. Carbonic anhydrases have been discussed as major secondary targets for COX-2 inhibitors at various points in this thesis. Some members of the carbonic anhydrase family are expressed on red blood cells and COX-2 radiotracers that carry a sulfonamide pharmacophore show very high retention in the blood pool as a result [4-6]. The experiments conducted by Uddin *et al*. are therefore likely to be representative of interactions between carbonic anhydrases and the radiotracer or reflective of changes in the blood pool and the vascularisation of tissue.

3 – Chemistry and Radiochemistry

We approached this study be focusing on four major characteristics of a successful COX-2 radiotracer, which are high inhibitory potency and selectivity for COX-2 in enzyme inhibition experiments, fast and high yielding radiosynthesis, COX-2 specific binding in cell experiments, high metabolic stability and COX-2 specific binding *in vivo*. To this end, we selected a COX-2 inhibitor previously reported by Swarbrick *et al*. and designed on the basis of pyrimidine scaffold

[7]. The compound showed excellent inhibitory potency against COX-2 (IC_{50} = 7 nM) and did not interact with COX-1 (IC_{50}> 100μM). As a result of these promising characteristics in enzyme inhibition assays, we derived the hypothesis for this study as "^{18}F-labeled small molecule compounds containing a central pyrimidine scaffold are suitable radiotracers for molecular imaging of COX-2 expression by positron emission tomography (PET)." The choice of ^{18}F as the radionuclide for this study was due to its favorable half-live (109.8 min) in comparison to ^{11}C (20.3 min). Since COX-2 is an intracellular target, slower binding kinetics are expected and longer imaging experiments required.

Fast and high yielding radiosynthesis was achieved by using 4-[^{18}F]fluorobenzylamine ([^{18}F]FBA) as a building block for the synthesis of lead radiotracer [^{18}F]**1a** (also referred to as [^{18}F]Pyricoxib). The building block [^{18}F]FBA could further be used to radiolabel the sulfonamide containing sister compound [^{18}F]**2a** in a quick and high yielding synthesis. Attempts to extend the building block approach for the radiosynthesis of sister compound [^{18}F]**3a**, which contains and ether pharmacophore in place of the secondary amine, were unsuccessful. Instead we employed a direct labeling strategy based on an iodyl precursor. Although the radiochemical yield for this radio-fluorination was low, this approach nonetheless constitutes a practical ^{18}F-labeling strategy. The site-specific incorporation of iodine in a molecule of interest is usually relatively trivial, the subsequent oxidation of iodine to iodyl can also be accomplished with most compounds. As a result, the iodyl direct labeling strategy affords the ability to quickly radio-fluorinate small molecules site-specifically.

4 and 5 – In vivo evaluation

An important conclusion of the literature review is the importance of the biological model to the study of potential COX-2 radiotracers *in vivo*. Many inflammation models and tumor models are inconsistent and unreliable in their expression of COX-2. The initial study of [^{18}F]**1a** in the ward colon tumor rat model suffered from some of these limitations. The initial *in vitro* and *in vivo* studies offered important insights to the pharmacokinetics of the radiotracer, but were not suited to draw definite conclusion as to *in vitro* and *in vivo* COX-2 specificity.

The subsequent evaluation in a colorectal cancer model offered a better platform to study the radiotracer in. The HCA-7 tumor / NIH-III mouse model has been reported as a suitable COX-2 positive tumor model [8], however, this is the first time this model is being used for the evaluation of a COX-2 radiotracer.

[^{18}F]**1a** was shown to specifically bind to COX-2 in both *in vitro* and *in vivo* experiments. The radiotracer includes a methyl sulfone pharmacophore is therefore unlikely to suffer from cross-affinity for carbonic anhydrases. We were able to show COX-2 specific binding through blocking studies *in vivo* by dynamic PET imaging and by biodistribution. Much of the experimental data presented in chapter 5 points towards the presence of non-COX-2 and non-specific interactions in addition to the partially COX-2 specific interaction of radiotracer [^{18}F]**1a**. These observed multiple non-COX-2 interactions of radiotracer [^{18}F]**1a** represent a major challenge. The non-specific interactions of COX-2 inhibitors might be inevitable due to their rather high lipophilic nature, which is necessary to cross biological membranes to reach the binding site of COX-2.

6 – Strucutre-activity relationship

Having established a reliable *in vivo* model, we further investigated the suitability of structurally similar sister compounds [^{18}F]**2a** and [^{18}F]**3a** to be used as COX-2 radiotracers. Interestingly, despite structural similarity and comparable inhibitory potency against COX-2, the *in vivo* and *in vitro* metabolic profiles of these radiotracers varied significantly. Neither [^{18}F]**2a** or [^{18}F]**3a** appear be retained in the pulmonary tissue upon first pass, while [^{18}F]**1a** shows slow lung clearance. [^{18}F]**2a** displays high retention in the blood pool, as is expected for a radiotracer that includes a sulfonamide pharmacophore. [^{18}F]**3a** shows fast elimination and a poor biological half-live. As a result, [^{18}F]**2a** or [^{18}F]**3a** are less suitable than [^{18}F]**1a** for COX-2 imaging in a tumor model. [^{18}F]**3a** exhibits some favorable characteristics as a neuro imaging agent and warrants further study in a neuroinflammation model. The short biological half-live of the radiotracer might be compatible with brain imaging studies, due to the lower background accumulation of radiotracer in brain tissue and resulting improved target to background ratios.

7 – Drug delievery using HSA

One of the clear disadvantages of the lead radiotracer [^{18}F]**1a** is the first-pass pulmonary retention it suffers from. This might have implications for the use of the tracer as a radiopharmaceutical in humans in the future as it leads to a higher radioactive dose delivered to the lung during the perfusion phase. We have attempted to identify by which mechanism the radiotracer is retained in the lung, but have not been able to draw conclusion based on experimental results. Chapter 7 includes a discussion on the mechanisms that might lead to retention of the radiotracer on first pass of the pulmonary tissue.

Drug delivery of [^{18}F]**1a** by human serum albumin reduced the first-pass pulmonary retention of the radiotracer. *In vivo* studies of [^{18}F]**1a** bound to HSA and not bound to HSA revealed that the accumulation of radiotracer in tumor, muscle and brain differs in the perfusion phase only; similar SUVs are found for bound and unbound tracer from 10 min post-injection onward. Delivery of [^{18}F]**1a** via HSA is a viable alternative, as it reduces the radiation exposure to the lung, while having a minimal effect on the pharmacokinetics of the radiotracer from 10 min post-injection onward.

8 – ^{125}I-labeled COX-2 inhibitors

Finally, due to the observation that effective perfusion to the active site of the COX-2 enzyme requires highly lipophilic compounds and the resulting high non-specific binding potential, we attempted to develop a longer-lived radiolabeled COX-2 inhibitor based on the pyrimidine scaffold. This would allow longer imaging experiments which might achieve more favorable target-to-background ratios.

A collaboration with McMaster University in Hamilton allowed us to develop an ^{125}I-labeled imaging agent. The affinity of this radiotracer for COX-2 is limited; however, the precursor and the radiochemistry developed here, especially the mild oxidation method using novel oxidant fluorous chloroamine-T (F-CAT) [9], might lead to the development of a suitable pyrimidine class tracer labeled with a long-lived halogen isotop in the future.

Note on the use of muscle as reference tissue

As part of the defence of this thesis and during the revision of this document, Dr. Vickie Baracos (who is a member of the examining committee) pointed out that a large tumor burden might induce

systemic inflammation in test animals which could lead to the expression of COX-2 in muscle tissue. If COX-2 is induced in the muscle tissues of test animals, the muscle should not be used as reference tissue since the term is misleading in that case. At the moment we are not not able to confirm the COX-2 negative properties of muscle in tumor bearing mice; however, there are cases reported in the literature were COX-2 expression is induced in muscle tissue in response to pathological events such as burn injuries [10], cancer [11] and ageing [12].

COX-2 expression in the muscle tissue would explain the relatively high retention of the radiotracers studied here in the muscle of the test animals. Wether the expression of COX-2 in the muscle has a significant effect on the uptake of radiotracer in comparison to uptake in tumor depends on the relative expression level of the enzyme in the respective tissue. There are literature reports that suggest that the expression of COX-2 in cancer is at least one order of magnitude higher than in inflammation [13]. The suitablility of muscle tissue to be used as COX-2 negative reference tissue in these animal models should be the subject of further investigation. The use of muscle as a reference tissue in radiopharmaceutical development is a convention that is difficult to revise in retrospect. If inflammation is systemic in tumor bearing animals it might be difficult to identify a tissue type that is entirely free of COX-2 expression.

9.2. Conclusion

The experimental results presented here show that ^{18}F-labeled small molecule compounds containing a central pyrimidine scaffold are suitable radiotracers for molecular imaging of cyclooxygenase-2 (COX-2) expression by positron emission tomography (PET).

Lead radiotracer [^{18}F]**1a** is a ^{18}F-labeled small molecule compound containing a central pyrimidine scaffold and was shown to (1) possess high affinity and selectivity for COX-2 in an enzyme inhibition assay; (2) be suitable for fast and high yielding radiosynthesis; (3) possess *in vitro* specificity for COX-2 in cell uptake experiments; (4) possess favorable *in vivo* radiopharmacology, including high metabolic stability and the ability to bind specifically to COX-2 *in vivo*.

These results underline that molecular imaging of intracellular targets in general and COX-2 specifically is possible. [^{18}F]**1a** is a promising candidate for molecular imaging of COX-2 in a clinical setting.

9.3. Significance

We have developed a novel PET imaging strategy for non-invasive detection of functional expression of COX-2 in cancer using radiolabeled COX-2 inhibitor [^{18}F]**1a**. This strategy has the potential to assess COX-2 expression *in vivo* which would be useful for monitoring COX-2 mediated effects on chemoprevention and radiosensitization using COX-2 inhibitors as an emerging class of therapeutics in cancer. To the best of our knowledge, this is the first time that a COX-2 radiotracer has been shown to interact with COX-2 specifically in an *in vivo* tumor model. Furthermore, we have extended the structure-activity understanding of a small compound library beyond the reach of conventional physiochemical and *in vitro* measures through dynamic small animal PET imaging. The information obtained here provides feedback on limitations of the molecular scaffold and specific chemical motifs, which enables advanced rational drug design.

The dynamic PET data that we have presented on the first-pass pulmonary retention properties of [^{18}F]**1a** might yield further information as to the origin and mechanisms that underline the extraction of drug molecules from the vascular into the pulmonary tissue. Dynamic PET analysis of radiotracer bound to HSA provides further insight into the effects of carrier proteins on the pharmacokinetic properties of drugs.

9.4. Future direction

Despite the relative success in imaging COX-2 reported here, the suitability of COX-2 as a target for molecular imaging remains unclear. The vast majority of radiopharmaceuticals in use or development today are designed to bind to extracellular targets. G-protein couple receptors, such as somatostatin receptors, chemokine receptors and gastrin-releasing peptide receptor, are especially popular in nuclear imaging. The advantages of targeting extracellular receptors are manifold. Access to the binding site is not restricted by a membrane, which allows the design of significantly less lipophilic targeting structures. These structures consequently display reduced non-specific uptake in fatty-tissues and better target-to-background ratios. The binding sites of receptor targets are less restrictive and allow for the use of larger targeting entities, such as peptides and antibodies, and a wider range of radionuclides and radiometals, such as ^{68}Ga, ^{64}Cu and ^{89}Zr, to be used.

The idea of using radiotracers labeled with isotops that have half-lives longer than 6 hours for COX-2 imaging was introduced in Chapter 8 and might present a viable avenue of future inquiry. The principal behind this concept is that the half-live of the radionuclide must match the pharmacokinetics of the targeting entity. This is a concept that is well established in antibody imaging. Although the ^{125}I radiotracer presented here showed low affinity for COX-2 and does not lend itself to PET imaging, the same precursor and similar radiochemistry could be used to label the compound with ^{76}Br. A bromine containing COX-2 inhibitor was reported in Chapter 3 (**1c**). **1c** displayed excellent affinity for COX-2 (IC_{50} = 18 nM) and no affinity for COX-1. ^{76}Br has a half-live of 16 hours and would therefore allow imaging studies exceeding 24 hours.

Another avenue of inquiry might be to obtain similar functional information on inflammatory events by targeting mediators and receptors of the prostaglandin pathway. Prostaglandin E_2 (PGE_2)

is believed to be the most important mediator of carcinogenesis [14, 15]. PGE_2 signaling is translated via four distinct prostaglandin E (EP) G-protein coupled receptors (EP1 – EP4). Recent research efforts have identified EP4 as the receptor most relevant to cancer [16, 17]. EP4 receptors were found to be overexpressed in a variety of cancers [18-20]. The experimental data on the involvement of PGE_2 in tumor development and progression coupled with the observed overexpression of EP4 in a variety of human tumors make EP4 a viable target for molecular imaging. EP4 is a membrane bound G-protein coupled receptor and therefore a preferred target for molecular imaging.

9.5. References

[1] Hanahan, D.; Weinberg, R. Hallmarks of cancer: The next generation. *Cell*, **2011**, 144, 646.

[2] Inoue, H.; Taba, Y.; Miwa, Y.; Yokota, C.; Miyagi, M.; Sasaguri, T. Transcriptional and posttranscriptional regulation of cyclooxygenase-2 expression by fluid shear stress in vascular endothelial cells. *Arterioscler. Thromb. Vasc. Biol.*, **2002**, 22, 1415.

[3] Uddin, M.; Crews, B.; Ghebreselasie, K.; Huda, I.; Kingsley, P.; Ansari, M.; Tantawy, M.N.; Reese, J.; Marnett, L.J. Fluorinated COX-2 inhibitors as agents in PET imaging of inflammation and cancer. *Can. Prev. Res.*, **2011**, 4, 1536.

[4] Weber, A.; Casini, A.; Heine, A.; Kuhn, D.; Supuran, C.T.; Scozzafava, A.; Klebe, G. Unexpected nanomolar inhibition of carbonic anhydrase by COX-2-selective celecoxib: New pharmacological opportunities due to related binding site recognition. *J. Med. Chem.*, **2004**, 47, 550.

[5] Supuran, C.T. Carbonic anhydrases: novel therapeutic applications for inhibitors and activators. *Nat. Rev. Drug Discov.*, **2008**, 7, 168.

[6] Kuge, Y.; Katada, Y.; Shimonaka, S.; Temma, T.; Kimura, H.; Kiyono, Y.; et al. Synthesis and evaluation of radioiodinated cyclooxygenase-2 inhibitors as potential SPECT tracers for cyclooxygenase-2 expression. *Nucl. Med. Biol.*, **2006**, 33, 21.

[7] Swarbrick, M.; Beswick, P.; Gleave, R.; Green, R.; Bingham, S.; Bountra, C.; et al. Identification of [4-[4-(methylsulfonyl) phenyl]-6-(trifluoromethyl)-2-pyrimidinyl] amines and ethers as potent and selective cyclooxygenase-2 inhibitors. *Bioorg. Med. Chem. Lett.*, **2009**, 19, 4504.

[8] Debucquoy, A.; Devos, E.; Vermaelen, P.; Landuyt, W.; De Weer, S.; Van Den Heuvel, F.; Haustermans, K. 18F-FLT and 18F-FDG PET to measure response to radiotherapy combined with celecoxib in two colorectal xenograft models. *Int. J. Radiat. Biol.,* **2009**, 85, 763.

[9] Dzandzi, J.P.K.; Beckford Vera, D.R.; Genady, A.R.; Albu, S.A.; Eltringham-Smith, L.J.; Capretta, A.; Sheffield, W.P.; Valliant, J.F. Fluorous Analogue of Chloramine-T: Preparation, X-ray Structure Determination, and Use as an Oxidant for Radioiodination and s-Tetrazine Synthesis. *J. Org. Chem.*, **2015**, 80, 7117.

[10] da Silva, N.T.; Quintana, H.T.; Bortolin, J.A.; Ribeiro, D.A.; de Oliveira, F. Burn injury induces skeletal muscle degeneration, inflammatory host response, and oxidative stress in wistar rats. *J. Burn Care Res.*, **2015**, 36, 428.

[11] Graves, E.; Ramsay, E.; McCarthy, D.O. Inhibitors of COX activity preserve muscle mass in mice bearing the Lewis lung carcinoma, but not the B16 melanoma. *Res. Nurs. Health.,* **2006**, 29, 87.

[12] Staunton, L.; Zweyer, M.; Swandulla, D.; Ohlendieck, K. Mass spectrometry-based proteomic analysis of middle-aged vs. aged vastus lateralis reveals increased levels of carbonic anhydrase isoform 3 in senescent human skeletal muscle. *Int. J. Mol. Med.*, **2012**, 30, 723.

[13] Zhang, H.; Fan, J.; Wang, J.; Dou, B.; Zhou, F.; Cao, J.; Qu, J.; Cao, Z.; Zhao, W.; Peng, X. Fluorescence Discrimination of Cancer from Inflammation by Molecular Response to COX-2 Enzymes. *J. Am. Chem. Soc.,* **2013**, 135, 17469.

[14] Wang, D.; DuBois, R.N. Eicosanoids and cancer. *Nat. Rev.*, **2010**, 10, 181.

[15] Wang, D.; Buchanan, F.G.; Wang, H.; Dey, S.K.; DuBois, R.N. Prostaglandin E2 enhances intestinal adenoma growth via activation of the Ras-mitogen-activated protein kinase cascade. *Cancer Res.*, **2005**, 65, 1822.

[16] Yokoyama, U.; Iwatsubo, K.; Umemura, M.; Fujita, T.; Ishikawa, Y. The Prostanoid EP4 Receptor and its Signaling Pathway. *Pharmacol. Rev.*, **2013**, 65, 1010.

[17] Konya, V.; Marsche, G.; Schuligoi, R.; Heinemann, A. E-type prostanoid receptor 4 (EP4) in disease and therapy. *Pharmacol. Therap.*, **2013**, 138, 485.

[18] Chandramouli, A.; Mercado-Pimentel, M.E.; Hutchinson, A.; Gibadulinová, A.; Olson, E.R.; Dickinson, S.; Shañas, R.; Davenport, J.; Owens, J.; Bhattacharyya, A.K.; et al. The induction of S100p expression by the Prostaglandin E_2 (PGE_2)/EP4 receptor signaling pathway in colon cancer cells. *Cancer Biol. Ther.*, **2010**, 10, 1056.

[19] Yang, L.; Huang, Y.; Porta, R.; Yanagisawa, K.; Gonzalez, A.; Segi, E.; Johnson, D.H.; Narumiya, S.; Carbone, D.P. Host and direct antitumor effects and profound reduction in tumor metastasis with selective EP4 receptor antagonism. *Cancer Res.*, **2006**, 66, 9665.

[20] Xin, X.; Majumder, M.; Girish, G.V.; Mohindra, V.; Maruyama, T.; Lala, P.K. Targeting COX-2 and EP4 to control tumor growth, angiogenesis, lymphangiogenesis and metastasis to the lungs and lymph nodes in a breast cancer model. *Lab. Invest.*, **2012**, 92, 1115.

APPENDIX A

Complete bibliography

A

Adam, M.J.; Wilbur, D.S. Radiohalogens for imaging and therapy. *Chem. Soc. Rev.*, **2005**, 34, 153.

Ahuja, N.; Singh, A.; Singh, B. Rofecoxib: An update on physicochemical, pharmaceutical, pharmacodynamic and pharmacokinetic aspects. *J. Pharm. Pharmacol.*, **2003**, 55, 859.

Alauddin, M.; Conti, P.; Mathew, T.; Fissekis, J.; Prakash, G.; Watanabe, K. Stereospecific fluorination of 1,3,5-tri-O-benzoyl-alpha-D-ribofuranose-2-sulfonate esters: Preparation of a versatile intermediate for synthesis of 2 '-[F-18]-fluoro-arabinonucleosides. *J. Fluorine Chem.*, **2000**, 106, 87.

Almansa, C.; Alfón, J.; de Arriba,A.F.; Cavalcanti, F.L.; Escamilla, I.; Gómez, L.A.; Miralles, A.; Soliva, R.; Bartroli, J.; Carceller, E.; Merlos, M.; Garcia-Rafanell, J. Synthesis and structure-activity relationship of a new series of COX-2 selective inhibitors: 1,5-diarylimidazoles. *J. Med. Chem.*, **2003**, 46, 3463.

Awara, W.M.; Alaa, E.E.; Magda, E.E.; Ahmed, E.G. The potential role of cyclooxygenase-2 inhibitors in the treatment of experimentally-induced mammary tumour: Does celecoxib enhance the anti-tumour activity of doxorubicin? *Pharmacol. Res.*, **2004**, 50, 487.

B

Balkwill, F.; Mantovani, A. Inflammation and cancer: back to Virchow? *Lancet*, **2001**, 357, 539.

Bakhle, Y.S. Pharmacokinetic and metabolic properties of lung. *Brit. J. Anaest.*, **1990**, 65, 79.

Bannwarth, B.; Berenbaum, F. Clinical pharmacology of lumiracoxib, a second-generation cyclooxygenase 2 selective inhibitor. *Expert Opin. Investig. Drugs.,* **2005**, 14, 521.

Bansal, P.; Sonnenberg, A. Risk factors in colorectal cancer in inflammatory bowl disease. *Am. J. Gastroenterol.*, **1996**, 91, 44.

Barrio, J.R.; Satyamurthy, N.; Huang, S.C.; Keen, R.E.; Nissenson, C.H.; Hoffman, J.M.; Ackermann, R.F.; Bahn, M.M.; Mazziotta, J.C.; Phelps, M.E. 3-(2'-[18F]fluoroethyl)spiperone: *In vivo* biochemical and kinetic characterization in rodents, nonhuman primates, and humans. *J. Cereb. Blood Flow Metab.*, **1989**, 9, 830.

Benesch, M.G.K.; Ko, Y.M.; McMullen, T.P.W.; Brindely, D.N. Autotaxin in the crosshairs: Taking aim at cancer and other inflammatory conditions. *FEBS Lett.*, **2014**, 588, 2712.

Beswick, P.J.; Blackaby, A.P.; Bountra, C.; Brown, T.; Browning, K.; Campbell, I.B.; Corfield, J.; Gleave, R.J.; Guntrip, S.B.; Hall, R.M.; Hindley, S.; Lambeth, R.F.; Lucas, F.; Mathews, N.;

Naylor, A.; Player, H.; Price, H.S.; Sidebottom, P.J.; Taylor, N.L.; Webb, G.; Wiseman, J. Identification and optimisation of a novel series of pyrimidine based cyclooxygenase-2 (COX-2) inhibitors: utilisation of a biotransformation approach. *Bioorg. Med. Chem. Lett.*, **2009**, 19, 4509.

Blondeau, P.; Berse, C.; Gravel, D. Dimerization of an intermediate during the sodium in liquid ammonia reduction of l-thiazolidine-4-carboxylic acid. *Can. J. Chem.*, **1967**, 45, 49.

Boer, F.; Bovill J.G.; Burm, A.G.L.; Hak, A. Effect of ventilation on first-pass pulmonary retention of alfentanil and sufentanil in patients undergoing coronary artery surgery. *Brit. J. Anaest.*, **1994**, 73, 458.

Boer, F. Drug handling by the lungs. *Brit. J. Anaest.*, **2003**, 91, 50.

Borrello, M.G.; Alberti, L.; Fischer, A.; Degl'Innocenti, D.; Ferrario, C.; Gariboldi, M.; Marchesi, F.; et al. Induction of a proinflammatory program in normal human thyrocytes by the *RET/PTC1* oncogene. *Proc. Natl Acad. Sci. USA,* **2005**, 102, 14825.

Braun, M.S.; Richman, S.D.; Quirke, P.; Daly, C.; Adlard, J.W.; Elliott, F.; Barrett, J.H.; et al. Predictive biomarkers of chemotherapy efficacy in colorectal cancer: results from the UK MRC FOCUS trial. *J. Clin. Onco.*, **2008**, 26, 2690.

Breder, C.D.; Dewitt, D.; Kraig, R.P. Characterization of inducible cyclooxygenase in rat brain. *J. Comp. Neurol.*, **1995**, 355, 296.

Buursma, A.; de Vries, E.; Garssen, J.; Kegler, D.; van Waarde, A.; Schirm, J.; Hospers, G.; Mulder, N.; Vaalburg, W.; Klein, H. [F-18]FHPG positron emission tomography for detection of herpes simplex virus (HSV) in experimental HSV encephalitis. *J. Virol.*, **2005**, 79, 7721.

Buvanendran, A.; Barkin, R. Lumiracoxib. *Drugs Of Today*, **2007**, 43, 137.

C

Cao, S.; Rustum, Y.M. Synergistic antitumor activity of irinotecan in combination with 5-fluorouracil in rats bearing advanced colorectal cancer: role of drug sequence and dose. *Cancer Res.*, **2000**, 60, 3717.

Cannon, C.P.; Cannon, P.J. COX-2 Inhibitors and Cardiovascular Risk. *Science*, **2012**, 336, 1386.

Chandramouli, A.; Mercado-Pimentel, M.E.; Hutchinson, A.; Gibadulinová, A.; Olson, E.R.; Dickinson, S.; Shañas, R.; Davenport, J.; Owens, J.; Bhattacharyya, A.K.; et al. The induction of S100p expression by the Prostaglandin E_2 (PGE_2)/EP4 receptor signaling pathway in colon cancer cells. *Cancer Biol. Ther.*, **2010**, 10, 1056.

Chang, H.C.; Weng, C.F. Cyclooxygenase-2 level and culture conditions influence NS398-induced apoptosis and caspase activation in lung cancer cells. *Oncol. Rep.*, **2001**, 8, 1321.

Copeland, R.A.; Williams, J.M.; Giannaras, J.; Nurnberg, S.; Covington, M.; Pinto, D.; Pick, S.; Trzaskos, J.M. Mechanism of selective inhibition of the inducible isoform of prostaglandin G/H synthase. *Proc. Natl. Acad. Sci. U S A*, **1994**, 91, 11202.

Coussens, L.M.; Werb, Z. Inflammation and cancer. *Nature,* **2002**, 420, 860.

D

da Silva, N.T.; Quintana, H.T.; Bortolin, J.A.; Ribeiro, D.A.; de Oliveira, F. Burn injury induces skeletal muscle degeneration, inflammatory host response, and oxidative stress in wistar rats. *J. Burn Care Res.*, **2015**, 36, 428.

Debucquoy, A.; Devos, E.; Vermaelen, P.; Landuyt, W.; De Weer, S.; Van Den Heuvel, F.; Haustermans, K. 18F-FLT and 18F-FDG PET to measure response to radiotherapy combined with celecoxib in two colorectal xenograft models. *Int. J. Radiat. Biol.,* **2009**, 85, 763.

deGroot, D.; de Vries, E.; Groen, H.; de Jong, S. Non-steroidal anti-inflammatory drugs to potentiate chemotherapy effects: from lab to clinic. *Crit. Rev. Oncol. Hematol.,* **2007**, 61, 52.

Dembo, G.; Park, S.B.; Kharasch, E.D. Central nervous system concentrations of cyclooxygenase-2 inhibitors in humans. *Anesthesiology*, **2005**, 102, 409.

de Vries, E.F.J.; van Waarde, A.; Buursma, A.R.; Vaalburg, W. Synthesis and *in vivo* evaluation of 18F-desbromo-DuP-697 as a PET tracer for cyclooxygenase-2 expression. *J. Nuc. Med.*, **2003**, 44, 1700.

deVries, E.F.J. Imaging of cyclooxygenase-2 (COX-2) expression: Potential use in diagnosis and drug evaluation. *Curr. Pharm. Des.*, **2006**, 12, 3847.

de Vries, E.F.J.; Doorduin, J.; Dierckx, R.A.; van Waarde, A. Evaluation of [11C]rofecoxib as PET tracer for cyclooxygenase 2 overexpression in rat models of inflammation. *Nucl. Med. Biol.*, **2008**, 35, 35.

DeWitt, D. Cox-2-selective inhibitors: The new super aspirins. *Mol. Pharmacol.*, **1999**, 55, 625.

Dollé, F. Fluorine-18-labelled fluoropyridines: advances in radiopharmaceutical design, *Curr. Pharm. Des.*, **2005**, 11, 3221.

Dollé, F. [18F]fluoropyridines: From conventional radiotracers to the labeling of macromolecules such as proteins and oligonucleotides, *Ernst Schering Res. Found Workshop*, **2007**, 62, 113.

Donohue, S.; Halldin, C.; Schou, M.; Hong, J.; Phebus, L.; Chernet, E.; Hitchcock, S.; et al. Radiolabeling of a high potency cannabinoid subtype-1 receptor ligand, N-(4-fluoro-benzyl)-4-(3-(piperidin-1-yl)-indole-1-sulfonyl) benzamide (PipISB), with carbon-11 or fluorine-18. *J. Labelled Compd. Radiopharm.*, **2008**, 51, 146.

Dubois, R.N.; Abramson, S.B.; Crofford, L.; Gupta, R.A.; Simon, L.S.; Van De Putte, L.B.A.; Lipsky, P.E. Cyclooxygenase in biology and disease. *FASEB J.*, **1998**, 12, 1063.

Duggan, K.C.; Hermanson, D.J.; Musee, J.; Prusakiewicz, J.J.; Scheib, J.L.; Carter, B.D.; Banerjee, S.; Oates, J.A.; Marnett, L.J. (R)-Profens are substrate-selective inhibitors of endocannabinoid oxygenation by COX-2. *Nat. Chem. Biol.*, **2011**, 7, 803.

Dzandzi, J.P.K.; Beckford Vera, D.R.; Valliant, J.F. A hybrid solid-fluorous phase radioiodination and purification platform. *J. labelled Compd Radiopharm.*, **2014**, 57, 551.

Dzandzi, J.P.K.; Beckford Vera, D.R.; Genady, A.R.; Albu, S.A.; Eltringham-Smith, L.J.; Capretta, A.; Sheffield, W.P.; Valliant, J.F. Fluorous Analogue of Chloramine-T: Preparation, X-ray Structure Determination, and Use as an Oxidant for Radioiodination and s-Tetrazine Synthesis. *J. Org. Chem.*, **2015**, 80, 7117.

E

Edwards, J.; Mukherjee, R.; Munro, A.F.; Wells, A.C.; Almushatat, A.; Bartlett, J.M.S. HER2 and COX2 expression in human prostate cancer. *Eur. J. Cancer*, **2004**, 40, 50.

Esser, R.; Berry, C.; Du, Z.; Dawson, J.; Fox, A.; Fujimoto, R.A.; Heston, W.; Kimble, E.F.; Koehler, J.; Peppard, J.; Quadros, E.; Quintavalla, J.; Toscano, K.; Urban, L.; van Duzer, J.; Zhang, X.; Zhou, S.; Marshall, P.J. Preclinical pharmacology of lumiracoxib: A novel selective inhibitor of cyclooxygenase-2. *Br. J. Pharmacol.*, **2005**, 144, 538.

F

Fiorucci, S.; Distrutti, E. COXIBs, CINODs and H2S-Releasing NSAIDs: Current Perspectives in the Development of Safer Non Steroidal Anti-Inflammatory Drugs. *Cur. Med. Chem.*, **2011**, 18, 3494.

Fischer, U.M.; Harting, M.T.; Jimenez, F.; Monzon-Posadas, W.O.; Xue, H.; Savitz, S.I.; Laine, G.A.; Cox, C.S. Pulmonary passage is a major obstacle for intravenous stem cell delivery: the pulmonary first-pass effect. *Stem cells Dev.*, **2009**, 18, 683.

FitzGerald, G.A. Coxibs and cardiovascular disease. *N. Engl. J. Med.,* **2004**, 351, 1709.

Fujisaki, Y.; Kawamura, K.; Wang, W.; Ishiwata, K.; Yamamoto, F.; Kuwano, T.; Ono, M.; Maeda, M. Radiosynthesis and *in vivo* evaluation of 11C-labeled 1,5-diarylpyrazole derivatives for mapping cyclooxygenases. *Ann. Nucl. Med.*, **2005**, 19, 617.

G

Gao, M.; Wang, M.; Miller, K.D.; Hutchins, G.D.; Zheng, Q. Synthesis of carbon-11 labeled celecoxib derivatives as new candidate PET radioligands for imaging of inflammation. *Appl. Radiat. Isot.*, **2009**, 67, 2019.

Gaulier, S.M.; Reuben, M.; Swain, N.A. A novel three-step synthesis of Celecoxib via palladium-catalyzed direct arylation. *Tetrahedron Lett.*, **2011**, 52, 6000.

Ghosh, N.; Chaki, R.; Mandal, V.; Mandal, S. COX-2 as a target for cancer chemotherapy. *Pharmacol. Rep.*, **2010**, 62, 233.

Giovannucci, E.; Rimm, E.; Stampfer, M.; Colditz, G.; Ascherio, A.; Willett, W. Asperin use and the risk for colorectal cancer and adenoma in male health professionals. *Ann. Intern. Med.*, **1994**, 121, 241.

Godsell, D.S. The molecular perspective: cyclooxygenase-2. *Oncologist*, **2000**, 5, 169.

Gong, L.; Thorn, C.F.; Bertagnolli, M.M.; Grosser, T.; Altman, R.B.; Klein, T.E. Celecoxib pathways: pharmacokinetics and pharmacodynamics. *Pharmacogenet. Genom.,* **2012**, 22, 310.

Graves, E.; Ramsay, E.; McCarthy, D.O. Inhibitors of COX activity preserve muscle mass in mice bearing the Lewis lung carcinoma, but not the B16 melanoma. *Res. Nurs. Health.,* **2006**, 29, 87.

Greenhough, A.; Smartt, H.; Moore, A.; Roberts, H.; Williams, A.; Paraskeva, C.; et al. The COX-2/PGE(2) pathway: Key roles in the hallmarks of cancer and adaptation to the tumour microenvironment. *Carcinogenesis*, **2009**, 30, 377.

Grosch, S.; Maier, T.J.; Schiffmann, S.; Geisslinger, G. Cyclooxygenase-2 (COX-2) independent anticarcinogenic effects of selective COX-2 inhibitors. *J. Nat. Cancer Inst.,***2006**, 98, 736.

Grossie Jr, V.B.; Mailman, D. Influence of the Ward colon tumor on the host response to endotoxin. *J. Cancer Res. Clin. Oncol.*, **1997**, 123, 189.

Guha, M.; Mackman, N. LPS induction of gene expression in human monocytes. *Cell Signal*, **2001**, 13, 85.

H

Habeeb, A.G.; Rao, P.N.P.; Knaus, E.E. Design and syntheses of diarylisoxazoles: Novel inhibitors of cyclooxygenase-2 (COX-2) with analgesic-antiinflammatory activity. *Drug. Dev. Res.*, **2000**, 51, 273.

Hagan, J.; Ratti, E.; Routledge, C.; et al. Use of cyclooxygenase- 2 inhibitors for the treatment of depressive disorders, WO, 2005048999 A3, **2005**.

Hanahan, D., Weinberg, R., Hallmarks of cancer: The next generation. *Cell*, **2011**, 144, 646.

Ho, L.; Pieroni, C.; Winger, D.; Purohit, D.P.; Aisen, P.S.; Pasinetti, G.M. Regional distribution of cyclooxygenase-2 in the hippocampal formation in alzheimer's disease. *J. Neurosci. Res.*, **1999**, 57, 295.

Hu, W.; Guo, Z.; Chu, F.; Bai, A.; Yi, X.; Cheng, G.; Li, J. Synthesis and biological evaluation of substituted 2-sulfonyl-phenyl-3-phenyl-indoles: A new series of selective COX-2 inhibitors. *Bioorg. Med. Chem.*, **2003**, 11, 1153.

Hull, M. Cyclooxygenase-2: how good is it as a target for chemoprevention? *Eur. J. Cancer.*, **2005**, 41, 1854.

Hwang, D.; Scollard, D.; Byrne, J.; Levine, E. Expression of cyclooxygenase-1 and cyclooxygenase-2 in human breast cancer. *J. Natl. Cancer Inst.*, **1998**, 90, 455-60.

I

Ilgan, S.; Yang, D.J.; Higuchi, T.; Zareneyrizi, F.; Bayhan, H.; Yu, D.; Kim, E.E.; Podoloff, D.A. 99mTc-ethylenedicysteine-folate: A new tumor imaging agent. synthesis, labeling and evaluation in animals. *Can. Biother. Radiopharm.*, **1998**, 13, 427.

Inoue, H.; Taba, Y.; Miwa, Y.; Yokota, C.; Miyagi, M.; Sasaguri, T. Transcriptional and posttranscriptional regulation of cyclooxygenase-2 expression by fluid shear stress in vascular endothelial cells. *Arterioscler. Thromb. Vasc. Biol.*, **2002**, 22, 1415.

Isakson, P.C.; Penning, T.D.; Talley, J.J.; Bertenshaw, S.R.; Carter, J.S.; Collins, P.W.; Docter, S.; Graneto, M.J.; Lee, L.F.; Malecha, J.W.; Miyashiro, J.M.; Rogers, R.S.; Rogier, D.J.; Yu, S.S.; AndersonG.D.; Burton E.G.; Cogburn J.N.; Gregory S.A.; Koboldt C.M.; Perkins, W.E.; Seibert, K.; Veenhuizen, A.W.; Zhang, Y.Y.; Isakson, P.C. Synthesis and biological evaluation of the 1,5-diarylpyrazole class of cyclooxygenase-2 inhibitors: Identification of 4-[5-(4-methylphenyl)-3-(trifluoromethyl)-1H-pyrazol-1-yl]benzenesulfonamide (SC-58635, celecoxib). *J. Med. Chem.*, **1997**, 40, 1347.

J

Jiménez, P.; García, A.; Santander, S.; Piazuelo, E. Prevention of cancer in the upper gastrointestinal tract with COX-inhibition, still an option? *Curr. Pharm. Des.*, **2007**, 13, 2261.

Joshi, A.; Raghavan, N.; Williams, R.; Takahashi, K.; Shingu, H.; King, S. Simultaneous quantification of an antiinflammatory compound (DuP-697) and a potential metabolite (X6882) in human plasma and urine by high-performance liquid chromatography. *J. Chromatogr., B: Anal. Technol. Biomed. Life Sci.,* **1994**, 660, 143.

K

Kabalka, G.; Mereddy, A.; Schuller, H. Synthesis of an iodine-123-labeled celecoxib analogue: A potential spect agent. *J. Labelled Compd. Radiopharmaceut.*, **2005**, 48, 295.

Karin, M. Nuclear factor-κB in cancer development and progression. *Nature,* **2006***,* 441, 431–436.

Kawamura, K.; Ishiwata, K. Improved synthesis of [C-11]SA4503, [C-11]MPDX and [C-11]TMSX by use of [C-11]methyl triflate. *Ann. Nucl. Med.*, **2004**, 18, 165.

Kershaw, E.E.; Flier, J.S. Adipose tissue as an endocrine organ. *J. Clin. Endocrinol. Metab.*, **2004**, 89, 2548.

Kim, D.; Jeong, H.-J.; Lim, S.; Sohn, M.-H. Recent Trends in the Nucleophilic [18F]-radiolabeling Method with No-carrier-added [18F] fluoride. *Nucl. Med. Mol. Imaging*, **2010**, 44, 25.

Kniess, T.; Laube, M.; Bergmann, F.; Sehn, F.; Graf, F.; Steinbach, J.; Wuest, F.; Pietzsch, J. Radiosynthesis of a 18F-labeled 2,3-diarylsubstituted indole via McMurry coupling for functional characterization of cyclooxygenase-2 (COX-2) *in vitro* and *in vivo*. *Bioorg. Med. Chem.*, **2012**, 20, 3410.

Koehler, L.; Gagnon, K.; McQuarrie, S.; Wuest, F. Iodine-124: a promising positron emitter for organic PET chemistry. *Molecules*, **2010**, 15, 2686.

Koehne, C.H.; Dubois, R.N. COX-2 inhibition and colorectal cancer. *Semin. Oncol.,* **2004**, 31, 12.

Konya, V.; Marsche, G.; Schuligoi, R.; Heinemann, A. E-type prostanoid receptor 4 (EP4) in disease and therapy. *Pharmacol. Therap.*, **2013**, 138, 485.

Koslowsky, I.; Mercer J.; Wuest, F.; Synthesis and application of 4-[18F] fluorobenzylamine: A versatile building block for the preparation of PET radiotracers. *Org. Biomol. Chem.*, **2010**, 8, 4730.

Krishnamoorthy, S.; Honn, K.V. Inflammation and disease progression. *Cancer Metastasis Rev.*, **2006**, 25, 481.

Kuge, Y.; Katada, Y.; Shimonaka, S.; Temma, T.; Kimura, H.; Kiyono, Y.; Yokota, C.; Minematusa, K.; Seki, K.; Tamaki, N.; Ohkura, K.; Saji, H. Synthesis and evaluation of radioiodinated cyclooxygenase-2 inhibitors as potential SPECT tracers for cyclooxygenase-2 expression. *Nucl. Med. Biol.*, **2006**, 33, 21.

Kuge, Y.; Obokata, N.; Kimura, H.; Katada, Y.; Temma, T.; Sugimoto, Y.; Aita, K.; Seki, K.; Tamaki, N.; Saji, H. Synthesis and evaluation of a radioiodinated lumiracoxib derivative for the imaging of cyclooxygenase-2 expression. *Nucl. Med. Biol.*, **2009**, 36, 869.

Kurumbail, R.G.; Stevens, A.M.; Gierse, J.K.; McDonald, J.J.; Stegeman, R.A.; Pak, J.Y.; Gildehaus, D.; Miyashiro, J.M.; Penning, T.D.; Seibert, K.; Isakson, P.; Stallings, W.C. Structural Basis for Selective-Inhibition of Cyclooxygenase-2 by Antiinflammatory Agents. *Nature*, **1996**, 384, 644.

Kurumbail, R.G.; Kiefer, J.R.; Marnett, L.J. Cyclooxygenase enzymes: Catalysis and inhibition. *Curr. Opin. Struct. Biol.*, **2001**, 11, 752.

L

Lacroix, S.; Rivest, S. Effect of acute systemic inflammatory response and cytokines on the transcription of the genes encoding cyclooxygenase enzymes (COX-1 and COX-2) in the rat brain. *J. Neurochem.*, **1998**, 70, 452.

Laube, M.; Kniess, T.; Pietzsch, J. Radiolabelled COX-2 inhibitors for non-invasive visualization of COX-2 expression and activity-A critical update. *Molecules.* **2013**, 18, 6311.

Lawrence, T.; Gilroy, D.W. Chronic inflammation: a failure of resolution? *Int. J. Exp. Pathol.*, **2007**, 88, 85.

Leblanc, Y.; Gauthier, J.; Ethier, D.; Guay, J.; Mancini, J.; Riendeau, D.; Tagari, P.; Vickers, P.; Wong, E.; Prasit, P. Synthesis and biological evaluation of 2,3-diarylthiophenes as selective COX-2 and COX-1 inhibitors. *Bioorg. Med. Chem. Lett.*, **1995**, 5, 2123.

Lehmann, L.; Stellfeld, T.; Graham, K.; Becaud, J.; Mu, L. Triaryl-sulphonium compounds, kit and methods for labeling positron emitting isotopes, US Patent, US/2012/0020881, **2012**.

Li, J.J.; Anderson, G.D.; Burton, E.G.; Cogburn, J.N.; Collins, J.T.; Garland, D.J.; Gregory, S.A.; Huang, H.; Isakson, P.C. 1,2-diarylcyclopentenes as selective cyclooxygenase-2 inhibitors and orally active anti-inflammatory agents. *J. Med. Chem.*, **1995**, 38, 4570.

Liao, Z.; Mason, K.; Milas, L. Cyclooxygenase-2 and its inhibition in cancer: is there a role? *Drugs*, **2007**, 67, 821.

Lin, X.B.; Farhangfar, A.; Valcheva, R.; Sawyer, M.B.; Dieleman, L.; Schieber, A.; Gänzle, M.G.; Baracos, V. The role of intestinal microbiota in development of irinotecan toxicity and in toxicity reduction through dietary fibres in rats. **2014**, e83644.

Littich, P.; Scott, P. Novel Strategies for Fluorine-18 Radiochemistry. *Angew. Chem., Int. Ed.*, **2012**, 51, 1106.

Luong, C.; Miller, A.; Barnett, J.; Chow, J.; Ramesha, C.; Browner, M.F. Flexibility of the NSAID binding site in the structure of human cyclooxygenase-2. *Nat. Struct. Biol.*, **1996**, 3, 927.

M

Mahalingam, A.; Xiongyu, W.; Yiqian, W.; Alterman, M. Scandium Triflate as an Efficient and Recyclable Catalyst for the Deprotection of Tert-Butyl Aryl Sulfonamides.*Synth. Commun.*, **2005**, 35, 95.

Majno, G. Chronic inflammation: links with angiogenesis and wound healing. *Am. J. Pathol.*, **1998**, 153, 1035.

Majo, V.; Prabhakaran, J.; Simpson, N.; Van Heertum, R.; Mann, J.; Kumar, J. A general method for the synthesis of aryl [C-11]methylsulfones: Potential PET probes for imaging cyclooxygenase-2 expression. *Bioorg. Med. Chem. Lett.*, **2005**, 15, 4268.

Mantovani, A.; Bottazzi, B.; Colotta, F.; Sozzani, S.; Ruco, L. The origin and function of tumor-associated macrophages. *Immunol. Today*, **1992**, 13, 265.

Mantovani, A.; Allavena, P.; Sica, A.; Balkwill, F. Cancer-related inflammation. *Nature,* **2008**, 454, 436.

McCarthy,T.J.; Sheriff, A.U.; Graneto, M.J.; Talley, J.J.; Welch, M.J. Radiosynthesis, *in vitro* validation, and *in vivo* evaluation of 18F-labeled COX-1 and COX-2 inhibitors. *J. Nuc. Med.*, **2002**, 43, 117.

Medzhitov, R. Origin and physiological roles of inflammation. *Nature*, **2008**, 454, 428.

Méric, J.; Rottey, S.; Olaussen, K.; Soria, J.; Khayat, D.; Rixe, O.; et al. Cyclooxygenase-2 as a target for anticancer drug development. *Crit. Rev. Oncol.*, **2006**, 59, 51.

Minghetti, L. Cyclooxygenase-2 (COX-2) in inflammatory and degenerative brain diseases. *J. Neuropath. Exp. Neuro.*, **2004**, 63, 901.

Moncada, S.; Gryglewski, R.J.; Bunting, S.; Vane, J.R. An enzyme isolated from arteries transforms prostaglandin endoperoxides to an unstable substance that inhibits platelet aggregation. *Nature*, **1976**, 263, 663.

Muller, W.A. Leukocyte-endothelia cell interactions in the inflammatory response. *Lab. Invest.*, **2002**, 82, 521.

N

Nagren, K.; Halldin, C. Methylation of amide and thiol functions with [C-11]methyl triflate, as exemplified by [C-11]NMSP, [C-11]flumazenil and [C-11]methionine. *J. Labelled Comp. Radiopharm*., **1998**, 41, 831.

O

Okamoto, T.; Hino, O. Expression of cyclooxygenase-1 and -2 mRNA in rat tissues: Tissue-specific difference in the expression of the basal level of mRNA. *Int. J. Mol. Med.*, **2000**, 6, 455.

Oldenhuis, C.N., Oosting, S.F., Gietema, J.A., de Vries, E.G., Predictive and prognostic value of biomarkers in oncology. *Eur. J. Cancer*, **2008**, 44, 946.

Ostrand-Rosenberg, S.; Sinha, P. Myeloid-derived suppressor cells: linking inflammation and cancer. *J. Immunol.,* **2009**, 182, 4499.

P

Pacelli, A.; Greenman, J.; Cawthorne, C.; Smith, G. Imaging COX-2 expression in cancer using PET/SPECT radioligands: current status and future directions. *J. Labelled Compd. Radiopharm.*, **2014**, 57, 317.

Penning, T.; Talley, J.; Bretenshaw, S.; Carter, J.; Collins, P.; Docter, S.; Graneto, M.; et al. Synthesis and biological evaluation of the 1, 5-diarylpyrazole class of cyclooxygenase-2 inhibitors: identification of 4-[5-(4-methylphenyl)-3-(trifluoromethyl)-1 H-pyrazol-1-yl] benzenesulfonamide (SC-58635, celecoxib). *J. Med. Chem.*, **1997**, 40, 1347.

Pinto, D.J.P.; Copeland, R.A.; Covington, M.B.; Pitts, W.J.; Batt, D.G.; Orwat, M.J.; Lam, G.N.; Joshi, A.; Chan, Y.; Wang, S.; Trzaskos, J.M.; Magolda, R.L.; Kornhauser, D.M. Chemistry and pharmacokinetics of diarylthiophenes and terphenyls as selective COX-2 inhibitors. *Bioorg. Med. Chem. Lett.*, **1996**, 6, 2907.

Prabhakaran, J.; Majo, V.; Simpson, N.; Van Heertum, R.; Mann, J.; Kumar, J. Synthesis of [C-11]celecoxib: A potential PET probe for imaging COX-2 expression. *J. Labelled Comp. Radiopharm.*, **2005**, 48, 887.

Prabhakaran, J.; Underwood, M.; Parsey, R.; Arango, V.; Majo, V.; Simpson, N.; van Heertum, R.; Mann, J.J.; Kumar, J.S. Synthesis and *in vivo* evaluation of [F-18]-4-[5-(4-methylphenyl)-3-(trifluoromethyl)-1H-pyrazol-1-yl]benzene-sulfonamide as a PET imaging probe for COX-2 expression. *Bioorg. Med. Chem.*, **2007**, 15, 1802.

Praveen Rao, P.N.; Amini, M.; Li, H.; Habeeb, A.G.; Knaus, E.E. Design, synthesis, and biological evaluation of 6-substituted-3-(4-methanesulfonylphenyl)-4-phenylpyran-2-ones: A novel class of diarylheterocyclic selective cyclooxygenase-2 inhibitors. *J. Med. Chem.*, **2003**, 46, 4872.

Puig, C.; Crespo, M.; Godessart, N.; Feixas, J.; Ibarzo, J.; Jiménez, J.; et al. Synthesis and biological evaluation of 3, 4-diaryloxazolones: a new class of orally active cyclooxygenase-2 inhibitors. *J. Med. Chem.*, **2000**, 43, 214.

Q

Quan, N.; Whiteside, M.; Herkenham, M. Cyclooxygenase-2 mRNA expression in rat brain after peripheral injection of lipopolysaccharide. *Brain. Res.*, **1998**, 802, 189.

R

Reitz, D.B.; Li, J.J.; Norton, M.B.; Reinhard, E.J.; Collins, J.T.; Anderson, G.D.; Gregory, S.A.; Koboldt, C.M.; Perkins, W.E. Selective cyclooxygenase inhibitors: Novel 1,2-diarylcyclopentenes are potent and orally active COX-2 inhibitors. *J. Med. Chem.*, **1994**, 37, 3878.

Riese, J.; Hoff, T.; Nordhoff, A.; DeWitt, D.L.; Resch, K.; Kaever, V. Transient expression of prostaglandin endoperoxide synthase-2 during mouse macrophage activation. *J. Leukoc. Biol.*, **1994**, 55, 476.

Rius, J.; Guma, M.; Schachtrup, C.; Akassoglou, K.; Zinkernagel, A.S.; Nizet, V.; Johnson, R.S.; Haddad, G.G.; Karin, M. NF-κB links innate immunity to the hypoxic response through transcriptional regulation of HIF-1α. *Nature,* **2008**, 453, 807.

Rodriguez, G.; Luis, A.; Cea-Soriano, L.; Tacconelli, S.; Patrignani, P. Coxibs: Pharmacology, Toxicity and Efficacy in Cancer Clinical Trials. *Prospects for Chemoprevention of Colorectal Neoplasia*, **2012**, 67.

Roerig, D.L.; Kotrly, K.J.; Dawson, C.A.; Ahlf, S.B.; Gualtieri, J.F.; Kampine, J.P. First-pass uptake of verapamil, diazepam, and thiopental in the human lung. *Anesth. Analg.*, **1989**, 69, 461.

Rovati, G.E.; Sala, A.; Capra, V.; Dahlén, S.E.; Folco, G. Dual COXIB/TP antagonists: a possible new twist in NSAID pharmacology and cardiovascular risk. *Trends Pharmacol. Sci.*, **2010**, 31, 102.

S

Satyamurthy, N.; Barrio, J. No-carrier-added nucleophilic [F-18] fluorination of aromatic compounds, WIPO Patent, WO/2010/117435, **2010**.

Scheiman, J.M. Unmet needs in non-steroidal anti-inflammatory drug-induced upper gastrointestinal diseases. *Drugs*, **2006**, 66, 15.

Schuller, H.M.; Mechanisms of smoking-related lung and pancreatic adenocarcinoma development. *Nat. Rev. Can.*, **2002a**, 2, 455.

Schuller, H.; Zhang, L.; Weddle, D.; Castonguay, A.; Walker, K.; Miller, M. The cyclooxygenase inhibitor ibuprofen and the FLAP inhibitor MK886 inhibit pancreatic carcinogenesis induced in hamsters by transplacental exposure to ethanol and the tobacco carcinogen NNK. *J. Cancer Res. Clin. Oncol.*, **2002b**, 128, 525.

Schuller, H.; Cekanova, M. NNK-induced hamster lung adenocarcinomas over-express β2-adrenergic and EGFR signaling pathways. *Lung Cancer*, **2005**, 49, 35.

Schuller, H.; Kabalka, G.; Smith, G.; Mereddy, A.; Akula,M.; Cekanova, M. Detection of overexpressed COX-2 in precancerous lesions of hamster pancreas and lungs by molecular imaging: Implications for early diagnosis and prevention. *Chem. Med. Chem.*, **2006**, 1, 603.

Seedher, N.; Bhatia, S. Reversible binding of celecoxib and vadecoxib with human serum albumin using fluorescence spectroscopic technique. *Pharmacol. Res.*, **2006**, 54, 77.

Seevers, R.H.; Counsell, R.E. Radioiodination techniques for small organic molecules. *Chem. Rev.*, **1982**, 82, 575.

Seibert, K.; Zhang, Y.; Leahy, K.; Hauser, S.; Masferrer, J.; Perkins, W.; Lee, L.; Isakson, P. Pharmacological and biochemical demonstration of the role of cyclooxygenase 2 in inflammation and pain. *Proc. Natl. Acad. Sci. U S A*, **1994**, 91, 12013.

Selinsky, B.S.; Gupta, K.; Sharkey C.T.; Loll, P.J. Structural analysis of NSAID binding by prostaglandin H2 synthase: time-dependent and time-independent inhibitors elicit identical enzyme conformations. *Biochemistry*, **2001**, 40, 5172.

Serhan, C.N.; Savill, J.; Resolution of inflammation: the beginning programs the end. *Nat. Immunol.*, **2005**, 6, 1191.

Serhan, C.N.; Chiang, N.; Van Dyke, T.E. Resolving inflammation: dual anti-inflammatory and pro-resolution lipid mediators. *Nat. Rev. Immunol.*, **2008**, 8, 349.

Shi, S.; Klotz, U. Clinical use and pharmacological properties of selective COX-2 inhibitors. *Eur. J. Clin. Pharmacol.*, **2008**, 64, 233.

Siegel, R.; Ma, J.; Zou, Z.; Jemal, A. Cancer statistics, 2014. *CA-Cancer J. Clin.*, **2014**, 64, 9.

Smith, C.J.; Zhang, Y.; Koboldt, C.M.; Muhammad, J.; Zweifel, B.S.; Shaffer, A.; Talley, J.J.; Masferrer, J.L.; Seibert, K.; Isakson, P.C. Pharmacological analysis of cyclooxygenase-1 in inflammation. *Proc. Natl. Acad. Sci. U S A*, **1998**, 95, 13313.

Staunton, L.; Zweyer, M.; Swandulla, D.; Ohlendieck, K. Mass spectrometry-based proteomic analysis of middle-aged vs. aged vastus lateralis reveals increased levels of carbonic anhydrase isoform 3 in senescent human skeletal muscle. *Int. J. Mol. Med.*, **2012**, 30, 723.

Supuran, C.T. Carbonic anhydrases: novel therapeutic applications for inhibitors and activators. *Nat. Rev. Drug Discov.*, **2008**, 7, 168.

Swarbrick, M.; Beswick, P.; Gleave, R.; Green, R.; Bingham, S.; Bountra, C.; et al. Identification of ⌈4-⌈4-(methylsulfonyl) phenyl]-6-(trifluoromethyl)-2-pyrimidinyl] amines and ethers as potent and selective cyclooxygenase-2 inhibitors. *Bioorg. Med. Chem. Lett.*, **2009**, 19, 4504.

Szabó, G.; Fischer, J.; Kis-Varga, A.; Gyires, K. New celecoxib derivatives as anti-inflammatory agents. *J. Med. Chem.*, **2008**, 51, 142.

T

Talley, J.J. Substituted pyrazolyl benzenesulfonamides. U.S. Patent No. 5,466,823. 14 Nov. **1995**.

Takashima-Hirano, M.; Takashima, T.; Katayama, Y.; Wada, Y.; Sugiyama, Y.; Watanabe, Y.; Doi, H.; Suzuki, M. Efficient sequential synthesis of PET probes of the COX-2 inhibitor [11C]celecoxib and its major metabolite [11C]SC-62807 and *in vivo* PET evaluation. *Bioorg. Med. Chem.*, **2011**, 19, 2997.

Tanaka, M.; Fujisaki, Y.; Kawamura, K.; Ishiwata, K.; Qinggeletu, Y.F.; Mukai, T.; Maeda, M. Radiosynthesis and evaluation of 11C-labeled diaryl-substituted imidazole and indole derivatives for mapping cyclooxygenase-2. *Biol. Pharm. Bull.*, **2006**, 29, 2087.

Teismann, P.; Tieu, K.; Choi, D.; Wu, D.; Naini, A.; Hunot, S.; Vila, M.; Jackson-Lewis, V.; Przedborski, S. Cyclooxygenase-2 is instrumental in parkinson's disease neurodegeneration. *Proc. Natl. Acad. Sci. U S A*, **2003**, 100, 5473.

Thun, M.; Namboodiri, M.; Calle E.; Flanders, W.; Heath, C. Aspirin use and risk of fatal cancer. *Cancer Res.*, **1993**, 53, 1322-7

Tian, H.; Lee, Z. Synthesis of 18F-labeled cyclooxygenase-2 (COX-2) inhibitor as a potential PET imaging agent. *J. Labelled Compd. Radiopharmaceut.*, **2006**, 49, 583.

Tietz, O.; Wang, M.; Marshall, A.; Sharma, S.; Way, J.; Wuest, M.; Wuest, F. 18F-Labelled radiotracers for molecular imaging of cyclooxygenase-2 (COX-2) expression in cancer. *J. Labelled Compd. Radiopharm.*, **2013a**, 56, S3.

Tietz, O.; Marshall, A.; Wuest, M.; Wang, M.; Wuest, F. Radiotracers for Molecular Imaging of Cyclooxygenase-2 (COX-2) Enzyme. *Curr. Med. Chem.,* **2013b**, 20, 4350.

Tietz, O.; Sharma, S.K.; Kaur, J.; Way, J.; Marshall, A.; Wuest, M.; Wuest, F. Synthesis of three ^{18}F-labelled cyclooxygenase-2 (COX-2) inhibitors based on a pyrimidine scaffold. *Org. Biomol. Chem.,* **2013c**, 11, 8052.

Tietz, O.; Wang,M.; Marshall, A.; Sharma, S.K.; Way, J.; Wuest, M.; Wuest, F. Functional imaging of COX-2 in cancer: A challenge for desgining a PET tracer and choosing the right *in vivo* model. *Mol. Imaging Biol.*, **2013d**, 15, S929.

Toyokuni, T.; Kumar, J.S.D.; Walsh, J.C.; Shapiro, A.; Talley, J.J.; Phelps, M.E.; Herschman, H.R.; Barrio, J.R; Satyamurthy, N. Synthesis of 4-(5-[18F]fluoromethyl-3-phenylisoxazol-4-yl)benzenesulfonamide, a new [18F]fluorinated analogue of valdecoxib, as a potential radiotracer for imaging cyclooxygenase-2 with positron emission tomography. *Bioorg. Med. Chem. Lett.*, **2005**, 15, 4699.

Tzeng, S.; Hsiao, H.; Mak, O. Prostaglandins and cyclooxygenases in glial cells during brain inflammation. *Curr. Drug Targets Inflamm. Allergy*, **2005**, 4, 335.

U

Uddin, M.; Crews, B.; Ghebreselasie, K.; Huda, I.; Kingsley, P.; Ansari, M.; Tantawy, M.N.; Reese, J.; Marnett, L.J. Fluorinated COX-2 inhibitors as agents in PET imaging of inflammation and cancer. *Can. Prev. Res.*, **2011**, 4, 1536.

V

Vane, J.R.; Bakhle, Y.S.; Botting, R.M. Cyclooxygenase-1 and 2. *Annu. Rev. Pharmacol.,* **1998**, 38, 97.

van Waarde, A.; Cobben, D.C.P.; Suurmeijer, A.J.H.; Maas, B.; Vaalburg, W.; de Vries, E,F,J.; Jager, P.L.; Hoekstra, H.J.; Elsinga, P.H. Selectivity of 18F-FLT and 18F-FDG for differentiating tumor from inflammation in a rodent model. *J. Nuc. Med.*, **2004**, 45, 695.

Verbruggen, A.M.; Nosco, D.L.; Van Nerom, C.G.; Bormans, G.M.; Adriaens, P.J.; De Roo, M.J. Technetium-99m-L,L-ethylenedicysteine: A renal imaging agent, labeling and evaluation in animals. *J. Nuc. Med.*, **1992**, 33, 551.

W

Wang, D.; Buchanan, F.G.; Wang, H.; Dey, S.K.; DuBois, R.N. Prostaglandin E2 enhances intestinal adenoma growth via activation of the Ras-mitogen-activated protein kinase cascade. *Cancer Res.*, **2005**, 65, 1822.

Wang, D.; DuBois, R.N. The role of COX-2 in intestinal inflammation and colorectal cancer. *Oncogene*, **2010a**, 29, 781.

Wang, D.; DuBois, R.N. Eicosanoids and cancer. *Nat. Rev.*, **2010b**, 10, 181.

Warner, T.D.; Mitchell, J.A. Cyclooxygenase-3 (COX-3): Filling in the gaps toward a COX continuum? *Proc. Natl. Acad. Sci. U S A*, **2002**, 99, 13371.

Way, J.; Wuest, F. Fully automated synthesis of 4-[18F] fluorobenzylamine based on borohydride/NiCl2 reduction. *Nucl. Med. Biol.*, **2013**, 40, 430.

Weber, A.; Casini, A.; Heine, A.; Kuhn, D.; Supuran, C.T.; Scozzafava, A.; Klebe, G. Unexpected nanomolar inhibition of carbonic anhydrase by COX-2-selective celecoxib: New pharmacological opportunities due to related binding site recognition. *J. Med. Chem.*, **2004**, 47, 550.

Weissman, G. Inflammation: Historical Perspectives in: Inflammation: Basic Principles and Clinical Correlates. *Raven Press, New York*, **1992**, 5.

Welch, M.J.; Dence, C.S.; Marshall, D.R.; Kilbourn, M.R. Remote system for production of Carbon-11 labelled palmitic acid. *J. labelled Compd. Radiopharm.*, **1983**, 10, 1087.

Wuest, F.; Kniess, T. Synthesis of 4-[F-18]fluoroiodobenzene and its application in sonogashira cross-coupling reactions. *J. Labelled Compd. Radiopharmaceut.*, **2003**, 46, 699.

Wüst, F.R.; Höhne, A.; Metz, P. Synthesis of 18F-labelled cyclooxygenase-2 (COX-2) inhibitors via stille reaction with 4-[18F]fluoroiodobenzene as radiotracers for positron emission tomography (PET). *Org. Biomol. Chem.*, **2005**, 3, 503.

Wuest, F.; Kniess, T.; Bergmann, R.; Pietzsch, J. Synthesis and evaluation *in vitro* and *in vivo* of a 11C-labeled cyclooxygenase-2 (COX-2) inhibitor. *Bioorg. Med. Chem.*, **2008**, 16, 7662.

X

Xin, X.; Majumder, M.; Girish, G.V.; Mohindra, V.; Maruyama, T.; Lala, P.K. Targeting COX-2 and EP4 to control tumor growth, angiogenesis, lymphangiogenesis and metastasis to the lungs and lymph nodes in a breast cancer model. *Lab. Invest.*, **2012**, 92, 1115.

Xue, H.; Sawyer, M.B.; Field, C.J.; Dieleman, L.A.; Baracos, V.E. Nutritional modulation of antitumor efficacy and diarrhea toxicity related to irinotecan chemotherapy in rats bearing the ward colon tumor. *Clin. Cancer Res.*, **2007**, 13, 7146.

Y

Yamada, S.; Kubota, K.; Kubota, R.; Ido, T.; Tamahashi, N. High accumulation of fluorine-18-fluorodeoxyglucose in turpentine-induced inflammatory tissue. *J. Nuc. Med.*, **1995**, 36, 1301.

Yang, D.J.; Bryant, J.; Chang, J.Y.; Mendez, R.; Oh, C.; Yu, D.; Ito, M.; Azhdarinia, A.; Kohanim, S.; Kim, E.E.; Lin, E.; Podoloff, D.A. Assessment of cyclooxygense-2 expression with 99m-Tc-labeled celebrex. *Anticancer Drugs*, **2004a**, 15, 255.

Yang, D.J.; Azhdarinia, A.; Wu, P.; Yu, D.F.; Tansey, W.; Kalimi, S.K.; Kim, E.E.; Podoloff, D.A. *In vivo* and *in vitro* measurement of apoptosis in breast cancer cells using 99mTc-EC-annexin V. *Can. Biother Radiopharm.*, **2004b**, 16, 73.

Yang, L.; Huang, Y.; Porta, R.; Yanagisawa, K.; Gonzalez, A.; Segi, E.; Johnson, D.H.; Narumiya, S.; Carbone, D.P. Host and direct antitumor effects and profound reduction in tumor metastasis with selective EP4 receptor antagonism. *Cancer Res.*, **2006**, 66, 9665.

Yasojima, K.; Schwab, C.; McGeer, E.G.; McGeer, P.L. Distribution of cyclooxygenase-1 and cyclooxygenase-2 mRNAs and proteins in human brain and peripheral organs. *Brain Res.*, **1999**, 830, 226.

Yokoyama, U.; Iwatsubo, K.; Umemura, M.; Fujita, T.; Ishikawa, Y. The Prostanoid EP4 Receptor and its Signaling Pathway. *Pharmacol. Rev.*, **2013**, 65, 1010.

Yoshida, K.; Fujino, H.; Otake, S.; Seira, N.; Regan, J.; Murayama, T. Induction of cyclooxygenase-2 expression by prostaglandin E2 stimulation of the prostanoid EP4 receptor via coupling to Gαi and transactivation of the epidermal growth factor receptor in HCA-7 human colon cancer cells. *Eur. J. Pharmacol.*, **2013**, 8, 408.

Yu, H.; Kortylewski, M.; Pardoll, D. Crosstalk between cancer and immune cells: role of STAT3 in the tumour microenvironment. *Nature Rev. Immunol.*, **2007**, 7, 41.

Yu, Y.; Ricciotti, E.; Scalia, R.; Tang, S.Y.; Grant, G.; Yu, Z.; Landesberg, G.; Crichton, I.; Wu, W.; Pure, E.; Funk, C.; FitzGerald, G. Vascular COX-2 Modulates Blood Pressure and Thrombosis in Mice. *Sci. Transl. Med.,* **2012**, 132.

Z

Zareneyrizi, F.; Yang, D.; Oh, C.; Ilgan, S.; Yu, D.; Tansey, W.; Liu, C.; Kim, E.E.; Podoloff, D.A. Synthesis of [Tc-99m]ethylenedicysteine-colchicine for evaluation of antiangiogenic effect. *Anticancer Drugs*, **1999**, 10, 685.

Zhang, J.; Yuan, J.; Wang, Y.; Bible, R.; Breau, A. Pharmacokinetics and metabolism of a COX-2 inhibitor, valdecoxib, in mice. *Drug Metab. Disposition.*, **2003**, 31, 491.

Zhang, H.; Fan, J.; Wang, J.; Dou, B.; Zhou, F.; Cao, J.; Qu, J.; Cao, Z.; Zhao, W.; Peng, X. Fluorescence Discrimination of Cancer from Inflammation by Molecular Response to COX-2 Enzymes. *J. Am. Chem. Soc.,* **2013**, 135, 17469.

Zheng, W.; Thorne, N.; McKew, J.C. Phenotypic screens as a renewed approach for drug discovery. *Drug Discov. Today*, **2013**, 18, 1067.